



**TOHOKU**  
UNIVERSITY

# **The 10<sup>th</sup> International Symposium on Water Environment Systems ---with Perspective of Global Safety**

(December 8<sup>th</sup> – 9<sup>th</sup>, 2022)

**Department of Civil and Environmental Engineering  
Graduate School of Engineering  
Tohoku University**



**SyDE** WISE Program for  
Sustainability in the  
Dynamic Earth  
変動地球共生学卓越大学院プログラム



## Sponsors



### GP-RSS Program

International Joint Graduate Program in Resilience and Safety Studies of Tohoku University

<http://gp-rss.tohoku.ac.jp/>



### SyDE Program

WISE Program for Sustainability in the Dynamic Earth of Tohoku University

<https://syde.tohoku.ac.jp/>



TOHOKU  
UNIVERSITY

### Tohoku University

Department of Civil and Environmental Engineering,  
Graduate School of Engineering, Tohoku University

<http://www.eng.tohoku.ac.jp/>

## Organizers

Dr. So KAZAMA	(Professor, Tohoku Univ)
Dr. Yu-You LI	(Professor, Tohoku Univ)
Dr. Daisuke SANO	(Professor, Tohoku Univ)
Dr. Keiko Udo	(Professor, Tohoku Univ)
Dr. Daisuke KOMORI	(Associate Professor, Tohoku Univ)
Dr. Kengo KUBOTA	(Associate Professor, Tohoku Univ)
Dr. Rajapaksha Mudiyansekage Janaka Bamunawala	(Associate Professor, Tohoku Univ)
Dr. Yusuke Hiraga	(Research Associate, Tohoku Univ)

## Secretariats

Dr. Yu QIN	(Assistant Professor, Tohoku Univ)
Dr. Tao YAMAMOTO	(Research Fellow, Tohoku Univ)
DC Student, Zibin LUO	(Tohoku Univ)
DC Student, Juntong HA	(Tohoku Univ)
DC Student, Shitong ZHOU	(Tohoku Univ)

# The 10<sup>th</sup> International Symposium on Water Environment Systems

---with Perspective of Global Safety

## PARTICIPANTS

- |           |  |  |
|-----------|--|--|
| <b>01</b> | <b>Agro-Environmental Protection Institute, <i>China</i></b><br>Haixin GUO<br>Bingkun CHEN                         | Professor<br>Student                       |
| <b>02</b> | <b>Fukushima University, <i>Japan</i></b><br>Yoshiyuki YOKOO<br>Sora MARUTA<br>Yuki KUSAKABE<br>Sheikh Hefzul BARI | Professor<br>Student<br>Student<br>Student |
| <b>03</b> | <b>National Research Centre, <i>Egypt</i></b><br>Samir I. GADOW  | Associate Professor                        |
| <b>04</b> | <b>King Mongkut's University of Technology Thonburi, <i>Thailand</i></b><br>Chaiwat EKKAWATPANIT                   | Associate Professor                        |
| <b>05</b> | <b>Shandong University, <i>China</i></b><br>Qigui NIU  | Associate Professor                        |
| <b>06</b> | <b>University of Moratuwa, <i>Sri Lanka</i></b><br>Luminda GUNAWARDHANA  | Senior Lecturer                            |
| <b>07</b> | <b>Tohoku Institute of Technology, <i>Japan</i></b><br>Keisuke ONO   | Lecturer                                   |
| <b>08</b> | <b>Malang State University, <i>Indonesia</i></b><br>Eli Hendrik SANJAYA  | Lecurer                                    |
| <b>09</b> | <b>Xi'an University of Architecture and Technology, <i>China</i></b><br>Xuanyu ZHAI<br>Xiaohuan YANG               | Student<br>Student                         |
| <b>10</b> | <b>Shanghai University, <i>China</i></b><br>Ruixin WU<br>Yanyan LI   | Student<br>Student                         |
| <b>11</b> | <b>China Agricultural University, <i>China</i></b><br>Jiahao ZHANG   | Student                                    |
| <b>12</b> | <b>Suzhou University of Science and Technology, <i>China</i></b><br>Yixiao LIU<br>Yuqin FAN                        | Student<br>Student                         |
| <b>13</b> | <b>Nanjing Tech University, <i>China</i></b><br>Xiang LI<br>Yang YANG<br>Chen-Shun LU                              | Student<br>Student<br>Student              |



# 14 Tohoku university, Japan

Tao YAMAMOTO	Postdoc Researcher
Kampachiro URASAKI	Student
Yanxiao WEI	Student
Wenzhao ZHAO	Student
Ziang HE	Student
Shitong ZHOU	Student
Weiyi WANG	Student
Juntong HA	Student
Abeygunasekara HASHANI	Student
Amalia Nafisah Rahmani IRAWAN	Student
Sartsin PHAKDIMEK	Student
Shoichi KUROSAWA	Student
Ayaka OKAMOTO	Student
Kumudu Madhawa KURUGAMA	Student
Atsuya IKEMOTO	Student
Andre FORTES	Student
Mohammad Naser SEDIQI	Student
Muthiah SADIDAH	Student

# Schedule(GMT+9)



## 8 Dec (THUR)

10:00~12:00 **Fieldwork**

## 9 Dec (FRI)

09:00~09:05 **Opening remarks**

09:05~09:10 **Group photo**

### Session 1 **Oral session I**

09:10~09:22 Development of a HCR-BrISH for detection of environmental microorganisms.

--Kampachiro URASAKI, *Tohoku Univsity.*

09:22~09:34 Removal of four RNA viruses from swine wastewater by AnMBR the interplay between adsorption, rejection and virus type.

--Xuanyu ZHAI, *Xi'an University of Architecture and Technology.*

09:34~09:46 Highlighting the key role of temperature and chemical environment in pathogen inactivation of anaerobic digestion of pig manure.

--Jiahao ZHANG, *China Agricultural University.*

09:46~09:58 Effective and Selective Removal of Phosphate from Water by Functional Carbon.

--Bingkun CHEN, *Agro-Environmental Protection Institute.*

09:58~10:10 Anammox Microorganisms Diversity in Sediment of Reservoir Located in Indonesia.

--Eli Hendrik Sanjaya, *Malang State University, Indonesia.*

10:10~10:22 Refractory dissolved organic matter as carbon source for advanced nitrogen removal from mature-landfill leachate: A review and prospective application.

--Ruixin WU, *Shanghai University.*

10:22~10:34 Achieving Stable Mainstream Partial Nitritation-Anammox Process by Successful Regulation of Nitrite-Oxidizing Bacteria.

--Yanxiao WEI, *Tohoku University.*

10:34~10:46 Experimental study on two-stage PN/HAP-A process for treating garbage methane fermentation liquid.

--Wenzhao ZHAO, *Tohoku University.*

10:46~10:58 Emerging onsite electron donors for advanced nitrogen removal from anammox effluent of leachate-treatment: A review and future applications.

--Yanyan LI, *Shanghai University.*

10:58~11:10 Preparation of a spherical biochar colloidal probe and its application in deciphering the mechanism of biochar mitigating membrane fouling.

--Xiaohuan YANG, *Xi'an University of Architecture and Technology.*

11:10~11:22 High solid of co-digestion performance of lipid waste and food waste by a thermophilic Hollow Fiber-anaerobic membrane bioreactor.

--Ziang HE, *Tohoku University*

11:22~11:34 Effects of oleate loads on methanogenesis under mesophilic and thermophilic conditions.

--Xiang LI, *Nanjing Tech University.*

11:34~11:46 Combining Steam Injection with Hydrodynamic Cavitation for Sludge Pretreatment to Improve Sludge-Solubility and Digestion Performance.

--Shitong ZHOU, *Tohoku University.*

11:46~11:58 Influence of nitrate as electron acceptor on Nap anaerobic biodegradation.

--Qigui NIU, *Shandong University.*

11:58~12:10 Current options in the treatment of agricultural drainage wastewater.

--Samir I.GADOW, *National Research Centre, Egypt.*

**12:10~13:00 Lunch break**

# Schedule(GMT+9)



13:00~14:30 | **Poster session**

## Poster exhibition (Room A)

An overview of sewage treatment for human health safety in the Song Dynasty.

--Yixiao LIU, *Suzhou University of Science and Technology*.

Performance comparison of Anammox process with EDTA chelation of Fe(III) and Fe(III) salts addition.

--Yang YANG, *Nanjing Tech University*.

Successful demonstration of a pilot-scale internal circulation reactor integrated with partial nitrification-anammox for the treatment of real membrane-manufacturing wastewater.

--Yujin FAN, *Suzhou University of Science and Technology*.

Impacts of different Biochar/Ni types on the anaerobic digestion of high salinity wastewater.

--Chen-Shun LU, *Nanjing Tech University*.

Effect of aeration intensity on a compact biofilm reactor for rural domestic sewage treatment in China: pollutant removal performance and hydrodynamic behavior.

--Weiyi WANG, *Tohoku University*.

Effect of up-flow anaerobic sludge blanket reactor treating methanolic wastewater by adding complex-accelerant.

--Juntong HA, *Tohoku University*.

## Poster exhibition (Room B)

Predictive numerical modeling of landslide susceptibility: A case study for Uma Oya catchment, Sri Lanka.

--Abeygunasekara HASHANI, *Tohoku University*.

Validation of watershed storage effects for the analysis of climate change.

--Sora MARUTA, *Fukushima University*.

Assessment of the chemical compositional characteristics as mass movements in granite zone.

--Yuki KUSAKABE, *Fukushima University*.

Population Movement caused by Flood Damage at City Level.

--Ayaka OKAMOTO, *Tohoku University*.

Innovative ensemble approach of spatial prediction of flood using bivariate index of entropy and support vector machine models.

--Kumudu Madhawa KURUGAMA, *Tohoku University*.

## Poster exhibition (Room C)

Understanding drought risk in the coastal region of Bangladesh using gridded meteorological data.

--Sheikh Hefzul BARI, *Fukushima University*.

Use of Irrigation reservoirs to reduce inundation depth by flooding.

--Atsuya IKEMOTO, *Tohoku University*.

Preliminary Analysis of Flood Events and Human-flood Interactions in Cascade Dams Area in Citarum-Watershed, Indonesia.

--Muthiah SADIDAH, *Tohoku University*.

Evaluation on high-altitude snow observation for snowmelt flood forecasting.

--Shoichi KUROSAWA, *Tohoku University*.

Satellite and UAV derived vegetative roughness in Nanakita river: case of Typhoon Hagibis.

--Andre FORTES, *Tohoku University*.



# Schedule(GMT+9)

## Session 2 | Oral session II

- 14:30~14:55 Climate risk and vulnerability assessment (CRVA) framework for the built environment:  
A case study in SEZAD industrial zone Yixiao LIU, Suzhou University of Science and Technology  
--Luminda GUNAWARDHANA, *University of Moratuwa*.
- 14:55~15:20 Climate Change Adaptation using Managed Aquifer Recharge.  
--Chaiwat EKKAWATPANIT, *University of Technology Thonburi*.
- 15:20~15:45 Minecraft as a tool for disaster education: A case study of flood inundation in Fukushima, Japan.  
--Keisuke ONO, *Tohoku Institute of Technology*.
- 15:45~16:00 Spatio-temporal projection of the change in sustainability of Kabul River Basin under SSP scenarios.  
--Mohammad Naser SEDIQI, *Tohoku University*.
- 16:00~16:15 Identifying Landslides Using SAR, Optical Imagery and Spatial indices in Google Earth Engine.  
--Sartsin PHAKDIMEK, *Tohoku University*.
- 16:15~16:30 Coffee break**
- 16:15~16:45 Decadal variations of drought indicators in Indonesia from 1981 - 2020.  
--Amalia Nafisah Rahmani IRAWAN, *Tohoku University*.
- 16:45~17:00 Study of Adaptation Measures for Flood Damage Mitigation by Adopting Effect of Climate Change.  
--Tao YAMAMOTO, *Tohoku University*.
- 17:00~17:25 A data-based modeling approach of rainfall-runoff processes: its development history and a blueprint for the future.  
--Yoshiyuki YOKOO, *Fukushima University*.

## 17:25~17:35 | Closing Remarks

## Development of an HCR-BrISH for environmental microorganisms

○ Kampachiro URASAKI<sup>1\*</sup>, Yu-You LI<sup>1</sup> & Kengo KUBOTA<sup>2</sup>

<sup>1</sup>Department of Civil and Environmental Engineering, Graduate School of Engineering, Tohoku University, Miyagi 980-8579, Japan.

<sup>2</sup>Department of Frontier Sciences for Advanced Environment, Graduate School of Environmental Studies, Tohoku University, Miyagi 980-8579, Japan.

\*E-mail: kampachiro.urasaki.pl@dc.tohoku.ac.jp

### Abstract

Electron microscopy enables to detect the microbial cells with high spatial resolution. *In situ* hybridization that can label the microbial with specific element has been developed (e.g., Gold-ISH). But there is no report that can label microbial cells phylogenetically with other element. In this study, we attempted to develop a novel bromine labelling method, “HCR-BrISH (hybridization chain reaction-bromine *in situ* hybridization)” to detect microbial cells phylogenetically by electron microscopy. An HCR-BrISH protocol was optimized based on HCR-FISH protocol. In HCR-BrISH protocol, some thymidines in amplifier probes were replaced to bromodeoxyuridines. As a result, Bromine signal was not obtained in EDX spectrograph although labelling amplifier probes to microbial cells was confirmed.

**Keywords:** HCR-ISH; Bromodeoxyuridine (BrdU); Scanning electron microscopy; Energy Dispersive X-ray Spectroscopy

### 1 Introduction

FISH (fluorescence *in situ* hybridization) is widely used in various fields because it can detect microorganisms at single-cell resolution without cell cultivation and DNA/RNA extraction. In recent years, detection using X-ray-based techniques, e.g., SEM (scanning electron microscopy), are becoming mainstream due to their high spatial resolution. For X-rays detection, labeling the microbial cells with heavy elements is necessary. In this study, bromine is selected as labelling element of the microbial cell. We proposed the TSA-BrISH (tyramide signal amplification-bromine *in situ* hybridization) in the previous report; however, in TSA-BrISH, bromine labeled to the microbial cell was not able to be detected by SEM-EDX [1]. In this report, we propose “HCR-BrISH (hybridization chain reaction-BrISH).” An HCR-BrISH protocol uses an HCR-FISH protocol [2] and BrdU (bromodeoxyuridine). HCR is an extension reaction of two amplifier probes. BrdU is a nucleoside analogue of dT (thymidine). In this report, we attempted to label microbial cells with a high density of bromine by performing HCR-BrISH using amplifier probes in which dT was replaced by BrdU.

### 2 Materials and methods

#### 2.1 Sample preparation

The strain used in this study was *Comamonas testosteroni*. The strain was cultivated in LB medium at 37°C with agitation. During exponentially growth phase, the cell was fixed in a 4% paraformaldehyde solution in phosphate buffered saline (PBS; 150 mM NaCl, 20 mM PO<sub>4</sub><sup>3-</sup> [pH7.4]) for 12 h at 4°C, and stored in ethanol/PBS solution at -20°C.

#### 2.2 HCR-BrISH

The scheme of HCR-BrISH is shown in Figure 1. The protocol was in accordance with “quick HCR-FISH” method [2] except the amplifier probes. The probe information was shown in Table 1. Two sets of amplifier probes were prepared. In set A, nine dTs were replaced to BrdU. In set C, 30 dTs were replaced to BrdU. Initiator probe and amplifier

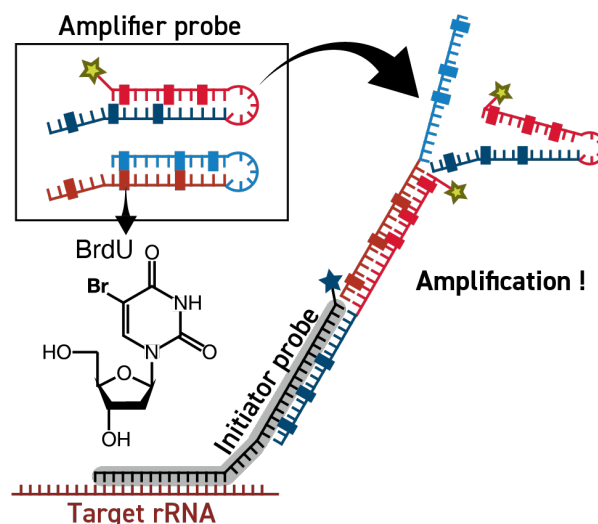


Figure 1 Scheme of HCR-BrISH

probe-H1 were labeled with Cyanine 5 and Alexa Fluor 488, respectively, in order to observe the microbial cells by epifluorescence microscopy. Initiator probe and amplifier probes were purchased from TSUKUBA OLIGO SERVICE CO., LTD and Japan Bio Services Co.,LTD, respectively.

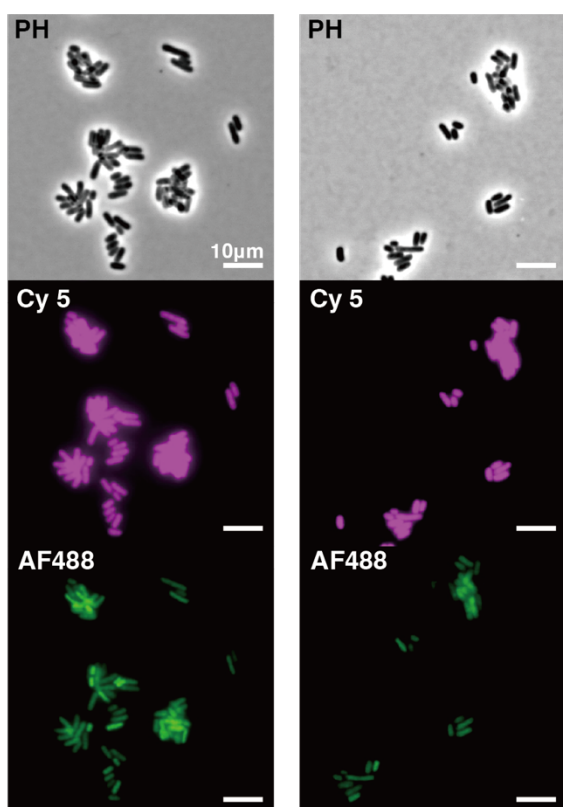
### 3 Results and discussion

Figure 2 shows the fluorescence images of *C.testosteroni* detected by epifluorescence microscopy. Cyanine 5 fluorescence signal (middle panel) indicates the initiator probe successfully hybridized with ribosomal RNA. Alexa Fluor 488 fluorescence signals (under panel) indicate the microbial cells were labeled with amplifier probes. The fluorescence signal of set C was tended to be weaker than that of set A. It is speculated that higher replace number of BrdU inhibited amplification efficiency.

Figure 3 shows the secondary electron images and EDX spectrograph of *C.testosteroni* obtained by SEM analysis. EDX spectrograph showed no bromine peak from the target cells whichever the amplifier probe used, set A or set C.

**Table 1** Probe sequence

Probe	Sequence (5' - 3' )
<b>Initiator</b>	
EUB338-H	c c g a a t a c a a a g c a t c a a c g a c t a g a a a a g c t g c c t c c c g t a g g a g t
<b>Amplifier set A. U=BrdU</b>	
H1-A	t c t a g t c g t g a t g c U t t g t a t t c g g c g a c a g a U a a c c g a a U a c a a a g c a U c
H2-A	c c g a a U a c a a a g c a U c a a c g a c U a g a g a t g c t U t g t a t t c g g t t a t c t g U c g
<b>Amplifier set C. U=BrdU</b>	
H1-C	U c U a g U c g U U g a U g c U U U g U a U U c g g c g a c a g a U a a c c g a a U a c a a a g c a U c
H2-C	c c g a a U a c a a a g c a U c a a c g a c U a g a U g c U U U g U a U U c g g U U a U c U g U c g



**Figure 2** Detection of *C.testosteroni* by epifluorescence microscopy. Right; set A, Left; set C.

#### 4 Conclusions

We attempted to develop “HCR-BrISH”, a novel high sensitive bromine labelling method. The labelling of amplifier probe to the microbial cells was confirmed; however, labeled bromine density was insufficient to be detected by SEM-EDX.

#### Reference

- [1] Kampachiro Urasaki, *et al.*, Development of a BrISH for environmental microorganisms, The 9th International Symposium on Water Environment Systems - with Perspective of Global Safety, 2021/11/25-26, Online, Poster.
- [2] Takashi Yamaguchi, *et al.*, (2015). Rapid and sensitive identification of marine bacteria by an improved in situ DNA hybridization chain reaction (quickHCR-FISH). *Systematic and applied microbiology*, 38(6), 400-405.

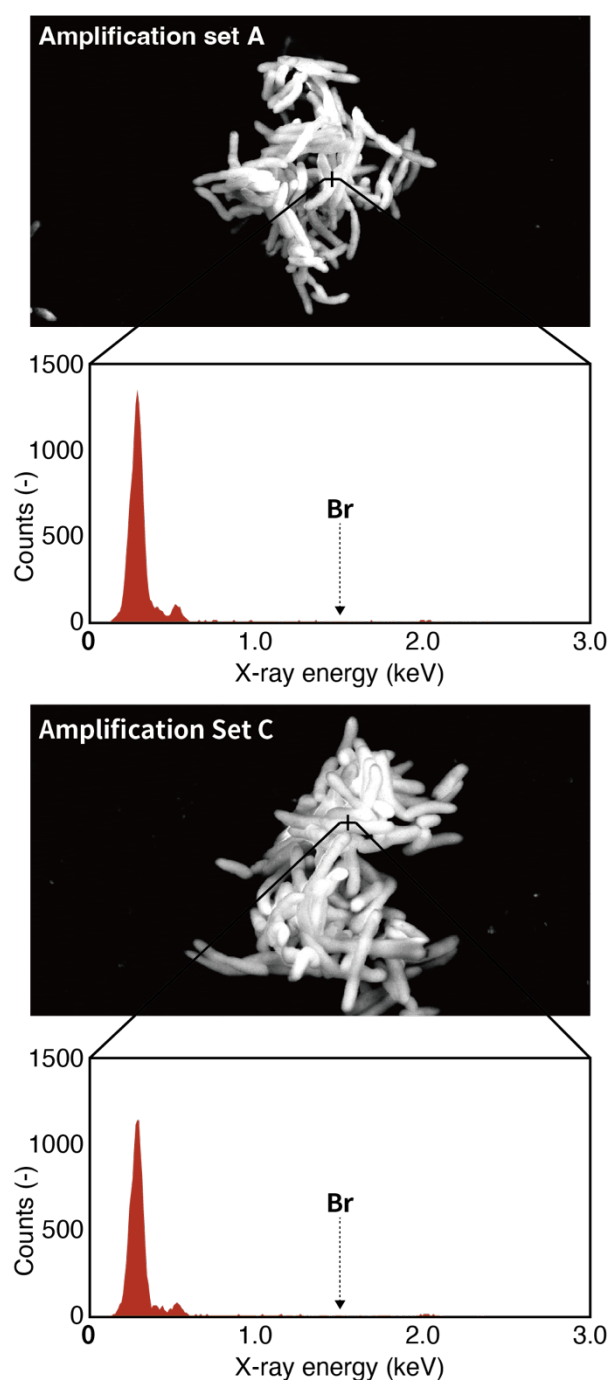


**Figure 3** Detection *C.testosteroni* by SEM-SEI and EDX.(A) set A and (B) set C

## Removal of four RNA viruses from swine wastewater by AnMBR the interplay between adsorption, rejection and virus type

○ Xuanyu Zhai<sup>1</sup>, Baolei Wu<sup>2</sup>, Jinfan Zhang<sup>1</sup> & Rong Chen<sup>1,3\*</sup>

<sup>1</sup> Key Lab of Environment Engineering, Shanxi Province, Xi'an University of Architecture and Technology, No. 13 Yanta Road, Xi'an 710055, PR China

<sup>2</sup> Vanke School of Public Health, Tsinghua University, Beijing 100008, PR China

<sup>3</sup> International S&T Cooperation Center for Urban Alternative Water Resources Development, Key Laboratory of Northwest Water Resource, Environment and Ecology, MOE, Xi'an University of Architecture and Technology, No. 13 Yanta Road, Xi'an 710055, PR China

\*E-mail: [chenrong@xauat.edu.cn](mailto:chenrong@xauat.edu.cn)

### Abstract

Anaerobic membrane bioreactor (AnMBR) is widely used in swine wastewater, but there were few studies on the removal of RNA viruses from swine wastewater by AnMBR. In this study, the interplay between adsorption, rejection and virus type of porcine hepatitis E virus (HEV), porcine kobuvirus (PKoV), porcine epidemic diarrhoea virus (PEDV), and transmissible gastroenteritis coronavirus (TGEV) was systematically investigated in AnMBR. Results revealed that the viruses concentration on the solid phase (73%~95%) was higher than in the liquid phase, indicating that most of the viruses were attached to the solids in the mixed liquor. In addition, membrane rejection experiments showed that membrane pore foulants (22%~76%) played a major role in the rejection of viruses by the membrane.

**Keywords:** Anaerobic membrane bioreactor (AnMBR); High concentration organic wastewater; Virus removal; Virus adsorption; Membrane fouling.

### 1 Introduction

Swine wastewater harbor a large amount of infectious viruses, in terms of the species and magnitude, among which RNA viruses was paid more attention for its higher mutation rates, cross-species transmission risk, and huge economic losses. Swine wastewater is characterized by high solids content and poor hydrolysis efficiency, while AnMBR enables the separation of sludge retention time (SRT) and hydrolysis retention time (HRT), enhancing further degradation of less biodegradable organic matter. Meanwhile, membrane in AnMBR can act as an important barrier against viruses.

In this study, the removal of HEV, PKoV, PEDV and TGEV from swine wastewater was investigated by AnMBR. The virus adsorption of the mixed liquor in the bioreactor was analyzed and the partitioning of viruses in the solid-liquid phase of the mixed liquor was studied. In addition, the virus rejection of fouled membrane was investigated.

### 2 Materials and methods

#### 2.1 AnMBR and operation condition

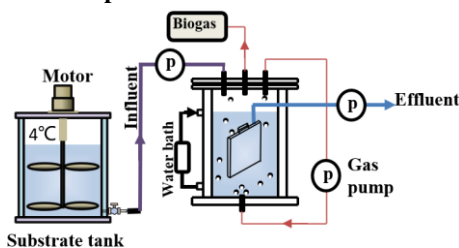


**Fig.1. Schematic of anaerobic membrane bioreactor**

A built-in submerged AnMBR with a working volume of 2.5 L was used in this study to treat swine wastewater (**Fig.1**). Polyvinylidene fluoride (PVDF) membrane was employed

with an average pore size of 0.22  $\mu\text{m}$ , HRT of 4 d. The mixed liquor suspended solids (MLSS) was maintained steady at  $72.10 \pm 1.93$  g/L.

#### 2.2 Samples

The influent and effluent were enriched by membrane and mixed liquor was separated into solid and liquid phases by centrifugation at 10,000g for 1 h. Determination of sample virus concentration by qPCR.

#### 2.3 Membrane contribution

Swine wastewater was filtered through the intact fouled membrane, and the log removal value (LRV) obtained represented the combined removal contribution of the cake layer, organic foulants, inorganic foulants, irrecoverable foulants and the pristine membrane. Subsequently, the membrane was rinsed with pressure water to remove the cake layer and then the swine wastewater was filtered through the membrane. The LRV obtained represented the combined removal contribution of organic foulants, inorganic foulants, irrecoverable foulants and the pristine membrane. The membrane was immersed in 0.1% NaClO solution for 24 h to remove organic fouling and then the sewage influent was filtered through the membrane. The LRV obtained represented the combined removal contribution of inorganic foulants, irrecoverable foulants and the pristine membrane. The fouled membrane immersed in a 10 g/L citric acid solution for 4 h and then the swine wastewater was filtered through the membrane. The LRV obtained represented the combined removal contribution of irrecoverable foulants and the pristine membrane. Finally, the pristine membrane was used to filter the swine wastewater and the LRV obtained represented the combined removal contribution of the pristine membrane.

### 3 Results and discussion

### 3.1 Virus removal performance

During the investigation period of the AnMBR, HEV, PKoV, PEDV and TEGV in the influent were  $10^{7.38 \pm 0.08}$ ,  $10^{8.14 \pm 0.32}$ ,  $10^{7.79 \pm 0.18}$  and  $10^{6.2 \pm 0.02}$  copies/L, respectively, while the virus concentrations in the effluent decreased gradually over time. The averaged overall LRVs for HEV, PKoV, PEDV and TGEV were  $1.62 \pm 0.17$ ,  $3.05 \pm 0.6$ ,  $2.41 \pm 0.35$  and  $1.34 \pm 0.31$  logs, respectively (Fig.2). Of these four viruses, the bioreactor had the highest removal efficiency for PKoV and was the least removal efficiency for TGEV.

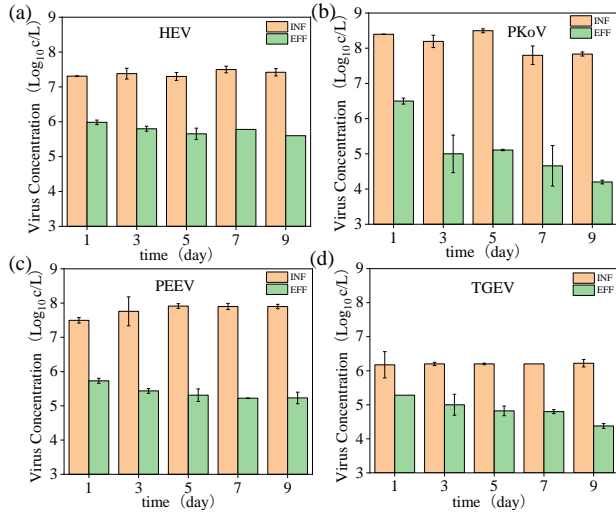


Fig. 2. Virus concentrations for (a)HEV, (b)PKoV, (c)PEDV, and (d)TGEV in the AnMBR influent and effluent.

### 3.2 biomass adsorption

The distribution of HEV, PKoV, PEDV and TGEV in the solid and liquid phases of the mixed liquor were shown in Fig.3. As shown in Fig.3a, most of the viruses were attached to suspended particles (73-95%). Specifically, of these four viruses, the sludge had the highest adsorption efficiency for PKoV (95%) and the lowest for TGEV (73%). The differential virus allocation rate between liquid and solid phases in this study was probably due to the specific virus type and surface characteristics. Indeed, Chaudhry<sup>[1]</sup> had reported that MS2, phiX174, and fr with similar surface electrical properties showed divergent biomass binding preference.

The averaged concentrations of HEV, PKoV, PEDV and TGEV in the solid phases were 1.16, 2.08, 1.30 and 0.26 LRV, respectively (Fig.3b). During the study period, the TMP increased from 12.0 to 35.1 kPa and the virus concentration in the mixed liquor was relatively constant, so the TMP was not related to the virus adsorbed by the biomass.

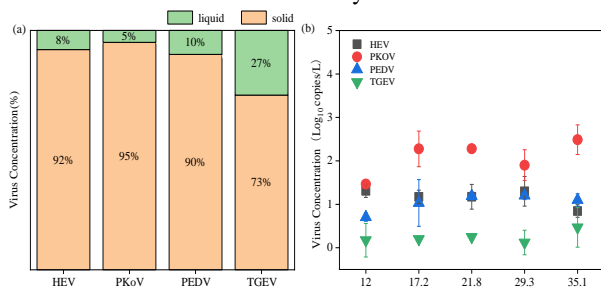


Fig. 3. Virus allocation rate in liquid and solid phases; (b) Virus concentrations in sludge particles at varying TMPs.

### 3.3 Virus rejection by each membrane fouling component

The pristine membrane rejection removal values for HEV, PKoV, PEDV and TGEV were 0.19, 0.40, 0.46, 0.66, respectively, which might be related to the size of the virus (Fig.4a). HEV is an RNA virus of approximately 27-34 nm in diameter, however the PVDF membrane employed in this study had a nominal pore size of 0.22 μm, which was approximately 10 times larger than the diameter of HEV. Therefore, smaller diameter viruses were less effectively retained by the pristine membrane and size sieving effect was the main virus rejection mechanism of the pristine membrane.

Virus rejection by fouled membranes could be divided into the five components acting on the viruses rejection: cake layer, organic foulants, inorganic foulants, irrecoverable foulants and pristine membrane, respectively (Fig.4). Specifically, inorganic, organic and irreversible foulants accounted for 1.53% of the total membrane resistance, they contributed 71.27%, 75.57%, 22.18% and 49.49% of the total membrane rejection rate for HEV, PKoV, PEDV and TGEV, respectively. The pristine membrane accounted for 0.22% of the total membrane resistance and retained 19-42% of the virus. The cake layer made up 98.25% of the total membrane resistance, but retained only 5-30% viruses. Therefore, viruses were primarily retained by the pore foulants, followed by the pristine membrane, and finally the cake layer. The pore foulants were the main contributor to viruses rejection by the fouled membrane, and the membrane resistance was low, so the rejection contribution per unit membrane resistance was significant.

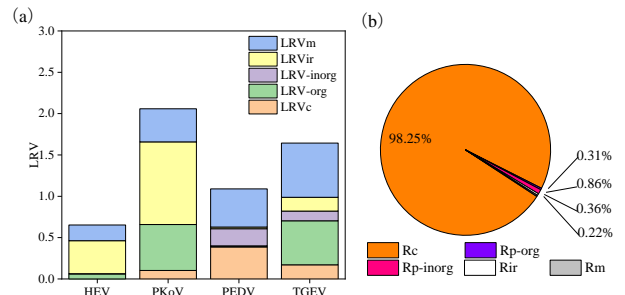


Fig.4. (a) The contribution of each membrane fouling component to virus rejection (b) The filtration resistance of each membrane fouling component.

## 4 Conclusions

The removal of viruses AnMBR was mainly achieved by the biological attachment and membrane rejection. Viruses accumulate heavily in the mixed liquor and were concentrated in the biomass (over 90%). The pore foulants and the pristine membrane were the main drivers of membrane rejection. In addition, the biomass attachment capacity and the pristine membrane rejection were related to the virus type.

## Reference

[1] Chaudhry R. M., Holloway R. W., Cath T. Y., et al. Impact of virus surface characteristics on removal mechanisms within membrane bioreactors, Water Research, (2015) 144-152

# Highlighting the key role of temperature and chemical environment in pathogen inactivation of anaerobic digestion of pig manure

○ Jia-Hao ZHANG<sup>1</sup>, Min LIN<sup>1</sup>, Wei QIAO<sup>1\*</sup> & Renjie DONG<sup>1</sup>

<sup>1</sup>College of Engineering, Biomass Engineering Center, China Agricultural University, Beijing 100083, China.

\*E-mail: qiaowei@cau.edu.cn; wayqiao@sina.cn

## Abstract

Cost-effective hygienization of animal manure through anaerobic digestion was a long-standing challenge. Two-stage AD process introducing 55 and 70 °C biological hydrolysis following a 37 °C reactor was thus studied and compared to a parallelly operated mesophilic reactor at the same total HRT (30 days). The numbers of *E. coli* and fecal coliforms in the effluent of both the two-stage AD systems were much low and comparable. The inactivation rate  $k_h$  of *E. coli* in the 70, 55, and 37 °C reactors was 19.768, 0.936, and 0.032 h<sup>-1</sup>, respectively, which indicated the importance of temperature. At 37 °C, acetate below 255 mg/L had no hygienization effects on *E. coli*, but ammonium bicarbonate of 2800 mg/L could completely inactivate *E. coli* in 24h. The chemical environment-derived impacts on pathogen inactivation were unexpected and need further studies.

**Keywords:** anaerobic digestion, pathogen inactivation, kinetics, temperature, chemical effects

## 1 Introduction

Anaerobic digestion (AD) is a widely used technology to treat manure for pollution control, energy recycling, and pathogen inactivation. However, mesophilic AD cannot effectively eliminate pathogens and the thermophilic process required too much energy even though it had better hygienization performance [1]. Two-stage AD that introduces high temperatures for pathogen inactivation and the subsequent mesophilic methane formation for process stability control and saving energy input is therefore more practical. During the AD process, the chemical environment had significant changes, i.e. high acetate concentration in the first stage and the formation of NH<sub>4</sub>HCO<sub>3</sub> in the second stage methane reactor. So far, if the chemical environment can contribute to pathogen inactivation and thus reduce the temperature level was still unclear.

Therefore, this study aimed to improve the sanitization of two-stage AD by introducing longer thermal treatment and verifying the temperature and chemical functional parameters of pathogen inactivation.

## 2 Materials and methods

### 2.1 Two-stage AD systems

TMAD system: 55 °C (5 d) + 37 °C (25 d)

HMAD system: 70 °C (5 d) + 37 °C (25 d)

MAD system: 37 °C (30 d)

All reactors were CSTR with a working volume of 4 L and a stirring speed of 100 rpm, and were fed once a day.

### 2.2 Pathogenic bacteria enumeration methods

Raw pig manure and AD effluent were sampled during the stable period for bacteria enumeration. The enumeration of *E. coli* was conducted according to GB 4789.38-2012 using VBR Agar-MUG. Fecal coliforms were enumerated using the procedures described in GB 4789.39-2013.

### 2.3 Inactivation kinetics

During a feed period (24h), effluent from 37 °C mono-reactor, 55 °C, and 70 °C reactors were sampled at irregular intervals for *E. coli* detection. The First-order model [1] was used to fit the *E. coli* inactivation, where  $C_N$  and  $C_0$  were the concentration of *E. coli* at a certain time and the beginning, respectively, and  $k_h$  was the inactivation rate constant.

$$\log\left(\frac{C_N}{C_0}\right) = -k_h t \quad (1)$$

## 2.4 Inhibition by chemicals

*E. coli* (ATCC 25922) type strain was selected for the inhibition test. According to the actual concentration in MAD, 255 mg/L acetate and 1600 mg/L NH<sub>4</sub>HCO<sub>3</sub> were added to the LB broth separately, and the pH was adjusted to 7.4. Then the tubes were inoculated with *E. coli* pure culture and incubated at 37±1 °C for 24 h. Serial concentrations (0~0.25 mol/L) of NH<sub>4</sub>CO<sub>3</sub>, NH<sub>4</sub>Cl, and NaHCO<sub>3</sub> were selected to explore their inhibitory effect.

## 3 Results and discussion

### 3.1 Performance of pathogens inactivation

In Figure 1, the fecal coliforms and *E. coli* in MAD effluent remained at 10<sup>3</sup>-10<sup>4</sup> CFU or MPN/ml, while two-stage AD systems reduced the fecal coliforms and *E. coli* that were below the limit of China and the European Commission. Although a small number of fecal coliforms was still present in the 55°C reactor, they became undetectable in the subsequent mesophilic reactor. A study reported that the number of fecal coliforms and enterococci in sludge remained high after 60 minutes of pasteurization at 80°C [2]. The recovery of coliform bacteria and *Enterococcus* spp. during the process of storage and farm utilization after the MAD with 60 minutes of pasteurization at 70°C was reported by Bagge and De. These results are inconsistent with this study, possibly because the longer thermal treatment time and other chemical factors have a positive effect on inactivating pathogens, which makes hygienization performance better.

### 3.2 Kinetic models for *E. coli* inactivation

The inactivation of *E. coli* in AD conformed to the first-order kinetic model shown in Figure 2. The constants  $k_h$  obtained for 70, 55, and 37 °C mono-reactor were 19.768, 0.936, and 0.032 h<sup>-1</sup>, respectively. It was reported the  $k_h$  of *E. coli* in the anaerobic storage of sludge was only 0.007 h<sup>-1</sup> at 15 °C [3]. The constants  $k_h$  of *E. coli* in the 25 °C storage and AD (37 °C and 52.5 °C) of dairy manure were 0.004, 0.024, and 0.075 h<sup>-1</sup> [4]. The  $k_h$  of MAD in the previous study is the same as the result of this study, but notably, the  $k_h$  of the high-temperature reactor is much lower than this study, perhaps

because the concentrations of ammonia or VFAs in our reactor are higher and the heat may exacerbate the inactivation of pathogens by these chemicals [1].

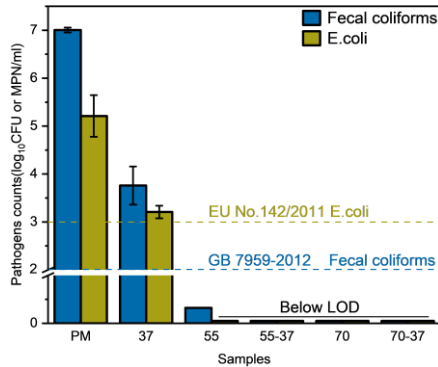


Figure 1 Reduction of fecal coliforms and *E. coli*

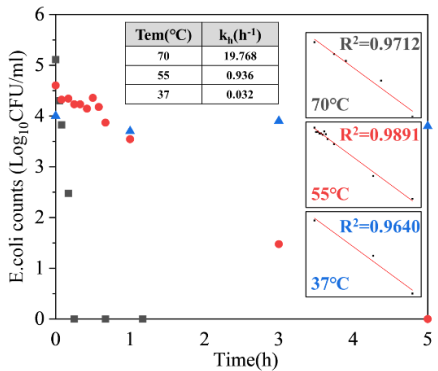


Figure 2 Inactivation of *E. coli* in a 24h feed cycle

### 3.3 Effects of chemicals on pathogen inactivation

The number of *E. coli* decreased at a slow rate in MAD and it was necessary to investigate the effect of chemicals in the MAD reactor. This study selected two intermediate products in the AD environment: acetate and  $\text{NH}_4\text{HCO}_3$ , and explored their inhibition on *E. coli*. The results showed (Figure 3) that 255 mg/L (pH7.4) acetate could not suppress the growth of *E. coli* at 37 °C. A study reported that the reductions of *E. coli* and fecal coliforms did not increase with raising concentrations of VFAs to 2500 mg/L (pH7.5) [5]. Free VFAs are more toxic than ionic VFAs because free VFAs can freely permeate the cell membrane, then make the cytoplasm acidified by ionizing to kill bacteria. However, few studies on free VFAs are currently available.

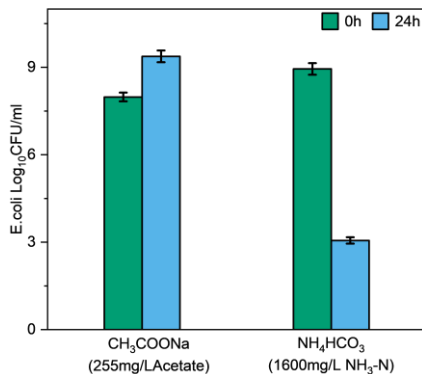


Figure 3 Effect of chemicals on the growth of *E. coli*.

### 3.4 Inhibition effects of $\text{NH}_4^+/\text{NH}_3$ on pathogen

The dose of 1600 mg/L for  $\text{NH}_4^+\text{-N}$  could effectively inactivate *E. coli*. Results showed (Figure 4) that  $\text{NH}_4\text{Cl}$

could not inhibit *E. coli*. But the inactivation effect was significant when adding the same moles  $\text{NH}_4\text{HCO}_3$ , which indicated that the inactivation of *E. coli* was mainly related to free ammonia and confirmed the previous study [1]. Park demonstrated that the addition of  $\text{Na}_2\text{CO}_3$  could enhance the inactivation of *E. coli* O157:H7 and *Salmonella Typhimurium* DT104 during the storage of cattle manure. There are few studies on the pathogens' inactivation of alkalinity, and its mechanism needs to be further explored.

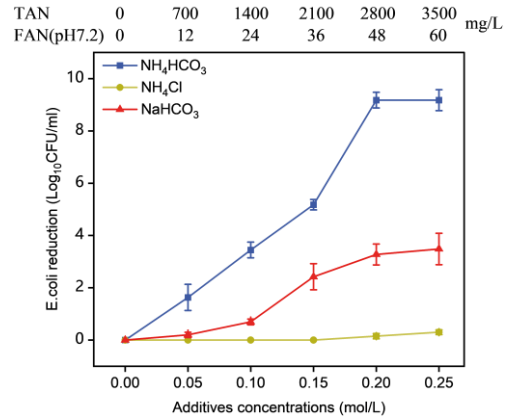


Figure 4 Inhibition of  $\text{NH}_4^+ / \text{NH}_3$  on *E. coli*

## 4 Conclusions

The hyperthermophilic temperature was not necessarily adopted since the thermophilic already has acceptable hygienization performance. In a well-stable mesophilic process, acetate was not a factor for the pathogens' inactivation. In contrast, the  $\text{NH}_4\text{HCO}_3$  that formed in the anaerobic degradation of organic matter was found to be significantly effective to eliminate *E. coli*. Taking the advantage of the naturally formed chemical environment to inactivate pathogens would save the energy input and high temperature would not be mandatory. Further studies are recommended to investigate the mechanism behind it.

## Reference

- [1] Jiang Y, et al. Inactivation of pathogens in anaerobic digestion systems for converting biowastes to bioenergy: A review. *Renew. Sust. Energ. Rev.* (2020) 120:109654.
- [2] Bonjoch X, et al. Resistance of Fecal Coliforms and Enterococci Populations in Sludge and Biosolids to Different Hygienisation Treatments. *Microb Ecol* (2009) 57:478–83.
- [3] Horan NJ, et al. Die-off of enteric bacterial pathogens during mesophilic anaerobic digestion. *Water Res.* (2004) 38:1113–20.
- [4] Pandey PK, et al. *Escherichia coli* persistence kinetics in dairy manure at moderate, mesophilic, and thermophilic temperatures under aerobic and anaerobic environments. *Bioprocess Biosyst. Eng.* (2015) 38:457–67.
- [5] Arias DE, et al. Biogas production, waste stabilization efficiency, and hygienization potential of a mesophilic anaerobic plug flow reactor processing swine manure and corn stover. *J. Environ. Manage.* (2021) 284:112027.

# Effective and Selective Removal of Phosphate from Water by Functional Carbon

○ Bingkun Chen,<sup>1</sup> Haixin Guo<sup>1\*</sup>

<sup>1</sup>Agro-Environmental Protection Institute, Ministry of Agriculture and Rural Affairs, Tianjin 300191, China

\*E-mail: haixin\_g@126.com

## Abstract

The waste plastic sheeting-derived functional carbon adsorbent doped with Ca metal was synthesized through pyrolysis carbonization mixture of plastic sheeting and Ca(OH)<sub>2</sub> with mechanochemical pretreatment. Characterization results (e.g. SEM-EDS, FTIR, XPS) showed that Ca was successfully loaded on waste plastic sheeting-derived functional carbon adsorbent. The phosphorus removal performance of Ca-PE was studied by batch adsorption experiments, and the mechanism of phosphate adsorption was studied by SEM-EDS, FTIR, XPS and XRD. The adsorption behavior of phosphates on the functional carbon prepared from waste plastic sheeting was investigated by batch adsorption experiment and the mechanism was studied by XPS and XRD. The adsorption isotherms of phosphate on this functional carbon were well described by the Langmuir model with high determination coefficients ( $R^2 > 0.96$ ) and the maximum adsorption capacity was 263.6 mg/g. The quasi-second-order kinetic model could fitted well with the adsorption data. This study provides an experimental basis for the effective and selective removal of phosphate from water by functional carbon and also provides a basis for the application of reducing the calcination temperature of carbon materials prepared by polyethylene.

**Keywords:** Functional Carbon; Phosphate adsorption; Polyethylene; Calcium hydroxide.

## 1 Introduction

Phosphorus is an indispensable nutrient element in the growth process of aquatic plants existing in various forms depending on the pH values of water, such as PO<sub>4</sub><sup>3-</sup>, HPO<sub>4</sub><sup>2-</sup> and H<sub>2</sub>PO<sub>4</sub><sup>-</sup>. With the growth in human activity such as household, agricultural and industrial, the phosphate contamination of water has become a great concern<sup>[1]</sup>. Because the increasing phosphate concentration in wastewater may cause eutrophication, leading to water hypoxia, death of aquatic plants and animals, and damage to water quality<sup>[2]</sup>. Current treatment processes for phosphate removal from wastewater include Chemical precipitation<sup>[3]</sup>, biological<sup>[4]</sup> and adsorption<sup>[5]</sup>. Compared with other technology, the adsorption method has received much more attention, because it is convenient, economical, highly selective, less potential for secondary pollution. Especially, functional carbon which could be synthesized from waste solid materials (e.g. agricultural solid waste, sewage sludge) has been the most widely used adsorbent in water treatment<sup>[6]</sup>.

Waste plastic sheeting, one kind of agricultural solid waste, has been widely used in the agricultural industry. Waste plastic sheeting exhibits high stability and causes environmental pollution. In this work, Ca- modified functional carbon materials were obtained from waste plastic sheeting by pyrolysis carbonization mixture of plastic sheeting and Ca(OH)<sub>2</sub>. The functional carbon performance of this adsorbent was determined by the adsorption capacity performance of the phosphate from water. The phosphorus absorption effect of prepared carbon material in water was studied by batch adsorption experiment. The morphology of the synthesized Ca-modified functional carbon materials was studied by various characterization methods, and its adsorption mechanism was studied.

## 2 Materials and methods

All the chemicals and materials were purchased from the Merck and Aldrich Chemical Reagent Co, Ltd (China). The prepared adsorbent compounds were characterized by SEM-EDS, FTIR (KBr), XPS and XRD spectra. The batch adsorption experimental of phosphate on the prepared functional carbon was studied with 200rpm shaken.

## 3 Results and discussion

In order to explore the structural characteristics of Ca-PE adsorbent, scanning electron microscopy (SEM) were performed on the samples to observe the microstructure information of the surface of the adsorbent material. As shown in Figure 1(a,b), the surface of Ca-PE-500 is relatively rough, while the surface of Ca-PE-800 is relatively smooth. It is stated that Ca(OH)<sub>2</sub> particles can better adhere to the surface of polyethylene at 500 °C, while the difference in pore structure in the material is attributed to the decomposition of Ca(OH)<sub>2</sub>, and the calcination temperature of 800 °C may make Ca(OH)<sub>2</sub> completely thermally decomposed, thereby making the surface smoother. Figure 1(c) is the product of polyethylene calcination alone, we found that the product is an oily substance, indicating that polyethylene calcination alone at this temperature can not prepare carbon materials, and calcination after incorporation of Ca(OH)<sub>2</sub> can form carbon materials as shown in Figure 1(d), which has a good ability to adsorb phosphate in water.

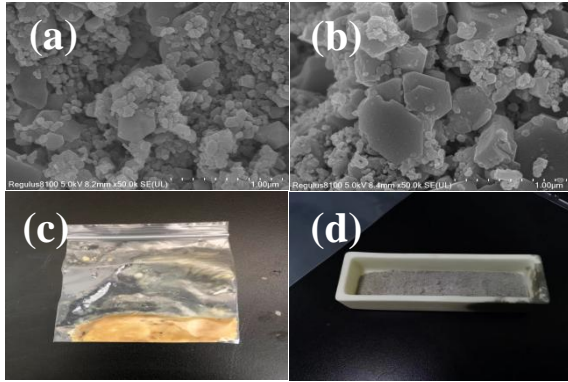


**Fig. 1. SEM images of (a) Ca-PE-500, (b) Ca-PE-800 and (c) carbon materials cannot be prepared by PE alone and (d) carbon materials made by mixing calcium**

The associated adsorption isotherms and kinetic parameters are shown in Table 1. The adsorption isotherms of phosphate on this functional carbon were well described by the Langmuir model with high determination coefficients ( $R^2 > 0.96$ ) and the maximum adsorption capacity was 263.6 mg/g. This indicates that the effective adsorption surface of Ca-PE in the process of phosphate adsorption is a monolayer homogeneous adsorption surface. The quasi-secondary kinetic model  $R^2$  of both adsorbents is greater than the quasi-first-order kinetic model  $R^2$ , and the quasi-second-order kinetic model assumes that the phosphorus removal process of the adsorbent is controlled by chemical rates (chemisorption). The chemical adsorption process is mainly the chemical reaction of the metal cations contained in the adsorbent with the phosphate anion in the solution to form an insoluble precipitate or crystallization, that is,  $\text{Ca}^{2+}$  combines with  $\text{PO}_4^{3-}$  to form hydroxyapatite (HAP) precipitation. This indicates that chemisorption plays a dominant role in the phosphate adsorption process.

**Table 1 Physical properties of biochar samples.**

Adsorbents	Langmuir model			pseudo-first-order model			pseudo-second-order model		
	$k_L$ (L/mg)	$q_{\max}$ (mg/g)	$R^2$	$k_1$ (h <sup>-1</sup> )	$q_e$ (mg/L)	$R^2$	$k_2$ (g/mg·h)	$q_e$ (mg/L)	$R^2$
Ca-PE-500	0.0124	263.6	0.966	20.1	0.483	0.937	0.005	231.2	0.998
Ca-PE-800	0.0125	260.3	0.958	19.9	0.483	0.933	0.008	240.8	0.998

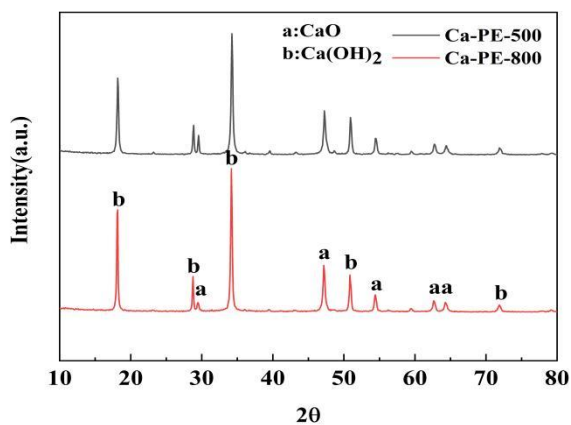


**Fig. 2. XRD spectra of Ca-PE-500 and Ca-PE-800 materials**

In order to investigate the effect of calcination temperature on the phase composition of functional carbon

adsorbents, XRD analysis was performed on Ca-PE-500 and Ca-PE-800. The data was analyzed and processed using Jade 6.0 and the results are shown in Figure 2. We can find that there is almost no difference between the diffraction peaks of the XRD patterns of the two materials, indicating that temperature treatment cannot change the composition of the materials. The main characteristic peaks of Ca-PE are from the  $\text{Ca(OH)}_2$  (PDF#04-0733) and  $\text{CaO}$  (PDF#28-0775) phases. It can be further proved that  $\text{Ca(OH)}_2$  is successfully loaded on polyethylene, and the appearance of  $\text{CaO}$  diffraction peak may be due to the reaction of  $\text{Ca(OH)}_2$  components with  $\text{H}_2\text{O}$  to form  $\text{CaO}$  during the calcined material.

#### 4 Conclusions

The combination of  $\text{Ca(OH)}_2$  and polyethylene calcination can successfully attach Ca to carbon materials, have high adsorption capacity for phosphate in water, and significantly reduce the calcination temperature of polyethylene carbonization to generate carbon materials. The adsorption isotherms of phosphate on this functional carbon were well described by the Langmuir model with high determination coefficients ( $R^2 > 0.96$ ) and the maximum adsorption capacity was 263.6 mg/g. The quasi-second-order kinetic model could fitted well with the adsorption data. Ca-PE removes the phosphate aqueous solution by chemical precipitation and electrostatic interaction with phosphate to form calcium phosphate. The maximum adsorption capacity was 263.6 mg/g. The characterization of SEM, XRD and other properties showed that the successful loading of  $\text{Ca(OH)}_2$  made carbon materials on polyethylene, and greatly reduced the calcination temperature of carbon materials prepared by polyethylene and reduced energy consumption. This study provides an experimental basis for the effective and selective removal of phosphate from water by functional carbon and also provides a basis for the application of reducing the calcination temperature of carbon materials prepared by polyethylene.

#### Reference

- [1] Tarayre, C.; De Clercq, L.; Charlier, R.; et al. New perspectives for the design of sustainable bioprocesses for phosphorus recovery from waste. *Bioresour. Technol.* 2016, 206, 264–274.
- [2] Yi, M.; Chen, Y. Enhanced phosphate adsorption on Ca-Mg-loaded biochar derived from tobacco stems. *Water Sci. Technol.* 2018, 78, 2427–2436.
- [3] Tang C C, Liu M, Chen H M, et al. Research progress of adsorption and phosphorus removal technology [J]. *Technology of Water Treatment*, 2014, 40(9):1-7, 12 (in Chinese).
- [4] Feng J M. Research on phosphorus removal performance and mechanism of the red soil substrate fillings in constructed wetlands [D]. Shanghai: Shanghai Jiao Tong University, 2014 (in Chinese).
- [5] Cai R. Capture and reuse of phosphorus in entropic water by iron-impregnated biochar [D]. Chang sha: Hunan Normal University, 2017 (in Chinese).
- [6] Mitrogiannis, D.; Psychoyou, M.; Baziotis, I.; et al. Removal of phosphate from aqueous solutions by adsorption onto  $\text{Ca(OH)}_2$  treated natural clinoptilolite. *Chem. Eng. J.* 2017, 320, 510–522.

## Anammox Microorganisms Diversity in Sediment of Reservoir Located in Indonesia

○ Eli Hendrik Sanjaya<sup>1\*</sup>, Sitoresmi Prabaningtyas<sup>3</sup>, Suharti<sup>1</sup>, Hong Chen<sup>4</sup>, Yan Guo<sup>5</sup> Mohd Fadhl

Md Din<sup>6</sup> & Annisa Elchamida<sup>3</sup>

<sup>1</sup>Department Chemistry, Malang State University, Indonesia.

<sup>2</sup>Biotechnology Program, Department of Applied Sciences, Malang State University, Indonesia.

<sup>3</sup>Department of Biology, Malang State University, Indonesia.

<sup>4</sup>Key Laboratory of Water-Sediment Sciences and Water Disaster Prevention of Hunan Province, School of Hydraulic Engineering, Changsha University of Science & Technology, Changsha 410004, China.

<sup>5</sup>Department of Environmental Engineering, School of Energy and Environmental Engineering, University of Science and Technology Beijing, Beijing 100083, PR China.

<sup>6</sup>Centre for Environmental Sustainability and Water Security (IPASA), School of Civil Engineering, Faculty of Engineering, Universiti Teknologi Malaysia, 81310 Skudai Johor, Malaysia.

\*E-mail: eli.hendrik.fmipa@um.ac.id.

### Abstract

Recently, anaerobic ammonium oxidation (anammox) process is common in treating ammonia rich wastewater. However, it is still very limited in developing country. In both laboratory scale research and its application in industry. Indonesia has a large waters area, which is very potential to be source of anammox microorganism. However, studies on the topic of anammox are still lacking. Therefore, as a preliminary study for anammox microorganisms isolation, this research investigated the diversity of anammox microorganism in the sediment of reservoir. The New generation sequencing (NGS) was used for analyzing the microbial diversity. The results show that the diversity of microorganisms in the sediments of the Selorejo and Karangates reservoirs has similarities at the level of medium diversity. At these two locations, several phyla, including the phylum *Firmiculus*, *Acidobacteria*, *Proteobacteria*, *Planctomycetes*, *Actinobacteria*, and *Bacteroidetes* was found. The phylum *Proteobacteria* has the most significant number of members, with four classes: *Alphaproteobacteria*, *Betaproteobacteria*, *Deltaproteobacteria*, and *Gammaproteobacteria*. Therefore, in both reservoir has a high potential to be a source of anammox microorganisms.

**Keywords:** Anammox, microbial diversity, reservoir

### 1 Introduction

The presence of anammox is found in various aquatic environments and widely distributed in marine environments [1] in estuaries [2][3] wetlands [4], lacustrine ecosystems [5][6], rivers [7] [8], in surface and subsystem freshwater [3][9] and subsurface natural wetlands and artificial wastewater treatment plant systems [10]. Research on the application of anammox microbes in wastewater treatment in several developed countries has been relatively developed. However, research on anammox microbes in Indonesia is still minimal. There is no Indonesian indigenous anammox microbe. Thus, as an initial study, it is necessary to analyze the diversity and potential of nitrite and ammonia-degrading bacteria (anammox) in the sediments/reservoirs of Karangates and Selorejo.

Currently, the method of microbial biodiversity analysis that has high accuracy is the analysis of the 16S rRNA gene using Next Generation Sequencing (NGS). The habitat of anammox bacteria is found in aquatic environments such as rivers, reservoirs, rice fields, to groundwater. In East Java, Indonesia has several dams, two of which are Karangates and Selorejo Dams.

Thus, in this study, biodiversity and its potential as a source of anammox microbes in sedimentary waters of Karangates (KRT) and Selorejo (SLRJ) were carried out based on NGS analysis of the 16S rRNA gene.

### 2 Materials and methods

Bacterial Biodiversity Testing with NGS (Next Generation Sequencing)

Parameters observed were the diversity, abundance, and distribution of bacteria based on 16S rRNA analysis using Next Generation Sequencing (NGS). The index was calculated by the Shann-Wiener index (diversity of bacterial communities), Simpson index (species dominance), Buzas-Gibson index (diversity and evenness), and Berger-Parker index (Species Abundance Distribution).

### 3 Results and discussion

Based on the results of the analysis of the 16S rRNA gene, it showed that the abundance of bacteria in both locations was relatively high and tended to have an overall similarity as indicated by the total number of OTUs (Operational Taxonomy Units) of 9643 (in SLRJ) and 9645 (in KRT). The Shanon-Wiener index of bacteria in SLRJ was 1247 and KRT 1322, indicating moderate diversity (1-3 moderate

categories). The data shows that the bacterial community tends to show an uneven distribution of species abundance (Species Abundance Distribution). In the case of a linear distribution, the fraction of the total individual sample contributed by the most abundant species, known as the Berger-Parker index, synthetically describes the SAD of the disturbed community.

There are similarities in discovering bacteria in the Selorejo and Karangates reservoirs, including the phylum *Firmiculus*, *Acidobacteria*, *Proteobacteria*, *Planctomycetes*, *Actinobacteria*, and *Bacteroidetes*. Phylum *Proteobacteria* has the most members, with four classes: *Alphaproteobacteria*, *Betaproteobacteria*, *Deltaproteobacteria*, and *Gammaproteobacteria*.

The comparison of microbial diversity in Karangater and Selorejo Reservoir is shown in **Table 1**.

**Table 1 Anammox Species Diversity in SLRJ and KRT**

	SLRJ	KRT
<i>Firmiculus</i>	<i>B thuringiensis</i> 2%, <i>Bacillus cereus</i> 0,9% Paenibacillus 1% Clostridium 1% <i>Paeniclostridium sordellii</i> 0.9 %	<i>Bacillus thuringiensis</i> 2%, <i>Bacillus cereus</i> 1%, <i>Bacillus asanii</i> 1% Paenibacillus 1% clostridiales 3%
<i>Acidobacteria</i>	<i>Luteitalea pratensis</i> 3%, <i>Candidatus solibacter usilatus</i> 5% <i>Candidatus koribacter versatilis</i> 7%, Terriglobus 1%, <i>Acidisarcina polymorpha</i> 1%	<i>Luteitalea pratensis</i> 4%, <i>Candidatus solibacter usilatus</i> 5% <i>Candidatus koribacter versatilis</i> 7%, Terriglobus 2%, <i>Acidisarcina polymorpha</i> 1%.
<i>Proteobacteria</i>	Rhodospirillaceae 1%, Xanthobacteraceae 0,9%, Methyloceanibacter 0,9%, Methylocystis 1%, Bradyryzhobium 1%, <i>Hyphomicrobium nitrativorans</i> 1%, <i>Rhodoplanes sp.</i> Z2-YC6860 6% Burkholderiaceae 2%	Rhodospirillales 1% Methylocystis 0,9%, Bradyryzhobium 0,9%, Hyphomicrobium 1%, <i>Rhodoplanes sp.</i> Z2-YC6860 5% <i>Varlovorax sp. PMC12</i> 2%, Cupriavidus 1%, Burkholderia 1%

<i>Desulfulrivibrio alkaliphilus</i> 1%	<i>Desulfulrivibrio alkaliphilus</i> 1%
<i>Haliangium ochraceum</i> 1%	<i>Haliangium ochraceum</i> 1%.
Enterobacteriaceae 1%	Enterobacterales 1%
Rhodanobacteraceae 1%	Rhodanobacteraceae 1%.
Xanthomonadaceae 1%	

<i>Planctomycetes</i>	<i>Limnoglobus roseus</i> 2%, <i>Tuwongella immobilis</i> 1%, <i>Aquisphaera giovannonii</i> 2%, <i>Planctomycetes bacterium ETA_AI</i> 1%	<i>Limnoglobus roseus</i> 1% <i>Aquisphaera giovannonii</i> 1%
-----------------------	---	---

#### 4 Conclusions

The diversity of microorganisms in the sediments of the Selorejo and Karangates reservoirs has similarities, as indicated by the total number of OTUs (Operational Taxonomy Units) of 9643 and 9645, respectively. At these two locations, several phyla, including the phylum *Firmiculus*, *Acidobacteria*, *Proteobacteria*, *Planctomycetes*, *Actinobacteria*, and *Bacteroidetes*. The phylum *Proteobacteria* has the most significant number of members. Thus, these two locations can be a source for isolating anammox microbes.

#### Reference

- [1] Schmid, M. C., et al., Anaerobic ammonium-oxidizing bacteria in marine environments: Widespread occurrence but low diversity, *Environ. Microbiol.*, 9, (2007) 1476–1484.
- [2] Trimmer, M., J. C. Nicholls, and B. Deflandre, Anaerobic ammonium oxidation measured in sediments along the Thames Estuary, United Kingdom, *Appl. Environ. Microbiol.*, 69, (2003) 6447–6454.
- [3] Wang, S., G. B. Zhu, Y. Z. Peng, M. S. M. Jetten, and C. Yin, Anammox bacterial abundance, activity, and contribution in riparian sediments of the Pear River Estuary, *Environ. Sci. Technol.*, 46, (2012) 8834–8842.
- [4] Zhu, G. B., S. Wang, Y. Wang, C. Wang, N. Risgaard-Petersen, and M. S. M. Jetten, Anaerobic

# Refractory dissolved organic matter as carbon source for advanced nitrogen removal from mature landfill leachate: A review and prospective application

Ruixin Wu<sup>1,\*</sup>, Yu-You Li<sup>2</sup>, Jianyong Liu<sup>1</sup>

<sup>1</sup>School of Environmental and Chemical Engineering, Shanghai University, 333 Nanchen Road, Shanghai 200444, China.

<sup>2</sup>Department of Civil and Environmental Engineering, Graduate School of Engineering, Tohoku University, 6-6-06 Aza, Aramaki, Aoba-ku, Sendai, Miyagi 980-8579, Japan.

\*E-mail: elisawuu@163.com

## Abstract

Partial nitrification-anammox is a promising process for treating mature landfill leachate, but there are still 11% nitrate to be removed. Denitrification or partial denitrification can be used to remove the nitrate in the presence of carbon source to achieve advanced nitrogen removal. However, there is a lack of biodegradable organic matter which can be used as denitrifying carbon source in mature landfill leachate. Fortunately, refractory dissolved organic matter (rDOM) was exploited to be used as a potential denitrifying carbon source in recent years. The performances, mechanisms of using rDOM as denitrification carbon source are summarized in this review. Furthermore, in order to improve the rDOM utilization efficiency, several methods to improve the biodegradability of rDOM are summarized, which include extended hydraulic retention time, sludge retention time, bioaugmentation and advanced oxidation processes. A novel integrated anammox-based process is proposed for mature landfill leachate treatment, in which ozonated nanofiltration concentrate is recirculated with many benefits.

**Keywords:** Mature landfill leachate; Anammox; Refractory dissolved organic matter (rDOM); Carbon source; Ozonation

## 1 Introduction

Mature landfill leachate contains high concentration of ammonia and low concentration of biodegradable organic carbon, which makes the conventional nitrification and denitrification processes difficult to carry out in leachate treatment to achieve nitrogen removal. As is known to all, although mature leachate contains high concentration of organic matter, the dissolved organic matter (DOM) in mature landfill leachate is mainly composed of refractory dissolved organic matter (rDOM), with a relatively low biochemical oxygen demand (BOD)/chemical oxygen demand (COD) ratio (less than 0.1). If simultaneous anammox and (partial) denitrification (SAD) process with rDOM as carbon source is feasible in mature leachate treatment, it can not only achieve advanced nitrogen removal, but also save the cost of aeration and additional carbon source.

However, due to the low utilization rate of rDOM, it is difficult to achieve advanced nitrogen removal only through using rDOM as carbon source in mature leachate. Therefore, some measures are needed to improve the utilization of rDOM as carbon source for denitrification. Measures such as extending HRT, prolonging sludge retention time (SRT), introducing rDOM degrading bacterial community and using advanced oxidation processes (AOPs) were used to increase the rDOM utilization rate. These measures can change rDOM into easily degradable organic matter, which can be used as carbon source for denitrification to remove the nitrate produced by PNA and then achieve advanced nitrogen removal. AOPs are generally used to remove all

the rDOM in the conventional landfill leachate treatment process. In fact, rDOM can also be converted into easily degradable organic matter by AOPs to provide carbon source for denitrification. However, it is not clear how to realize it in leachate treatment process.

In this review, the shortage of readily biodegradable organic matter and the mechanisms of utilizing rDOM as the carbon source are summarized and discussed from the perspective advanced nitrogen removal from mature landfill leachate. Based on the literature summary, an integrated process of treating mature landfill leachate with rDOM as the carbon source is proposed, in which ozonated nanofiltration concentrate is recirculated.

## 2. The deficiency of carbon source for denitrification in mature leachate

The DOM in mature landfill leachate is mainly composed of volatile fatty acids and the rDOM, such as humic substances accounting for most of DOM in leachate (up to 60%). As a result, the relatively low BOD/COD ratio leads to the few carbon sources available for denitrification, as shown in Table 1.

The mature landfill leachate contains only a small amount of readily degradable organic matter, which decreased with the increase of landfill age.

The rDOM is difficult to remove by conventional biological processes, which means microorganisms can hardly use it as carbon source for denitrification. However, if the rDOM can be explored and utilized, the amount of carbon source in mature landfill leachate can satisfy the need of advanced nitrogen removal treatment.

### 3. Feasibility of rDOM as carbon source for advanced nitrogen removal

Previous studies showed that rDOM was partially degraded to biodegradable organics by specific heterotrophs (e.g., Chloroflexi and Chlorobi) in the anammox-based system, which could serve as the electron donor for denitrification to achieve advanced nitrogen removal. rDOM in SAD is a potential carbon source that can be utilized by denitrifying bacteria.

Mechanism of rDOM in anammox-based treatment of mature landfill leachate was shown in Fig. 1.

EPS adsorption-biodegradation was the key mechanism for the removal of rDOM. The anammox bacteria can be stimulated to produce more EPS by the addition of fulvic acid in the process of treating mature landfill leachate. EPS provide more extracellular enzymes and nutrients for microorganisms, and EPS contribute to the formation of biofilms, which can protect the anammox activity, enabling it to achieve stable nitrogen removal efficiency even in the presence of organic matter.

Table 2 summarized the bacterial communities that can degrade rDOM in the SNAD process. As can be seen from Table 2, when anammox process was used to treat wastewater containing high concentrations of ammonia nitrogen and rDOM, anammox bacteria can coexist with bacteria which can degrade rDOM (Wang et al., 2019). Adequate adaption time is the key to enrich the rDOM degrading bacterial community.

### 4. Enhancing degradation of rDOM to provide carbon source for SAD

In order to promote the degradation of rDOM, some methods such as increasing HRT and SRT in SAD, the bioaugmentation technology in SAD, and advanced oxidation technology were adopted.

Longer HRT allowed bacteria to have sufficient time to absorb rDOM in the mature landfill leachate and then associate enzymes to decompose them into small organic molecules.

The longer SRT, which could be realized in the biofilm or MBR systems, could promote the enrichment of distinct microbial communities degrading rDOM.

To enhance the release of carbon source from rDOM biodegradation, activated sludge contained enriched rDOM-degrading bacteria could be introduced into SAD systems to enhance the release of carbon source from rDOM biodegradation.

AOPs, such as Fenton, photocatalytic, ozonation and electrochemical technology, could generate highly active hydroxyl radical (OH $\cdot$ ) for the degradation of rDOM and increasing biodegradability of organic compounds. Ozone oxidation process can effectively improve the biodegradability of different wastewater, as shown in Table 3 (Chen et al., 2019).

### 5. Enhancing degradation of rDOM to provide carbon source for SAD

Based on the above proposed idea, an innovative anammox-based process is proposed to achieve advanced nitrogen removal of mature landfill leachate.

Ozonation can improve the biodegradability of the NFC and recycling ozonated NFC into SAD to can provide carbon source for (partial) denitrification. On the premise of satisfying the carbon source required by SAD, the

remaining organic matter in the ozonated NFC can be introduced into AD to further recover the bioenergy.

Firstly, NFC is an urgent secondary pollutant in the treatment of mature landfill leachate. Controlling the ozonation process to maximize biodegradability of rDOM can not only reduce the cost of ozonation, but also realize recycling of the ozonated NFC into the SAD reactor as carbon source for denitrification, thus reducing the cost of carbon source.

Secondly, the optimum pH for treating NFC with ozonation process is between 8 and 9 because the hydroxide ion could induce the ozone molecules to produce hydroxyl radicals in the water. The pH of SAD effluent is usually above 8, so ozone process is suitable to improve its biodegradability. However, if Fenton method is used, the pH (optimal pH is 2-4) needs to be adjusted firstly. In the acidic environment, large amounts of H<sub>2</sub>O<sub>2</sub> and Fe<sup>2+</sup> to produce moderate hydroxyl radicals, which makes Fenton expensive and produces large amounts of iron mud resulting in secondary pollution. Therefore, it can be seen that the proposed process is economically and environmentally friendly and technically feasible.

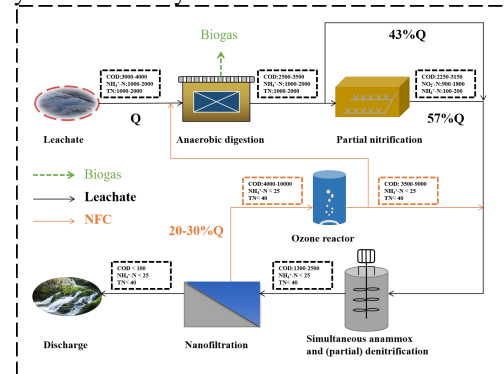


Fig. 1. An innovative integrated process for advanced nitrogen removal using rDOM as carbon source in mature leachate treatment.

### 6. Conclusion

Through sludge adsorption-degradation, rDOM in mature landfill leachate could be biodegraded by bacteria such as Chloroflexi as denitrifying carbon source, which promoted advanced nitrogen removal in anammox-based process. In order to improve the biodegradability of rDOM and reduce the carbon source addition cost, some measures such as extended HRT, SRT, bioaugmentation and AOPs can be taken. An innovative integrated process based on SAD was proposed, which could simultaneously remove ammonia nitrogen and rDOM from mature landfill leachate. In this process, recycling ozonated NFC could not only avoid secondary pollution, but also provide carbon source for (partial) denitrification and achieve advanced nitrogen removal.

### Reference

- [1] Chen, W., Zhang, A., Jiang, G., Li, Q., 2019. Transformation and degradation mechanism of landfill leachates in a combined process of SAARB and ozonation. Waste Manag 85, 283-294.
- [2] Wang, Y.M., Lin, Z.Y., He, L., Huang, W., Zhou, J., He, Q., 2019. Simultaneous partial nitrification, anammox and denitrification (SNAD) process for nitrogen and refractory organic compounds removal from mature landfill leachate: Performance and metagenome-based microbial ecology. Bioresource Technology 294, 11.

# Achieving Stable Mainstream Partial Nitrification-Anammox Process by Successful Regulation of Nitrite-Oxidizing Bacteria

○ Wei Yanxiao<sup>1\*</sup>, Xia Weize<sup>1</sup>, Ye Min<sup>1</sup> & Yu-You Li<sup>1,2</sup>

<sup>1</sup>Department of Environmental Engineering, Environmental University, Miyagi 980-8579, Japan.

<sup>2</sup>Department of Water Environment, Engineering University, Miyagi 980-8579, Japan.

\*E-mail: wei.yanxiao.q5@dc.tohoku.ac.jp

## Abstract

The long-term stable operation is still a challenge for partial nitrification and anammox (PN/A) process in the treatment of low-strength ammonium wastewater. The nitrite oxidizing bacteria (NOB) growth can destroy the stability of part of the PNA system. This study explores solutions to the NOB growth problem using a laboratory-scale reactor. The results showed that NOB reduced the nitrogen removal efficiency from up to around 85% to 32.5% in mainstream condition. NOB inhibition strategies such as intermittent aeration and FA inhibition were applied but did not successfully in controlling NOB growth. The final enhanced Anammox activity brought the removal rate up to 76.3 again. Based on the analysis on the physicochemical properties of the granules, the size decreased to around 280 $\mu$ m in mainstream. The dissolution granules of may be the reason for the weakened anammox activity, which favored NOB growth. These results provide an alternative NOB inhibition method to maintain a healthy PN/A process in mainstream.

**Keywords:** Anammox; Nitrite oxidizing bacteria; Partial nitrification; Hydroxyapatite; Mainstream.

## 1 Introduction

The partial nitrification/anammox (PN/A) process is considered to have the potential to update the currently widely used traditional nitrification and denitrification processes due to its advantages such as energy saving and reduction of greenhouse gas emissions. Although PN/A process has been successfully applied to high strength ammonium wastewater in sidestream, the application of PN/A process to treat low-concentration ammonium wastewater such as mainstream municipal wastewater remains a big challenge. For example, uncontrolled nitrite oxidizing bacteria (NOB) growth can significantly reduce nitrogen removal efficiency. NOB competes with ammonia oxidizing bacteria (AOB) and anammox in substrate utilization and thus can interfere with the PN/A system. The widely reported inhibition strategies such as using free ammonia (FA), free nitrous acid and dissolved oxygen (DO) control do not always work. The long-term stable operation of the mainstream PN/A process still needs further research.

To achieve long-term stable nitrogen removal efficiency in the mainstream PN/A process, this study used a laboratory-scale air-lift reactor. The variation of nitrogen removal efficiency and factors affecting the balance between partial nitrification, and anaerobic ammonia oxidation system were assessed by analyzing physicochemical properties to find ways to rebuild and maintain a healthy nitrogen removal system. The spatial distribution and microbial community structure of different functional bacteria are analyzing to finally elucidate the competitive relationship between NOB and the PN/A system.

## 2 Materials and methods

### 2.1 Reactor Setup

The experimental apparatus includes the main body of the bioreactor, the water influent system, and the aeration system, which is shown in Fig. 1.

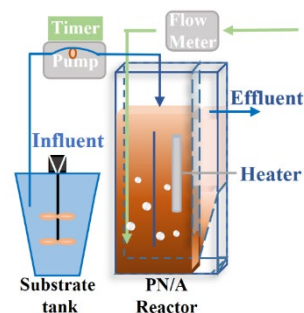


**Fig. 1. Schematic diagram of the experimental setup**

### 2.2 Operation Phases

The PN/A reactor was inoculated with the sludge from the effluent of another PN/A reactor treating mainstream. The PN/A reactor was continuously fed with synthetic wastewater. Additional trace elements were added as previous study reported [1]. The PN/A reactor was continuously operated for 325 days. And the entire procedure can be divided for 8 phases (Table 1).

**Table 1 Operation Phases.**

Phases	Day(d)	HRT(h)	N <sub>inf</sub> (mg/L)	NLR (kg/m <sup>3</sup> /d)
1	1-2	12	100	0.2
2	3-113	6	100	0.4
3	114-153	3	50	0.4
4	154-199	3	50	0.4
5	200-215	24	500	0.5
6	216-291	24	500	0.5
7	292-310	24	500	0.4
8	311-325	3	50	0.4

### 2.3 Analytical methods

NH<sub>4</sub><sup>+</sup>-N, NO<sub>2</sub><sup>-</sup>-N, NO<sub>3</sub><sup>-</sup>-N, P<sup>-</sup> and Ca<sup>2+</sup> concentrations were measured by capillary electrophoresis (Agilent 7100, Agilent Technologies, USA). DO concentration was measured by DO meter (DM-31P). Other tests were analyzed according to APHA standard methods [3]. Sludge samples were collected at the end of each phase for Fluorescence in situ hybridization, 16S rRNA gene sequencing and qPCR test.

### 3 Results and discussion

The nitrogen removal performance of PN/A during the 8 phases is illustrated in Fig. 2. After successful start-up in phase 1, HAP granules with excellent sedimentation performance were cultivated in phase 2. The nitrogen removal efficiency (NRE) up to around 85% was obtained. When the HRT was shortened to 3h and the influent ammonia nitrogen concentration was reduced to 50 mg/L, NOB started its activity. NRE finally reduced to 62.4% in phase 3.

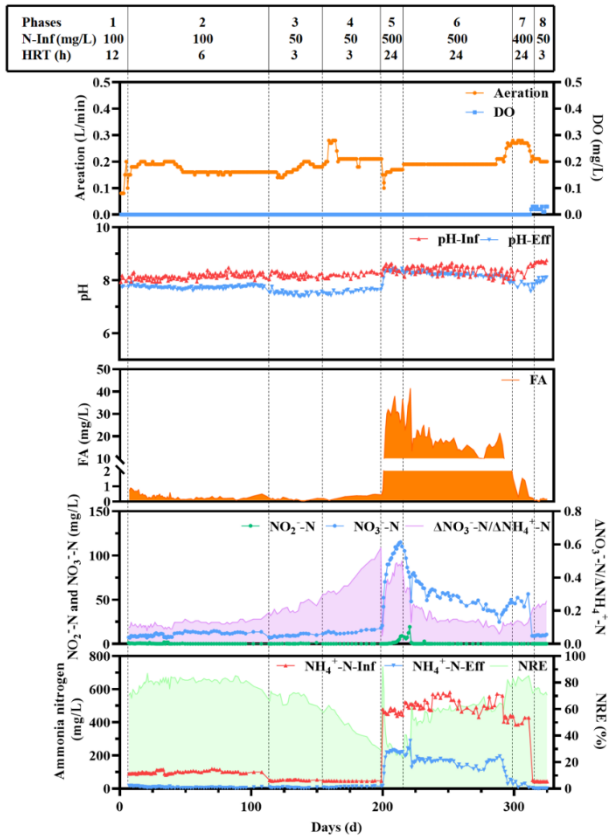


Fig. 2. Operation performance

To control the NOB activity, intermittent aeration was applied in phase 4. But it did not limit the continued growth of NOB with NRE decreased to 32.5%. According to the nitrogen balance, NOB competed better than anammox in nitrite utilization in phase 4. Around 35 mg/L FA was provided in phase 5. The FA concentration was set to achieve inhibition on NOB with less side effects on anammox [2]. However, NOB activity was only slightly suppressed. The NO<sub>3</sub><sup>-</sup> to ΔNH<sub>4</sub><sup>+</sup> ratio decreased from 0.58 to 0.50. The reason for that may be that anammox activity has been compromised to utilize normal levels of nitrite, which has been confirmed by activity tests (data are not shown here). To enhance the anammox activity, 0.5 g/L MLVSS Anammox was additionally added for twice. The NOB existed in the system

finally was controlled. Returning to the mainstream again, the NRE reached a maximum of 76.3% with the average ratio of 0.22.

From the above data it can be seen that the enhanced activity of Anammox fully utilizes nitrite and ultimately eliminates NOB from the system.

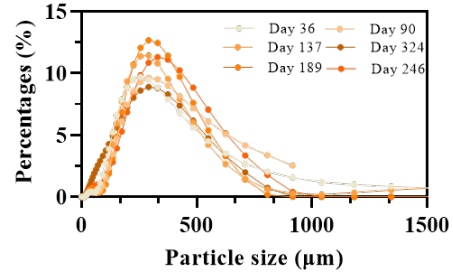


Fig. 3. HAP granule size

As shown in Fig. 3, Hydroxyapatite (HAP) granule size was tested. It can be found that the proportion of large particles is reduced under mainstream conditions, and then recovered in sidestream. The maximum mean size was 452μm in phase 1 and decreased to around 280μm in phase 4. Compared with other studies, the mean size of around 338μm granule was obtained [1]. The granule size is proportional to pH and is also related to the microbial activity. HAP granules provide shelter for anammox growth while improving sludge settling properties. The smaller particle size indicates disintegration of the particles, which may be responsible for the decreased activity of Anammox and the NOB dominance.

Regarding the microbiological data, it is still being tested. Those results will be helpful to analyze the growth of NOB and changes in its competition with anammox.

### 4 Conclusions

- (1) The PNA reactor was successfully started, and up to 83% total nitrogen removal efficiency was achieved at HRT 6h and relatively large HAP granules (mean size 452μm) were obtained.
- (2) Strategies such as intermittent aeration and FA inhibition were not successful in controlling NOB growth. At low nitrogen loads, decreased anammox activity was responsible for NOB dominance. But it was successfully reversed the direction of the nitrogen oxidation by enhancing Anammox.
- (3) HAP granules are difficult to maintain stable under mainstream conditions.

### Reference

[1] Chen, R., Ji, J., ... & Li, Y. Y. (2019). Successful operation performance and syntrophic micro-granule in partial nitrification and anammox reactor treating low-strength ammonia wastewater. *Water research*, 155, 288-299.

[2] Chen, Y., Feng, G., Guo, G., Luo, Z., Rong, C., Wang, T., ... & Li, Y. Y. (2022). Nitrogen removal by a Hydroxyapatite-enhanced Micro-granule type One-stage partial Nitritation/anammox process following anaerobic membrane bioreactor treating municipal wastewater. *Bioresource Technology*, 348, 126740.

[3] APHA, 2005. Standard Methods for the Examination of Water and Wastewater. APHA-AWWA-WEF, Washington, DC, USA.

# Experimental study on two-stage PN/HAP-A process for treating garbage methane fermentation liquid

○ Wenzhao Zhao<sup>1\*</sup>, Ying Song<sup>1</sup>, Yi Xue<sup>2</sup> & Yu-You Li<sup>1,2</sup>

<sup>1</sup>Department of Civil and Environmental Engineering, Tohoku University, Graduate School of Engineering, Miyagi 980-8579, Japan

<sup>2</sup>Department of Frontier Science for Advanced Environment, Graduate School of Environmental Studies, Tohoku University, Miyagi 980-8579, Japan

\*E-mail: zhao.wenzhao.q5@dc.tohoku.ac.jp

## Abstract

A two-stage partial nitrification/hydroxyapatite-Anammox (PN/HAP-A) system was set up to verify the application of the system on garbage methane fermentation liquid. The PN reactor had good ability to convert ammonium to nitrite. Moreover, HAP-anammox reactor, the critical core of the system, had a good nitrogen removal performance. This study focuses on the efficiency and stability of the system in dealing with high-strength garbage fermentation liquid. Through 200-days operation, the stable removal performance of system was obtained. The system nitrogen loading rate (NLR) increased from of 1.0 g-N·(L·d)<sup>-1</sup> to 2.9 g-N·(L·d)<sup>-1</sup>, the nitrogen removal efficiency maintained at 85.6%. The study achieved an enhancement on nitrogen loading rate when treating methane fermentation liquid by Partial nitrification/HAP-Anammox process, which the results can also be promoted to pilot and full-scale on the high-strength ammonium wastewater treatment.

**Keywords:** Anammox; methane fermentation; HAP; AOB.

## 1 Introduction

High-strength ammonium sewage is widespread in wastewater treatment process, especially as a by-product in the drainage after anaerobic treatment, such as garbage fermentation liquid. Based on this problem, anaerobic ammonium oxidation (Anammox) process is a suitable way to be applied which can significantly reduce the energy consumption and operating cost, and at the same time achieve efficient total nitrogen removal, which is an environmentally friendly sewage treatment process<sup>[1]</sup>. The new denitrification process is a feasible solution to face the challenges in low-carbon society, sustainable development and circular economy which these trends have become more important in the development of human society.

Considering the stability in operation, using two-stage PN/HAP-A (Partial Nitrification/HAP-Anammox) system may be the better solution in the engineering for actual wastewater treatment. The process will separate AOB and Anammox into two reactors and operate individually, which can easily control and enrich corresponding functional microorganisms. In addition, cultivated HAP-anammox granular sludge are using in the study. The granular sludge retention capacity would also be a key factor which can avoid the functional microorganism washing out.

In this study, the treatment of fermentation liquid from biogas production center by two-stage anammox process using HAP-anammox granule sludge at 25°C was evaluated by long-term continuous experiments, which the results can provide a reference for practical applications.

## 2 Materials and methods

### 2.1 Reactor configuration and operation

The substrate using in the experiment was periodically collected from a garbage biogas power generation center located in Nagaoka City, Niigata Prefecture, Japan. The main composition of the substrate is showed in **Table 1**.

**Table 1 Operation Conditions**

Phase	I	II	III	IV	V
pH	8.13	8.22	8.21	8.29	8.31
NH <sub>4</sub> <sup>+</sup> -N (mg·L <sup>-1</sup> )	1446	1495	1783	1761	1810
COD (mg·L <sup>-1</sup> )	553	609	664	694	653
Alkalinity (mg-CaCO <sub>3</sub> ·L <sup>-1</sup> )	8320	8040	8240	8140	8040
P (mg·L <sup>-1</sup> )	16.2	35.6	19.8	24.2	44.9
Ca (mg·L <sup>-1</sup> )	34.2	66.1	58.1	58.3	90.4
Fe (mg·L <sup>-1</sup> )	7.5	7.6	7.4	7.4	6.5
Mg (mg·L <sup>-1</sup> )	31.0	36.4	33.7	35.8	50.4

As demonstrated in **Fig.1**, the PN reactor (working volume of 10 L) and EGSB reactor (working volume of 5 L) were applied for PN and Anammox, respectively. Both reactors were controlled at 25 °C. The throughput varied from 12 L·d<sup>-1</sup> to 24 L·d<sup>-1</sup> using raw fermentation liquid.

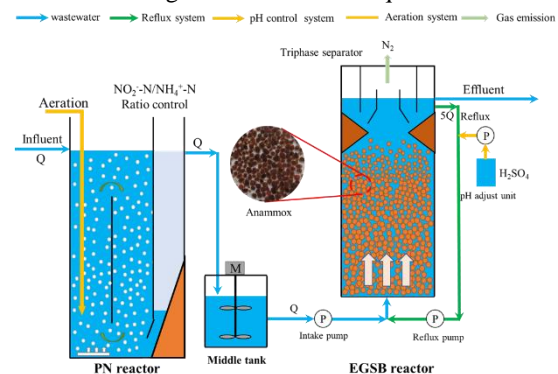


**Fig. 1 Schematic diagram of the System**

### 2.2 Analysis of liquid samples

Liquid samples of influent and effluent were filtered with a 0.45 μm filter. Ammonium, nitrite and nitrate were analyzed by capillary electrophoresis (Agilent 7100). IC/TOC was determined using a total organic carbon analyzer (Shimadzu, TOC-L, Japan). Alkalinity, mixed liquor volatile suspended solids (MLVSS) and mixed liquor suspended solids (MLSS) were analyzed according to APHA standard methods.

### 3 Results and discussion

The performance of the two-stage system is shown in **Fig.2** and **Fig.3** for PN reactor and Anammox reactor, respectively. The influent contained 1500 to 1800 mg·L<sup>-1</sup> ammonium during the operation and the system had an average TN removal efficiency of 85.6%.

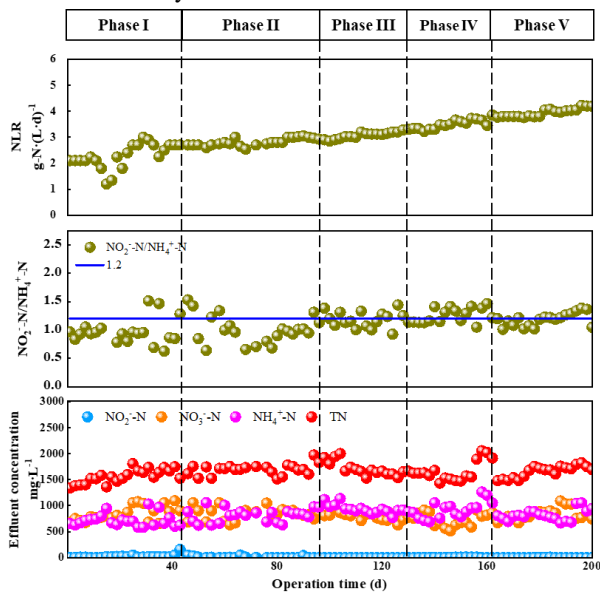


**Fig. 2** Operation performance of PN reactor

The garbage fermentation liquid was fed into the PN unit without dilution with ammonium concentration of 1466±51 mg·L<sup>-1</sup> in the phase I. The NLR increased from 2 to 4 g·N·(L·d)<sup>-1</sup> in the operation. The NO<sub>2</sub>-N/NH<sub>4</sub><sup>+</sup>-N ratio is not controlled well during the early phases because of the

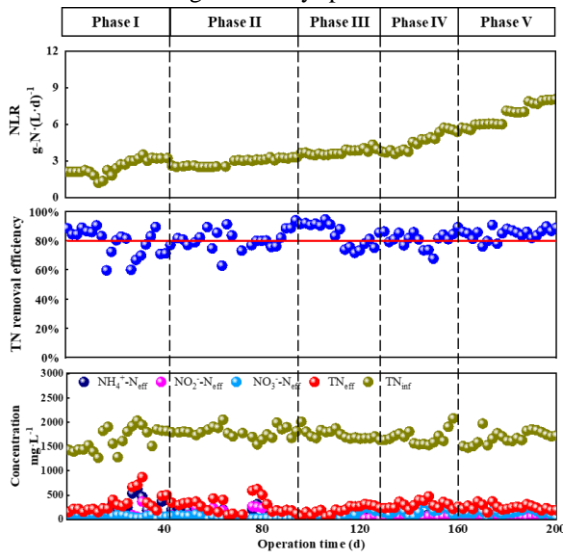


**Fig. 3** Operation performance of HAP-Anammox reactor

limitation of aeration ability and oxygen transfer rate. When enter the Phase III, a well-controlled ratio at 1.2 can make the effluent of PN reactor suitable for Anammox unit. The alkalinity consumed in the reactor has a proportional linear relationship with the ammonium in the influent water, which the value can be defined between 4.5-5 (**Table.2**).

**Table 2** Average operation results of system

Phase	I	II	III	IV	V
NRE	75.9	78.4	84.1	83.2	85.6
NO <sub>2</sub> -N/NH <sub>4</sub> <sup>+</sup> -N	0.96	0.90	1.15	1.19	1.21
ΔIC/ΔNH <sub>4</sub> <sup>+</sup> -N	1.58	1.46	1.17	1.42	1.55
ΔAlkalinity/ΔNH <sub>4</sub> <sup>+</sup> -N	6.86	5.86	5.24	4.67	4.78
ΔCOD (mg·L <sup>-1</sup> )	103	120	174	166	156
ΔCa (mg·L <sup>-1</sup> )	6.1	26.1	23.7	41.5	38.6
ΔP (mg·L <sup>-1</sup> )	7.4	20.1	6.4	16.8	17.8
ΔCa/ΔP	0.82	1.3	1.45	2.47	2.17

The NLR in EGSB reactor increased to the 8.2 g·N·(L·d)<sup>-1</sup> in the phase V and the reactor still showed a good performance on TN removal at 82.4%, while also had a 57% removal of phosphorus. The effluent showed that the nitrate is the main factor influencing the TN removal efficiency. The HAP granular sludge distributions in HAP-A reactor is showed in **Fig.4**.

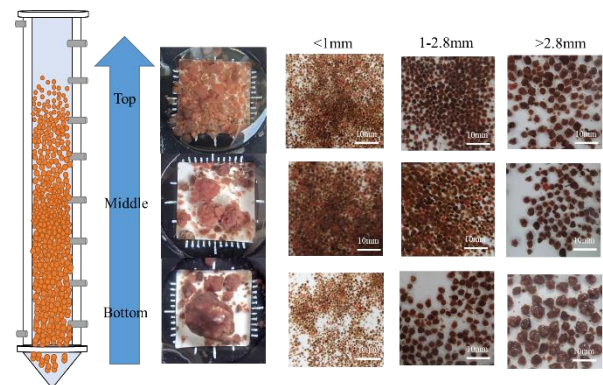


**Fig. 4** HAP granular sludge in HAP-A reactor

### 4 Conclusions

(1) The efficiency and stability of the two-stage PN/HAP-A process was evaluated and confirmed for the treatment of the garbage fermentation liquid. The NLR of PN/HAP-A system is 2.9 g·N·(L·d)<sup>-1</sup> while the NRE is 85.6%. The NLR of the PN and HAP-Anammox reactor can maintain at 4 g·N·(L·d)<sup>-1</sup> and 8.2 g·N·(L·d)<sup>-1</sup>, respectively.

(2) The conversion rate of ammonium should be maintain at 55% in PN reactor, while the ratio of alkalinity to ammonium is between 4.5-5 to demonstrate sufficient alkalinity in the PN reactor.

### Reference

[1] Valenzuela-Heredia D, Panatt C, Belmonte M et al,2022. Performance of a two-stage partial nitrification-anammox system treating the supernatant of a sludge anaerobic digester pretreated by a thermal hydrolysis process. Chemical Engineering Journal, 429, 131301.

# Emerging onsite electron donors for advanced nitrogen removal from anammox effluent of leachate treatment: A review and future applications

○ Yanyan Li<sup>1\*</sup>, Yanxu Liu<sup>1</sup>, Jinghuan Luo<sup>1</sup>, Yu-You Li<sup>2</sup>, Jianyong Liu<sup>1</sup>

<sup>1</sup>School of Environmental and Chemical Engineering, Shanghai University, 333 Nanchen Road, Shanghai 200444, China.

<sup>2</sup>Department of Civil and Environmental Engineering, Graduate School of Engineering, Tohoku University, 6-6-06 Aza, Aramaki, Aoba-ku, Sendai, Miyagi 980-8579, Japan.

\*E-mail: li.yanyan.s5@dc.tohoku.ac.jp.

## Abstract

Partial nitrification-anammox process is promising in leachate treatment, but the 11% residue nitrate limits the total nitrogen removal efficiency. Denitrification or partial denitrification and anammox are both practical polishing processes of anammox effluent, requiring extra electron donors. Fortunately, there are organic matter, sulfide and methane in leachate or produced by leachate treatment, which can serve as onsite electron donors. In this review, the mechanisms and processes using these three kinds of electron donors for residue nitrate reduction in anammox effluent of leachate are systematically summarized and discussed. It can be concluded that, biodegradable organic matter is an effective electron donor, sulfide is a promising electron donor, methane is a potential electron donor. Two possible applications in future based on anammox treatment of fresh and mature leachate using sulfide and methane as onsite electron donors are proposed. Through sulfide reutilization, energy-saving with about 14% of aeration reduction can be achieved.

**Keywords:** Leachate; Anammox; Advanced nitrogen removal; Electron donors; Sulfide; Methane.

## 1 Introduction

Municipal solid waste leachate contains a high ammonium nitrogen concentration, which usually can be up to 2000 mg N/L or higher. Partial nitrification (PN)-anammox process can remove nitrogen efficiently with less aeration amount, carbon source demand, and waste sludge production (reducing by 63%, 100%, 90%, respectively) compared with the traditional nitrification and denitrification process, which has become a research hotspot for decades. In 2009, the application of the full-scale anammox process in leachate treatment was reported for the first time. So far, the engineering application of anammox process has been realized in wastewaters with high ammonium nitrogen.

Theoretically, the maximum nitrogen removal efficiency of anammox process is 89%, while 11% of the total nitrogen (TN) is converted into nitrate. As for nitrogen removal from leachate using anammox process, the residue nitrate concentration will be as high as 200 mg N/L, which is still too high for discharge directly. The residue nitrate needs to be removed by biological methods such as complete denitrification or partial denitrification (PD, providing nitrite for anammox), during which electron donor is required. There are a few kinds of mass in leachate that can serve as electron donors for residue nitrate reduction.

In this review paper, the mechanisms and processes using three emerging onsite electron donors (organic matter, sulfide, and methane) for residue nitrate reduction in anammox effluent are systematically summarized and discussed. Some research prospects are put forward. Specifically, two possible applications in future based on anammox of fresh and mature leachate treatment are proposed to achieve the purpose of advanced nitrogen removal, energy recovery, full utilization of electron donors and reduction of energy consumption.

## 2 Biodegradable organic matter is an effective electron donor

Fresh leachate contains a high concentration of organic matter, and the proportion of biodegradable organic matter is high. Biodegradable organic matter can be used as an electron donor for complete denitrification or PD through different kinds of processes, such as returning the anammox effluent to the AD reactor or using leachate as an electron donor directly.

Mature leachate contains a certain concentration of organic matter, and the proportion of biodegradable organic matter is very low. Recent studies have shown that ROM such as humus can be biodegraded by anammox process and can be used for denitrification.

As a novel and effective biological nitrogen removal process, anammox process is proved to be effective for the degradation of ROM. Recent studies have shown that ROM in leachate can be used as an electron donor to achieve advanced nitrogen removal and the removal efficiency of ROM and TN removal efficiency were 67.7% and 94.9%, respectively. The removal mechanism of ROM is that it is first adsorbed by anammox sludge, and then mineralized or biodegraded into small molecule biodegradable organic matter for utilization by denitrifying bacteria.

## 3 Sulfide is a promising electron donor

Landfill leachate contains a certain amount of sulfate, ranging from 8 to 7750 mg/L. Sulfate is reduced to H<sub>2</sub>S by heterotrophic reduction, and the solubility of H<sub>2</sub>S in water is high, so it dissociates into sulfide in water. Under the neutral condition of AD, sulfide in anaerobic effluent mainly exists in the form of HS<sup>-</sup>. Some autotrophic denitrifying bacteria can use sulfide as an electron donor and nitrate as an electron

acceptor to achieve simultaneous removal of nitrogen and sulfide. Sulfide can be completely oxidized to  $\text{SO}_4^{2-}$  and can be partially oxidized to  $\text{S}^0$ . The N/S molar ratio will affect the formation of the final product during sulfide-oxidizing autotrophic denitrification (SOAD). In recent years, sulfate with strong oxidation capacity can be used as an electron acceptor of anammox has attracted attention. Compared with the conventional NirAnammox process, PN is not required in the Sulfammox process. Therefore, the reduction of energy consumption and the minimum production of sludge can be achieved. New Sulfammox process can provide great potential for energy saving, environmental protection and efficient removal of ammonium and sulfate in wastewater. Because the growth environment of AnAOB and Sulfammox bacteria is similar, and the optimal pH is 7–8.5, the coexistence of Sulfammox and NirAnammox is possible[1].

#### 4 Methane is a potential electron donor

The biogas produced by AD cannot be fully recovered because some of the biogas will be dissolved in the water, and the solubility is affected by some factors. Under different partial pressure of methane, the amount of dissolved methane in anaerobic wastewater is 10–25 mg/L. Methane can be oxidized aerobically or anaerobically in two different microbial processes, both of which can be combined with denitrification. A batch experiment showed that the activities of methane aerobic oxidation, denitrification, nitrification and anammox could exist at the same time. AMOB were successfully enriched by AOB biomass from the PN reactor, and dissolved methane was oxidized to methanol. PN-ANAMMOX process has been proved to be feasible in membrane-aerated biofilm reactor, which can successfully regulate the layer distribution and symbiosis of AOB and AnAOB. Therefore, the integration of AME-D and PN-ANAMMOX may be feasible. By supplying oxygen in the hollow fibre membrane of MBfR, anaerobic wastewater containing ammonium and dissolved methane exists in bulk liquid. It then forms layered biofilm on the membrane surface with aerobic layer, microaerobic layer, and anaerobic layer from the inside to the outside.

#### 5 Possible applications of advanced nitrogen removal using anammox based processes

SOAD, PN and ANAMMOX processes are proposed for fresh leachate treatment to use different S species repeatedly to minimize the electron donors waste (Fig. 1). On the one hand, the use of sufficient sulfide as an electron donor can not only realize advanced nitrogen removal, but also avoid the oxidization of sulfide back to sulfate. The energy consumption of sulfide oxidization during the PN stage can be reduced or avoided through as an electron donor of nitrate in anammox effluent during SOAD between AD and PN-ANAMMOX. On the other hand, sulfate can become the substrate for anammox and is converted to elemental sulfur, reducing the demand for nitrite, that is, reducing the amount of aeration and saving energy. Fresh leachate is firstly introduced into AnMBR for AD. The effluent of PN-ANAMMOX containing nitrate is recycled to SOAD reactor, residue nitrate from anammox can be removed by using sufficient sulfide as an electron donor to achieve advanced nitrogen removal. Finally, nanofiltration (NF) is used in the treatment of PN-ANAMMOX effluent to ensure that the leachate discharge meets the requirements of the standard.

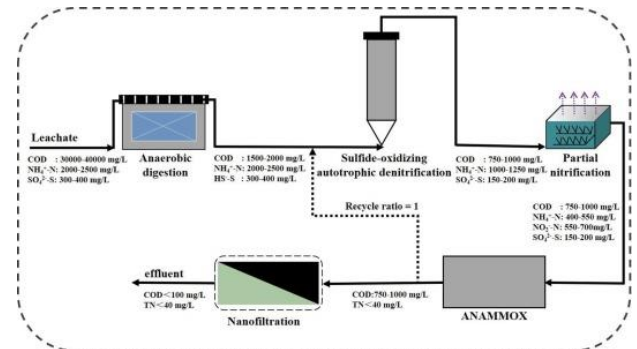


Fig. 1. A possible application in future for advanced nitrogen removal from anammox effluent of fresh leachate treatment.

Mature leachate contains low concentrations of organic matter and sulfate but a higher concentration of ammonium nitrogen. The biodegradable part of organic matter is converted into methane during AD, including dissolved methane. Using dissolved methane as an electron donor can not only avoid greenhouse gas emissions, but also realize advanced nitrogen removal. Therefore, the integrated process of methane oxidation coupled with PD is most suitable for mature leachate treatment, achieving cost-saving and full utilization of electrons. MBfR should be selected to avoid dissolved methane being blown into the atmosphere. On the one hand, the oxygen in the membrane lumen can oxidize ammonium nitrogen to nitrite as the substrate for anammox. On the other hand, it can oxidize the methane to organic matter. An integrated process is proposed for mature leachate treatment (Fig. 2).

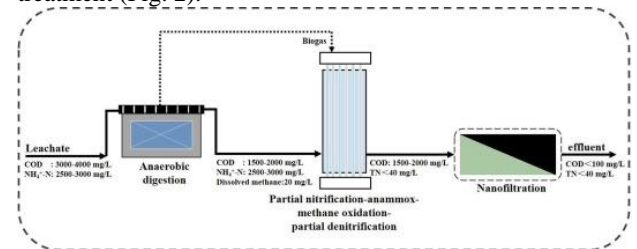


Fig. 2. A possible application in future for advanced nitrogen removal from anammox effluent of mature leachate treatment.

#### 6 Conclusions

Organic matter, sulfide, and methane can be used as onsite electron donors for residue nitrate reduction in anammox effluent of leachate treatment. Biodegradable organic matter is an effective electron donor, sulfide is a promising electron donor, methane is a potential electron donor. For fresh leachate, sulfide-oxidizing autotrophic denitrification, partial nitrification and anammox are suggested as novel optimized processes to achieve energy saving with about 14% of aeration reduced and sulfide reutilization. For mature leachate, membrane biofilm reactor for simultaneous partial nitrification, anammox, methane oxidation coupled with partial denitrification is a potential alternative.

#### Reference

- [1] L. Wu, Y. Peng, et al., Low temperature advanced nitrogen and sulfate removal from landfill leachate by nitrite-anammox and sulfate-anammox. *Environ. Pollut.*, 259 (2020), Article 113763

# Preparation of a spherical biochar colloidal probe and its application in deciphering the mechanism of biochar mitigating membrane fouling

○ Xiaohuan YANG<sup>1</sup>, Silian XIA<sup>1</sup>, Litu Hao<sup>1</sup> & Rong Chen<sup>1,2\*</sup>

<sup>1</sup>Key Lab of Environmental Engineering, Shaanxi Province, Xi'an University of Architecture and Technology, No.13 Yanta Road, Xi'an, 710055, PR China.

<sup>2</sup>International S&T Cooperation Center for Urban Alternative Water Resources Development, Key Laboratory of Northwest Water Resource, Environment and Ecology, MOE, Xi'an University of Architecture and Technology, No.13 Yanta Road, Xi'an, 710055, PR China.

\*E-mail: 1090633365@qq.com.

## Abstract

To better unravel biochar's interface behavior and mitigation mechanism on membrane fouling, spherical biochar colloidal probes were prepared by adhering microspheres to the free end of the cantilever and used to quantitatively determine adhesion force in a foulant-biochar-membrane system. The study investigated the differences in physicochemical properties of biochars and their mitigation effect on membrane fouling. Results indicated that dosing biochars can strengthen the electrostatic repulsion between BSA and membrane, mitigating BSA adhesion or deposition on the membrane surface. Additionally, the regular biochar (SBC and HC) exhibited better mitigation on membrane fouling than irregular biochar due to better physicochemical properties, adsorption capacity, and more porous fouling layer structure composed of microparticles, which caused a higher BSA rejection and loading factor over the membrane. Importantly, the stronger adhesion force of SBC-PVDF (0.90 mN/m) than BSA-PVDF (0.50 mN/m) alleviated membrane fouling in the initial stage of the filtration, and the adhesion force of SBC-BSA (0.049mN/m) alleviated membrane fouling in the later stage, resulting in higher water flux. The interaction force between aged SBC and BSA was comparable to that between BSA and BSA (0.14 mN/m) and stronger than that between original SBC and BSA (0.051 mN/m), implying further mitigating membrane fouling.

**Keywords:** biochar; membrane fouling; hydrothermal carbonization, colloidal probes, interfacial forces.

## 1 Introduction

In recent years, membrane-based technologies are widely used in wastewater treatment, whereas membrane fouling hinders the practice application. It is reported that carbon-based materials show great promise in membrane fouling control. As common additives, powder activated carbon (PAC) and granular activated carbon (GAC) have been applied to retard membrane fouling. However, compared to activated biochar, biochar was produced by a simple and low-cost pyrolysis process without activation. The feasibility of biochar in mitigating membrane fouling has been proven in membrane bioreactors, so it is a good alternative to GAC and PAC for membrane fouling control [1].

There are not many studies involved in biochar's influence on membrane fouling. Limited by the diversity and complexity of the fouling process, the potential mechanisms of biochar were mainly summarized by changes in reactants and products. Therefore, measuring microscopic interfacial forces in a mixed biochar-foulant-membrane system is of great significance to explore the mechanism of biochar on membrane fouling.

In this study, a spherical biochar probe was prepared and utilized to quantitatively determine the adhesion forces of biochar-membrane, and biochar-foulant, which will provide a theoretical method to improve membrane fouling control of biochar.

## 2 Materials and methods

### 2.1 Preparation of biochar colloidal probes

Spherical biochar (SBC) was prepared by a two-stage process: hydrothermal carbonization (230°C, 5 h) and pyrolysis (500°C, 2 h). Spherical biochar colloidal probes were prepared by adhering biochar microspheres to the free end of the probe's cantilever (Fig.1) and then were used to quantitatively determine adhesion force in a foulant-biochar-membrane system.

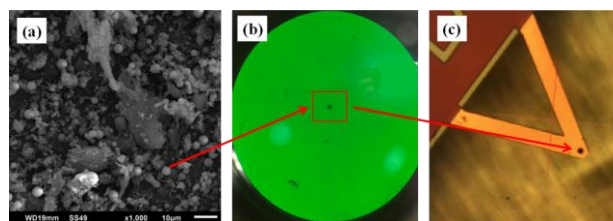


**Fig. 1.** (a) The SEM image of biochar microspheres, (b) the image of biochar microspheres under the microscope, and (c) the image of the probe adhered with a biochar microsphere under the AFM scope.

### 2.2 Membrane filtration experiments

Bovine serum albumin (BSA) filtration experiments with the addition of conventional biochar (CBC), hydrochar (HC), and SBC were constructed. Corn cob was a feedstock for biochar preparation. For CBC, dried fragments of corn cob were directly pyrolyzed in a non-circulated air atmosphere for 2.0 h at 500°C. HC was prepared by hydrothermal carbonization with a reaction temperature of 230°C for 5 h.

The membrane filtration system was performed using a dead-end setup consisting of a feed solution system, a dead-end membrane cell, a draw solution system, and an online

balance monitoring system. The membrane flux  $J$  and BSA rejection ( $R$ ) were calculated by the following equations:

$$J = V / (A \cdot t) \quad (1)$$

$$R = (C_f - C_p) / C_f \times 100\% \quad (2)$$

Where,  $V$  is the change of permeate volume (L),  $A$  is the effective membrane sample area (m<sup>2</sup>), and  $t$  is the sampling time (h).  $C_f$  and  $C_p$  are the concentrations of BSA (mg/L) in the feed and permeate, respectively.

### 3 Results and discussion

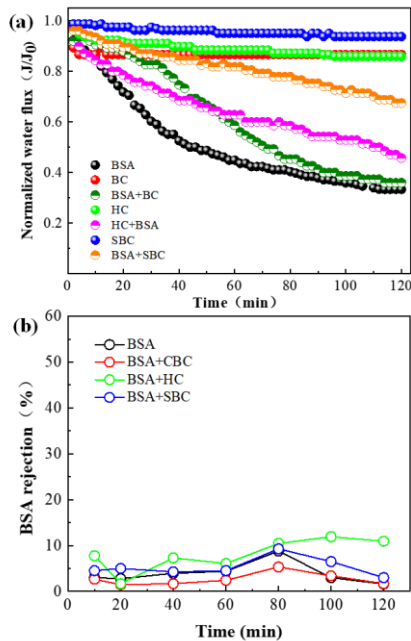


**Fig. 2. (a) The normalized water flux curves of individual foulant BSA and biochar, and BSA with biochar addition and (b) BSA rejection vary with time over the filtration experiments.**

In Fig.2(a), the normalized water flux curves of individual foulant BSA and biochar demonstrated that protein-like substances were representative of the organic matter triggering membrane fouling and biochar did not cause excessive membrane fouling. The permeate flux of BSA with biochar indicated that biochar contributed to mitigating BSA membrane fouling. In addition, it was obvious that the SBC exerted a remarkable mitigating effect on BSA fouling, followed by HC and CBC, namely, the regular spherical biochar was better than irregular biochar in alleviating membrane fouling. In Fig.2(b), BSA rejection of all filtration tests was less than 10%. In a single BSA microfiltration system, BSA rejection was mainly attributed to the adsorption and deposition of BSA in or on the membrane. In the BSA-biochar system, BSA rejection of BSA-HC- and BSA-SBC- fouled membrane were higher than that of BSA-fouled membrane. This may be due to the BSA adsorption by biochar.

A spherical biochar colloidal probe was successfully prepared and applied to uncover biochar's influence on membrane fouling. In Fig.3, the stronger adhesion force of SBC-PVDF (0.90 mN/m) than BSA-PVDF (0.50 mN/m) alleviated membrane fouling in the initial stage of the

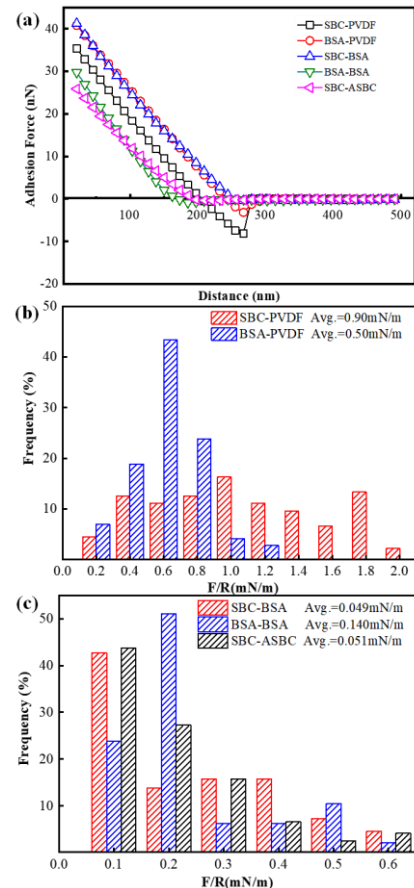


**Fig. 3. (a) Representative adhesion force-distance curves of membrane-foulant and foulant-foulant, and the frequency distributions of the (b) membrane-foulant, and (c) foulant-foulant.**

and the adhesion force of SBC-BSA (0.049 mN/m) alleviated membrane fouling in the later stage, resulting in higher water flux. The interaction force between aged SBC and BSA was comparable to that between BSA and BSA (0.14 mN/m) and stronger than that between original SBC and BSA (0.049 mN/m), implying further mitigating membrane fouling.

### 4 Conclusions

- (1) Due to higher adsorption ability and more porous fouling layer formation, SBC and HC exhibited better mitigation effects on membrane fouling than CBC, causing higher BSA rejection and loading factor over the membrane.
- (2) At the micro-interface, the adhesion force data indicated that the existence of spherical biochar can alleviate membrane fouling in the initial stage and later stage of the filtration process. Aged SBC possessed further mitigation on membrane fouling.

### Reference

[1] Z. Lei, Y. Ma, J. Wang, X.C. Wang, Q. Li, R. Chen, Biochar addition supports high digestion performance and low membrane fouling rate in an anaerobic membrane bioreactor under low temperatures, *Bioresour. Technol.* 330 (2021) 124966.

# High solid of co-digestion performance of lipid waste and food waste by a thermophilic Hollow Fiber anaerobic membrane bioreactor

○ **Ziang HE**<sup>1</sup>, Yuanyuan REN<sup>2</sup>, Chen WANG<sup>2</sup>, Yu-You LI<sup>1,2\*</sup>

*Department of Frontier Science for Advanced Environment, Graduate School of Environmental Sciences, Tohoku University, Sendai 980-8579, Japan.*

*<sup>2</sup>Department of Civil and Environmental Engineering, Graduate School of Engineering, Tohoku University, Sendai 980-8579, Japan;*

\*E-mail: he.zi.ang.p8@dc.tohoku.ac.jp.

## Abstract

The co-digestion performance of thermophilic (55°C) HF-AnMBR in treating lipid waste and food waste for 280 days was investigated. The OLR were increased from 7.34 to 18.37 g-COD/L/d by increasing the lipids content from 10%, 30%, 50% and 70% on dry based. The COD conversion efficiency for methane was 80.14%, 91.13%, 92.07% and 83.87%, and the sludge yield was 0.015, 0.016, 0.016, 0.011 g VSS/g COD at OLRs of 7.34, 10.69, 14.78 and 18.37 g-COD/L/d, respectively. The COD, protein and carbohydrate concentrations in permeate was stable, with an average of 3674.21, 1753.77 and 148.77 mg/L, respectively. During lipids hydrolysis, the main long chain fatty acid (LCFA) were C16 and C18 in lipid content of 10%. When the lipid content increasing, the proportion of C18 is stable, but the proportion of C16 is decreasing from 34% to 17%. It indicates that  $\beta$ -oxidation from C18 to C16 is rate-limiting step. The ultra long chain fatty acids like C20 and C24 are also increasing in high lipid content. The long-term stable performance of the AnMBR indicated that the co-digestion of lipid waste and food waste was effectively decomposed.

**Keywords:** Anaerobic membrane bioreactor; lipid waste, food waste, biogas production, LCFAs.

## 1 Introduction

Around 1.6 billion tonnes of food prepared for human consumption is wasted according to the report of the Food and Agriculture Organization (FAO), and the carbon footprint of food waste is approximately 3.3 billion tonnes of the CO<sub>2</sub> equivalent of greenhouse gas into the atmosphere per year. The past methods of disposing of food waste, such as landfilling, incineration and composting, generate large quantities of greenhouse gases, which is not a desirable scenario, and more than 70% of economic entities in the world have committed to achieving carbon net-zero emissions by the middle of the century. A suitable countermeasure for disposing of food waste is urgently needed. Moreover, between 8.3% and 21% of the content of food waste is lipids which produce greater amounts of biogas than protein and carbohydrate during methane fermentation. That is, a huge amount of bioenergy is contained in food waste, and the efficient use of lipid rich food waste in methane fermentation has yet to be fully explored.

Anaerobic membrane bioreactor (AnMBR) technology could be defined as an anaerobic digestion treatment with membrane separation. The unique function of the AnMBR is retaining solids in the reactor and discharging permeate via membrane filtration. Due to this unique function, total biomass retention, excellent effluent quality, low sludge yield and energy recovery can be achieved. However, the sustainable flux of membrane filtration is hard to maintain, especially for high concentration substrates like food waste, which has total solids content (TS) of around 14% to 25. In addition, membrane fouling is inevitable and directly affects the operating efficiency of the AnMBR. Therefore, despite the huge methane production potential of the digestion of lipids, significant challenges remain to the engineering

applications for the digestion of high concentration lipids rich food waste. Hence, the first purpose of this study is to demonstrate the potential of the methane fermentation of rich lipid food waste by the AnMBR. The second purpose is to investigate the effect of food waste with different lipid ratios during methane fermentation at 55°C.

## 2 Materials and methods

**Table 1 operation condition**

Item	Unit	Start up	Phase I	Phase II	Phase III	Phase IV
TS-Lipids/TS-FW	%	10	10	30	50	70
HRT	day	30	15	15	15	15
SRT	day	30	30	30	30	30
pH		4.1	4.1	4.2	4.9	4.5
TS	g/L	105.1	105.1	120.5	140.2	160.2
VS	g/L	98.1	98.1	116.4	133.1	150.1
VS/TS	%	96.7	96.7	96.5	94.9	95.9
T-COD	g/L	110.1	110.1	160.4	221.7	275.56
S-COD	g/L	46.76	46.76	49.55	48.49	47.49
T-Carbohydrate	g/L	49.4	49.4	50.3	59.3	58.3
S-Carbohydrate	g/L	8.65	8.65	8.41	8.63	8.77
T-Protein	g/L	27.8	27.8	26.3	30.2	31
S-Protein	g/L	7.03	7.03	7.14	7.23	7.13
Lipids	g/L	10.51	10.51	30.5	49	70.1

### 3 Results and discussion

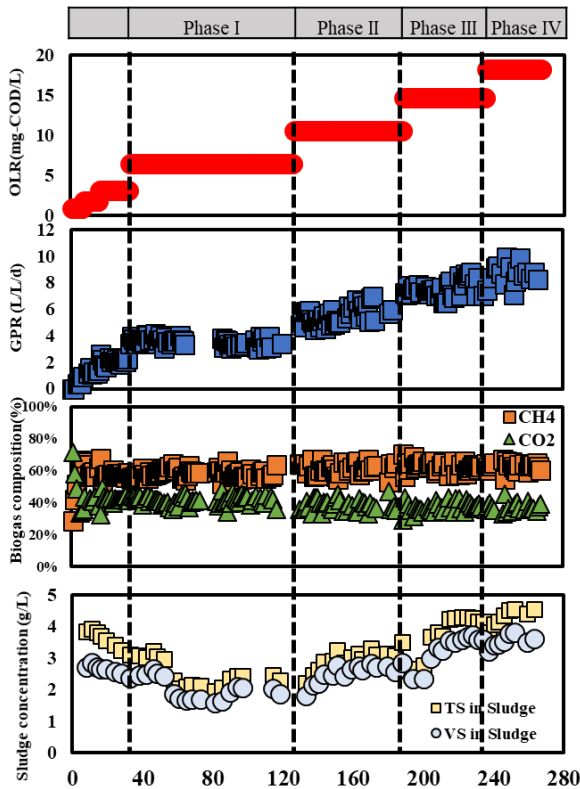
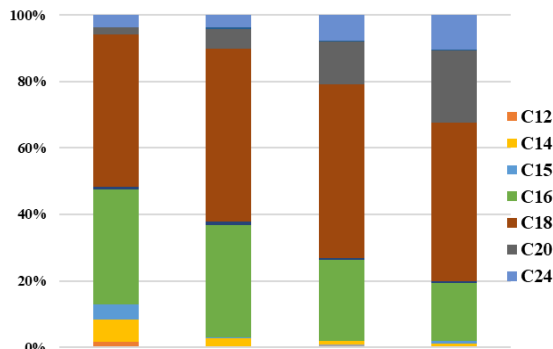


Fig.1. Long term performance of reactor



lipid=10% lipid=30% lipid=50% lipid=70%

Fig.2. The compositions of LCFAs in different lipid contents.

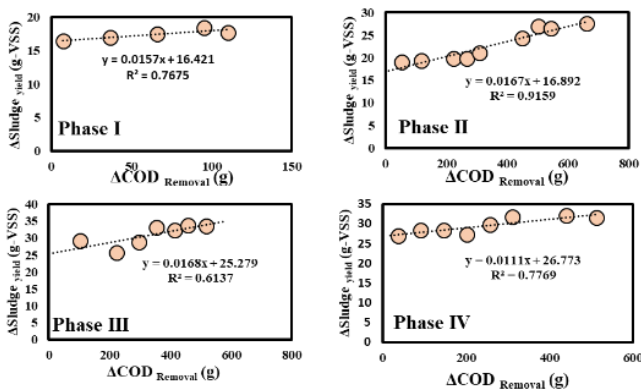


Fig.3. Sludge yield of different lipid content

The long-term continuous experiment was operated in 4 phases. In phase I, the TS of the substrate was 10% and the HRT was 30d. After a successful start-up, the HRT of phase II, phase III and phase IV was shortened to 15d and TS of the food waste was 10%. Then the OLR of rest phases was increased by rising the lipid content from 10%, 30%, 50% to 70%. Figure 2 presents the operation performance of the experiment considering three typical operational factors: gas production rate, methane composition and sludge concentration. These were stable in all phases, indicating that this reactor was operated successfully for 280d, even at a COD loading rate up to 18.37g-COD/L/d. With the rising lipid content, the biogas production rate increased dramatically, with biogas production rates of 3.55±0.15, 5.5±0.25, 7.56±0.31, 8.56±0.34 L/L/d, for corresponding methane fraction of 58.6, 62.1, 63.0, 63.1%, respectively, and corresponding OLRs of 7.34, 10.69, 14.78 and 18.37g-COD/L/d from phase I to phase IV. Considering these results, the increase in biogas production is the most active point in the long-term performance since the methane production potential of lipids is theoretically much higher than that of protein and carbohydrates. The results demonstrate that the co-digestion of lipids with artificial food waste at a rate of 10%, 30%, 50% and 70% lipid content in the TS of the substrate results in a 54.9-141.1% increase in the biogas production rate.

With the increasing of lipid content, the composition of accumulated-long chain fatty acid in sludge was changed. In lipid content of 10%, the main LCFA is C16 and C18. When the lipid content increasing, the proportion of C18 is stable, but the proportion of C16 is decreasing from 34% to 17%. It indicates that  $\beta$ -oxidation from C18 to C16 is rate-limiting step.

The sludge yield in each phases was evaluated. Due to the high methane production potential for lipid, the sludge yield was very low. It was 0.015, 0.016, 0.016, 0.011 g VSS/g COD at OLRs of 7.34, 10.69, 14.78 and 18.37 g-COD/L/d, respectively. So for the reason of high methane production and low sludge yield, it indicates that the lipid was suitable for anaerobic digestion.

### 4 Conclusions

In this study, we applied the HF-AnMBR to digest the artificial lipid-rich food waste with different contents of lipid.

- (1) Operating the HF-AnMBR treating lipid-rich food waste with around 10%-70% of lipid resulted in stable long-term performance.
- (2) The main LCFAs were C16 and C18 in lipid content of 10%. When the lipid content increasing, the proportion of C18 is stable, but the proportion of C16 is decreasing from 34% to 17%. It indicates that  $\beta$ -oxidation from C18 to C16 is rate-limiting step.

### Reference

- [1] Li, Y.Y., Sasaki, H., Yamashita, K., Saki, K., Kamigochi, I., 2002. High-rate methane fermentation of lipid-rich food wastes by a high-solids co-digestion process. *Water Sci. Technol.* 45, 143–150. <https://doi.org/10.2166/wst.2002.0420>

## Effects of oleate loads on methanogenesis under mesophilic and thermophilic conditions

Xiang Li<sup>1</sup>, Yijuan Yan<sup>1</sup>, Yong Hu<sup>1\*</sup>

<sup>1</sup> School of Environmental Science and Engineering, Nanjing Tech University, Nanjing 211816, PR China

\*E-mail: huyong333@163.com

### Abstract

This study investigated the influence of oleate loads (mM-oleate/g-VS) on methanogenesis under mesophilic and thermophilic conditions. Generally, mesophilic anaerobic system is more stable than thermophilic system, which embodied in higher initial microbes' abundance and higher oleate tolerance. Furthermore, oleate not only presents its negative effects on methanogenesis, it also presents its potential to produce methane. This paper provides noticeable and avoidable oleate loads under different experimental conditions as a guidance for future anaerobic bioreactor of lipidic waste biodegradation.

**Keywords:** oleate loads; acetoclastic methanogenesis; hydrogenotrophic methanogenesis; temperature.

### 1 Introduction

The amount of lipidic waste such as fat, oil and grease (FOG) increases yearly due to population growth and catering industry development. As a critical step in biodegradation of FOG, long chain fatty acids (LCFAs) have long pathway of  $\beta$ -oxidation which become the rate-limiting step in AD process (He and Yan 2016). LCFAs can adsorb to the cell membrane of anaerobic microorganisms, and generate block layers to obstruct cell membrane and prevent microbes from obtaining essential nutrients for their vital movement (Kurade et al. 2019). Meanwhile, the accumulation of LCFAs can poison anaerobic microbes and destroy their homeostasis, leading to damages such as transformation and death to microbes (Elsamadony et al. 2021). Therefore, LCFAs have been widely recognized as inhibitors of AD system.

Previous study has shown that different sludge volatile solid contents mediate hydrolytic conversion efficiency of anaerobic sludge, but they will be apt to poisoned on account of LCFAs accumulation (Mahmoud et al. 2004). LCFA loads (mM-LCFA/g-VS) is utilized to further manifest the relationship between LCFAs concentration and sludge volatile solid contents. From these above discussions, there are few systematical researches focusing on the influence of LCFA loads on methanogenic activity under different experimental conditions.

As a typical unsaturated LCFA, oleate (C<sub>18:1</sub>) has continuously attracted much attention for their abundance in wastewater (Alves et al. 2009). In this paper, we utilize oleate as a representative inhibitor in anaerobic serum vial bottles. Firstly, we analyze the initial microbial community composition of mesophilic and thermophilic sludge by 16S rRNA identification to further verify subsequent conclusions. Then we carried out another batch experiment to explore the influence of oleate loads on methanogenic activity under acetoclastic or hydrogenotrophic pathways by utilizing initial mesophilic and thermophilic sludge.

### 2 Materials and methods

#### 2.1. 16S rRNA analysis

The microbial community of initial mesophilic and thermophilic sludge was analyzed by 16S rRNA cloning and sequencing. The detailed operation procedure about genomic

sampling and analysis was carried out according to previous thesis (Jing et al. 2013).

#### 2.2. Seed sludge and substrate

Sufficient seed sludge derived from a continuous-stirred tank reactor (CSTR). It was cultivated under mesophilic and thermophilic conditions in the incubator for three days respectively to recover methanogenesis activity. 2000 mg-COD/L sodium acetate was configured to cultivate acetate-utilizing methane producing archaea (MPA).

#### 2.3 Experiment design

Firstly, seed sludge, phosphate buffer, substrate, sodium oleate and distilled water were added in each anaerobic serum vial bottles. Subsequently, we compressed the bottle with a butyl stopper and sealed it with an aluminum crimp caps. The headspace was swilled by N<sub>2</sub> when utilizing acetate as substrate. On the other hand, H<sub>2</sub>/CO<sub>2</sub> (80:20, v/v) was used to fill the headspace when cultivating hydrogen-utilizing MPA. Finally, 250 mg/L Na<sub>2</sub>S·9H<sub>2</sub>O was injected into all bottles. The liquid volume containing anaerobic sludge, phosphate buffer, substrate, and sodium oleate was maintained at 50 mL. Subsequently, these bottles were statically cultivated at mesophilic (35°C) and thermophilic (55°C) conditions respectively in a shaker (MMS-220, EYELA) for heating and shaking. Each experiment was performed in three parallel vial bottles. **Table 1.** lists the detailed experimental condition of diverse oleate concentration and volatile solid contents respectively. Gas production was measured three times a day until total COD almost converts into theoretical biogas yield.

**Table 1.** Detailed experimental conditions

Number	VS (g/L)	Oleate concentration (mM)	Number	VS (g/L)	Oleate concentration (mM)
MA1	2	0	MA2	2	0.5
MA3	4	0	MA4	4	0.5
MA5	6	0	MA6	6	0.5
MA7	8	0	MA8	8	0.5
MA9	10	0	MA10	10	0.5
MH1	2	0	TH1	2	0
MH2	2	1.5	TH2	2	1.5
MH3	4	0	TH3	4	0
MH4	4	1.5	TH4	4	1.5
MH5	6	0	TH5	6	0
MH6	6	1.5	TH6	6	1.5
MH7	8	0	TH7	8	0
MH8	8	1.5	TH8	8	1.5
MH9	10	0	TH9	10	0
MH10	10	1.5	TH10	10	1.5

#### 2.4. Analytical methods

Sludge volatile solid contents were detected according to standard methods (American Public Health Association, 2012). Biogas production was measured by glass syringe. The pH value was measured by a handheld pH meter (LAQUAtwin, Horiba Ltd., Albany, NY). The composition of biogas was determined by a gas chromatography (Shimadzu GC 2014) equipped with a flame ionization detector and a StabilwaxR-DA capillary column (Resteck, Bellefonte, PA, USA).

### 3 Results and discussion

In general, **Fig. 1.** presents that the abundance of microbes' species in mesophilic serum bottles surpass that in thermophilic bottles, especially acetate-utilizing and hydrogen-utilizing archaea for methane production. Therefore, though thermophilic condition promotes substrate hydrolyzation process and has higher theoretically potential to produce methane, anaerobic mesophilic reactors used for lipidic waste degradation are more stable and reliable than thermophilic ones because they possess larger microbe's quantity and more abundant microbe's species (Labatut et al. 2014).

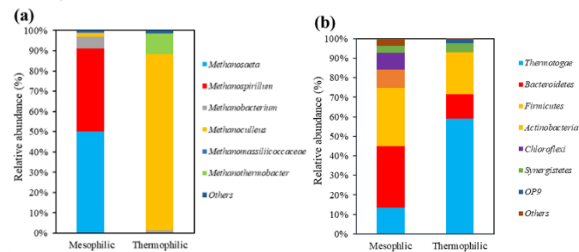


**Fig. 1.** Microorganism composition (a) archaea genus composition in mesophilic and thermophilic sludge (b) bacteria phylum composition in mesophilic and thermophilic sludge

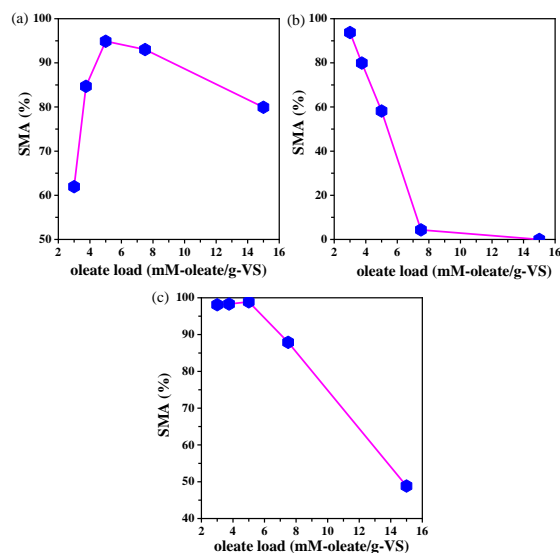


**Fig. 2.** The relationship between oleate loads and SMA percentage (a) acetoclastic SMA in mesophilic sludge (b) hydrogenotrophic SMA in mesophilic sludge (c) hydrogenotrophic SMA in thermophilic sludge.

**Fig. 2.** presents the relationship between oleate loads and AD results, the IC<sub>50</sub> of **Fig. 2.** (b) is 6.68 mM-oleate/g-VS. However, in **Fig. 2.** (a) and (c), the optimal oleate load is both 5 mM-oleate/g-VS. This indicates that moderate oleate load not only detracts slightly to anaerobic microbes, but also owns bioavailable potential, which accords with the conclusion that LCFAs have high methane production

potential (1010 mL CH<sub>4</sub>/g VS) theoretically (Kim et al. 2004, Raposo et al. 2012). Therefore, in the future FOG biodegradation anaerobic reactor, we should not only take the adverse effect of oleate loads on anaerobic sludge into consideration so that we can maintain the stability of AD reactor as much as possible, but also consider their biogas production potential.

### 4 Conclusions

Generally, 16S rRNA analysis manifests the abundance of initial archaea and other bacteria decrease as temperature rises which shows an unstable omen to thermophilic AD system for lipidic waste treatment. On the other hand, oleate loads (mM-oleate/g-VS) is a critical index in anaerobic bioreactor because 6.68 mM-oleate/g-VS will result in 50% decrease of methane production in hydrogenotrophic mesophilic sludge. Meanwhile, this paper provides a guidance of noticeable and avoidable oleate loads for future anaerobic lipidic waste digestion bioreactor.

### Reference

- American Public Health Association (APHA), American Water Works Association, Water Environment Federation, 2012. Standard Methods for the Examination of Water and Wastewater, 22nd Edition, Standard Methods.
- Alves, M.M., Pereira, M.A., Sousa, D.Z., Cavaleiro, A.J., Picavet, M., Smidt, H. and Stams, A.J. (2009) Waste lipids to energy: how to optimize methane production from long-chain fatty acids (LCFA). *Microb Biotechnol* 2(5), 538-550. <http://doi.org/10.1111/j.1751-7915.2009.00100.x>
- Elsamadony, M., Mostafa, A., Fujii, M., Tawfik, A. and Pant, D. (2021) Advances towards understanding long chain fatty acids-induced inhibition and overcoming strategies for efficient anaerobic digestion process. *Water Res* 190, 116732. <http://doi.org/10.1016/j.watres.2020.116732>
- He, X. and Yan, T. (2016) Impact of microbial activities and hydraulic retention time on the production and profile of long chain fatty acids in grease interceptors: a laboratory study. *Environmental Science: Water Research & Technology* 2(3), 474-482. <http://doi.org/10.1039/c6ew00013d>
- Jing, Z., Hu, Y., Niu, Q., Liu, Y., Li, Y.Y. and Wang, X.C. (2013) UASB performance and electron competition between methane-producing archaea and sulfate-reducing bacteria in treating sulfate-rich wastewater containing ethanol and acetate. *Bioresour Technol* 137, 349-357. <http://doi.org/10.1016/j.biortech.2013.03.137>
- Kim, S.H., Han, S.K. and Shin, H.S. (2004) Kinetics of LCFA inhibition on acetoclastic methanogenesis, propionate degradation and beta-oxidation. *J Environ Sci Health A Tox Hazard Subst Environ Eng* 39(4), 1025-1037. <http://doi.org/10.1081/ese-120028411>
- Kurade, M.B., Saha, S., Salama, E.S., Patil, S.M., Govindwar, S.P. and Jeon, B.H. (2019) Acetoclastic methanogenesis led by Methanosarcina in anaerobic co-digestion of fats, oil and grease for enhanced production of methane. *Bioresour Technol* 272, 351-359. <http://doi.org/10.1016/j.biortech.2018.10.047>
- Labatut, R.A., Angenent, L.T. and Scott, N.R. (2014) Conventional mesophilic vs. thermophilic anaerobic digestion: A trade-off between performance and stability? *Water Research* 53, 249-258. <http://doi.org/10.1016/j.watres.2014.01.035>
- Mahmoud, N., Zeeman, G., Gijzen, H. and Lettinga, G. (2004) Anaerobic stabilisation and conversion of biopolymers in primary sludge - effect of temperature and sludge retention time. *Water Research* 38(4), 983-991. <http://doi.org/10.1016/j.watres.2003.10.016>
- Raposo, F., De la Rubia, M.A., Fernández-Cegrí, V. and Borja, R. (2012) Anaerobic digestion of solid organic substrates in batch mode: An overview relating to methane yields and experimental procedures. *Renewable and Sustainable Energy Reviews* 16(1), 861-877. <http://doi.org/10.1016/j.rser.2011.09.008>

# Combining Steam Injection with Hydrodynamic Cavitation for Sludge Pretreatment to Improve Sludge Solubility and Digestion Performance

○ Shitong ZHOU<sup>1\*</sup>, Guangze GUO<sup>1</sup>, Yemei LI<sup>2,3</sup>, Yu-You LI<sup>1,2</sup>

<sup>1</sup>Department of Frontier Science for Advanced Environment, Graduate School of Environment Studies, Tohoku University, 6-6-06 Aoba, Aramaki-Aza, Sendai, Miyagi 980-8579, Japan.

<sup>2</sup>Department of Civil and Environmental Engineering, Graduate School of Engineering, Tohoku University, 6-6-06 Aoba, Aramaki-Aza, Sendai, Miyagi 980-8579, Japan.

<sup>3</sup>Material Cycles Division, National Institute for Environmental Studies, Tsukuba 305-8506, Japan  
\*E-mail: zhou.shitong.q2@dc.tohoku.ac.jp.

## Abstract

Two novel pretreatment methods (VT-SI and IH-SI) that integrated steam injection into hydrodynamic cavitation (HC) in different ways were applied to improve sludge solubility as well as digestion performance. The raw sludge and pretreated sludge were digested in a thermophilic anaerobic membrane bioreactor (ThAnMBR) respectively. The analysis for sludge properties revealed a significant enhancement in sludge solubility after VT-SI and IH-SI pretreatment, with the ratio of soluble COD to total COD increased by around 91.3% and 84.6% respectively. Besides, sludge digestion performance was also improved, with the biogas production rate (L/L/d) increasing by 6.9% and 5.8%, and the organics to methane conversion efficiency (L-CH<sub>4</sub>/g-VS) rising from 0.289 to 0.372 and 0.338 L-CH<sub>4</sub>/g-VS<sub>fed</sub>. And the energy balance analysis found that in ThAnMBR scenario, either the raw sludge or pretreated sludge, the energy recovery could not satisfy the energy consumption. But in case of traditional AD reactor, regardless the energy used for sludge recycle and permeate extracting, the VT-SI could realize higher net energy production than that of raw sludge, presenting a promising application prospect in future.

**Keywords:** Sludge Pretreatment; Hydrodynamic Cavitation; Sludge Solubility; Biogas Production; Energy Recovery

## 1 Introduction

Anaerobic digestion (AD) has commonly been applied as a low-cost and energy-producing technology for sludge treatment in wastewater treatment plants (WWTPs), since it can remove organic pollutants and simultaneously produce biogas. However, the complex sludge structure including extracellular polymeric substances (EPS) matrix, cell wall, etc., greatly strains the full utilization of organics in the sludge, resulting in low biodegradability degree, slow hydrolysis rate, and limited biogas production efficiency. Sludge pretreatment has been proposed to disrupt sludge structure and release more biodegradable organics. There have been various pretreatment methods developed and many of them have been verified effective, but the most commonly applied ones, such as thermal hydrolysis, alkali addition, and ultrasonic treatment, require either high energy cost, new treatment facility construction or a large amount of chemical dosage. It is necessary and important for WWTPs to look for more electricity-saving and cost-effective methods for sludge pretreatment to pursue energy self-sufficiency and carbon neutrality.

Hydrodynamic cavitation (HC) has aroused more and more interests recently, as it presents multiple merits like low operation cost, convenient application, effective organic removal and so on. The effect of HC is attributed to instant and dramatic change of pressure in the fluid, which lead to the formation, growth and expansion and further explosion of cavities. Commonly applied HC instruments like venturi tube or orifice plate all have simple configurations and are very easy to operate, showing high applicability in WWTPs, since sludge pretreatment can be realized by changing the pipeline design. Apart from HC, what else can we do to

enhance the pretreatment effect and increase the energy efficiency in the WWTPs? In fact, the recovery of the waste heat generated has always been a neglected but very promising source, and there is a large amount of steam generated in WWTPs. This part of the steam, if utilized, will not only improve the HC performance but also increase the efficiency of energy utilization in wastewater treatment plants, as the high-temperature steam not only heats the sludge but also promotes cavitation.

Therefore, this study is to investigate the effect of the combination of steam injection and HC on sludge biodegradability and methane conversion performance in a thermophilic AnMBR system with two different pretreatment methods. The energy balance under different scenarios was also estimated.

## 2 Materials and methods

### 2.1 Substrate and Pretreatment methods

The substrate was concentrated excess sludge collected from S WWTPs in Sendai. Two pretreatment methods were applied before sludge digestion, both of which combined the steam injection and HC, but presented different steam utilization ways. One was a venturi tube-type with steam injection (VT-SI) and another was a steam inflowing type (IH-SI). The schematic diagram of these two methods is shown in fig.1-a, 1-b. The VT-SI was based on the venturi tube with an injection inlet designed in the throat so that the steam could be injected at a high speed to promote the cavitation. In the IH-SI, the sludge passed through a nozzle which was surrounded by the steam transporting pipe. The sludge, as well as the steam, were mixed in the sequent area where the cavitation occurred. In this process, the sludge

was heated from 30 °C to 50 °C due to the injection of large amount of high-temperature steam.

### 2.2 Experimental Device and Operation Conditions

A thermophilic anaerobic membrane bioreactor (shown in fig.1-c) was applied for sludge digestion to investigate the methane production performance. The raw excess sludge as well as two pre-treated sludge were fed as the substrate, respectively. The TS concentration of the bulk sludge in the system was kept at around 30 g/L by controlling the daily sludge discharge volume.

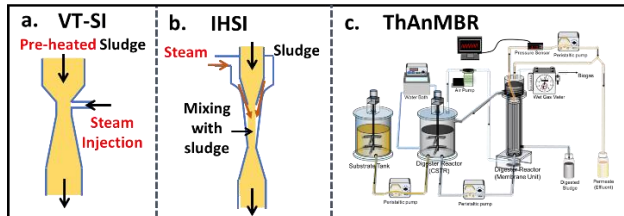


Fig. 1. The schematic diagram of the pretreatment methods and experimental device. a. VT-SI; b. IHSI; c. ThAnMBR

## 3 Results and discussion

### 3.1 Significant Sludge Solubility Improvement

Different analyses were conducted to investigate the effect of pre-treatment on sludge properties. It showed that TS and SS concentrations decreased after VT-SI and IHSI pretreatment. The result of the particle size distribution also presented a smaller mean particle size compared with the untreated sludge. This implied the great crushing solid removal effect of these two methods. More importantly, there were significant soluble organics raised, in terms of proteins(PN), polysaccharides (PS), and COD. Taking the ratio of soluble organics to total organics as the indicator representing sludge solubility, it was found that the sludge solubility increased by about 91% and 85%, respectively after VT-SI and IHSI treatment. Besides, it was noted the dramatic increase of soluble protein content, was nearly four times compared to the untreated one. This was because the sludge was rich in protein but most of which was protected inside the EPS or cellular structure, and the HC helped destroy such structure and release more biodegradable organics.

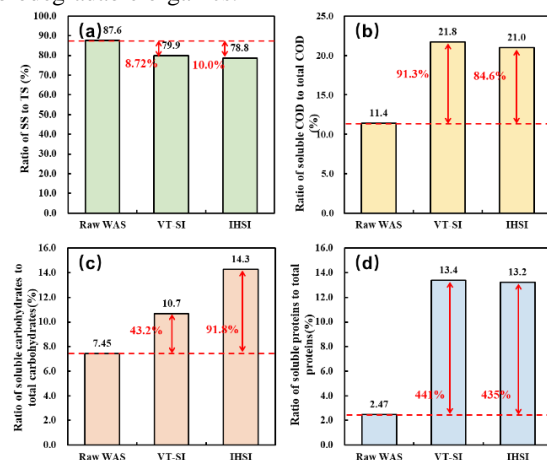


Fig. 2. Soluble substances concentration in sludge before and after pretreatment

### 3.2 Enhanced Biogas Production Performance

All three kinds of sludge had been fed as the substrate in a ThAnMBR system to evaluate the methane conversion efficiency under thermophilic condition. The biogas

production rate as well as biogas yield efficiency were calculated in each stage based on the biogas production and component data. The calculated results showed the biogas production rate were 0.954, 1.02, and 1.01 L/L/d in the stage of untreated sludge, VT-SI, and IHSI, respectively, and the biogas yield efficiency were 0.289, 0.372, and 0.338 L-CH<sub>4</sub>/g-VS<sub>fed</sub>, accordingly, implying a 6.9% and 5.8% increase in biogas production rate and a 28.7% and 17.0% enhancement in methane yield efficiency. The material balance based on COD was also conducted, and it was found the ratio of COD converting to methane has increased from 42.0% to 46.2% and 46.0% after VT-SI and IHSI treatment. It can be seen that the improvement effect on methane production seemed not as effective as that on sludge solubility, which might be attributed to the masking effect of thermophilic digestion, namely the relatively high biodegradation degree and methane conversion efficiency of thermophilic digestion itself.

Table 1 The biogas production performance of each sludge

Substrate/Pretreatment method	Unit	Raw WAS	VT-SI	IHSI	
Biogas Composition	CH <sub>4</sub>	%	63.1	65.0	63.3
	CO <sub>2</sub>	%	34.3	33.6	34.4
	H <sub>2</sub> S	ppm	500	527	588
Biogas production rate	(L/L-reactor/d)	0.954	1.02	1.01	
Methane Yield Efficiency	L-CH <sub>4</sub> /g-VS <sub>fed</sub>	0.289	0.372	0.338	

### 3.3 Energy Analysis

The energy balance analysis was also conducted to estimate the economic benefits when introducing these two pretreatment methods. The energy recovery mainly came from biogas production, heat energy recovered by AnMBR and pretreatment, while the energy consumption including pretreatment, heating, biogas sparging, feeding, sludge cycle, mixing, permeate extracting and heat loss. The calculated results showed that in every stage, the energy recovery could not satisfy the energy demand to operate the thermophilic AnMBR, since the sludge recycle and permeate extracting take a great deal of energy. It seemed that the energy consumed on pumps has long been underestimated. However, in a case of a regular sludge digestion reactor, such as CSTR, when the energy consumed on sludge cycle and permeate extracting were omitted, the net energy production could be realized in raw sludge and VT-SI scenario, with the net energy production were 1.501 and 2.018 kJ/g-VS, respectively. This indicated that VT-SI possess advantages over IHSI due to the less energy consumption on pretreatment but similar biogas improvement effect, and there was still a promising application prospect of such an integrated pretreatment method.

## 4 Conclusions

- VT-SI and IHSI greatly improved the sludge solubility, with the soluble COD in sludge nearly doubled.
- VT-SI and IHSI also enhanced the sludge digestion performance, as the VS to methane conversion efficiency increased by 28.7% and 17.0, respectively.
- In a traditional digester scenario, the VT-SI could realize high net energy production than raw sludge.

## Reference

[1] Guo, G., Li, Y., Zhou, S., Chen, Y., Qin, Y., & Li, Y. Y. (2022). Enhanced degradation and biogas production of waste activated sludge by a high-solid anaerobic membrane bioreactor together with in pipe thermal pretreatment process. *Bioresource Technology*, 346, 126583.

## Influence of nitrate as electron acceptor on Nap anaerobic biodegradation

○ Qigui Niu<sup>1,2,3\*</sup>, Yilin Yao<sup>1</sup> & Jingyi Li<sup>1</sup>

<sup>1</sup>School of Environmental Science and Engineering, Shandong University, 72#Jimo Binhai Road, Qingdao, Shandong Province, 266237, China.

<sup>2</sup>China–America CRC for Environment & Health, Shandong University, 72#Jimo Binhai Road, Qingdao, Shandong Province, 266237, China.

<sup>3</sup> Shandong Provincial Key Laboratory of Water Pollution Control and Resource Reuse, Shandong University, Qingdao, Shandong 266237, China.

\*E-mail: niuqg@sdu.edu.cn.

### Abstract

Simultaneous methanogenesis, denitrification, and Nap anaerobic biodegradation in the up-flow anaerobic sludge blanket reactor (UASB). This study focuses on the promotion of adding nitrate as electron acceptor on naphthene (Nap) biodegradation. After 106 d domestication period, the biological removal of Nap reached 5.38 mg/(L·d). With the nitrate addition as electron acceptor, the biological removal of Nap increased 2.3 times. Interesting, with the nitrate addition, the absorption by sludge of Nap also increased with the ratio of Nap absorption by sludge/ Nap biodegradation increased from 0.55 to 1.36. The concentration of extracellular polymeric substances (EPS) changed with the nitrate addition. And EPS became less hydrophobicity to absorb more Nap. This research confirms that adding nitrate is a promising strategy for the biodegradation of refractory organic compounds.

**Keywords:** Nap anaerobic biodegradation; Methanogenesis; Electron acceptor; Extracellular polymeric substances.

### 1 Introduction

PAHs are lipophilic and mutagenic that have attracted worldwide attention owing to their ubiquity, abundance, persistence, and toxicity. Aerobic PAHs degradation has been well studied and the associated mechanism of biotransformation was clearly. However, PAHs do not extensively present in oxic environments, but have markedly increased longevity in anoxic environments, such as petroleum-polluted soil, deep subsurface oil reservoirs, underground water, and saturated sediments.

Anaerobic digestion (AD) possesses a perfect electron utilization system including electron production, electron transport and electron consumption, for which organic compounds provide electrons as electron donor and these electrons are subsequently used for producing methane. The syntrophic association between the electroactive bacteria and methanogens can maintain the stable performance of AD. Electroactive bacteria decompose organic compounds, such as PAHs then generate and transfer electrons to methanogens directly or indirectly. However, seldom of research focus on adding electron acceptor to promote the microbial behavior.

In this study, the AD electron utilizes the system in the up-flow anaerobic sludge blanket (UASB) reactor (7.5 L work volume) was specifically constructed, and then Nap was added as another electron donor, while NO<sub>3</sub><sup>-</sup> was incorporated as another electron acceptor to explore the promotion on Nap anaerobic digestion, which can provide a reference for subsequent practical studies.

### 2 Materials and methods

#### 2.1 Reactor Setup and Operation

UASB reactor was used with work volume of 7.5 L. The operating conditions of the reactor were shown in Table 1. The whole 250 d experiment was divided into four stages

based on varied electron donor and acceptor concentrations. During stage I (phase I, II and III), cyclodextrin was used as carbon source and electron donor to build AD system. Then in stage II (phase IV, V, VI and VII), Nap was added as another electron donor. Next in stage III (VIII, IX and X), KNO<sub>3</sub> was added as another electron acceptor. Finally in stage IV (phase XI, XII, XIII, XIV and XV), COD was reduced by half. Gas production and methane production were recorded. The effluent samples from the reactor were collected every two days to determine chemical oxygen demand (COD), Nap, ORP, pH, NO<sub>3</sub><sup>-</sup> and NO<sub>2</sub><sup>-</sup>. And sludge samples were collected to determine Nap in sludge every two days. At the end of every phase, sludge samples were collected to extract EPS according to our previous study.<sup>1</sup>

Table 1 Operation conditions

Stage	Phase	Cyclodextrin (g/COD/L)	Nap(mg/L)	KNO <sub>3</sub> (mg/L)	TS(%)	VS(%)	HRT(d)	COD/KNO <sub>3</sub>
Stage I	I(0-13d)	0.75	0	0	14.18±2.77	6.66±0.54	2	
	II(13-24d)	1.50	0	0	8.74±0.16	4.70±0.22	2	
	III(24-36d)	3.00	0	0	10.20±0.33	5.69±0.06	2	
	IV(36-50d)	3.00	10	0	10.95±0.38	5.92±0.18	2	
Stage II	V(50-72d)	3.00	20	0	11.87±0.26	6.28±0.17	2	
	VI(72-92d)	3.00	30	0	10.60±0.59	5.72±0.17	2	
	VII(92-106d)	3.00	60	0	10.55±0.32	5.66±0.13	2	
Stage III	VIII(106-120d)	3.00	60	100	10.26±0.26	5.46±0.07	2	30:1
	IX(120-127d)	3.00	60	200	11.81±0.07	5.91±0.20	1	15:1
Stage IV	X(127-133d)	3.00	60	500	10.76±0.35	5.67±0.12	1	6:1
	XI	0	0	0			1	
	XII	1.50	60	0	10.86±0.78	5.84±0.46	1	
	XIII	1.50	60	100	10.87±1.36	5.74±0.25	1	15:1
	XIV	1.50	60	300	11.61±0.35	5.87±0.15	1	5:1
	XV	1.50	60	500	8.73±0.89	4.93±0.36	1	3:1

#### 2.2 Sampling and analytical methods

COD, pH, ORP, NO<sub>3</sub><sup>-</sup>, NO<sub>2</sub><sup>-</sup>, TS and VS were analyzed according to standard methods. And the composition of methane was detected by absorbing CO<sub>2</sub> at standard atmospheric pressure. Nap was measured by High-Performance Liquid Chromatography (HPLC) as described in our previous study.<sup>2</sup>

### 3 Results and discussion

This part is Results and discussion. The reactor performance is shown in Figure 1 during 270 d in a continuous UASB

reactor. It was divided into four major stages including 15 phases. The pH and ORP were stable during the operation. In stage II, the Nap influent concentration was increased from the value of 10 mg/L to 60 mg/L, the production of methane raised from 957.82±169.5 mgCOD/(L\*d) to 1333.54±176.62 mgCOD/(L\*d). Meanwhile, the Nap removal rate increased from 2.45±0.21 mg/(L\*d) to 5.38±0.54 mg/(L\*d). In stage III, when the NO<sub>3</sub><sup>-</sup> was added as the electron acceptor, the Nap removal rate increased from 5.38±0.54 m/(L\*d) to 6.50±2.64 mg/(L\*d) and NO<sub>3</sub><sup>-</sup> removal efficiency reached 97.26%.

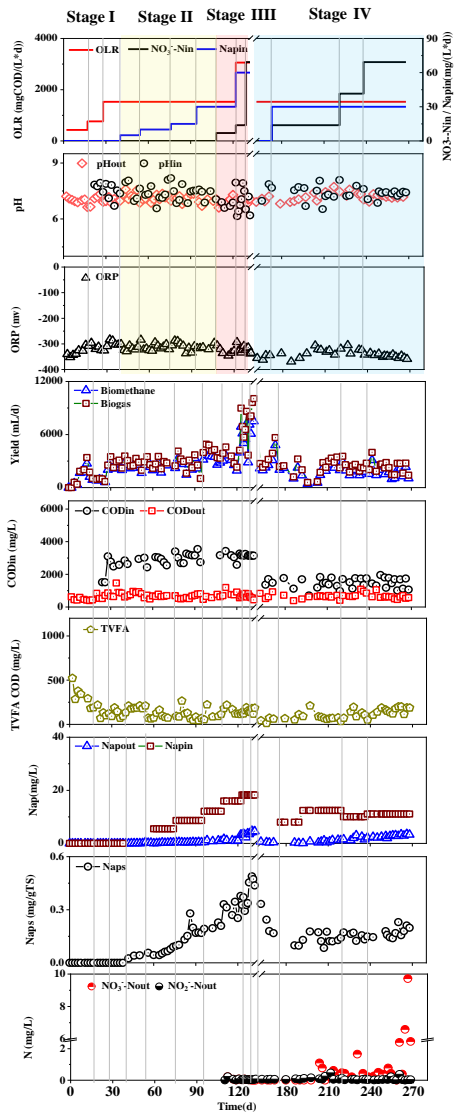


Fig. 1. Reactor performance

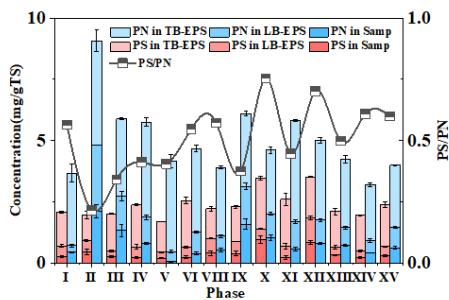


Fig. 2. Proteins (PN), polysaccharides (PS) in EPS and the ratio of PN/PS

It could be inferred that NO<sub>3</sub><sup>-</sup> as the electron acceptor could promote the biodegradation of Nap. Some electrons might flow to denitrifying bacteria, which promoted the utilization of electrons. Then, HRT was changed from 2d to 1d, and the removal concentration of Nap increased significantly from 6.50±2.64 mg/(L\*d) to 14.04±2.27 mg/(L\*d), which explained the potential of removing Nap. During stage IV, CODin changed from 3000 mg/L to 1500 mg/L, with the CODin/NO<sub>3</sub><sup>-</sup> ratio declined to 3:1. As a result, more electrons might flow to denitrifying bacteria, causing methane production decreased from 901.57±79.03 mg COD/(L\*d) to 735.37±238.80 mg COD/(L\*d). Meanwhile, the Nap removal rate to decrease from 11.37±2.38 mg/(L\*d) to 7.46±2.78 mg/(L\*d), while the removal rate of nitrate remained above 95%. It is quite important to point out that the Nap in effluent is maintained at a very low level. Almost all the Nap were removed in an airtight reactor, since 40%-50% of Nap were removed by biodegradation and the rest were absorbed by the sludge. With the NO<sub>3</sub><sup>-</sup> addition as the electron acceptor, the ratio of Nap biodegradation / Nap absorption by sludge decreased from 1.36 in stage II (phase V) to 0.55 in stage III (phase X) (Figure S2). EPS plays a key role in the Nap adsorption and it will be further analyzed in this work.

It is well known that EPS could effectively protect microbes against the harm of toxic substances by absorbing organic compounds. During stage II (Figure 2), with Nap increasing, PN decreased from 5.89± 0.52 mg/gTS to 4.68 ± 0.24 mg/gTS and the ratio of PS/PN increased from 0.34 to 0.55. With the NO<sub>3</sub><sup>-</sup> addition, PS/PN further increased to the value of 0.76 indicating that the hydrophobicity of EPS decreased, which is consistent with the increased adsorption capacity of Nap (Figure 1h).

## 4 Conclusions

Simultaneous methanogenesis, denitrification, and Nap anaerobic biodegradation in the UASB reactor. Adding electron acceptor could promote the biodegradation of Nap. Efficient synergistic Nap biodegradation and methane production was realized by regulating the ratio of CODin/NO<sub>3</sub><sup>-</sup>. Nap biodegradation reached the highest 14.04 mg/(L\*d) at CODin/ NO<sub>3</sub><sup>-</sup>=6:1, which was three times than without nitrate. With nitrate addition as electron acceptor, EPS became less hydrophobicity, which resulted more Nap was absorbed by sludge.

## Reference

- (1) Li, J.; Yao, Y.; Shi, Y.; Tang, J.; Gadaw, S. I.; Liu, R.; Niu, Q. [Bmim]FeCl<sub>4</sub> mediated inhibition and toxicity during anaerobic digestion: Dose-response kinetics, biochar-dependent detoxification and microbial resistance. *Water Res.* **2022**, *210*, 117969.
- (2) Song, L.; Song, Y.; Li, D.; Liu, R.; Niu, Q. The auto fluorescence characteristics, specific activity, and microbial community structure in batch tests of mono-chicken manure digestion. *Waste Manag* **2019**, *83*, 57-67.

## Current options in the treatment of agricultural drainage wastewater

○ Gadow I. Samir <sup>1\*</sup>, Saber M. <sup>1</sup> & Zaghoul A. <sup>1</sup>

<sup>1</sup>National Research Centre, Cairo, Egypt.

At the time being, water is a restricted indispensable resource for sustainable development worldwide. In Egypt, water resources are fairly inadequate and the challenges for achieving the highest possible water use efficiency are not that easy. Decision-makers in Egypt adopted several strategies to secure water allocation and distribution including the reuse of low-quality water particularly agricultural drainage water that is already used in farming on a large scale. Most of the agricultural drainage water in Egypt is apt to many types of pollutants coming from varied sources. Those pollutants are contentiously disposed of in agricultural drains and could be destroying the soil ecosystem when used in farming. In Egypt, climate change is expected especially in the summer season, these warming conditions had some adverse impacts on the agro-environmental ecosystem. This, however, when linked to the low quality of irrigation water, would need urgent and fast actions. This research covered the biological and chemical

characteristics of two agricultural drainage waters at Belbeis and El-Rahawy, as well as assessing the efficiency of four remediation techniques, i.e., DHS, wetland, micro-algae and the combined action of certain biological, chemical and mineral remediate amendments. The overall results showed that surface water was more polluted with different pollutants during the rainy season compared dry season, especially TCOD which was detected in the wide range concentration of 553.4 to 924.3mg L-1 and 544.3 to 821.5mg L-1at Belbeis and El Rahawy drains during dry and rainy seasons, respectively. Our results confirmed that there was a variation in pollutant levels with seasons. TCOD, SCOD, BOD5, EC, pH and potential toxic elements levels in all water samples generally exceeded Egyptian water quality guidelines for the protection of agricultural water uses. The obtained results confirmed that El-Rahawi and Belbeis water samples exhibited high intensities with pathogenic bacteria compared to river Nile water. River Nile water

samples were free from either *Salmonella* or *Shigella*, with the lowest numbers of *Campylobacter* sp. *E. coli* and *E. coli* O157 ( $3 \times 10^2$ , 30 and 1, respectively). El-Rahawi water samples (after Hadar site) had the highest density of *E. coli* ( $5 \times 10^4$ ) and *Salmonella* sp. ( $4 \times 10^3$ ), while Belbeis (at El-Kantara site) had a lower density of *Salmonella* (10) and *Shigella* sp. (20) and the highest density of *Campylobacter* sp. ( $6 \times 10^4$ ). The studied indigenous microorganisms included total bacteria, total fungi, *Azotobacter* sp., *Clostridium* sp., *Pseudomonas* sp., phosphate-dissolving bacteria and cellulose decomposers. Results revealed that the counts of bacteria, fungi, *Azotobacter* sp., *Clostridium* sp., *Pseudomonas* sp., phosphate dissolving bacteria and cellulose decomposers were  $93 \times 10^6$ ,  $1 \times 10^6$ ,  $1 \times 10^3$ ,  $6 \times 10^6$ ,  $27 \times 10^6$ ,  $1 \times 10^6$ ,  $2 \times 10^6$  and  $18 \times 10^6$ ,  $2 \times 10^6$ ,  $1 \times 10^4$ ,  $7 \times 10^6$ ,  $25 \times 10^6$ ,  $25 \times 10^6$ ,  $2 \times 10^6$  respectively at El-hod and El-hadar sites at El-Rahawi agriculture drain. Whereas, the counts of bacteria, fungi, *Azotobacter* sp., *Clostridium* sp., *Pseudomonas* sp., phosphate dissolving bacteria and cellulose decomposers were within the range of  $62 \times 10^6$ ,  $1 \times 10^6$ ,  $1 \times 10^2$ ,  $30 \times 10^6$ ,  $20 \times 10^6$ ,  $1 \times 10^6$  and  $7 \times 10^6$  and  $50 \times 10^6$ ,  $2 \times 10^6$ ,  $1 \times 10^4$ ,  $79 \times 10^7$ ,  $6 \times 10^6$ ,  $88 \times 10^6$  and  $75 \times 10^6$  respectively at the Bridge and Mosque sites at Belbeis agriculture drain. However, the counts of bacteria, fungi, *Azotobacter* sp., *Clostridium* sp., *Pseudomonas* sp., phosphate dissolving bacteria and cellulose decomposers were within the range of  $57 \times 10^6$ ,  $2 \times 10^4$ ,  $1 \times 10^2$ ,  $45 \times 10^6$ ,  $7 \times 10^6$ ,  $1 \times 10^6$  and  $2 \times 10^6$  respectively in River Nile water.

## Climate risk and vulnerability assessment (CRVA) framework for the built environment: A case study in SEZAD industrial zone

○ Luminda GUNAWARDHANA<sup>1\*</sup> & Mahad BAAWAIN<sup>2</sup>

<sup>1</sup>Department of Civil Engineering, University Moratuwa, Katubedda, Sri Lanka.

<sup>2</sup>Ministry of Labor, Muscat, Sultanate of Oman.

\*E-mail: lumindang@uom.lk

### Abstract

According to the Intergovernmental Panel on Climate Change (IPCC), potential variability in future climate will place greater pressure on economic, environmental, and social assets. Subsequent damages to the built environment can be substantially reduced by assessing the climate change impacts on vulnerable sectors in the early stages of the project planning and implementing appropriate adaptation measures. The objective of this climate risk vulnerability assessment (CRVA) is to examine climate change threats to the Special Economic Zone Authority at Duqm (SEZAD) area in Oman to determine to what extent the infrastructure and natural environment are vulnerable to climate change and to recommend measures that will improve the climate resilience. The SEZAD area is expected to develop as a industrial economic center based on a seaport, ship repair yard, and dry-dock complex. Surface air temperature, rainfall, wind speed, and sea level rise were considered for the CRVA analysis. Meteorological records at Masirah observational station during the 2004-2019 period were used to define the baseline climate. Future projections from five general circulation models (GCMs) and two representative concentration pathways (RCP 4.5: stabilization scenario and RCP 8.5: business-as-usual) were downscaled using stochastic models to the local scale. These projections were incorporated in risk assessment in two future periods: 2040-2059 and 2060-2079. Results show that the severity of the extreme temperature and rainfall effects will continue to rise in the future. A 12.5% of annual occurrence probability of a heat wave in the baseline period is likely to reach 41.5% in the 2060-2079 period according to the RCP 8.5 scenario. The estimated 1% annual exceedance probability (AEP) of 1-day rainfall in the baseline period (return level = 288.5 mm/day) will likely increase to a 2.7% AEP level during the 2040-2059 period as projected by the RCP 8.5 scenario. Extreme droughts are likely possible even though such events have not occurred during the baseline period. A significant change in the days with strong winds (1-hr gust more than 15 m/s) was projected in all future periods compared to observations in the baseline period. Results also showed that these strong winds will not likely be strengthened up to destructive levels on the Saffir-Simpson Hurricane Scale. Total inundation land along a 90 km coastal line ranges from about 6 km<sup>2</sup> to 50 km<sup>2</sup> corresponding to 0.5 m to 5.0 m sea level rise, respectively. The impacts of hazards were assessed in terms of economic, environmental, social, and public safety, and the resulting climate risk was calculated under 5 categories ranging from negligible risk to extreme risk. Several adaptation measures were then outlined to cope with the potential damages.

**Keywords:** GCM; RCP; Duqm; Saffir-Simpson Hurricane Scale; Multi-Model Ensembles.

### 1 Introduction

In recent decades, governments in the Middle East region invest extensively in the built environment focusing on the economic development of the nations. Most of these designs are based on the stationarity assumption, which considers the same probability characteristics of hydro-meteorological events that occurred in the past to be continued to the future. However, the intensity and the frequency of the extreme events are likely to increase under climate change resulting in exacerbating infrastructure damages, disrupting critical systems, and increasing operational and maintenance costs [1].

The Climate Risk vulnerability assessment (CRVA) is used to quantify climate risks that may occur during the design period of the project and propose the best cause of action to mitigate or very least reduce the subsequent damages. Vulnerability to climate change is defined as the degree to which a system is susceptible to, or unable to cope with, adverse effects of climate change including climate variability and extremes. Risk of the climate change can be assessed by considering both the consequence of an event

occurring and the likelihood that the same event occurs. The likelihood is used as a general description of probability or frequency, that is, how likely it is that a hazardous event will occur. A consequence is the outcome or impact of an event. A risk assessment process such as the 'risk matrix' is a structured way of identifying impacts, adaptive responses, and vulnerability to climate change [2].

SEZAD area in Oman is expected to develop as a world-scale industrial economic center based on a seaport, ship repair yard and dry-dock complex, to international standards. The purpose of this CRVA is to understand the climate and assess climate change threats to the SEZAD area, to determine to what extent the infrastructure and natural environment is vulnerable to climate change, and to recommend measures that will improve the climate resilience.

### 2 Study area

The entire SEZAD development area is about 123,000 ha. Predominant land use area is allocated for industrial and residential zones. In addition, about 2,400 ha has been designated to develop as tourism projects. The designated

area is featured five main rivers (locally known as wadis) that channel the water from the hilly area toward the sea (Fig. 1). Among these, Wadi Jurf flows directly in the middle of the planned industrial area. Wadi Saay flows from the south to the Arabian Sea through the area of the new port expansion. In order to lower the flood risk downstream, large artificial channel areas; Jurf and Saay dams were designed on the upstream sides of the catchments. When designing the channels, it was expected that two dams are able to reduce a 1000-year peak discharge to a 100-year peak discharge by routing floodwater through the reservoirs.

Surface air temperature, rainfall, wind speed, and sea level rise were considered for the CRVA analysis. Meteorological records at Masirah observational station during the 2004-2019 period were used to define the baseline climate. The climate in Duqm is characterized by arid to hyper-arid. According to the available data in Masirah from 2004 to 2019, temperature varies from 47.2 °C maximum to 11.7 °C minimum with an average of 26.7 °C. Annual total rainfall averaged over the same period in Masirah is about 57 mm. In general, the total rainfall amount and intensity are higher in June. For example, tropical storm Ashobaa brought 213 mm/day of rainfall intensity to Masirah in June 2015.

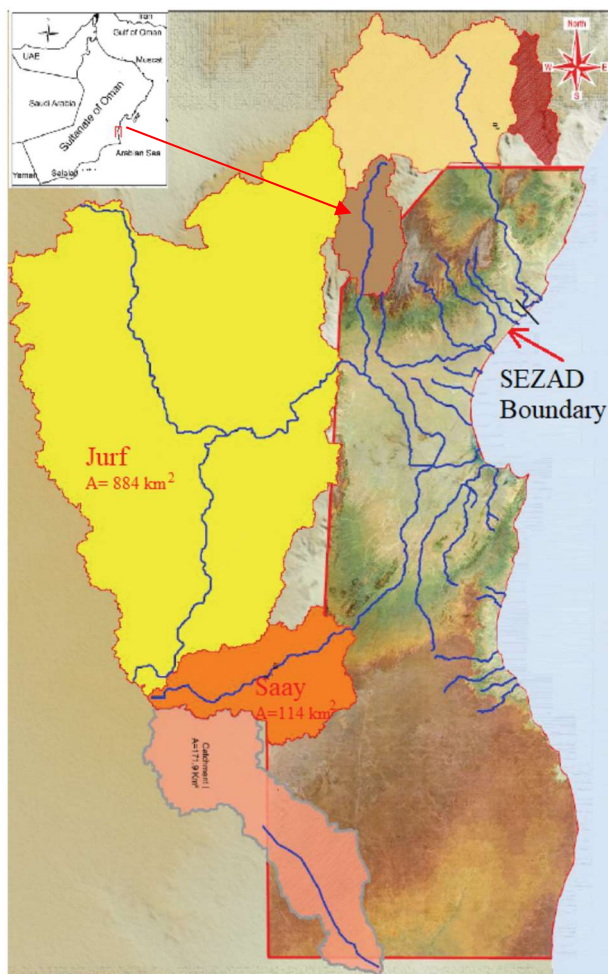


Fig. 1. SEZAD area with Jurf and Saay watersheds

### 3 Methodology

When determining how climate change may influence a project, the standard approach is to determine current climate

parameters, identify how they will change due to global climate change, assess how these climate hazards may affect the project design or impact the project assets, and then determine how to adapt the project specifications. This CRVA implements this approach to the extent possible.

### 3.1 Rainfall indices

When the changes in extreme rainfall are considered, previous research found that the contribution from extreme rainfall to the annual total rainfall has steadily increased in two major cities: Muscat and Salalah in the Sultanate of Oman during the 1990-2009 period [3]. Therefore, the following set of rainfall indices that explore the potential changes of extreme rainfall in the future was considered.

1. 100-year 1-day and 5-day maximum rainfall in the baseline and future periods,
2. annual exceedance probability of the baseline 100-year return level of the maximum 1-day and 5-day rainfall (%),
3. annual exceedance probability of a day with daily rainfall exceeding 25 mm (%),
4. annual exceedance probability of a day with daily rainfall exceeding 50 mm (%),
5. annual exceedance probability of a 5-days event with total rainfall exceeding 50 mm,
6. annual exceedance probability of a 5-days event with total rainfall exceeding 100 mm, and
7. the number of droughts in the baseline and future periods.

Although rainfall is a major indicator of the availability of water, the temperature is also an important factor that can influence the availability of water as it controls the rates of evapotranspiration. Under climate change, large increases in potential evapotranspiration (PET) in a warmer climate may cause an increase in widespread drying. Therefore, the Standardized Precipitation Evapotranspiration Index (12-month SPEI) was used for assessing the temporal variation of droughts. The Hargreaves method was used for estimating PET. Data requirements include daily maximum and minimum temperatures. SPEI scale used for categorizing the severity of the drought is as follows.

- Extreme droughts:  $SPEI \leq -2$ ,
- Severe droughts:  $-2 < SPEI \leq -1.5$ , and
- Moderate droughts:  $-1.5 < SPEI \leq -1$ .

### 3.2 Maximum temperature indices

In Duqm area, the following indices were used to estimate potential variations of maximum temperature in future periods relative to the baseline period.

1. Monthly averaged daily maximum temperature of the warmest month,
2. maximum daily temperature estimated for different percentiles starting from 90th to 99.9th,
3. average number of days per year with daily maximum temperature above 40°C,
4. number of heat waves, and
5. yearly probability of occurrence of heat waves, at least one time, at least two times, at least three times, and more than three times.

According to the Task Team on the Definition of Extreme Weather and Climate Events commissioned by the World Meteorological Organization, a heat wave is defined as a period of marked unusual hot weather (maximum, minimum,

and daily average temperature) over a region persisting at least three consecutive days during the warm period of the year based on local (station-based) climatological conditions, with thermal conditions recorded above-given thresholds. Accordingly, a heat wave in Duqm area was defined as an event, which satisfied the following three conditions.

1. During a period of five consecutive days, the maximum daily temperature reached at least the 98th percentile of maximum temperature in the baseline period (38.8 °C) in at least three days,
2. during these five days, the mean maximum daily temperature was at least 38.8 °C, and
3. during which, the maximum daily temperature did not drop below the 90th percentile of maximum temperature in the baseline period (36.0 °C).

### 3.3 Extreme wind

The wind climate is very important for the port as the wind-generated waves may limit operations at the port. Accordingly, the following indices were used for assessing changes in extreme wind.

1. The average number of days per year with maximum wind speed (1-hr gust) of more than 15 m/s in the baseline and future periods,
2. annual exceedance probability of Category 1 and Category 3 winds (60-sec gust) based on the Saffir-Simpson Hurricane Scale in the baseline and future periods, and
3. annual exceedance probability of 100-year return level estimated from the baseline period and future periods.

The observed wind speeds are on an hourly scale. Therefore, an appropriate gust factor must be used to match the estimations with the Saffir-Simpson Hurricane Scale. In this CRVA study, guidelines from the WMO were applied and a gust factor of 1.28 was used [4].

### 3.4 Sea level rise

The IPCC AR5 projected that the global mean sea-level rise rate during the 21st century will exceed the historical rate observed during the 1971–2010 period for all RCPs. Between 0.26 and 0.55 m of sea-level rise are projected for RCP 2.6 by 2100, and between 0.52 and 0.98 m of sea-level rise are projected under RCP 8.5 by 2100. Estimates of regional sea-level rise can differ from global estimates. The Second National Communication Report (NCR-2) used sea-level rise scenarios from 0.2 m up to 5 m added to mean high tide for estimating inundation areas in Oman. In this CRVA, sea level rise scenarios adapted in NCR-2 were considered with high-resolution DEM data (5 m × 5 m) in Duqm area.

### 3.5 Climate projections

IPCC AR5 produced climate change projections for a range of representative concentration pathways (RCPs) based on different greenhouse gas (GHG) emissions scenarios. In this study, projections of RCP 4.5 and RCP 8.5 scenarios were used from 5 general circulation models (GCMs). A stochastic weather generator (Long Ashton Research Station-Weather Generator; LARS-WG v5.5) was used to downscale the coarse resolution rainfall and temperature future projections at the daily scale to the local scale. The two-parameter Weibull distribution, which is long been established as a useful probability distribution for representing wind speeds,

was used for downscaling wind speed. Frequency analysis of climate variables was performed using the Generalized Extreme Value (GEV) distribution function.

### 3.6 Multi-model ensemble

Weighting individual GCM based on model performance has been used as a way to reduce the unwanted uncertainty in climate model projections. The rationale is that uncertainties can be reduced if the results from the better-performing models are given greater weight in the ensemble when used to produce probabilistic projections. In this study, different weights were calculated based on the ability of the GCMs to represent climate in the baseline period. To compute the GCM weight, the bias  $B$  (%) was found first and then  $B$  was converted to a weight ( $W$ ) using the following transformation.

$$B = 100 \left[ \frac{P_{GCM}}{P_{Obs}} - 1 \right] \quad (1)$$

$$W = 1 + B/100, \quad B < 0 \quad (2)$$

$$W = \frac{1}{1+B/100}, \quad B > 0 \quad (3)$$

Here  $P_{GCM}$  and  $P_{Obs}$  are the interest climate variables from GCM and observations, respectively in the baseline period. The application of Equation 1 for temperature, rainfall, and wind speed is however different and depends on the extreme feature that we are interested in capturing from GCM.

### 3.7 Vulnerability and risk matrix

In this CRVA study, likelihoods were assigned based on consideration of both the historical occurrence and the level of confidence associated with the climate projections, for the key hazards. The consequence of a climate change impact can be identified as either minor, moderate, major, severe, or catastrophic. Depending on the likelihood of the hazard and the consequence, a single value for the risk was calculated based on the guidelines in Fig. 2.

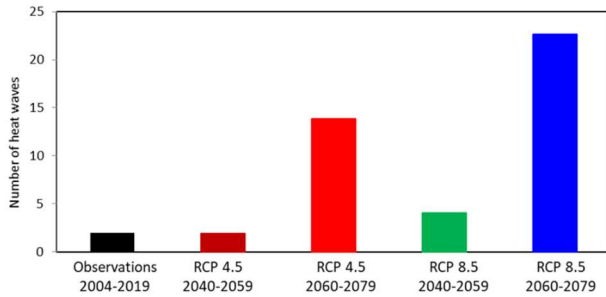
Consequence	C5: Catastrophic	Yellow	Orange	Red	Red	<b>R5</b> Extreme risk: Immediate controls required <b>R4</b> High risk: High priority control measures required <b>R3</b> Moderate risk: Some controls required to reduce risks to lower levels <b>R2</b> Low risk: Controls not likely required <b>R1</b> Negligible risk: Scenarios do not require further consideration
	C4: Severe	Blue	Yellow	Orange	Red	
	C3: Major	Blue	Blue	Yellow	Orange	
	C2: Moderate	Green	Blue	Blue	Yellow	
	C1: Minor	Green	Green	Blue	Yellow	
		L1: Rare	L2: Unlikely	L3: Possible	L4: Likely	
Likelihood						

Fig. 2. Risk evaluation matrix

## 4 Results and Discussion

Projections for all emission scenarios indicate that the annual average daily maximum temperature increases in the future in Duqm area. Under the high emission scenario (RCP 8.5), the maximum temperature in the warmest month is projected to increase by 1.5 °C. An increasing number of studies have documented that temperature above a certain high level remains for a few consecutive days is significantly associated with human mortality. Figure 3 shows that the number of heatwaves projected in the 2060-2079 period by both RCP scenarios is considerably higher than that was

calculated from observed temperatures or projected for the 2040-2059 period. When compared with the baseline period, RCP 4.5 and RCP 8.5 scenarios projected 5.5- and 9.1-times higher numbers of heat waves in the 2060-2079 period. The frequency analysis of heat waves estimated that even though heat waves did not happen more than once per year during the 2004-2019 period, heat waves more than twice or thrice per year are also likely to occur in future climates (Table 1).



**Fig.3. Number of heat waves in different periods.**

**Table 1: Annual occurrence (%) of heat waves.**

Time period	At least 1 time	At least 2 times	At least 3 times	More than 3 times
Baseline (2004-2019)	12.5	0.0	0.0	0.0
RCP 4.5 (2040-2059)	4.9	2.0	1.2	0.8
RCP 4.5 (2060-2079)	28.5	20.3	11.4	7.1
RCP 8.5 (2040-2059)	7.7	7.7	2.8	2.1
RCP 8.5 (2060-2079)	41.5	28.1	18.5	10.2

Rainfall intensities projected by the RCP 4.5 scenario for different return periods show only some minor changes (positive changes for return periods less than 50-year and negative changes for return periods more than 50-year) compared to the intensities estimated from observations. In contrast, RCP 8.5 projected consistently higher rainfall intensities in both future periods. In particular, RCP 8.5 in the 2040-2059 period projected approximately 80% increases in rainfall intensity for a 100-year return period (Fig. 4).

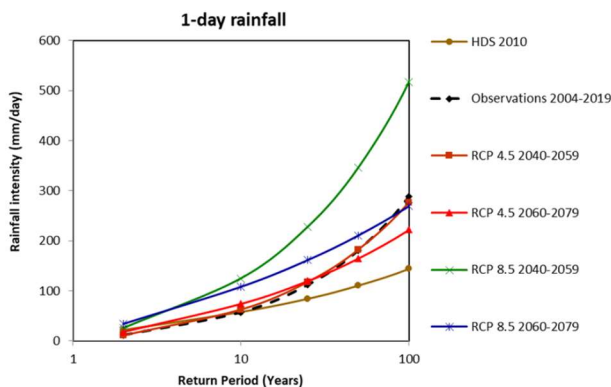


**Fig.4. A comparison of 1-day rainfall intensity-frequency curves.**

The 5-day rainfall projections generally have higher rainfall amounts than the observations for return periods of less than 50-year. In contrast to 1-day rainfall intensities, 5-days

rainfall amounts projected by the RCP 8.5 scenario are smaller than the rainfall amounts calculated from observations for return periods greater than 50-year. On the other hand, RCP 4.5 scenario projected consistently greater rainfall amounts during the 2040-2059 period. For example, the 100-year 5-day rainfall from observations is about 385.9 mm (1% AEP), which according to RCP 4.5 in the 2040-2059 period is about 535.5 mm.

A comparison of the temporal variations of droughts estimated in the baseline period with two of the projections in the future is shown in Fig. 5. All four future scenarios projected that the overall proportion of time spent in drought would only change marginally. These scenarios however indicate that extreme droughts are likely possible even though such events have not occurred during the baseline period in Duqm. From all scenarios, RCP 4.5 projected the greatest changes in the 2060-2079 period compared to the experienced droughts in the past. When two future periods are compared, the occurrence of droughts in all categories in the 2060-2079 period is expected to be higher than in the 2040-2059 period. In addition to the potential variations of monthly total rainfall, this difference can be attributed to the increases in evapotranspiration because of greater warming in the 2060-2079 period than in the 2040-2059 period.

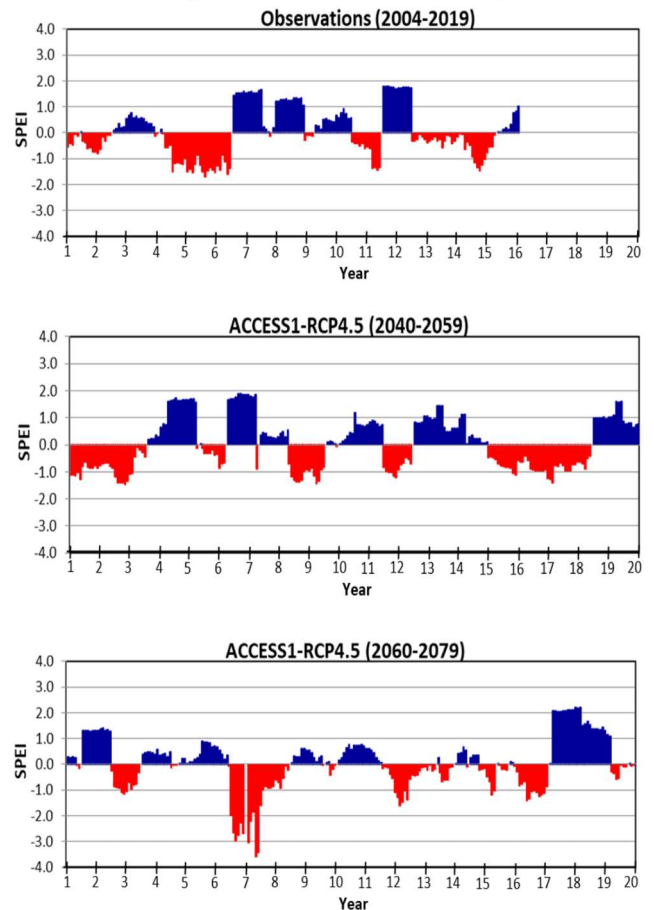


**Fig. 5. Temporal variation of the droughts.**

A significant change in the days with strong winds (1-hr gust more than 15 m/s) was projected in all future periods compared to observations in Duqm during the 2004-2019 period (Fig. 6). The greatest of which, the RCP 4.5 scenario estimated 23 days of strong winds per year in the 2040-2059

period compared to 1.6 days/year observed during the baseline period in Duqm. Results also showed that these strong winds would not likely be strengthened up to destructive levels on the Saffir-Simpson Hurricane Scale. According to the comparison of return-level and return period plots of 60-sec gust wind speed between observations and future projections, three out of four future scenarios indicated slightly smaller wind speeds than the estimated values from the observations in Duqm. The RCP 4.5 scenario alone showed increased wind speeds in the 2040-2059 period than the observations. Consequently, this scenario projected that the AEP of the Category 1 and Category 3 winds will be increased by 0.64% and 0.15%, respectively.

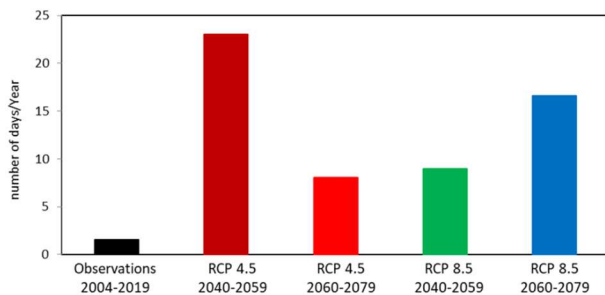


**Fig. 6. The Average number of days per year with a maximum wind speed (1-hr gust) of more than 15 m/s.**

In this study, potential inundation areas (IA) were calculated for a coastal belt of approximately 90 km long. Total IA ranges from about 6 km<sup>2</sup> with a sea level rise under 0.5 m to over 50 km<sup>2</sup> under a sea level rise of 5 m which corresponds to conditions of storm surge due to tropical cyclones.

Depending on the likelihood of the hazard and the consequence, climate risk was calculated (Table 2) and categorized as follows.

- R1, Negligible risk: Scenarios do not require further consideration
- R2, Low risk: Controls not likely required
- R3, Moderate risk: Some controls are required to reduce risks to lower levels
- R4, High risk: High-priority control measures required
- R5, Extreme risk: Immediate controls required

#### 4 Conclusions and Recommendations

In accordance with the findings of the risk analysis, several options were proposed to manage the climate risks. The most important recommendations of those are mentioned below.

- The PMP of 580 mm/day used for designing Jurf and Saay dams has a 285-years return period according to the observations in the baseline period. The annual exceedance probability of a such event is about 0.35% (R2 risk). According to the highest impact scenario (RCP 8.5 in the 2040-2059 period), such rainfall event has an annual exceedance probability of 0.8%. Should SEZAD wish to reduce the associated risk, the non-overspill crest (NoC) level of the dam can be increased.

- Similarly, 500-year 24-hour rainfall event in HDS (2010), which was used for the Drainage network master plan, has an approximately 100-year return period according to the observations in the baseline period. The annual exceedance probability of a such event is about 1% (R2 risk). According to the highest impact scenario (RCP 8.5 in the 2040-2059 period), such rainfall event has an annual exceedance probability of 3.2%. Should SEZAD wish to reduce the associated risk, the embankment level can be increased in critical places after a detailed study.

- Future designs in Duqm are required to consider the local rainfall records with a full set of past data and potential changes in the future.

- Use flood-proof design and construction methods for industrial, commercial, and residential complexes and tourist hotels anticipating both surface flooding and underground flooding due to groundwater level rise.

- Implement a groundwater-monitoring program to investigate the variation in groundwater level and quality.

- Installing weather stations covering the entire catchment area and piloting an Early Warning System (EWS) is highly recommended.

#### Reference

[1] Gunawardhana L.N., Al-Rawas G.A., Al-Hadhrami G., Quantification of the changes in intensity and frequency of hourly extreme rainfall attributed climate change in Oman, *Natural Hazards*, 92 (2018) 1649-1664.

[2] ISO 31000, 2009: Risk management-principles and guidelines

[3] Gunawardhana, L.N., Al-Rawas, G.A., A comparison of trends in extreme rainfall using 20 years data in three major cities in Oman. *The Journal of Engineering Research*, 13 (2016) 137-148.

[4] Harper, B.A., Kepert, J.D., Ginger, J.D., Guidelines for converting between various wind averaging periods in tropical cyclone conditions, *World Meteorological Organization TD-No. 1555* (2008) 1-64.

**Table 2 A summary of climate change risk.**

#	Climate Change Parameter	Risk: 2040 – 2059	Risk: 2060 – 2079
1	Max Temp Heat Wave: 4 types of impact: M/C, community health, livestock/agriculture & tourism	RCP 4.5: 1 x R1 & 3 x R2 RCP 8.5: Same	RCP 4.5: 1 x R2 + <b>3 x R3</b> RCP 8.5: 1 x R3 + <b>3 x R4</b>
2	High-Intensity Extreme Rainfall: 4 types: Wadis, Roads, Port & Maintenance	RCP 4.5: 1 x R1 & 3 x R2 RCP 8.5: Same	RCP 4.5: 1 x R1 & 3 x R2 RCP 8.5: Same
3	Prolonged Rainfall Intensity >5 days: 3 types: Roads, Flooding & Structure	RCP 4.5: 2 x R2 & <b>1 x R3</b> RCP 8.5: 1 x R1 & 2 x R2	RCP 4.5: 1 x R1 & 2 x R2 RCP 8.5: 2 x R2 & <b>1 x R3</b>
4	Droughts: 3 types: GW, Crops & Ecology	RCP 4.5: 1 x R2 & <b>2 x R3</b> RCP 8.5: Same	RCP 4.5: 1 x R3 & <b>2 x R4</b> RCP 8.5: Same
5	High Winds: 3 types: Port Ops/Coastal Topping, Bldgs/Infra, Dust Impacts on public health	RCP 4.5: 2 x R1 & <b>1 x R4</b> RCP 8.5: Same	RCP 4.5: 2 x R1 & <b>1 x R4</b> RCP 8.5: Same
6	Sea Level Rise: 3 types: Corrosion/damage, erosion/shoreline, loss of freshwater/agriculture	RCP 4.5: 3 x R2 RCP 8.5: 1 x R2 + <b>2 x R3</b>	RCP 4.5: 1 x R2 & <b>2 x R3</b> RCP 8.5: Same

## Climate Change Adaptation using Managed Aquifer Recharge

○ Chaiwat EKKAWATPANIT<sup>1\*</sup>, Chanchai PETPONGPAN<sup>1</sup>, &

Duangrudee KOSITGITTIWONG<sup>1</sup>

<sup>1</sup>Civil Engineering Department, King Mongkut's University of Technology Thonburi, 126 Prachautit Rd. Bangkok 10140, Thailand.

\*E-mail: chaiwat.ekk@kmutt.ac.th

### Abstract

Among numerous approaches to responding to hydro-climatic extreme events such as floods and drought, the conjunctive use of surface water and groundwater is one effective option. Flooding can be mitigated by keeping surplus water during the wet season in the aquifer and, meanwhile, using the groundwater storage to deal with a water deficit issue in the dry season. The purpose of this study is to investigate the Managed Aquifer Recharge approaches for the holistic management of surface water and groundwater. The SWAT-MODFLOW model is performed to simulate the surface water-groundwater regime of the vulnerable region in Thailand under the future climate scenarios from 2021–2040. The results show that about 2,000 recharge wells can be installed in the most suitable areas to inject the water into the aquifer layer. Under the minimum and maximum Green House Gas emission scenarios (RCPs 2.6 and 8.5), recharging groundwater at 550-900 m<sup>3</sup>/day causes 22x10<sup>6</sup> m<sup>3</sup> of groundwater storage while reducing 500x10<sup>6</sup> m<sup>3</sup> of flood volume. From 2031–2040, the groundwater storage can be increased by 48x10<sup>6</sup> m<sup>3</sup> due to a recharge rate of 1,000–1,400 m<sup>3</sup>/day under RCP 2.6 and 1,400–1,800 m<sup>3</sup>/day under RCP 8.5. The surface water seems to have decreased by 940x10<sup>6</sup>-1,120x10<sup>6</sup> m<sup>3</sup>. The achieved approaches can be applied to create primary proactive plans in the conjunctive use of water to prepare for climate change impacts in the future.

**Keywords:** Managed Aquifer Recharge; Surface water-Groundwater simulation; Climate change; Hydrological modeling.

### 1 Introduction

The conjunctive use of surface and groundwater relates to the combined management and development of surface water and groundwater for sustainable water use in general. The purpose of this water management strategy is to improve the holistic resilience of water supply, particularly in areas with high water availability throughout the seasons, by utilizing surface water and groundwater systematically. As mainly focused, groundwater is used to play an advantageous role in water storage, distribution, and treatment for increasing water supply coupled with improving water quality and distribution (Bertule et al., 2017).

In recent years, Managed Aquifer Recharge (MAR) has become an essential strategy for water resources management under the rising intensity of climate extremes from climate change. Groundwater is intentionally recharged into aquifers for a variety of reasons, including maintaining groundwater level and pressure, storing and recovering water for future use, and protecting the environment (land subsidence and salt-water intrusion prevention). Research regarding MAR in terms of economics, governance, operation, risk assessment, and public acceptance has been undertaken. Over the past few decades, the MAR project has been implemented at an average of 5% per year, but it is not sufficient to respond to an increase in groundwater extraction (Dillon et al., 2019).

Thus, it is demonstrated that the conjunctive use of surface water and groundwater plays an increasingly important role in the climate change adaptation strategy. This study takes into account the potential of this water resources

management approach to cause an effective implementation with the least impact on the local people. The conjunctive use of surface water and groundwater approaches is applied to a simultaneous simulation of surface water and groundwater under the various climate scenarios in the future by using the SWAT-MODFLOW model.

### 2 Materials and methods

#### 2.1 Study area

The study area covers about 55,362 km<sup>2</sup> of the Yom and Nan River basins in northern Thailand by defining the outlets at runoff stations Y.5 and N.8A (Fig.1). The ground surface elevation is between 25 and 2,091 m(MSL). The climate conditions are mainly influenced by the depression, Southwest monsoon, and Northwest monsoon of the South China Sea, especially during July-September. Over the period of 36 years (1981–2016), annual rainfall in the Yom River basin is almost 1,200 mm, while the Nan River basin is 1,300 mm. 90% of rainfall in both basins occurs between May and October, with the highest value occurring in September at 240-250 mm. Maximum-minimum air temperatures have similar patterns in that maximum air temperatures begin an upward trend in January at 32°C and hit a peak at 37.3°C in April, then decrease continuously until the end of the year. The minimum air temperature increases from 18.7°C in January to 25°C in April, then reduces by 1.5 °C in October and further drops to the same level as in January in December. Drought events are mainly affected by long periods of intermittent rainfall that cause severe impacts on non-irrigated areas as rainfall is the main water source for

agriculture. Furthermore, immersed floods are easily caused by inconsistencies between transportation routes and water-drained sections. The Yom River basin seems to be more severely affected by flood and drought issues than the Nan River basin due to insufficient storage for storing and recovering the upstream water, while the Nan River basin has Sirikit dam.

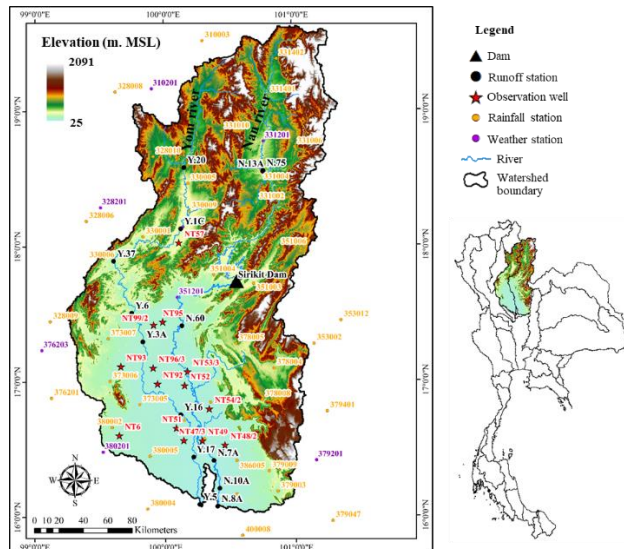


**Fig. 1. Yom and Nan River basins, Northern Thailand**

## 2.2 Methods

The SWAT-MODFLOW model, integrating the source codes of SWAT 2012 Rev.591 with MODFLOW-NWT by Bailey et al. (2016), was applied to simultaneously simulate the surface water–groundwater regime. The model was constructed by referring to the proposed in Petpongpan et al. (2021) because the model demonstrated high performance in the simulation of surface water-groundwater regimes in the Yom and Nan River basins. The daily river discharges in the calibration and validation periods have similar patterns and quantities to the observation data at 15 runoff stations. In addition, the monthly groundwater heads in both the calibration and validation periods show similar seasonal variations to the measured data at 14 observation wells.

The study area is spatially analyzed to define a suitable area for implementing conjunctive use of water in the approach of Managed Aquifer Recharge (MAR). According to the DGR report in 2020, the suitability level depends on the geology, geomorphology, soil permeability, and slope of the area. The raster files of these variables are overlaid by defining weighted factors at 0.9 (geology), 0.8 (geomorphology), 0.7 (soil permeability), and 0.6 (slope). The watershed area is classified into four suitability levels, including Unsuitable, Low Suitable, Moderate Suitable, and High Suitable (Department of Groundwater Resources, 2020).

The future climate conditions depend on the outputs of the Global Climate Model (GCM), proposed as the Representative Concentration Pathways (RCPs) by the Coupled Model Intercomparison Project 5 (CMIP5). Outputs for the historical period from numerous GCMs are initially screened by comparing them with the observation data due to different assumptions and formulas of the GCMs. Because of its significant impact on hydrologic processes, precipitation is the primary concern variable in this case. As proposed in

Petpongpan et al. (2020), MIROC5 has the most similar monthly rainfall to measured rainfall data in the Yom and Nan River basins over the period of 1981–2005. Monthly rainfall intensity presented by MIROC5 provides more significant consistency with observation data than the other nine GCMs, whether in quantity or seasonal variation. To minimize uncertainties, the original outputs of MIROC5 are adjusted to remove the systematic distributional biases from a different grid size between the global scale and regional scale. It is adequate to adjust biases for only precipitation and air temperature due to their higher influences on hydrologic processes than the other variables (Hanasaki et al., 2013). The bias correction method, namely the Change Factor Method (CFM) (Zahmatkesh et al., 2015), is applied because of its simplicity and straightforward application.

The conjunctive use of surface water and groundwater is included in the future scenario simulation to find effective adaptation approaches under various climate conditions in the future. The Managed Aquifer Recharge method is applied as the conjunctive use of water approach dealing with water resources management under the minimum (RCP 2.6) and maximum (RCP 8.5) GHG emission scenarios throughout 2021–2040. The groundwater recharge wells (dry wells) are indicated for construction near the existing groundwater pumping wells in the most suitable areas for groundwater recharge by excluding the forest area to avoid environmental impacts. During the wet season, the MODFLOW model's Wells package generates recharge wells to harvest a surplus water volume in the shallow aquifer layer for reducing flood volume and water supply in the dry season. The recharge rate is defined as a positive pumping volume by considering the expected increasing groundwater use in the Yom and Nan River basins.

## 3 Results and discussion

In the calibration period (2007–2011), the Nash-Sutcliffe Efficiency (NSE) and coefficient of determination ( $R^2$ ) values obtained from all 15 calibrated stations in the Yom and Nan River basins were higher than 0.75. For the Yom River basin, the highest values of NSE and  $R^2$  are at station Y.16 in the downstream area. The lowest value for both NSE and  $R^2$  is displayed at station Y.6, located in the middle of the basin. In the Nan River basin, stations N.60, N.7A, N10A, and N8A located in the lower part below the Sirikit dam show higher NSE and  $R^2$  values than those obtained at stations N.75, N13A, and the inflow of the dam in the upstream area. This is because of the defined outflow release of the dam, which forces a behavior of streamflow in the downstream area, especially in the dry season (November–April). The percent bias (PBIAS) values are in a range of -5.2%–12.7% for the Yom River basin and -6.4%–10.3% for the Nan River basin. Based on their positive PBIAS values, the river discharge in the Yom and Nan River basins are mostly underestimated by 0.8%–12.7%, except for stations Y.1C, Y.37, Y17, Y5, and the inflow of the Sirikit dam, for which PBIAS is negative, suggesting that flows are overestimated by 0.8%–6.4%. The greatest underestimation is 12.7% at station Y.16 and 10.3% at station N.60 for the Yom and Nan River basins, respectively. For the validation period (2012–2016), in both the Yom and Nan River basins, almost all stations show NSE and  $R^2$  values greater than 0.65. PBIAS are between -28.5% and 14.9%. All stations located in the middle and upper parts of the watershed provide positive

PBIAS values, implying that the simulated river discharge in these areas is underestimated by 1.9%–14.9%. Whereas in lower parts, river discharges are overestimated by 2.2%–28.5%, referring to their negative PBIAS. The maximum overestimation is 28.5% at station Y.16, while the maximum underestimation is 14.9% at station N.13A.

In general, the daily river discharge simulated by the SWAT-MODFLOW model is very consistent with the observation data in both patterns and quantity (Fig. 2). The simulated results are acceptable based on the NSE and R2 values. In the validation period, daily river discharges in the downstream reaches of both the Yom and Nan River basins are overestimated, even though they are underestimated during the calibration period. This may be due to the effect of calibrating the model to the high discharge rates of the great flood year of 2011. Nevertheless, the simulated daily river discharges obtained in this study present an improvement to Petpongpan et al. (2020), who simulated surface water and groundwater of the Yom and Nan River basins via the SWATMOD-Prep interface. Despite the difference in the numbers of the assessed stations, their study obtained NSE and R2 values higher than 0.75 during the calibration period (2007–2011) and higher than 0.60 during the validation period (2012–2016), which is consistent with this study. However, the simulated results of their study are mainly overestimated, especially in the Yom River basin. Most of the stations show a negative PBIAS and the highest value is -35.6%, which is higher than in this study that the estimated model error on either of these simulations is in a range of  $\pm 30\%$ .

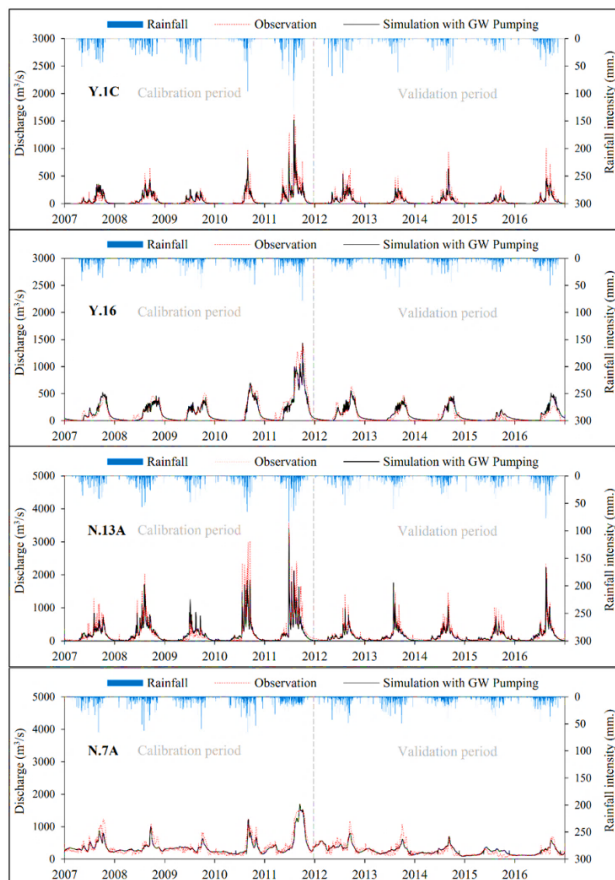


**Fig. 2. Comparison of daily river discharge from simulation and observation during 2007-2016**

**Fig. 3** presents examples of comparing monthly simulated and observed groundwater heads for simulations with and without groundwater pumping. Including groundwater pumping is more consistent with the observed data than excluding them, with the no-pumping scenario overestimating groundwater levels. The monthly groundwater levels from simulation with pumping have similar patterns and magnitude of fluctuation compared to the observed data, likely due to the seasonal drawdown and recovery patterns caused by the pumps operating during the growing season and then being shut off, as well as transpiration in both the growing and non-growing seasons.

These results indicate that the application of groundwater pumping has a significant impact on groundwater storage in the aquifer system and is necessary for the accuracy of the model. The simulated results in some locations and periods are different from observed data due to uncertainties in applying a grid-based model to a large-scale watershed such as grid cell size or spatial variability of inputs. PBIAS values show a consistent groundwater simulation with Petpongpan et al. (2020) that the groundwater heads are overestimated in the calibration period and underestimated in the validation period. However, the PBIAS numbers obtained in this study are about twice as low as in their study. Moreover, the NSE and R2 values provided in this study are greater than 0.80 for both periods of the calibration and validation, which is higher than the mainly displayed between 0.71 and 0.80 in the study of Petpongpan et al. (2020).

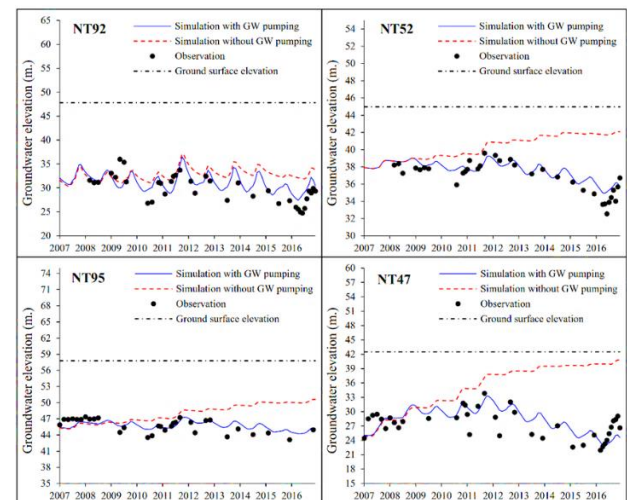


**Fig. 3. Comparison of monthly groundwater elevation from simulation and observation during 2007-2016**

The managed aquifer recharge is generated through the groundwater recharge wells (dry wells) separated into four parts (**Fig. 4**). The recharge wells are classified due to the individual surface hydrological systems and water resources management of the Yom and Nan River basins, including a different potential for groundwater recharge between the upper and lower parts of the watershed area. The lower area is defined as having higher recharge rates than the upper area because of greater topographical suitability, surface water yield, and the number of irrigation projects, which means more facilities for recharging the groundwater.

Over the period of 2021–2030, the groundwater recharge rates during the wet season at 550–600 m<sup>3</sup>/day in the upper watershed area and 820–850 m<sup>3</sup>/day in the lower area can

provide more than  $22 \times 10^6$  m<sup>3</sup> annual groundwater volume under the scenario RCP 2.6. While, in order to provide the same amount of additional groundwater volume under the scenarios RCP 8.5, the recharge rates are increased to 650-700 m<sup>3</sup>/day in the upper area and to 850-900 m<sup>3</sup>/day in the lower area. Due to these managed aquifer recharge approaches, the surplus surface water volume can be reduced by about  $530 \times 10^6$  m<sup>3</sup> under the scenario RCP 2.6 and  $570 \times 10^6$  m<sup>3</sup> under the scenario RCP 8.5, on average. During 2031–2040, a recharge rate at 1,400, 1,800, 1,200, and 1,650 m<sup>3</sup>/day in the upper Yom, lower Yom, upper Nan, and lower Nan River basins, respectively, causes more than  $48 \times 10^6$  m<sup>3</sup> annual groundwater volume and a decrease of  $1,120 \times 10^6$  m<sup>3</sup> surface water volume under the scenario RCP 2.6. Under RCP 8.5, a  $48 \times 10^6$  m<sup>3</sup> of groundwater volume can be added to a  $940 \times 10^6$  m<sup>3</sup> of surface water volume from recharge rates of 1,150 (upper) and 1,500 (lower) m<sup>3</sup>/day in the Yom River basin, as well as 1,000 (upper) and 1,400 (lower) m<sup>3</sup>/day in the Nan River basin.

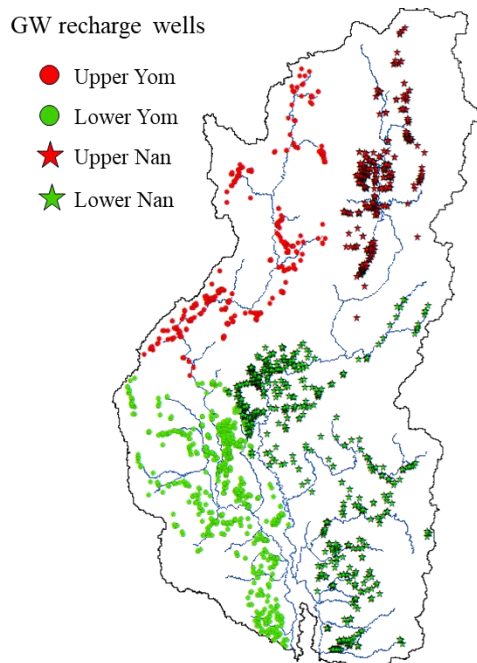


**Fig. 4. Classification of groundwater recharge wells for the managed aquifer recharge**

Under scenarios RCP 2.6 and RCP 8.5, the managed groundwater recharge rate in the upper Yom River basin is lower than the upper Nan River basin, while it seems higher in the lower area. whereas, under both GHG emission scenarios, the Yom River basin recharge rates are greater than those of the Nan River basin in both upper and lower areas between 2031 and 2040. In addition, the managed recharges to the aquifer in the whole watershed area defined during 2031–2040 under the scenario RCP 8.5 have lower rates than under the scenario RCP 2.6. Because of the effects of climate change, a high amount of annual rainfall combined with slightly decreasing air temperatures can result in less groundwater recharge required. However, due to the limited capacity of the groundwater recharge wells applied as the dry well method, it might not be able to harvest the targeted amount of water in some years. Therefore, increasing the number of recharge wells should be taken into account for

more contributing to groundwater recharge responding to increments in air temperature and water demand in the future.

#### 4 Conclusions

Almost 2,000 groundwater recharge wells can be generated in the highly suitable areas near the existing groundwater pumping wells for conjunctive use of surface water and groundwater using the managed aquifer recharge method. Recharging groundwater with a rate of 550-700 m<sup>3</sup>/day in the upper and 820-900 m<sup>3</sup>/day in the lower Yom and Nan River basins during 2021–2030 under the scenarios RCP 2.6 and RCP 8.5 can produce more annual groundwater storage volume at  $22 \times 10^6$  m<sup>3</sup> coupled with a decreasing  $530 \times 10^6$ - $570 \times 10^6$  m<sup>3</sup> surplus volume of surface water. Under scenario RCP 2.6 (RCP 8.5), the recharge rate for the upper Yom, lower Yom, upper Nan, and lower Nan River basins is 1,400 (1,150), 1,800 (1,500), 1,200 (1,000), and 1,650 (1,400) m<sup>3</sup>/day, respectively, to increase a  $48 \times 10^6$  m<sup>3</sup> of groundwater volume during 2031-2040. Based on this managed aquifer recharge, the surplus surface water is reduced to  $1,120 \times 10^6$  m<sup>3</sup> under scenario RCP 2.6 and to  $940 \times 10^6$  m<sup>3</sup> under scenario RCP 8.5, on average.

#### Reference

- [1] Bertule, M., Rosendahl, L., Spensley, J., Lærke, S. and Naswa, P., A Practitioner's Guide to Adaptation Technologies for Increased Water Sector Resilience, Climate Change Adaptation Technologies for Water, (2017).
- [2] Bailey, R.T., Wible, T.C., Arabi, M., Records, R.M. and Ditty, J., Assessing regional-scale spatio-temporal patterns of groundwater-surface water interactions using a coupled SWATMODFLOW model, Hydrological Processes, 30 (2016) 4420-4433.
- [3] Dillon, P., Stuyfzand, P., Grischek, T., Lloria, M., Pyne, R.D.G., Jain, R.C., Bear, J., Schwarz, J., Wang, W., Fernandez, E., Stefan, C., Pettenati, M., Gun, J.V.D., Sprenger, C., Massmann, G., Scanlon, B.R., Xanke, J., Jokela, P., Zheng, Y., Rossetto, R., Shamrukh, M., Pavelic, P., Murray, E., Ross, A., Bonilla Valverde, J.P., Palma Nava, A., Ansems, N., Posavec, K., Ha, K., Martin, R. and Sapiena, M., Sixty years of global progress in managed aquifer recharge, Hydrogeology Journal, 27 (2019) 1-30.
- [4] Department of Groundwater Resources, Managed Aquifer Recharge approaches in Thailand, (2020).
- [5] Hanasaki, N., Fujimori, S., Yamamoto, T., Yoshikawa, S., Masaki, Y., Hijioka, Y., Kainuma, M., Kanamori, Y., Masui, T., Takahashi, K. and Kanae, S., A global water scarcity assessment under Shared Socio-economic Pathways - Part 2: Water availability and scarcity, Hydrology and Earth System Sciences, 17 (2013) 2393-2413.
- [6] Petpongpan, C., Ekkawatpanit, C. and Kositgittiwong, D., Climate Change Impact on Surface Water and Groundwater Recharge in Northern Thailand, Water, 12 (2020) 1029.
- [7] Petpongpan, C., Ekkawatpanit, C., Bailey, R.T. and Kositgittiwong, D., Improving integrated surface water-groundwater modelling with groundwater extraction for water management, Hydrological Sciences Journal, 66 (2021) 1-18.
- [8] Zahmatkesh, Z., Karamouz, M., Goharian, E. and Burian, S.J., Analysis of the Effects of Climate Change on Urban Storm Water Runoff Using Statistically Downscaled Precipitation Data and a Change Factor Approach, Journal of Hydrologic Engineering, 20 (15).

# Minecraft as a tool for disaster education: A case study of flood inundation in Fukushima, Japan

○ Keisuke ONO<sup>1\*</sup>

<sup>1</sup>Department of Civil Engineering and Management, Tohoku Institute of Technology,  
Miyagi 982-8577, Japan.

\*E-mail: onokeisuke@tohtech.ac.jp

## Abstract

Education is key for reducing children's risks to disasters. This study developed a 1/1-scale flood hazard map in the game Minecraft, one of the most popular video games among kids. The city data in a 3D format was derived from Project PLATEAU by the Ministry of Land, Infrastructure, Transport and Tourism (MLIT), and transformed into a format readable in Minecraft. Finally, the hazard map in Minecraft was developed and compared with a hazard map in a 2D format. The developed world successfully represented actual topography, shape of buildings and roads, and flood inundation area in the watershed, where game players can manipulate their avatar and experience the flood hazard in the reproduced virtual 3D world. This result indicated that the flood hazard map in Minecraft can be a potential tool for disaster education.

**Keywords:** Minecraft; disaster education; flood inundation area; hazard map

## 1 Introduction

Floods are becoming more frequent throughout the world in a changing climate. In Japan, serious floods are causing inundation damage almost every year. As a non-structural countermeasure against floods, Japanese river administrators, such as the Ministry of Land, Infrastructure, Transport and Tourism (MLIT), and prefectural governments, designate potential areas of flood inundation as "flood inundation areas", covering 99% of major river streams in the country. Based on the inundation areas designated, municipalities prepare and disseminate flood hazard maps to the residents. Many reports indicate that the hazard map demonstrated a high reliability in several historical floods in the country.

Regarding the use of flood hazard maps by citizens, municipalities disseminate the maps in a paper format, make them available in their city websites, and conduct disaster drills based on the maps. These activities have improved the understanding of flood risk among citizens who have a high degree of disaster awareness and who are capable to access to related disaster information. On the other hand, youth citizen in compulsory education, such as elementary or junior high school students, sometimes have a less awareness or less access to disaster information. Given the basic idea of disaster prevention and mitigation in Japan is based on a self-help and mutual-help, it is important to provide disaster information in an improved format for the youth, so that they can understand the flood hazard in their community and make appropriate decision by themselves in a moment of floods.

Past studies reported the usefulness of video games in city planning and disaster education. For example, a United Nations project used the game Minecraft to have citizens virtually build improvements in their communities [1]. UNDRR made an online game on disaster risk reduction where students can play multiple disaster scenarios including tsunami, wildfire, and earthquake [2]. However, these studies targeted certain scenarios in a fictional area, which unable students to play the game in their actual life space; the watershed where their community belong.

Education is key for reducing children's risks to disasters. Given the fact that appropriate evacuation action depends on the flood hazard in the areas, it is important to present the flood hazard in a format which is easy for students to understand. Therefore, this study developed a hazard map in the game Minecraft, one of the most popular video games among kids, where students can learn the hazard posed by flood inundation. As a pilot case study, this study targeted Koriyama city in Fukushima, Japan, which experienced a serious flood inundation in recent years. Finally, this study gives an insight of advantages of the developed map, challenges, and future works.

## 2 Materials and methods

### (1) Minecraft

Minecraft is a java base first person multiplayer sandbox game. Categorized as virtual world game, Minecraft is a game about placing blocks, where player is requires gathering object to create environment around it at will. Minecraft is a game that created and published by Mojang, an indie game Developer Company in 2009 for home computer and later the mobile version for iOS and android in 2012. Minecraft is the best-selling video game of all time, with over 238 million copies sold and nearly 140 million monthly active players as of 2021. This study used Minecraft Java Edition to create flood hazard map in the virtual world.

### (2) Dataset

The 3D data of terrain, building shape, road shape, water body (e.g., rivers and lakes), and flood inundation area, were downloaded from the website of Association for Promotion of Infrastructure Geospatial Information Distribution. In the website, "Project PLATEAU", a leading program of 3D city data by MLIT, disseminate the data for free of charge [3]. The data format is CityGML for terrain, building shape, and road shape, and Geodatabase for water body and flood inundation area.

### (3) Data transformation

Development of virtual world in Minecraft needs a data transformation from CityGML and Geodatabase to a format which Minecraft can import. The data transformation was conducted by FME Desktop software developed by Safe Software Inc. This software is the data integration platform that allows users to connect and transform data between hundreds of systems, with the best support for spatial data. In the transformation, all of the 3D data were converted to a format of Minecraft with a scale of 1/1, where one block represent an object of 1m<sup>3</sup> (1 m x 1 m x 1 m) in the actual world.

### 3 Results and discussion

The figure 1 shows an overview of flood hazard map in 2D format in a website [4] and 3D format in Minecraft. In the map of Minecraft, the virtual world shows ground surface with blocks of “Grass” (Green), building with blocks of “Podzol” (Brown), road with blocks of “Rocks” (Grey), water body with blocks of “Ice” (Light Blue), and inundation area with blocks of “Water” (Blue). The world successfully reproduces the flood inundation area in Minecraft. The blocks precisely describe the terrain of watershed, the shapes of buildings and roads, and inundation areas overlaid on the ground, where game players can manipulate their avatar and experience the flood hazard (i.e., inundation depth) in the reproduced 3D world. The area of domain modeled was 16 km<sup>2</sup>, the number of building objects processed was 20000, and total blocks placed was 100,000,000 blocks, approximately. The data transformation took about one hour for the calculation, by a personal computer with Apple M1 Pro chip and 16 GB of RAM.

The flood hazard map in Minecraft was successfully developed. However, the result raised some challenges as follows.

1) The outer edge of inundation area does not follow its surrounding terrain since the spatial resolution of flood inundation area was 25 m x 25 m.

2) The building has monochromatic and does not represent actual building color. An integration of texture data of buildings in CityGML could enable a better color representation with colorful blocks.

3) Possible domain of the world is limited to the area of the Project PLATEAU since the Project has developed the 3D data in only 56 cities selected in Japan.

### 4 Conclusions

This case study developed a 1/1-scale flood hazard map in Fukushima in the popular game Minecraft, deriving the 3D data of city from Project PLATEAU by MLIT. The developed world successfully represented actual topography, shape of buildings and roads, and flood inundation area in the watershed, indicating that the flood hazard map in Minecraft can be a potential tool for disaster education in elementary and junior high school. As a future work of this study, we have a plan of on-site lecture in a community school to demonstrate applicability of the developed world for disaster education.

### Reference

- [1] UN Habitat, Using Minecraft for Youth Participati on in Urban Design and Governance, <https://unhabitat.org/using-minecraft-for-youth-participation-in-urban-design-a-aa-governance>
- [2] UNDRR, Stop Disasters, <https://www.stopdisastersg ame.orghttps://www.mlit.go.jp/plateau/>
- [3] Ministry of Land, Infrastructure, Transport and To urism, Project PLATEAU, <https://www.mlit.go.jp/plateau>
- [4] Ministry of Land, Infrastructure, Transport and To urism, Portal site of hazard maps, <https://disaportal.gsi.g o.jp>

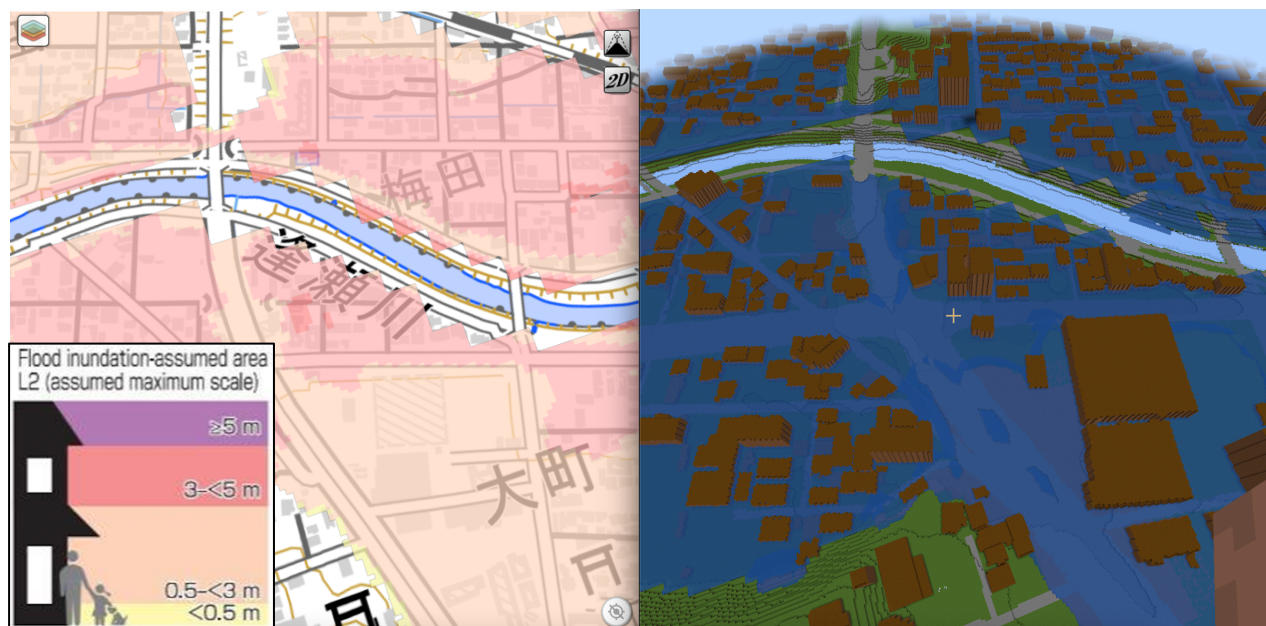


Fig. 1. Comparison of flood inundation map along Ouse river in Koriyama, Fukushima (Left: 2D inundation map derived from a website, Right: 3D inundation map in Minecraft)

# Spatio-temporal projection of the change in sustainability of Kabul River Basin under SSP scenarios

○ Mohammad Naser SEDIQI<sup>1\*</sup>, Daisuke KOMORI<sup>1,2</sup>

<sup>1</sup>Graduate School of Environmental Studies, Tohoku University, Sendai 980-8579, Japan.

<sup>2</sup>Graduate School of Engineering, Tohoku University, Sendai 980-8579, Japan

\*E-mail: [mohammad.naser.sedqi.p4@dc.tohoku.ac.jp](mailto:mohammad.naser.sedqi.p4@dc.tohoku.ac.jp)

## Abstract

In this study, reliability (Rel), resilience (Res), and vulnerability (Vul) concept, together with the 3-month standardized runoff index (SRI-3) and 12-month standardized runoff index (SRI-12), was used to assess the sustainability of the Kabul River Basin due to drought during historical (1975-2014), near future (2020-2059) and far future (2060-2099). Three downscaled global climate models (GCMs) from Coupled Model Intercomparison Project Phase 6 (CMIP6) under two shared socioeconomic pathways (SSP2-4.5 and SSP5-8.5) were used to generate the climate variables. The performance assessment of the basin was based on two thresholds level, which represent the normal and moderate dryness condition. The soil and water assessment tool (SWAT) model was used to estimate the surface runoff. The results revealed that the basin would be in an unsustainable condition compared to the historical period and would be in a very low performance level when not considering adaptation. The sustainability of the Kabul river basin would be low in the far future compared to the near future, and it would be much lower for SSP5-8.5 compared to SSP2-4.5. The study provides information on driving factors of sustainability in water resources and help policy makers in planning adaptation to climate change.

**Keywords:** Sustainability; Standardized runoff index; CMIP6-GCMs; Shared socioeconomic pathways; Kabul River Basin.

## 1 Introduction

Drought among other natural disasters has extensive and adverse impacts on the water resources, ecosystem, environment and socioeconomic development of a country, particularly in arid regions.

Drought indices are generally used to assess drought events, including their severities and durations. There are many drought indices, for instance, the Standardized precipitation index (SPI), standardized precipitation evapotranspiration index (SPEI), and standardized runoff index (SRI). Shukla & Wood, (2008) developed the SRI index to assess hydrological drought considering runoff data. The process of calculating the SRI index is the same as the SPI index and is widely used due to fewer data requirements and calculation processes.

Global climate models (GCMs) are essential for climate change and are usually used to project climatic variables (Sedqi et al., 2022). Coupled Model Intercomparison Project (CMIP) is a standard experimental framework developed by more than 30 institutions worldwide for analyzing the outputs of GCMs. The latest version of CMIP is CMIP6, which is based on the shared socioeconomic pathways (SSP) scenarios and includes future climate adaptation and mitigation.

The reliability, resilience and vulnerability (RRV) concept which was initially introduced by (Hashimoto et al., 1982) is a widely used approach to assess sustainability of a system under normal or failure conditions. Reliability measures the capability of the watershed to be in acceptable no drought condition during a period. Resilience shows the performance of the basin, where how quickly it bounces back from drought to the acceptable stage after getting to the failure state. Vulnerability measures the amount of drought severity. The critical step in RRV analysis is to introduce the threshold value, which is the transition zone between failure and

satisfactory state, and it gets a different level of performance by changing the threshold value.

The objective of this study is to assess the change in water resources sustainability of KRB, using 3-month and 12-month SRI for the two future periods based on RRV framework under different dryness conditions.

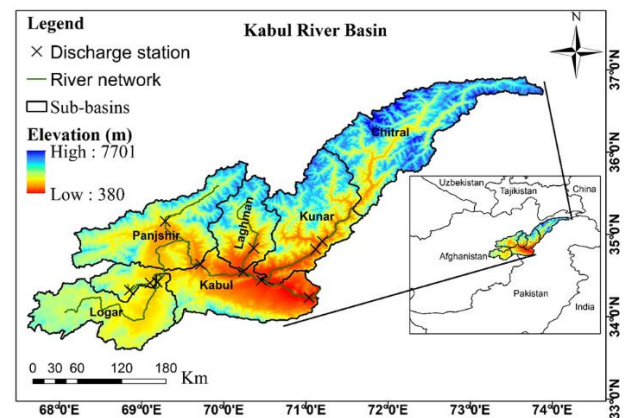


Fig. 2: Study area with its topography

## 2 Materials and methods

The meteorological data, including daily, monthly maximum (Tmax), and minimum (Tmin) air temperatures and precipitation (P), were collected from the Ministry of Energy and Water of Afghanistan. In this study, the multi-model mean ensemble of three monthly GCMs, namely ACCESS-CM2, MPI-ESM1-2-LR, and FIO-ESM-2-0, from CMIP6 which had the highest skill among other GCM models for climate change assessment over Afghanistan (Sedqi et al., 2022) used to assess sustainability of the basin

future periods of 2020-2099 under two (SSP2-4.5 and SSP58.5) scenarios.

The SWAT model was used in this study to estimate the surface runoff under future climate change scenarios. SWAT-CUP was used for calibration during from 2010 to 2020. The SRI index can be calculated by using gamma distribution function (GDF) for fitting monthly runoff data using the following equation (Thom, 1966).

$$g(x) = \frac{1}{\beta^\alpha \Gamma(\alpha)} x^{\alpha-1} e^{-\frac{x}{\beta}}, x \geq 0 \quad (1)$$

where  $\Gamma$  is an ordinary GDF,  $\alpha$  and  $\beta$  are shape and scale parameters. SRI index based has been divided into different categories shown in the table.1

**Table 1: SRI index categories**

No	Category	SRI Value
1	Mild drought	$-1 \leq \text{SRI} < 0$
2	Moderate drought	$-1.5 \leq \text{SRI} < -1$
3	Severe drought	$-2 \leq \text{SRI} < -1.5$
4	Extremely drought	$\text{SRI} \leq -2$

we selected two threshold values to assess future river basin health conditions. First, the SRI index value of -0.1, indicated the normal dryness condition. Second, the SRI index value of -0.7 that corresponds to the future average of 20 percent of the time, was chosen to represent the future drought probability condition. The RRV framework can be calculated as follows:

$$Rel = 1 - \sum_{j=1}^M \frac{d(j)}{T} \quad (2)$$

$$Res = \left\{ \frac{1}{M} \sum_{j=1}^M d(j) \right\}^{-1} \quad (3)$$

$$Vul = \frac{1}{M} \sum_{i=1}^T \left\{ \frac{L_{obs}(i) - L_{std}(i)}{L_{std}(i)} \times H \times (L_{obs}(i) - L_{std}(i)) \right\} \quad (4)$$

$$Sus = [Rel \times Res \times (1 - Vul)]^{1/3} \quad (5)$$

where M is the number of “unsatisfactory states”, d(j) is the duration of the j-th “unsatisfactory state” (the number of months spent in an unsatisfactory state), T is the total record duration (here, 12 months), Lobs(i) is the SRI value of the i-th month, and Lstd(i) is the threshold (here, threshold=-0.1, -0.7). H is the Heaviside function, which can ensure that the Vulnerability calculation only involves an “unsatisfactory state”—if M= 0, then H=0, and if M > 0, then H=1,

The sustainability index was divided into five classes, as shown in table (2)

**Table 2: SRI index categories**

No	Category	Sustainability index
1	Very high	$0.81 \leq S_{us} < 1$
2	High	$0.61 \leq S_{us} < 0.81$
3	Moderate	$0.41 \leq S_{us} < 0.61$
4	Low	$0.21 \leq S_{us} < 0.41$
5	Very low	$0 \leq S_{us} < 0.21$

### 3 Results and discussion

Fig.1 shows the calibration and validation results at Tangi Gulbahar station from 2010 to 2020. The result shows that the R2 increased to 0.84, and NSE increased to 0.74 after calibration. Validation also has a higher value of R2=0.81

and NSE=0.7. Therefore, SWAT was calibrated very well for the runoff simulation.

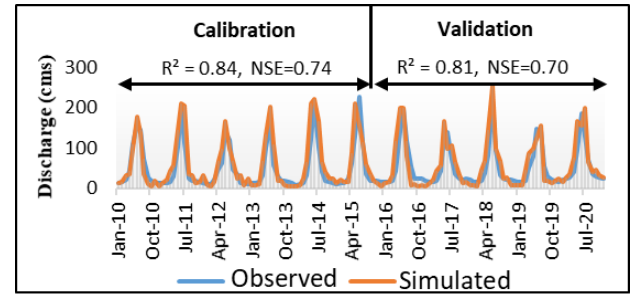


**Fig.2. Calibration and Validation of SWAT model.**

Fig.3 indicated the spatial category of based on SRI-3 and SRI-12 for two future periods and two SSPs scenarios under the threshold of -0.1 and -0.7, respectively. Under the -0.1 threshold, most of the areas of the basin for SSP5-8.5 has projected to low sustainable condition, while for SSP2-4.5 during the near and far future, only upstream of the basins falls under high to very high sustainable category. Under the -0.7 threshold, for SSP2-4.5 and SSP5-8.5, the basin's sustainability is projected to increase from very low or low to moderate, high, or even very high.

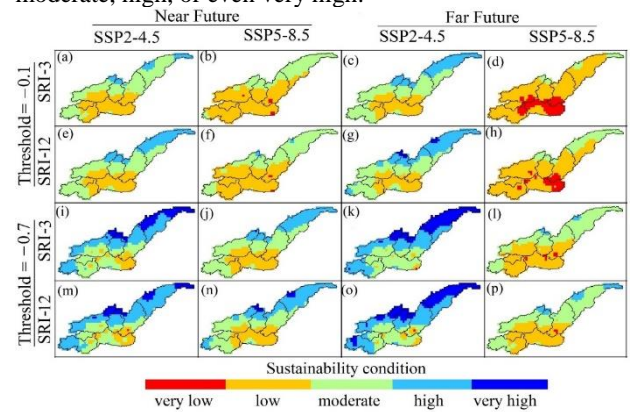


**Fig. 3. Spatial variability of reliability based on 3-month and 12-month SRI drought indicator.**

### 4 Conclusions

This study highlights the importance of improving water resources management for the KRB, where the climate is changing, and more resources are needed for irrigation due to the increasing population. RRV approach in this study has successfully quantified the impact of future climate variability on watershed sustainability.

### Reference

- [1] Sediqi MN, I., Hendrawan, A., & Komori, D. (2022). Climate Projections Over Different Climatic Regions of Afghanistan under Shared Socioeconomic Scenarios. Theoretical and Applied Climatology, 0123456789, 1–22. <https://doi.org/10.1007/s00704-022-04063-y>
- [2] Shukla, S., & Wood, A. W. (2008). Use of a standardized runoff index for characterizing hydrologic drought. Geophysical Research Letters, 35(2), 1–7. <https://doi.org/10.1029/2007GL032487>

[3] Hashimoto, T., Stedinger, J. R., & Loucks, D. P. (1982). Reliability, Resiliency, and Vulnerability Criteria. *Water Resources Research*, 18(1), 14–20.

# Identifying Landslides Using SAR, Optical Imagery and Spatial Indices in Google Earth Engine

○ Sartsin PHAKDIMEK<sup>1\*</sup>, Daisuke KOMORI<sup>1</sup>

<sup>1</sup>Graduate School of Environmental Studies, Tohoku University, Miyagi, 980-0845, Japan.

\*E-mail: sartsin.p@gmail.com, sartsin.phakdimek.q3@dc.tohoku.ac.jp

## Abstract

The study aims to detect landslides area and type using satellite images, spectral indices, and topography condition in Ehime prefecture, Japan on 2018. The sentinel-1 and sentinel-2 are utilized to calculate Normalized Difference Indices (NDIs) and amplitude change detection which detect landslides that apply with classification and regression tree (CART) on Google Earth Engine (GEE). As result of landslide detection using amplitude change detection and differential of spectral indices, the accuracy of the assessment of the landslide detection is sufficient to identify landslide which are useful for a rapid mapping after landslide event. The accuracy of model can obtain about 67.78-85.71% of detection percentage and 55.72-58.76% of quality percentage, which are moderately good for landslide detection.

**Keywords:** Landslides; Normalized Difference Indices; Amplitude change; Google Earth Engine.

## 1 Introduction

Landslides occur anywhere in the world, causing damage to humans and properties and economic losses. Rapid response to landslide events is necessary to assess the damage and save human life and properties. The detailed landslide inventories are location, land cover, morphology, type of landslide and trigger. These are used to improve understanding of landslide occurrence location, erosion quantification, and secondary hazards observation (debris flow, landslide dams, Etc.) [1]. Therefore, detecting landslides occurrence, it is necessary to develop tools with freely available data that can be used to map the landslide after catastrophic events.

Several studies have used satellite-based optical images, such as Landsat-8 and Sentinel-2, and aerial images with manual mapping approaches to provide high-quality information for landslides, floods, and other types of natural hazard mapping [2]. They are limited in terms of quick response because optical imagery requires sunlight and cloud and shadow-free conditions to identify landslides accurately. The satellite-based synthetic aperture radar (SAR) can minimize these limitations of optical imagery.

Synthetic aperture radar (SAR) can penetrate clouds and acquire data day and night. That can be beneficial for rapid mapping of event landslides triggered by intense or prolonged rainfall, but its limitation is geometric shading and distortion). The SAR radar amplitude and coherence-based change detection can also be used to identify landslides when there are changes in ground surfaces properties (reflectance, roughness, dielectric properties) pre- and post-landslide events [3]. The coherence-based change detection methods work well in urban areas because the coherence is generally high before a landslide event, and the coherence reduces from damage after the event. In mountainous areas with dense vegetation where landslides occur, the amplitude-based change detection method outperforms the coherence-based method. The coherence change is always low, while the amplitude change is apparent.

The main objective of this study was to investigate how multi-temporal image composite approaches can be used to improve accuracy of landslide detection in change detection images on Google Earth Engine (GEE), which combine SAR

for minimize limitation of optical image by Sentinel-1 and spectral indices by Sentinel-2 from open-source satellite images, the classification and regression trees (CART) is applied to evaluate in the identification of landslide in the classification phase. As part of this study, landslide inventories were obtained from previous researches and manually satellite image identification. Then, this study explored change detection approaches with machine learning, with sentinel-1 images with VV- and VH-polarized data, and with NDVI, BSI, and BI in sentinel-2 images.

## 2 Materials and methods

Study site is Ehime prefecture, Japan. Ehime landslide event were triggered by more than 400 mm of precipitation on 5 to 8 July 2018. There were 413 landslide disaster sites, and the minimum, mean, and maximum slope angle is 5, 25, and 33 degrees, respectively.

This study uses SAR amplitude data from the Copernicus Sentinel-1 (S1) satellite constellation. Satellite S1 carries a C-Band radar sensor with a wavelength of 5.6 cm. The spatial resolution of the S1 Ground Range Detected (GRD) Interferometric Wide Swath (IW) product is 20 x 22 m. The Ground Range Detected (GRD) products on GEE are processed to remove thermal noise and are radiometric and terrain calibrated using the SRTM DEM. Potential landslides examining the change in amplitude, Aratio, defined as the pre-event stack minus post-event stack,  $A_{pre} - A_{post}$ ,  $A_{pre} - A_{post}$  is equivalent to the standard amplitude ratio approach following Eq. (1).

$$A_{ratio} = \log_{10} \frac{A_{pre}}{A_{post}} \quad (1)$$

where  $A_{pre}$  is amplitude of pre-event and  $A_{post}$  is amplitude of post event. Aratio can be either positive or negative, with positive values corresponding to a decrease in SAR amplitude after a landslide event. The SAR amplitude changes following landslide events because landslides cause major changes in ground surface properties that alter the radar reflectance, hillslope geometry, roughness, and dielectric properties [3].

Sentinel-2 images have been used to analyze pre- and post-landslide event. The data selection was made based on the

cloud cover estimates (<10%) provided by the European Space Agency (ESA) on the Google Earth Engine (GEE). To detect landslide by spectral indices, normalized difference vegetation index (NDVI), bare soil index (BSI), and brightness index (BI) are calculated by Eq (2) to (4).

$$NDVI = \frac{(NIR-RED)}{(NIR+RED)} \quad (2)$$

$$BSI = \frac{(SWIR+RED)-(NIR+BLUE)}{(SWIR+RED)+(NIR+BLUE)} \quad (3)$$

$$BI = \sqrt{BLUE^2 + GREEN^2 + RED^2} \quad (4)$$

The results of the processing routine indicate a normalized percentage of the NDVI gained or lost. The rdNDVI is lost as potential landslide and rdNDVI is gain as non-potential landslide. The differential bare soil index (dBSI) and brightness index (dBI) take the spectral response before and after the landslide event. The area with presence of landslides will appear with negative values. [3,4]

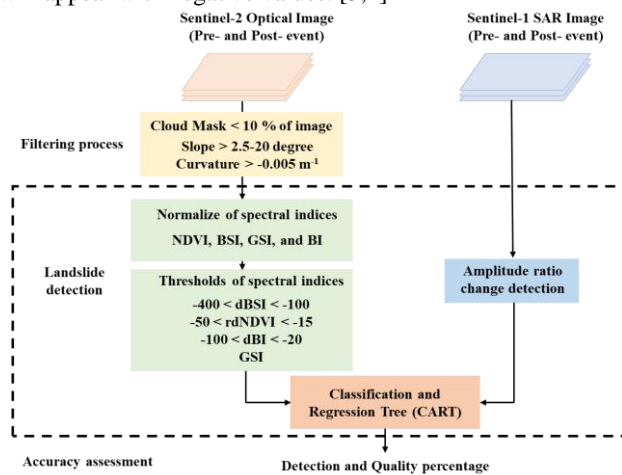


Fig. 1. Landslide detection framework.

### 3 Results and discussion

As a result of landslide detection using amplitude change detection and differential of spectral indices, the accuracy of the assessment of the landslide detection model was obtained for the total number of landslides and area detected by classification and regression tree (CART) based on semi-automatic classification. Wise accuracy for all landslide in the study area in the Ehime landslide event are provided in Fig. 2. The model's accuracy could obtain about 67.78-85.71% of detection percentage and 55.72-58.76% of quality percentage, which are moderately good for landslide detection. However, the false detection of the model is bare soil areas such as roads, farmland., and urban areas, which have shown on the low slope. The slope filtering has been applied with a landslide detection model to solve this issue. Figure 3 presented a slope filtering application with a landslide detection model. The 7.5 to 15-degree results were high in detection percentage and fitted with actual landslide scars. The detection percentage of 7.5 to 15 degree of slope filtering is 80.04-85.71%. For slope filtering 2.5-5 degrees, the false detection was bare soil area on low area, but the slope filtering 17.5-20 degrees, the detection percentage decreased by missing detection on landslide area. The detection percentage of 2.5-5 and 17.5-20 degree of slope filtering is 67.78-72.65%.

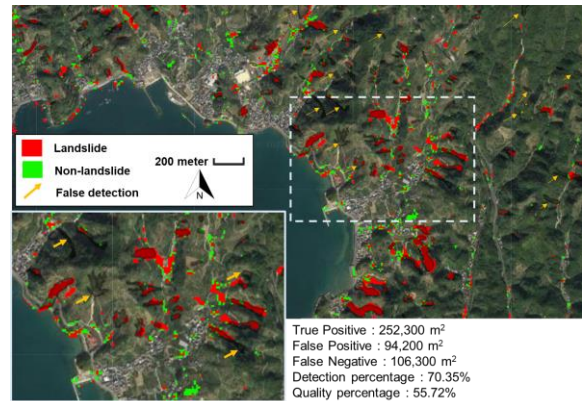


Fig. 2. Landslide detection with slope filtering 5 degree at Ehime landslide events.

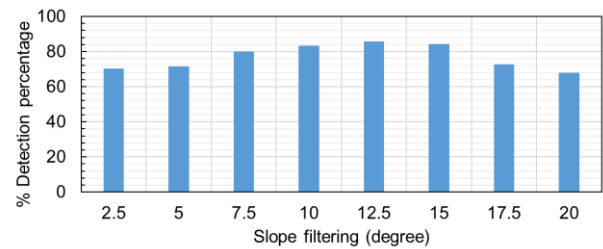


Fig. 3. Detection percentage of landslide detection model with slope filtering in Ehime landslide event.

### 4 Conclusions

Rapid response to landslide events is necessary to assess the damage and save human life and properties. Therefore, the landslide detection model is necessary to develop tools with freely available data that can be used to map the landslide after catastrophic events. As a result of the amplitude changes detection, rdNDVI, dBSI, dBI indices, and slope filtering with classification and regression tree (CART, semi-automatic) on GEE is sufficient to identify landslides which are useful for rapid mapping after landslide events. The accuracy of the model can obtain about 67.78-85.71% of detection percentage and 55.72-58.76% of quality percentage, which are moderately good for landslide detection.

### Reference

- [1] Kirschbaum, D. and Stanley, T. (2018) Satellite-based assessment of rainfall-triggered landslide hazard for situational awareness, *Earth's Future*. 6(3), 505-523,
- [2] Scheip, C.M. Wegmann, K.W., (2021). HazMapper: A global open-source natural hazard mapping application in Google Earth Engine. *Nat. Hazards Earth Syst. Sci.* 21 (5), 1495-1511, 2021.
- [3] Handwerker, A. L., Jones, S. Y., Huang, M.-H., Amatya, P., Kerner, H. R., and Kirschbaum, D. B. (2020). Rapid landslide identification using synthetic aperture radar amplitude change detection on the Google Earth Engine, *Nat. Hazards Earth Syst. Sci.*, <https://doi.org/10.5194/nhess-2020-315>.
- [4] Alexander, A., Norma, A.D., Hannah, K., Gerhard Kemper. (2021) Landslide detection in central America using the differential bare soil index, *The international archives of the photogrammetry, Remote Sensing and Spatial Information Science*, XXIV ISPRS Congress.

## Decadal variations of drought indicators in Indonesia from 1981 - 2020

○ Amalia Nafisah Rahmani IRAWAN<sup>1\*</sup> & Daisuke KOMORI<sup>1,2</sup>

<sup>1</sup>Graduate School of Environmental Studies, Tohoku University, Miyagi 980-8572, Japan.

<sup>2</sup>Department of Civil and Environmental Engineering, Tohoku University, Miyagi 980-8579, Japan.

\*E-mail: amalia.nafisah.rahmani.irawan.q3@dc.tohoku.ac.jp

### Abstract

The Intergovernmental Panel on Climate Change (IPCC) reported that the world's temperature is expected to increase by around 1.5°C in 2030. One of the impacts of this temperature increase is the variability of the rainfall pattern and the rainfall amount which is not evenly distributed globally. This condition can lead to more severe drought disasters in some regions. Because drought event can reduce the water availability, both surface and groundwater, eventually it will also affect human aspect which has a high dependency on water for various sector like domestic, industry, agriculture, and so on. Many drought indexes have been developed for drought assessment, one of them is the Standardized Precipitation Index (SPI) found by McKee et al., in 1993 which only requires long term precipitation data for the input. Based on probability distribution and normalization, SPI is able to assess the wet and dry conditions.

This research used SPI-3 to assess various drought indicators including frequency, duration, severity, and intensity in Indonesia from 1981 – 2020. The precipitation dataset was obtained from the Multi-Source Weighted-Ensemble Precipitation (MSWEP) which provide monthly precipitation with 0.1° resolution from 1979 – present date. Based on the assessment, the drought frequency, duration, severity, and intensity tend to increase in the recent decade especially in South Sumatera and Java Island. However, the worst drought event occurred in 1991 – 2000 where the precipitation was recorded as the lowest compared to the other decades. This study will be beneficial to assess the hotspot region to consider the appropriate drought mitigation and preparedness.

**Keywords:** Drought; SPI; Decadal Variation; Indonesia.

### 1 Introduction

There are many hazards related to the climate that affect human life, one of them is drought. According to the World Meteorological Organization (WMO), drought can be defined as a slow on-set phenomenon caused by a lack of rainfall. Drought is often called a creeping disaster because unlike floods that occur during relatively short periods of time, drought impacts build overtime and take a quite longer time compared to other climatological hazards, for example floods or landslides.

According to Wilhite [8], there are four types of droughts which can be understood simply as the deficiency of different variables of hydrological process. The first one is meteorological drought which started from the deficiency of precipitation that could cause less water going to soil and higher evapotranspiration rate. Over time, the agricultural drought will occur because of the depletion of soil moisture [3] that affected crop production. Hydrological drought occurs when there is low water supply on surface and groundwater. If there is still lack of precipitation, the socioeconomic drought when demands exceed supply might occur and affect the social, economic, and environmental aspect. From this understanding, many precipitation-based indexes were developed for drought assessment, one of which is Standardized Precipitation Index (SPI).

SPI was found by McKee et al., in 1993 [4] that it can be used for drought assessment and only needs the long-term precipitation data (minimum 20-30 years). By using the probability density function and normalization, the SPI can assess the wet and dry conditions over any regions (drought occurred where  $SPI \leq -1$ ). Another benefit of SPI is the

temporal versatility so it can be calculated for various timescale according to user's interest (WMO, 2012) [9]. In this research, SPI-3 was chosen as the drought index that represent not only the rainfall deficiency but also as the appropriate temporal scale to examine drought impact to vegetation [1,2,5]. This research was conducted to assess the decadal variations of drought event in Indonesia from 1981 – 2020. Further study of this research will be beneficial to examine the hotspot region to consider the appropriate drought mitigation and preparedness.

### 2 Materials and methods

The SPI analysis was conducted using monthly precipitation obtained from the MSWEP dataset over Indonesia with 0.1° resolution from January 1981 – December 2020. Then various drought indicators were assessed as follows:

#### 1. Frequency

Frequency is the total number of drought event. According to McKee et al., [4] drought event is defined as a period when the SPI value is -1 until it becomes positive.

#### 2. Duration

The duration of a drought event can be calculated as the number of months between its start (included) and end month (not included) [6].

#### 3. Severity

Drought severity is the absolute value of the cumulative SPI values during the drought event [7].

#### 4. Intensity

Drought intensity can be defined as the ratio between drought severity and drought duration for each drought event

[7]. The larger the drought intensity value means more severe drought event.

### 3 Results and discussion

#### (1) Drought frequency

Figure S1 in the appendix shows that drought event becomes more frequent in the recent decades, especially in West Kalimantan, South Sumatera, and Java Island. However, the period from 1991 – 2000 was the decade with the most frequent drought events. According to the precipitation analysis show in Fig. 1., this is occurred because during that period the precipitation distribution was the lowest compared to other decades, especially during the dry season from May – October.

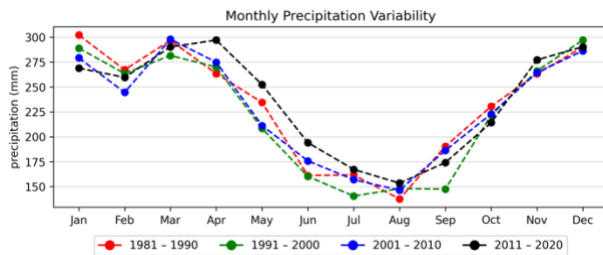


Fig. 1. Monthly precipitation variability.

#### (2) Drought duration

Figure S2 in the appendix also shows that drought event tends to be longer in recent decades, especially in Java Island, Sulawesi Island, and South Sumatera. The result showed that those regions suffered from drought condition with a total of 45 – 65 months or around 37.5 – 55% of its months is a drought month within a decade. Moreover, considering that those regions is the main producer of agricultural product (especially Java Island), more attention is needed to reduce the drought impact to agricultural sectors in the future.

#### (3) Drought severity

Figure S3 in the appendix shows the total of drought severity for each decade. Like the previous indicators, the drought severity also has a tendency to become more bigger in the recent years. But, due to the precipitation variability as shown in Fig. 1., the period from 1991 – 2000 was a decade with the biggest total drought severity in Indonesia.

#### (4) Drought intensity

Lastly, Figure S4 in the appendix shows the drought intensity for each decade. This result also indicated the average of drought intensity for one drought event in a specific region. The darker blue color indicated that those region during the specific decades suffered from more severe drought. If we compared it with the result of drought frequency, we could distinguish the region into two categories: 1) has more frequent but with a relatively less severe drought event and 2) has less frequent but with a relatively more severe drought event.

It can be seen that Java Island as the main producer of agricultural product is belong to the former category, the region which suffered from more frequent drought event with less severity. Thus, the attention to adapt and mitigate the drought impact should be put into those regions. It can be achieved by developing the appropriate drought preparedness and mitigation system in order to reduce the drought impact in the future, especially to ensure the food security.

### 4 Conclusions

This drought assessment was conducted to examine the decadal variation of drought indicators in Indonesia from 1981 – 2020. The result showed that the frequency, duration, severity, and intensity of drought events tends to be longer and bigger in recent years. However, the period from 1991 – 2000 can be categorized as the most extreme drought events indicated by the most frequent drought events, most longer drought duration, and most bigger drought severity and intensity. This extreme drought decade caused by the lowest precipitation distribution compared to other decades, especially during the dry season.

Based on the result, the Java Island as the main producer of agricultural product in Indonesia is the region which we should put more attention into with the characterization of drought event in those regions that occurred more frequent compared to the others, even though with less severity. The development of appropriate drought mitigation and preparedness is important to reduce the drought impact, especially, to ensure the food security in the upcoming decades where the food demand is expected to increase along with the population increase.

### References

- [1] Ali, U.K. (2001). Using the SPI to Analyze Spatial and Temporal Patterns of Drought in Turkey. Drought Network News (1994- 2001). Paper 49.
- [2] Ji, L., & Peters, A. J. (2003). Assessing vegetation response to drought in the northern Great Plains using vegetation and drought indices. Remote Sensing of Environment, 87(1), 85–98. doi:10.1016/s0034-4257(03)00174-3.
- [3] Legesse G. (2010), Agricultural Drought Assessment Using Remote Sensing and GIS Techniques. MSc. Thesis, Addis Ababa University, Ethiopia.
- [4] McKee, T. B., Doesken, N. J. and Kleist, N. J. (1993): The relationship of drought frequency and duration to time scales. Proceedings, 8th Conference on Applied Climatology, 17-22 January, 1993, Anaheim, pp. 179-184.
- [5] Patel, N. R., Chopra, P., & Dadhwal, V. K. (2007). Analyzing spatial patterns of meteorological drought using standardized precipitation index. Meteorological Applications: A journal of forecasting, practical applications, training techniques and modelling, 14(4), 329-336.
- [6] Spinoni, J.; Naumann, G.; Carrao, H.; Barbosa, P.; Vogt, J. World drought frequency, duration, and severity for 1951–2010. Int. J. Climatol. 2014, 34, 2792–28.
- [7] Tan, C., Yang, J., & Li, M. (2015). Temporal-spatial variation of drought indicated by SPI and SPEI in Ningxia Hui Autonomous Region, China. Atmosphere, 6(10), 1399-1421.
- [8] Wilhite, D. A. (2000). Drought as a natural hazard: concepts and definitions
- [9] World Meteorological Organization, 2012: Standardized Precipitation Index User Guide (M. Svoboda, M. Hayes and D. Wood). (WMO-No. 1090), Geneva.

## Appendix

### Decadal Variation of Drought Frequency

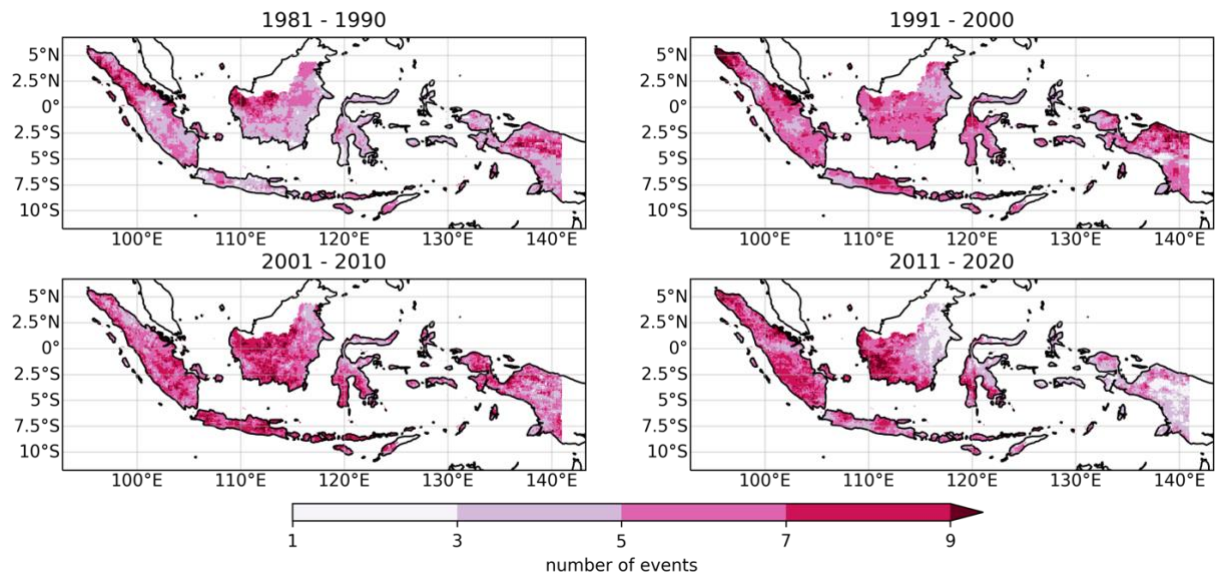


**Figure S 1** The decadal variation of drought frequency in Indonesia from 1981 – 2020.

### Decadal Variation of Total Drought Duration

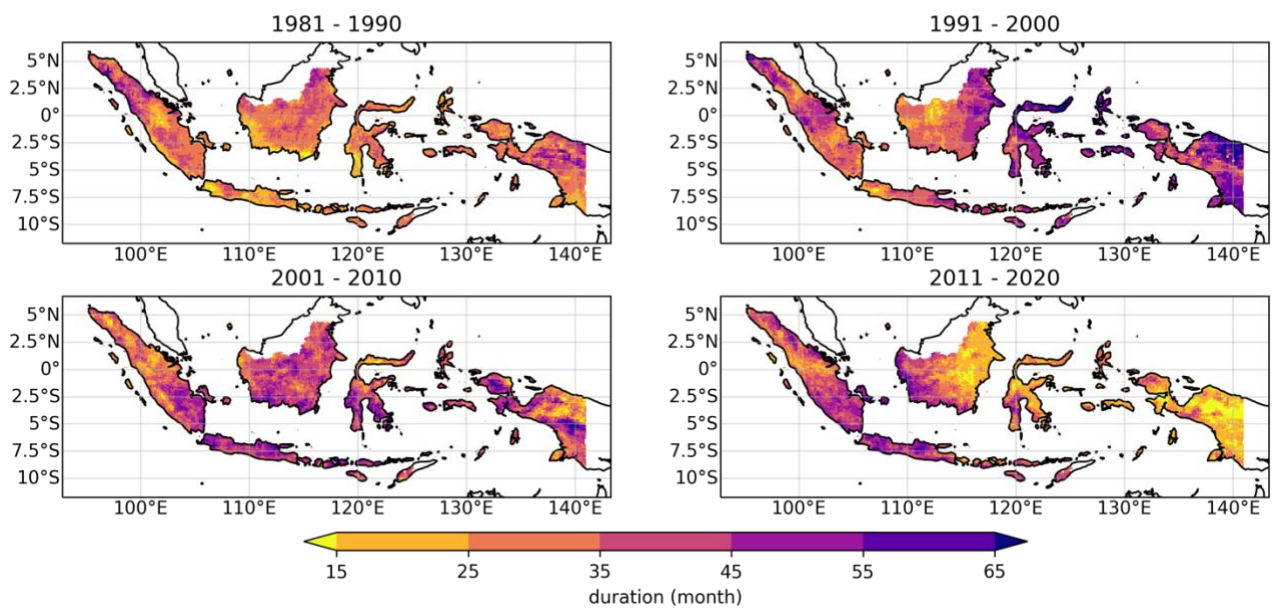


**Figure S 2** The decadal variation of drought duration in Indonesia from 1981 – 2020.

### Decadal Variation of Total Drought Severity

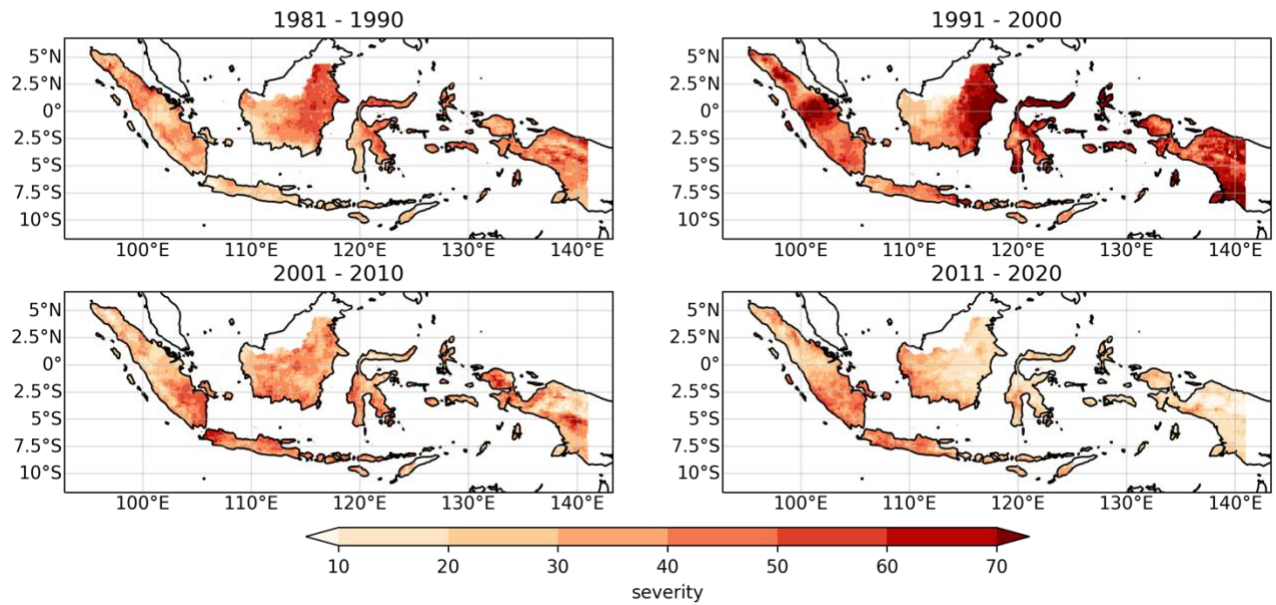


**Figure S 3** The decadal variation of drought severity in Indonesia from 1981 – 2020.

### Decadal Variation of Total Drought Intensity

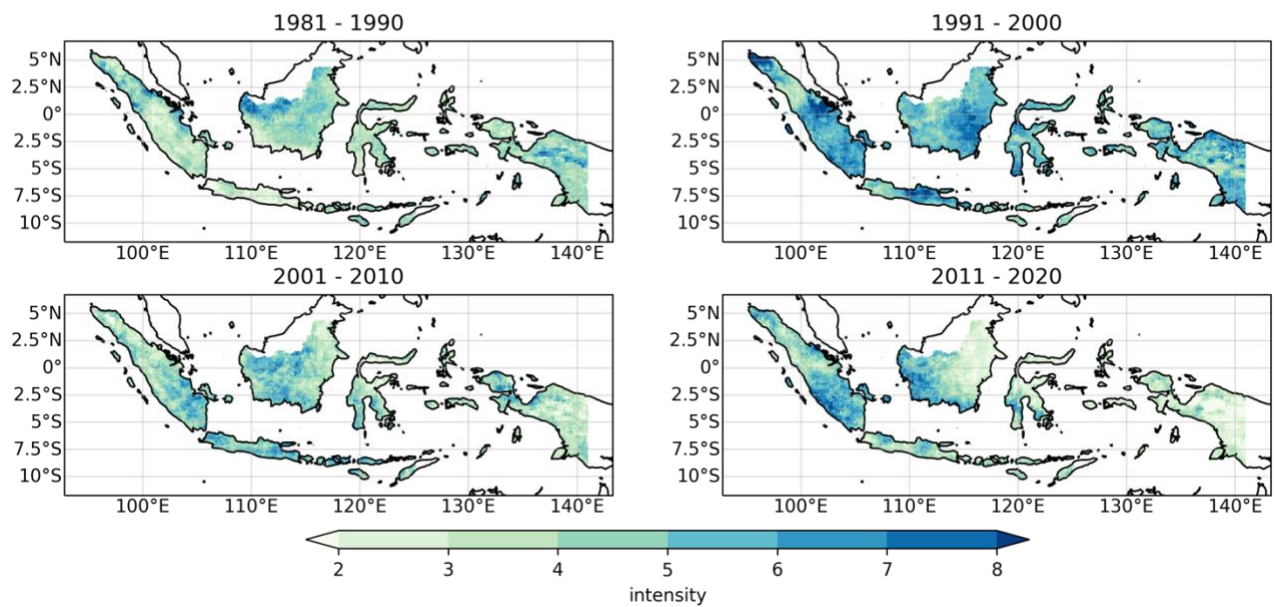


**Figure S 4** The decadal variation of drought intensity in Indonesia from 1981 – 2020.

# Study of Adaptation Measures for Flood Damage Mitigation by Adopting Effect of Climate Change

○ Tao Yamamoto<sup>1</sup>, So Kazama<sup>1</sup>

<sup>1</sup>Department of Civil Engineering, Tohoku University, Miyagi 980-8579, Japan.

\*E-mail: tao.yamamoto.b7@tohoku.ac.jp

## Abstract

In order to clarify effect of climate change on flood control planning, this study evaluated how the future reduction of flood damage cost changed by changing the rainfall scenario that served as the basis for flood control planning. CSIRO-Mk3-6-0 was selected as climate prediction data. There were three target periods, the late 20<sup>th</sup> century, the near future, and the late 21<sup>st</sup> century. Flood inundation simulations were performed using two-dimensional unsteady flow model. The river channel elevation was reduced by the depth obtained from flood inundation simulations corresponding to the flood control safety level. This reduced depth was changed based on flood inundation of late 20<sup>th</sup> century, 21<sup>st</sup> century under RCP2.6 or RCP8.5. From these analyses, the possibility has been raised to decrease flood damage by developing flood control level based on future climate.

**Keywords:** flood control planning; two-dimensional unsteady flow model; maladaptation.

## 1. Introduction

In recent years, there is concern about the expansion of flood damage due to the effects of climate change in Japan. As an example, in August 2022, flooding occurred in the Tohoku and Hokuriku regions, causing inundation and landslides. The Ministry of Land, Infrastructure, Transport and Tourism formulated “Integrated flood management” [1]. This is the first initiative to compile an overall vision of flood control measures through the cooperation of all parties concerned, based on a bird’s eye view of the entire basin, considering the increasingly severe and frequent disasters caused by climate change in recent years. In this project, flood control planning will be shifted from planning based on past phenomena to planning that considers climate change. **Table 1** shows the rate of change in precipitation, etc. due to climate change as indicated by the Japanese government. A number of studies have assessed the effects of climate change on precipitation and discharge [2],[3], but few have estimated the effectiveness of flood damage mitigation measures based on these effects. This study evaluates how the future flood control effectiveness changes by changing the rainfall scenario that serves as the basis for flood control planning.

## 2. Datasets and methods

As climate prediction data, daily precipitation data downscaled to a 1-km resolution (Regional Climate Projection Dataset NARO2017-V2.7r, National Agriculture and Food Research Organization) were used [4]. In this dataset, CSIRO-Mk3-6-0 was selected, and the two target scenarios were RCP8.5 and RCP2.6. Three target periods were considered: 1981–2000 (the late 20<sup>th</sup> century), 2031–2050 (the near future), and 2081–2100 (the late 21<sup>st</sup> century).

**Table 1. Rate of change in precipitation, etc. due to climate change as indicated by Japanese government**

GHG Scenario	Precipitation	Discharge	Flooding Frequency
2°C increase	Approx. 1.1 times	Approx. 1.2 times	Approx. 2 times
4°C increase	Approx. 1.3 times	Approx. 1.4 times	Approx. 4 times

Using this future daily precipitation, an extreme value analysis using the GEV distribution was conducted to determine the rate of increase in future extreme value precipitation. **Figure 1** shows the distribution of the rate of change in precipitation of the 100-year return period.

The stochastic flood-contributing precipitation distribution was used as daily precipitation data for the late 20<sup>th</sup> century. This precipitation distribution is weighted to make the extreme precipitation distribution have equal probability of discharge at any given location. The scales of precipitation were 30, 50, 100, and 200 return period.

A two-dimensional unsteady flow model was used for the flood inundation simulations. The spatial resolution used was the fifth order mesh resolution (approximately 250m × 250 m). Then, the unit price was set for each inundation depth for

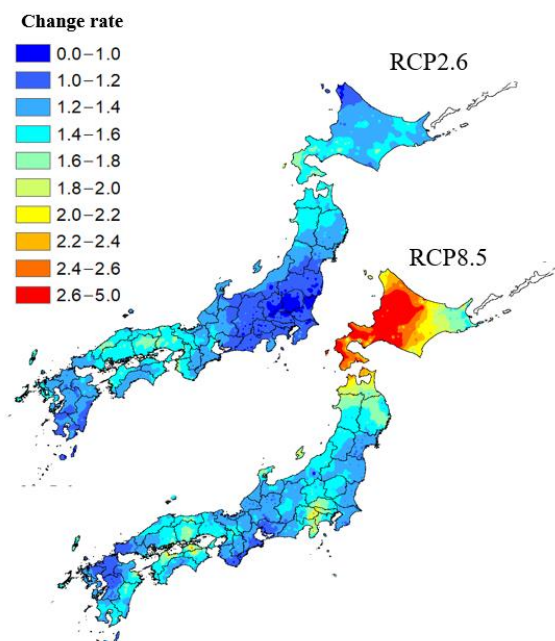


**Figure 1. Change rate of 100y return period precipitation (late 21<sup>st</sup> century)**

each land use type, and the damage cost was calculated for each cell. The details are described in Yamamoto et al. [5].

This study used the method of Tanaka et al. [6] as a method for expressing flood control levels. The method of Tanaka et al. was as follows: 1) The depth of the river channel required to safely flow the 5-, 10-, 30-, 50-, 70-, 100-, 150-, and 200-year floods was determined from flood simulations; 2) A flood control safety level was set for each river section based on the flood return period; 3) The channel elevation was reduced by the depth of the channel corresponding to the flood control safety level. In the flood simulation in 1), three standards for flood control planning were established by calculating three patterns: late 20<sup>th</sup> century, late 21<sup>st</sup> century RCP 2.6, and late 21<sup>st</sup> century RCP 8.5. The flood control safety level in 2) is assumed to be maintained as planned at the late 21<sup>st</sup> century, and the flood control safety level was assumed to be 50% at the late 20<sup>th</sup> century.

### 3. Results and discussion

Figure 2 shows Estimated Annual Damage Cost. If flood control was promoted based on the precipitation at the late 20<sup>th</sup> century, the damage cost increased by 17.0% under the RCP2.6 scenario and by 58.3% under the RCP8.5 scenario in the late 21<sup>st</sup> century. If flood control improvements were made based on the precipitation in the RCP2.6 scenario at the late 21<sup>st</sup> century, the EADC at the late 21<sup>st</sup> century would decrease by 4.3% in the RCP2.6 scenario and increase by 37.3% in the RCP8.5 scenario. If flood control improvements were made based on the precipitation in the RCP8.5 scenario at the late 21<sup>st</sup> century, the EADC at the late 21<sup>st</sup> century would decrease by 21.2% in the RCP2.6 scenario and increase by 7.2% in the RCP8.5 scenario. Future-standard flood control improvements, which were set up to accommodate higher discharge, reduced the EADC more than past-standard flood control improvements.

Even if flood control improvements were based on past phenomena, EADC would increase due to the effects of climate change. Therefore, in order to mitigate EADC in the future, flood control measures must be based on future precipitation. On the other hand, there was a large difference in precipitation between the RCP2.6 scenario and the RCP8.5

scenario, and therefore, the cost of flood control was also expected to differ greatly between the two scenarios.

The average depth of excavation was calculated as a helpful indicator of cost. The average depth of excavation based on the late 20<sup>th</sup> century was 0.39 m, based on RCP 2.6 - late 21<sup>st</sup> century was 1.02 m, and based on RCP 8.5 - late 21<sup>st</sup> century was 1.84 m. The difference of 0.82 m was caused by the different RCP scenarios. The cost of constructing levees and excavating river channels to cover this difference in height is significant. However, the flood control criteria should be discussed in consideration of the rework required to revise the flood control plan and the loss of leaving highly vulnerable areas until the completion of the improvement. There is also a problem to select which GCM for determining the future flood control level. Only one scenario was used for this analysis. Referring to Yamamoto et al. [5], the distributions and increase rates of precipitation was significantly different from each GCMs. Therefore it is important to select carefully which future predictions we use, and to use more future predictions as much as possible.

### 4. Conclusions

When flood control was developed based on the past climate, flood damage increased due to the effects of climate change. However, there is a possibility to decrease flood damage by developing flood control level based on future climate.

### Reference

- [1] Konami, T., Koga, H., Kawatsura, A., Role of pre-disaster discussions on preparedness on consensus-making of integrated flood management (IFM) after a flood disaster, based on a case in the Abukuma River Basin, Fukushima, Japan, *International Journal of Disaster Risk Reduction*, Volume 53(2021), 102012.
- [2] Iizumi, T., Takayabu, I., Dairaku, K., Kusaka, H., Nishimori, M., Sakurai, G., Ishizaki, N. N., Adachi, S. A., and Semenov, M. A., Future change of daily precipitation indices in Japan: A stochastic weather generator-based bootstrap approach to provide probabilistic climate information, *J. Geophys. Res.*, 117(2012), D11114.
- [3] S. Tezuka, H. Takiguchi, S. Kazama, A. Sato, S. Kawagoe, R. Sarukkalige, Estimation of the effects of climate change on flood-triggered economic losses in Japan, *International Journal of Disaster Risk Reduction*, Volume (2014), Pages 58-67.
- [4] Nishimori, M., Y. Ishigooka, T. Kuwagata, T. Takimoto and N. Endo, SI-CAT 1km-grid square Regional, Climate Projection Scenario Dataset for Agricultural Use (NARO2017). *J Jpn Soc Simul Technol*, 38(2019), 150-154 (in Japanese with English title)
- [5] Yamamoto, T., Kazama, S., Touge, Y. et al., Evaluation of flood damage reduction throughout Japan from adaptation measures taken under a range of emissions mitigation scenarios. *Climatic Change* 165(2021), 60.
- [6] Tanaka Y, Kazama S, Tada T, Yamashita T, Komori D, Assessment of the risk on flood and storm surge with flood control facilities. *J Jpn Soc Civ Eng Ser B1 (Hydraul Eng)* 75(2) (2019), I\_109-I\_114 (in Japanese)

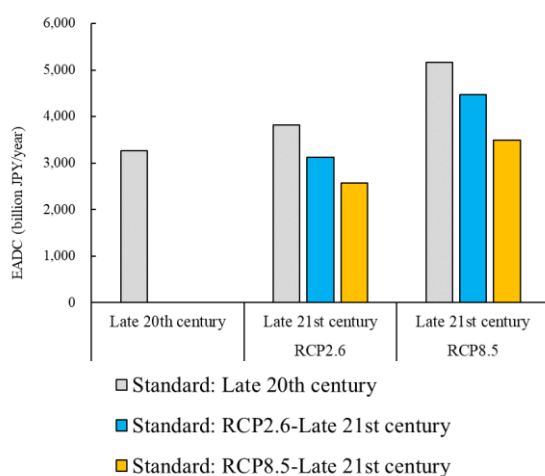


Figure 2. Estimated Annual Damage Cost (EADC)

# A data-based modeling approach of rainfall-runoff processes: its development history and a blueprint for the future

○ Yoshiyuki YOKOO<sup>1\*</sup>

<sup>1</sup>Faculty of Symbiotic Systems Science, Fukushima University, Fukushima 960-1296, Japan.

\*E-mail: yokoo@sss.fukushima-u.ac.jp.

## Abstract

Rainfall-runoff models have been developed for estimating river flows and used for explaining the hydrological processes that induced flood and drought events by today. Yet, they stand on many assumptions that were not validated enough by field measurements or observe data. The author think that this is the critical weakness of current rainfall-runoff models, because a rainfall-runoff model based on wrong assumptions would derive a right answer for the wrong reasons. To reduce the weakness, the author's research group have been developed a data-based modeling approach that can simultaneously identify the structure and the parameters of a rainfall-runoff model with least assumptions. This article attempts to summarize its development history and share a blueprint for the future for more reliable rainfall-runoff modeling.

**Keywords:** discharge; storage; recession time constant; calibration; understandings.

## 1. Introduction

Modeling of natural processes reflects our understandings of the processes to seek for their governing theories, hence it is a strong measure to advance sciences of nature together with field measurements. In rainfall-runoff modeling, most of studies apply existing models and their validities are not verified enough in most of the cases. These facts would prevent the advances in the theoretical aspects of rainfall-runoff modeling. Besides, most of the existing rainfall-runoff models used today have the problem of uncertainties in their structures and their parameters even today. In other words, most of the models are constructed based on assumptions that are not verified enough. This is the critical weakness of the rainfall-runoff models used today.

As one of the countermeasures for this problem of uncertainties, the author's research group have been developed a methodology to identify the structure and the parameters of rainfall-runoff models. In this short article, the author introduces the development history of our data-based modeling approach and a blueprint for the future toward the developments of more reliable models for science of hydrology and its contribution to the society.

## 2. Development history

The data-based modeling approach of rainfall-runoff processes was developed based on the inspiration from the unique research by Kirchner [1].

We first tested the original method of Kirchner [1] in order to test the applicability of the method in Japanese mountainous watershed that has relatively complex rainfall-runoff processes compared to the watersheds tested in Kirchner [1]. In Yokoo *et al.* [2], we confirmed the original method of Kirchner [1] estimates watershed-scale storage only for quick flows after rainfall events.

To adjust the methodology of Kirchner [1] in watersheds with more complex hydrological processes, we recalled that we would be able to use the filter-separation method of Hino and Hasebe [3]. We showed our first results of the methodology of Kirchner [1] applied after hydrograph separation method of Hino and Hasebe [3] and Kobayashi

and Yokoo [4]. The results indicated that we can significantly improve the estimated changes of storage in Japanese mountainous watersheds. Later we confirmed in Yokoo *et al.* [5] that the storage estimations in mountainous watersheds in the northern Thailand can be significantly improved than the original method of Kirchner [1]. As an application of our methodology, we compared estimated storage under heavy rainfall events that caused slope failure in Hiroshima between the Soil Water Index of Okada and our method in Kobayashi and Yokoo [6]. There we found that the Soil Water Index is of near surface storage

We then noticed that storage-discharge relationships for all the separated discharge components can be approximated as linear relationships rather than the original power-law relationships from the storage-discharge relationships. Hence we examined if we can linearize the storage-discharge relationships for all the discharge components in Chiba *et al.* [7]. The results showed that we can approximate by the linear relationships for all the storage-discharge relationships. These results suggested that our data-based modeling approach to identify storage-discharge relationships for different discharge components can be used for identifying the structures and parameters of the Tank model of Sugawara [8] that employs linear storage-discharge relationships for all the discharge components.

Based on the above-mentioned expectation, we investigated if we can identify structures and parameters of the Tank model of Sugawara [8]. In the end, we noticed that we can identify structure and parameters simultaneously if we identify them from the bottom tank of the Tank model of Sugawara [8]. We summarized our theoretical investigations on the simultaneous identifications of structures and parameters of the model in Yokoo *et al.* [9]. This achievement allowed us to construct a Tank model of Sugawara [8] without any trial and errors nor complex parameter calibrations, which would be an epoch-making improvement the applicability of the Tank model of Sugawara [8]. It also allowed our data-based interpretations of rainfall-runoff processes, which would open a new way to investigate rainfall-runoff processes.

One of the examples would be the interpretations of rainfall-runoff processes that form the unique shape of the

flow duration curve of a watershed. Leong and Yokoo [10], [11] attempted to explain why the shapes of flow duration curves of watersheds under different climate regions by using our data-based modeling approach. They succeeded to explain that different rainfall-runoff processes cause the unique shapes of flow duration curves in watersheds under different climate regions by using the modeling approach. Their paper contributed to significantly advance our understanding on the shape of flow duration curves.

### 3. A blueprint for the future

Based on the development history mentioned above, the author wants to list up further development directions as a blueprint for the future of our data-based modeling approach of rainfall-runoff processes.

One of the directions would be using the approach for the verifications of spatially distributed rainfall-runoff processes, because the data-based modeling approach was initially developed for identifying structures and parameters of lumped rainfall-runoff models. The identified model structure and parameters can contribute to constrain or identify the structure and the range of parameters of distributed models. Almost all the distributed models are developed uniquely in terms of structure and parameters, hence it would be beneficial if we can constrain or identify the structure and parameters of distributed models from the identified structure and parameters of lumped models.

As another direction, we can explore storage-discharge mechanisms at a watershed scale by using the data-based modeling approach. Kobayashi and Yokoo (2013) showed an example to investigate the storage-discharge mechanisms at a watershed scale. The author think it would be a hint to explore hysteresis of storage discharge relationships caused by the multiple linear relationship between storage and discharge. If it rains, a watershed would increase storages of rainwater from near surface zones to the deeper zones, which results in increase of discharge to the rivers in the watershed. On the contrary, rainwater storage would decrease the storages from near surface zones to deeper zones. Hence, the author expects that the simulated total storage and total discharge at a watershed scale would exhibit hysteresis in the storage-discharge relationship.

The other direction would be developing a methodology to partition observed rainfall into evapotranspiration and effective rainfall to rainfall-runoff processes. Yokoo *et al.* (2017) succeeded to estimate effective rainfall but they did not how to partition it. If we can succeed to partition it, then our data-based modeling approach of rainfall-runoff process would be regarded as it was completed. The author is now working on the development of this methodology.

### 4. Summary

The author attempted to introduce the development history and a blueprint for the future of our data-based modeling approach of rainfall-runoff processes in this short article. As described in its history, the author's group has succeeded to develop and utilize the methodology by today. Yet, it still need to complete this methodology about rainfall-partitioning near the ground surface, toward further applications of the methodology. Hence, we would try to complete this methodology for conducting its application

studies as exemplified in the blueprint for the future, and we are looking forward to work these studies with you.

### Acknowledgments

This work was supported by JSPS KAKENHI (20H00256, 20H02249, 16KK0142, 16K06501, 24760388).

### Reference

- [1] Kirchner JW, Catchments as simple dynamical systems: Catchment characterization, rainfall-runoff modeling, and doing hydrology backward. *Water Resources Research* 45 (2009) W02429.
- [2] Yokoo Y, Kobayashi S, Kawasaki M, Toward estimations of watershed-scale storage and storage potential in Japanese mountainous watersheds, *Annual Journal of Hydraulic Engineering, JSCE*, 56 (2012), I\_475-I\_480. (In Japanese with English abstract).
- [3] Hino M, Hasebe M, Identification and prediction of nonlinear hydrologic systems by the filter-separation autoregressive (AR) method: Extension to hourly hydrologic data, *Journal of Hydrology*, 68 (1984), 181–210.
- [4] Kobayashi S, Yokoo Y, Estimating watershed-scale storage changes from hourly discharge data in mountainous humid watersheds: toward a new way of dominant process modeling, *Hydrological Research Letters*, 7 (2013), 97–103.
- [5] Yokoo Y, Wattanakarn C, Wattanakarn S, Semcharoen V, Promasakha na Sakolnakhon K, Soralump S, Storage under the 2011 Chao Phraya river flood: An interpretation of watershed-scale storage changes at two neighboring mountainous watersheds in northern Thailand, *Hydrological Research Letters*, 8 (2014), 1-8.
- [6] Kobayashi S, Yokoo Y, Relationship between soil water index and estimates of watershed-scale storage, *Journal of Japan Society of Civil Engineers, Series B (Hydraulic Engineering)*, 70 (2014), I\_349-I\_354 (In Japanese with English abstract).
- [7] Chiba T, Yokoo Y, Revision of estimation method of watershed-scale rainwater storage and its effect, *Journal of Japan Society of Civil Engineers, Series B (Hydraulic Engineering)*, 71 (2015), I-289-294 (In Japanese with English abstract).
- [8] Sugawara M, Tank model. In *Computer models of watershed hydrology*, V. P. Singh (Ed.), *Water Resources Publications* (1995), 165-214.
- [9] Yokoo Y, Chiba T, Shikano Y, Leong C, Identifying dominant runoff mechanisms and their lumped modeling: a data-based modeling approach, *Hydrological Research Letters*, 11 (2017), 128-133.
- [10] Leong C, Yokoo Y, An interpretation of the relationship between dominant rainfall-runoff processes and the shape of flow duration curve by using data-based modeling approach, *Hydrological Research Letters*, 13 (2019), 62-68.
- [11] Leong C, Yokoo Y, A multiple hydrograph separation technique for identifying hydrological model structures and an interpretation of dominant process controls on flow duration curves, *Hydrological Processes*, 36 (2022), e14569.

**POSTER**



# An overview of sewage treatment for human health safety in the Song Dynasty

○ Yixiao LIU<sup>1\*</sup>

<sup>1</sup>School of Social Development and Public Administration, Suzhou University of Science and Technology, Suzhou 215009, China

\*E-mail: 1720128460@qq.com

## Abstract

In today's globalized world of development, how to remedy water pollution has become a hot topic of discussion. The importance attached to the issue of pollution reflects the depth of modern human understanding of environmental health. The problem of environmental pollution is not unique to modern society. It is evident from the surviving historical texts that the ancient people suffered from environmental pollution as well, and quite severely. The high economic prosperity of the Song Dynasty was also bound to bring about some pollution problems. The diversity of sources of pollution was concentrated in the areas of production and life, and many sources of pollution from production and life had a huge impact on water bodies.

**Keywords:** Sewage treatment; China history; Song dynasty; Health safety; Social development

## 1. Introduction

Since ancient times, the development of human society has been inseparable from water sources. During the Song Dynasty, there were many rivers and waterways, and not only did most of the inhabitants live along the rivers, but also most of the handicraft production sectors were built on the water. A large amount of domestic and production sewage was discharged into the nearby waters without being treated, causing great harm to the environment.

### 1.1 Domestic sewage

The Song Dynasty saw unprecedented social and economic development, as well as a significant increase in urbanisation and a burgeoning urban population. According to Mr. Qi Tao, "the actual populations of Kaifeng and Lin'an in the Northern Song Dynasty in the first year of Chongning (1102) both exceeded one million inhabitants." [1] With a large number of densely packed buildings in a limited urban space, the daily life of the inhabitants had an impact on the public health of the city and the surrounding water environment. The frequent occurrence of epidemics in Song cities was closely related to the contamination of rivers, waterways, lakes and underground drinking water. In Bianjing, the capital of the Northern Song Dynasty, there was a large amount of household waste in the rivers and drains, causing congestion and pollution. According to "Dongjing Dreams and Records": "every spring, the government sent people to supervise the panning in the city drains, and opened a pit to hold the panned mud, called "mud basin". Waiting for the official to come to inspect the party cover cover, night access, the moon darkness should also take care of." From the dredging of ditches in Bianjing, it is easy to see that the ditches were filled with a large amount of dirt, and this situation was mostly caused by the residents of Bianjing throwing their daily rubbish into the ditches. This was the case in the capital city, not to mention the local pollution. The river in Danyang County, Zhenjiang Province, is often filled with "dung, especially at the Hu Gong Land Bridge, where it is as high as the bridge".

### 1.2 Production of wastewater

The main sources of pollution from handicraft production during the Song Dynasty were paper making and printing, mining and smelting and textile printing and dyeing, and

these handicraft production sectors caused a certain amount of pollution to the surrounding environment during their operations. Let's talk about the paper-making industry first. The paper-making process relied heavily on clarified water sources to bleach and wash the raw materials, and the "Paper Recipe" contains information about the waters of the Jinjiang River in Sichuan during the Song Dynasty, where paper was made "with the water of the Ronghuatan, so it was good. It is also water that is suitable." Numerous paper mills were built along the river to meet the huge demand for paper from all over the country, working day in and day out on both sides of the river, and the frequent bleaching and washing of the paper process polluted the surrounding waters. The frequent bleaching and washing of paper pollutes the surrounding waters. The pollution caused to the nearby drinking water sources can be imagined in the long run.

The smelting industry was also more harmful to water bodies than ever before. The Song Dynasty was rich in gold and silver mineral resources, and there were only three silver-producing places in the country, with fifty-one. The main method used to pluck alluvial gold in the Song Dynasty is to pluck gold from the water or soil at a convenient place near the alluvial gold deposit, without processing to get the net gold and stop. Such as "Pingzhou can talk about" in the Beijing East Road area: "deng, Lai gold pit household, stop with a large wooden saw cut, leave edge marks, cast sand on it, flood with water, sand to go, gold in the saw, very easy to get". However, this method of panning for gold by impacting

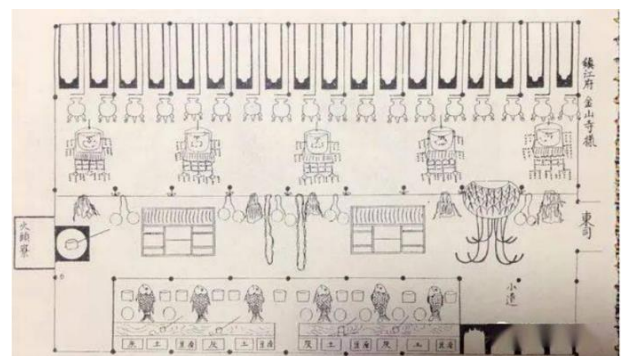


Fig. 1. Toilets in Song Dynasty

sediments with water is very easy to pollute water sanitation due to the lack of protective measures. The rivers where gold panning is carried out contain large amounts of heavy metal ions, acids and alkalis and suspended solids, which pose a threat to the health and safety of the surrounding population and the survival of other plants and animals.

## 2. Governance measures

The development of handicraft industry was relatively rapid during the two Song dynasties, and according to Mr Ji Ziya, "the development of handicraft industry during the Song dynasty was greatly enhanced in terms of breadth and depth, composition, division of labour and technological level compared to previous generations." However, behind the economic prosperity was a damaged environment, as the smelting and smelting activities of the crafts and the daily life of the inhabitants of the two Song dynasties caused a certain amount of pollution to the nearby waters. These polluted waters were complex in composition, containing acids, alkalis and heavy metals, which were not easily degraded. During the production process, some waste water is also discharged into the surrounding waters, changing the original structure of the water bodies. Some toxic and non-degradable pollutants pose a great threat to the survival of fish and shrimps and other aquatic products in the water, and also have a certain impact on the health and safety of the residents on both sides of the river. Due to the limitations of the times and the development of technology, the Song people naturally did not understand the composition of waste water from handicraft production, but they were aware of the hazards of sewage. The government of the two Song dynasties reduced the pollution of the waters by setting up artificial ponds for smelting and dedicated sewage, and by filtering the printing and dyeing effluent.

In mining and smelting production, artificial pools were set up to replace the previous direct washing and filtering operations in the river water. For example, the Song dynasty's Zhao Yanwei recorded in the <Yunlu Manchu> that during the Shaoxing period (1131-1162), the Ruiying field in Songxi County, Jianning Province (now Songxi County, Fujian Province), in the process of refining fine silver in the silver mines, "roughly six times overhand, pit households called over pools, over pools, lead pools, ash pools and the like is also." As can be seen, the silver ore was panned and filtered by setting up numerous artificial pools, which reduced the pollution of the surrounding waters to a certain extent, as opposed to working directly in the river. In the early years of the Northern Song Dynasty, the Jinshui River was polluted by the waste water discharged from the surrounding dye houses. A series of measures were put in place by the court to combat this. In 1015, Emperor Zhenzong of the Northern Song Dynasty ordered that "short walls be erected on both sides of the Jinshui River to protect the river from the polluted water." By setting up short walls, the two banks of the river were restrained from discharging water to the Jinshui River. This was followed by the opening of small ponds and the installation of bucket gates to control the water and filter the sewage. The west courtyard open pool five, five place the bucket door, put water to fill wash things silk, in the event of making that open the bucket door, night under the stack lock closed. If you open a small pool, set the bucket door, put water to wash the bolt section, when the water is

muddy, back into the protection of the Dragon River, spin put clear water.



Fig. 2. Urban Drainage in Song Dynasty

At the same time, a retreat ditch was dug to drain some of the waste water from the dyeing and dyeing process to the Dragon Protection River (a trench outside the palace), thus reducing the direct pollution of the city's waters. The domestic sewage was mostly due to the washing and other waste water from the daily lives of the residents along the river, and the frequent encroachments on the water during the Song Dynasty exacerbated the pollution of the waters. The pollution of the waters caused by domestic waste water and rubbish was much easier to degrade than that caused by handicraft production. During the Song dynasty, the government discharged sewage from the city to the rivers, lakes and seas outside the city by repairing the city's drains and underground ditches, leaving it to degrade naturally. For example, Meng Yuanlao wrote in his description of the imperial street in Bianjing: "There are two brick and stone ditches in the fork." Lu You also writes that the dark ditches in Bianjing City are crisscrossed and extremely wide, "The ditches in the capital are extremely deep and wide, and many dead people hide in them." It can be seen that the underground sewers in Bianjing were very well developed in the Song Dynasty. These sewers discharged large amounts of waste water directly into the rivers outside the city, thus reducing the pollution of the waters around the city. The fast flowing, fast circulating river water itself has a high dissolved oxygen content, so its self-cleaning ability is also very strong.

## 3. Conclusions

In terms of the standard of treatment of waste water today, the Song dynasty has only demonstrated the most basic treatment techniques in the treatment of waste water, and is still in a state of natural digestion and decomposition for the treatment of waste water caused by production and living. However, there is no doubt that the official response to the pollution problem was positive and relatively less polluting to the surrounding waters, while at the same time restraining the expansion of the pollution.

## Reference

[1] Qi Tao, Ancient Economic History of China, Jinan: Shandong University Press, December 1999, p. 335.

# Performance comparison of Anammox process with EDTA chelation of Fe (III) and Fe (III) salts addition

Yang Yang<sup>1</sup>, Li Wen Cao<sup>1</sup>, Yong Hu<sup>1\*</sup>

<sup>1</sup> School of Environmental Science and Engineering, Nanjing Tech University, Nanjing 211816, PR China

\*E-mail: huyong333@163.com

## Abstract

This study investigated the performance comparison of Anammox process with EDTA chelation of Fe (III) and Fe (III) salts addition. Generally, adding iron is one of the strategies to enhance Anammox, which embodied in higher growth and enrichment of Anammox bacteria and higher denitrification performance of UASB. Although the low concentration of iron can promote Anammox process, high concentration can inhibit it. This paper will complete the research of iron enhanced Anammox and serve as guidance for future engineering application of Anammox process.

**Keywords:** Anammox; Iron; Enhancement; Denitrification

## 1 Introduction

Anaerobic ammonium oxidation (Anammox) has been deemed to be a novel and promising process for treating high ammonium wastewater in the last decades. Under anaerobic conditions, the Anammox bacteria use nitrite as electron acceptor to oxidize ammonia nitrogen to nitrogen. Compared with traditional nitrification and denitrification, Anammox has significant advantages of no need for organic carbon resources, saving aeration and reducing the amount of sludge generated. As a result, it has been considered as one of the most cost-effective biological denitrification technologies for wastewater treatment.

However, Anammox bacteria (AnAOB) grow very slowly, with a long generation cycle of 7–20 days and are quite sensitive to surrounding environment. In view of these problems, the strengthening of the Anammox process has always been the most concerned problem. Many strategies have been conducted to strengthen the Anammox process. The addition of iron is the cost-effective methods to enhance Anammox process because iron is the most abundant metal element in the earth, which is widely available, cheap and easy to obtain.

As a typical organic sequestering agent, EDTA has continuously attracted much attention for that it can promote the bioavailability of metal. In this paper, we compare with two forms of Fe (III) (Fe (III) (chelated by EDTA) and FeCl<sub>3</sub>). Firstly, we start up the reactor by addition of FeSO<sub>4</sub>·7H<sub>2</sub>O. Then we carried out continuous experiment to explore the performance comparison of the addition of EDTA chelation of Fe (III) and Fe (III) salts. Therefore, two identical reactors were operated and nitrogen removal performance, sludge characteristic, EPS (extracellular polymeric substances), and community structure of reactors were investigate

## 2 Materials and methods

### 2.1 Experimental setup and operation strategy

Experimental work was conducted in two lab-scale UASB reactors (R1, R2). The reactor was made of plexiglass and an effective volume of 2 L. The simulated wastewater was pumped into the reactor by a peristaltic pump, and the nitrogen conversion was completed during the upflow movement. The gas was emitted from the top air chamber, and the effluent was discharged from the overflow weir. The reactors were inoculated with Anammox mature

granule sludge collected from Jia Yi environmental Protection Company. The volatile suspended solids (VSS) concentration of each reactor was 20.4 g/L. In R1 and R2, the concentrations of iron added into the water were 5mg/L, respectively, and they were provided in the form of FeCl<sub>3</sub> (R1) and Fe (III) (chelated by EDTA) (R2). Operational temperature was maintained at 35°C, and hydraulic retention time (HRT) was 24 h.

Operation strategies are summarized in **Table1** and were the same for two reactors. After reaching the stable state, nitrogen loading rate (NLR) was raised by increasing the influent nitrogen concentration and/ or HRT. Water samples were taken to determine the concentrations of nitrogen compounds. At the end of each phase, the mixed liquor was withdrawn from the reactors for subsequent batch tests.

**Table1.** Experimental conditions of continuous experiments.

Phase	NH <sub>4</sub> <sup>+</sup> -N (mg/L)	NO <sub>2</sub> <sup>-</sup> -N (mg/L)	HRT (h)	NLR (g-N/(L·d))
I	52.5	69.3	24	0.12
II	90.4	119.3	24	0.21
III	128.3	169.3	24	0.29
IV	166.1	219.3	24	0.39
V	204.1	269.3	24	0.47
VI	204.1	269.3	12	0.95
VII	204.1	269.3	6	1.89

### 2.2. Synthetic wastewater

The synthetic wastewater was composed of substrates, trace elements and inorganic solution. Nitrogen resource was provided by (NH<sub>4</sub>)<sub>2</sub>SO<sub>4</sub> and NaNO<sub>2</sub>, and the initial NH<sub>4</sub><sup>+</sup>-N and NO<sub>2</sub><sup>-</sup>-N concentration in influent were 52.5 and 69.3 mg N/L respectively. Trace elements were supplied at a dosage of 0.125 mL per liter of wastewater. One liter of the trace metals solution contained: 0.5375 mg ZnSO<sub>4</sub>·7H<sub>2</sub>O, 0.0175 mg H<sub>3</sub>BO<sub>4</sub>, 0.2375 mg NiCl<sub>2</sub>·6H<sub>2</sub>O, 1.2375 mg MnCl<sub>2</sub>·4H<sub>2</sub>O, 0.275 mg CoCl<sub>2</sub>·6H<sub>2</sub>O, 0.3125 mg CuSO<sub>4</sub>·5H<sub>2</sub>O, and 0.275 mg Na<sub>2</sub>Mo<sub>4</sub>·2H<sub>2</sub>O. The inorganic solution consisted of MgSO<sub>4</sub>·7H<sub>2</sub>O (102.5 mg/L), NaHCO<sub>3</sub> (500 mg/L), KH<sub>2</sub>PO<sub>4</sub> (50 mg/L), CaCl<sub>2</sub>·2H<sub>2</sub>O (108 mg/L), KCl (570 mg/L). Influent pH was adjusted to 7.2 ± 0.2.

### 2.3. Analytical methods

Effluent samples were collected every two days, then filtrated through 0.45 μm membranes. NH<sub>4</sub><sup>+</sup>-N, NO<sub>2</sub><sup>-</sup>-N,

NO<sub>3</sub><sup>-</sup>-N were measured according to standard analytical procedures (American Public Health Association, 2012). Sludge volatile suspended solid and suspended solid contents were detected according to standard methods. Gas production was measured by gas flowmeter. The pH value was measured by a handheld pH meter. The composition of gas was determined by a gas chromatography equipped with a flame ionization detector and a StabiliwaxR-DA capillary column. Sludge samples were collected for elemental composition analysis using energy dispersive spectroscopy (EDS). According to the previous methods, the functional genes were analyzed with qPCR and the microbial community was analyzed with high throughput 16S rRNA gene sequencing.

### 3 Results and discussion

During the whole experimental period, the two reactors have been successfully operated for three phases. Phase I and phase II was the start-up phase. Phase III has begun to explore the performance comparison of the two reactors.

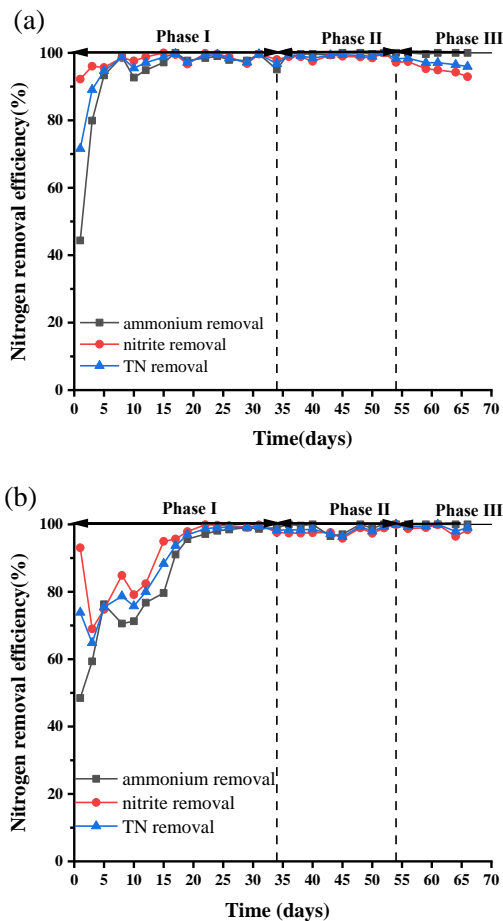


Fig.1. Performance of the Anammox granular reactor as a function of operating time: (a) R1; (b) R2.

Fig.1 and 2. show the variation of nitrogen removal performance, nitrogen loading rate (NLR) and nitrogen removal rate (NRR) of the two reactors after 66 days of operation. During the phase I, the influent NH<sub>4</sub><sup>+</sup>-N and NO<sub>2</sub><sup>-</sup>-N concentrations were 52.5 mg/L and 69.3 mg/L, respectively. NLR was 0.12 g-N/(L·d). After approximately 2 weeks start-up time of R1, excellent treatment results were obtained quickly without big fluctuation. Ammonium and nitrite have been simultaneously removed. The gas component analysis indicated that over 99% of the produced

gas was N<sub>2</sub>. The result indicates that the Anammox reactor was successfully started up. But approximately 3 weeks start-up time was used to start up R2. At the end of this period, the nitrogen removal rate (NRR) of the two reactors had stabilized at 0.12 g-N/(L·d) and the NH<sub>4</sub><sup>+</sup>-N and NO<sub>2</sub><sup>-</sup>-N removal efficiencies were above 99% and 99.5%, respectively. During phase II, the influent NH<sub>4</sub><sup>+</sup>-N and NO<sub>2</sub><sup>-</sup>-N concentrations were increased to 90.4 mg/L and 119.3 mg/L, the NLR reached to 0.21 g-N/(L·d). The performance of two reactors remained stable.

The start-up period was shorter than reactors with other types of sludge and similar to (Ni et al., 2011), showing that the inoculation of mature Anammox granules was a good idea to start-up a new reactor. Nearly complete influent NH<sub>4</sub><sup>+</sup>-N and NO<sub>2</sub><sup>-</sup>-N were removed from the wastewater, which fully indicated that high activities of Anammox bacteria were achieved in the reactor.

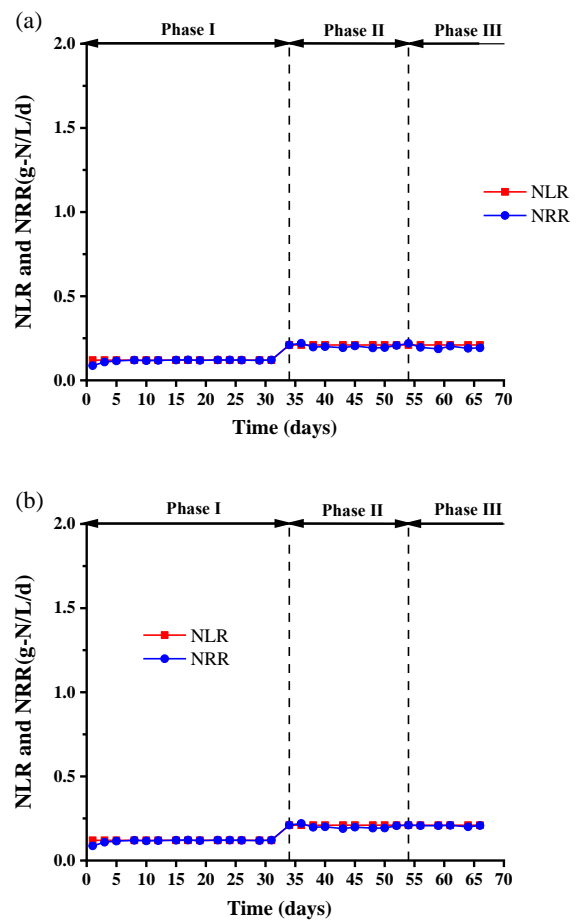


Fig.2. Nitrogen loading rate (NLR) and nitrogen removal rate (NRR) of two Anammox reactors: (a) R1; (b) R2.

### 4 Conclusions

Generally, the performance of two identical UASB reactors have been excellent and similar, the result shows that Anammox reactor was successfully started up. The inoculation of mature Anammox granules can be a good idea to start-up a new reactor and the start-up time was 2-3 weeks. The successful start-up of the reactors prepare for subsequent continuous experiments.

## Reference

American Public Health Association (APHA), American Water Works Association, Water Environment Federation, 2012. Standard Methods for the Examination of Water and Wastewater, 22nd Edition, Standard Methods.

Ni S Q, Gao B Y, Wang C C, et al. Fast start-up, performance and microbial community in a pilot-scale anammox reactor seeded with exotic mature granules, *Bioresour Technol*, 2011, 102: 2448-54

# Successful demonstration of a pilot-scale internal circulation reactor integrated with partial nitrification-anammox for the treatment of real membrane-manufacturing wastewater

○ Yuqin FAN<sup>1</sup>, Yong HUANG<sup>1,2</sup>, Dapeng LI<sup>1,2</sup>, Zhe KONG<sup>1,2\*</sup>

<sup>1</sup>School of Environmental Science and Engineering, Suzhou University of Science and Technology, Suzhou 215009, China

<sup>2</sup>National and Local Joint Engineering Laboratory of Municipal Sewage Resource Utilization Technology, Suzhou 215009, China \*E-mail: zhekong@mail.usts.edu.cn

## Abstract

A pilot-scale system integrating internal circulation and partial nitrification-anammox successfully treated real high-strength membrane-manufacturing wastewater in this study. With this pilot-scale system, a high chemical oxygen demand (COD) removal efficiency of 85% and a nitrogen removal of 90% are achieved at an organic loading rate of 6.0 kg COD/m<sup>3</sup>/d. The nitrogenous organic matters in the internal circulation zone are degraded into ammonia nitrogen. In the partial nitrification zone, nitrite accumulation is achieved, providing a suitable NH<sub>4</sub><sup>+</sup>-N/NO<sub>2</sub><sup>-</sup>-N ratio for anammox reaction. Partial nitrification is achieved by maintaining an operational temperature at 30-35 °C, free ammonia concentration at 5-7 mg/L and dissolved oxygen at 0.4 to 0.7 mg/L with a reflux ratio of 150%. The COD to nitrogen ratio in the internal circulation effluent is maintained below 3.0 to inhibit nitrite oxidizing bacteria. This study demonstrates that a pilot-scale system can efficiently remove organic matters and nitrogen from wastewater of membrane-manufacturing industry.

**Keywords:** Membrane-manufacturing wastewater; Anaerobic digestion; Partial nitrification; Anammox; internal circulation; Pilot-scale

## 1 Introduction

Membrane-manufacturing wastewater (MMW) with high concentrations of biotoxic wastewater discharged during the production of various membrane products are hazardous to the environment. Although conventional activated sludge has been widely used for wastewater treatment, they are considered less suitable for treating high-strength industrial organic wastewater. The goal of wastewater treatment is to develop a sustainable green technology. Anaerobic digestion (AD) can produce CH<sub>4</sub> for energy recovery and carbon emission reduction, while the partial nitrification-anammox process saves energy consumed by the aeration process and reduces biomass production. In this experiment the MMW was degraded by AD of organic matter and produced NH<sub>4</sub><sup>+</sup>-N, half of the NH<sub>4</sub><sup>+</sup>-N was converted to NO<sub>2</sub><sup>-</sup>-N under partial nitrification conditions and subsequently successfully denitrifying by anammox process. This study provides new ideas for the anaerobic treatment of high-strength industrial organic wastewater such as MMW, and brings solid engineering experience to the promotion of the IC-PN/A process in practical applications.

## 2 Materials and methods

### 2.1 Reactor Setup and Operation

The entire IC-PN/A system has an operational volume of 2 m<sup>3</sup> and is equipped with a peristaltic pump, blower and pH online monitor. A fluidized bed biological filler with a filling rate of 30% is added to the PN zone. The actual MMW is fed continuously into the IC, PN and AMX zones. Air is pumped into the PN zone by a blower for the nitrification reaction. Finally a percentage of the effluent from the AMX zone is recycled to the IC zone for enhanced denitrification by means of an air lift system. The reactor temperature was controlled

at 30-35 °C. The IC zone was inoculated with black anaerobic granular sludge. The PN zone was inoculated with activated sludge from the wastewater treatment plant. The AMX zone was inoculated with anammox granular sludge. The actual MMW in this study was diluted 10 times and fed into the reactor for reaction. NH<sub>4</sub><sup>+</sup>-N, NO<sub>2</sub><sup>-</sup>-N, NO<sub>3</sub><sup>-</sup>-N, TN and COD were measured regularly in the effluent of each zone of the reactor. DO and PH were monitored in real time inside the PN zone using an online monitoring device model (PHS-3T Digital pH Meter/WTW Multi 9430).

Stage (day)	COD (mg/L)	COD <sub>RE</sub> (%)	NH <sub>4</sub> <sup>+</sup> -N* (mg/L)	HRT (day)	TN <sub>RE</sub> (%)
I	1050±25	83.3±3.1	79.3±10.1		
II	1520±40	81.5±2.2	125.6±4.6	0.75	
III	2023±22	82.6±1.8	156.5±12.3		—
IV	2046±36	82.9±1.9	169.5±6.8	1	
V	2550±37	83.9±0.7	198.5±21.5	1.25	
VI	2550±42	84.5±1.3	206.5±9.5	1.67	55.6±13.2
VII	3051±47	85.3±0.4	168.5±78.5	2	80.5±11.1

The operation condition is shown in Table 1.

NH<sub>4</sub><sup>+</sup>-N\*:NH<sub>4</sub><sup>+</sup>-N released from IC effluent

## 2.2 Sampling and analytical methods

Water samples were measured through the analytical methods for water quality and wastewater monitoring (the 4th Edition) issued by the State Ministry of Environmental Protection. The analytical items are  $\text{NH}_4^+\text{-N}$ ,  $\text{NO}_2^-\text{-N}$ ,  $\text{NO}_3^-\text{-N}$ , TN, COD, MLSS and MLVSS. The values of pH, DO and temperature were monitored online with a WTW multifunctional meter (WTW, Germany).

## 3 Results and discussion

This study was divided into seven stages, containing the initial domestication and the stable operation stage. As shown in Fig. 1, in stage I, the anaerobic digestion sludge achieved a COD removal efficiency of 79.4-85% at an influent organic load of 4-6  $\text{kg}/\text{m}^3/\text{d}$ , indicating that the sludge gradually adapted to the MMW and was successfully domesticated. When the organic load is increased to 8  $\text{kg}/\text{m}^3/\text{d}$ , the IC-COD removal efficiency decreases to 75% and aerobic oxidation of COD occurs in the PN zone. The organic load was restored to 6  $\text{kg}/\text{m}^3/\text{d}$  in order not to affect the subsequent PN/A denitrification performance, but the subsequent operation was stable enough to continue the load increase. As the COD concentration increased, the ammonia nitrogen in the IC effluent was raised from 80 $\text{mg}/\text{L}$  to 200 $\text{mg}/\text{L}$ . The ammonia nitrogen conversion efficiency in the PN zone was controlled at 50-58% by adjusting the aeration. A high FA (5-7 $\text{mg}/\text{L}$ ) was obtained mainly through the combined regulation of high  $\text{NH}_4^+\text{-N}$  (150-200 $\text{mg}/\text{L}$ ) and low DO (0.4-0.7 $\text{mg}/\text{L}$ ) in the PN zone to jointly suppress NOB and obtain a stable nitrite accumulation efficiency (80%). This process provided continuous  $\text{NO}_2^-\text{-N}/\text{NH}_4^+\text{-N}$  for the subsequent anammox reaction and the NRE was increased from 57.6% to 90%. During the experiments it was found that competition for DO from aerobic heterotrophic bacteria in the IC effluent led to a significant decrease in  $\text{NO}_2^-\text{-N}$  and  $\text{NO}_3^-\text{-N}$  in the PN effluent when the COD/TN was above 2.05. Therefore, maintaining a stable operation of the IC is a key step in the subsequent denitrification. Last but not least, the anammox process is significantly dependent on a stable nitritation process. At reflux ratios greater than 150%, the  $\text{NH}_4^+\text{-N}$  in the PN zone is diluted to 95  $\text{mg}/\text{L}$  resulting in a weakened NOB inhibition in the PN zone. Gas lifting reflux sends  $\text{NO}_3^-\text{-N}$  from the AMX zone back to the IC zone for internal enhanced denitrification, and refluxes below 150% reduce the overall denitrification performance of the IC-PN/A. Therefore, a guaranteed reflux ratio of 150% will result in high denitrification efficiency.

This pilot-scale integrated IC-PN/ a process is the first report to investigate MMW treatment. This result provides solid evidence that the IC-PN/ a system has good potential for treating actual MMW.

## 4 Conclusions

This study successfully demonstrates for the first time a pilot-scale IC-PN/A system for the anaerobic treatment of real high-strength MMW. During the long-term operation, the entire IC-PN/A system succeeded in the synergetic removal of both organic matters and ammonia nitrogen, achieving over 85% and 90% removal of COD and TN, respectively. The division of work is also realized through the integrated three-stage design of the system. The results of this study provide solid research experience for the future application in practical industrial organic wastewater

treatment process and also contribute to the promotion of the IC-PN/A process.

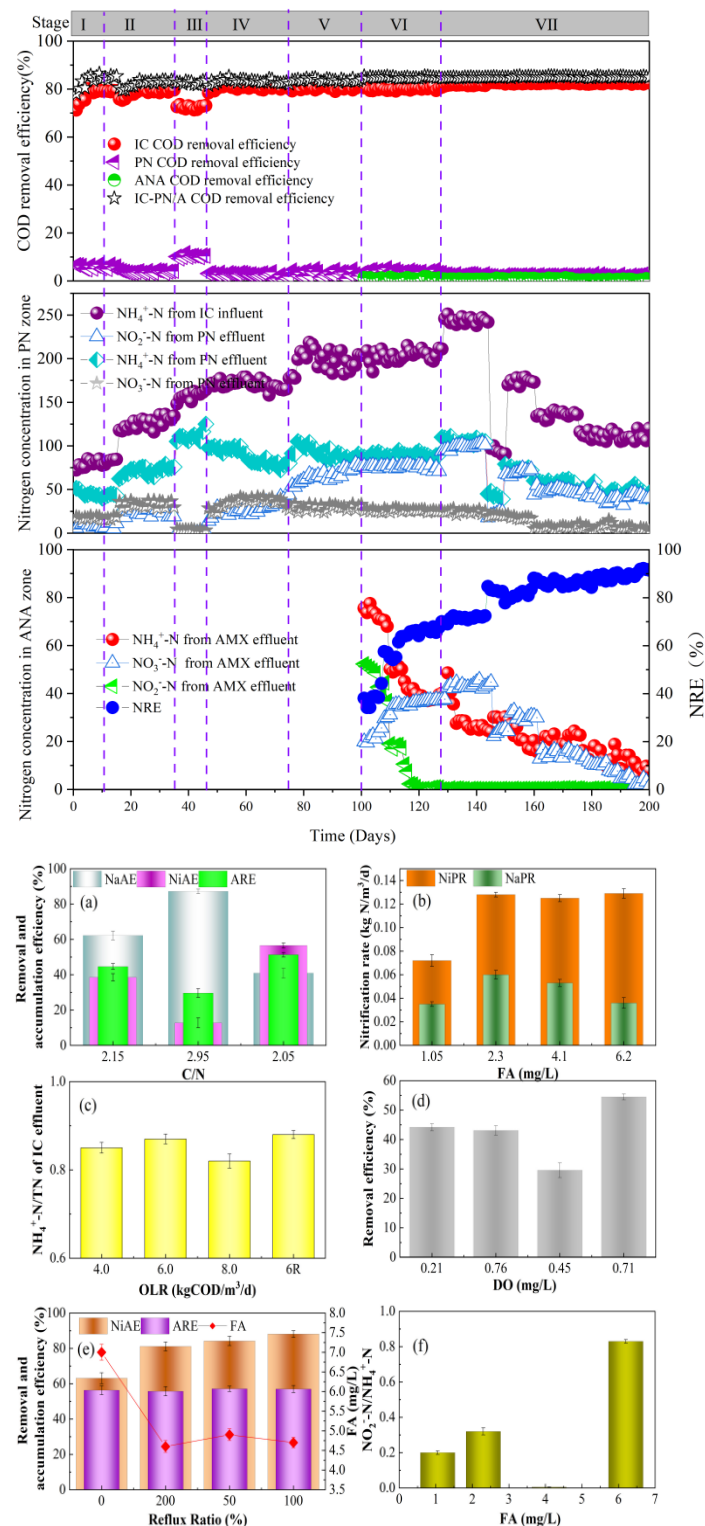


Fig. 1. Long-term performance of IC-PN/A

## Reference

[1] Issaoui, M. 2022. Membrane technology for sustainable water resources management: Challenges and future projections. Sustainable Chemistry and Pharmacy, 25, 100590.

## Impacts of different Biochar/Ni types on the anaerobic digestion of high salinity wastewater

○ Chen-shun Lu<sup>1\*</sup>, Jin-ming Qiu<sup>1</sup> & Yong Hu<sup>1</sup>

<sup>1</sup>School of Environmental Science and Engineering, Nanjing Tech University, Nanjing 211816, China.  
\*E-mail: cs999v@163.com.

### Abstract

For the anaerobic biological treatment of high salinity wastewater, anaerobic digestion (AD) is currently a possibility, even though elevated salt concentrations can be a major obstacle. To ameliorate the negative effects of high salinity, adding materials has been reported as an effective way. Biochar plays an active role in anaerobic digestion and high salinity wastewater treatment due to its excellent properties. Due to the different characteristics of the biochar raw materials, the biochar made by pyrolysis also have different characteristics, and the biochar loaded with nickel ions has been proved to be a possibility of anaerobic digestion. In this study, we focused on the impacts of biochar/Ni made by pyrolysis of three different kinds of wastes (shrimp shells, pine wood and residual sludge) on the treatment of high salinity wastewater by granular sludge. Besides, the impacts of different addition amount and different load nickel ion concentration were also considered. The addition of 2 g/L biochar/Ni can promote the methane production rate and activity, while the addition of 10 g/L can slightly delay the methane fermentation. High concentration can strongly inhibit the methane production rate, while the cumulative methane production is only 56.8% of the unadded.

**Keywords:** Biochar/Ni; Anaerobic digestion; Cumulative methane production; High salinity.

### 1 Introduction

High-salinity wastewater is produced from various industries, such as textile-dyeing, tanning, petroleum and food-processing industries. It is reported that about 5% of industrial effluents are saline or high salinity. A variety of physical, chemical and biological technologies have been applied to the treatment of saline wastewater. Compared to physical and chemical treatment processes, the biological processes are energy conservation, no secondary pollution and more convenient. Especially, anaerobic treatment of high salinity industrial wastewater has attracted considerable attention over the past decades because of the recovery of net energy, the reduction to sludge production and the possibility to handle higher volumetric loading rates if the formation of granular or immobilized biomass is possible. However, high salinity is regarded as a stress factor that severely hampers the performance of biological systems, negatively affecting biomass retention. High salinity can induce a significant increase in osmotic pressure, which resulting in a decrease in cell activity and eventually leading to cell plasmolysis and cell death.

The effect of biochar as an additive in anaerobic digestion has become a research hotspot. A variety of biomass types can be used as feedstock for pyrolysis, and the type of feedstock selected affects the biochar properties. supporting bacteria colonies, conducting electron transfer between species, and adsorbing indirect inhibitors could be mechanisms that biochar uses to promote methanogenesis [1]. The variability of these specific effects is controlled by the physicochemical properties of the biochar, which is attributed to the feedstock types and pyrolysis conditions used for its production. In addition, nickel (Ni) is one of the necessary nutrient elements for the synthesis of microbial, which was involved in the synthesis of CO dehydrogenase,

acetyl-CoA synthase and methyl coenzyme reductase cells in the process of anaerobic microbial growth and reproduction, and plays an important role in methanogens. The addition of biochar and the cations were considered to be effective strategies in anaerobic digestion, but few studies discussed their respective roles in the anaerobic treatment of high salinity wastewater, let alone the combined impacts of biochar/Ni.

Thus, this study focused on the impacts of biochar/Ni made by pyrolysis of three different kinds of wastes (shrimp shells, pine wood and residual sludge) on the treatment of high salinity wastewater by granular sludge, and investigated the impacts of different addition amount and different load nickel ion concentration.

### 2 Materials and methods

#### 2.1 Reactor set-up and operation

Two 1 L working volume up-flow anaerobic sludge blanket (UASB) reactors named R1 and R2 were conducted. Both reactors were covered with a water jacket to control the temperature at  $35 \pm 1$  °C. In the present study, glucose was added as the sole organic carbon source to the substrate at a concentration of 2812 mg/L (COD of 3 g/L). The two reactors had similar performance and were used as the source of batch experimental seed sludge. The concentration of the total sodium in the substrate was maintained at 10 g/L.

The operation condition is shown in Table 1

Stage	Time (days)	HRT (d)	OLR (g-COD/L/d)	Na <sup>+</sup> (g/L)
1	0-57	2	1.5	10
2	58-108	1	3	10
3	109-127	0.5	6	10

## 2.2 Biochar preparation

Shrimp shell, pine wood and residual sludge were used to produce biochar. It was put into quartz tube reactor and slowly pyrolyzed in a tube furnace with a highly purified nitrogen gas environment. The slow pyrolysis was performed at the temperature of 600 °C for 2 h and the heating rate was 10 °C/min. Samples were washed three times with deionized water to remove impurities and dried in the oven at 105 °C.

The static adsorption experiments were carried out in 1 L conical flasks. 500 mL of Ni<sup>2+</sup> solution with a desired concentration and 5 g of shrimp shells biochar (SBC), pine wood biochar (PBC) and residual sludge biochar (RBC) were added into each conical flask. Then conical flasks were placed at a constant temperature shaker, where the temperature and the rotational speed were 30 °C and 150 r/min, respectively. After 24 h of adsorption, biochar and solutions were separated by a suction filter with 0.22 μm membrane. National standard (GB) method was used to test concentrations.

## 2.3 Batch experiment

Batch anaerobic digestion experiments were carried out in 100 mL serum bottles. Seed sludge is derived from the granular sludge cultured by UASB. Each serum bottle had 2 g of granular sludge (100 mg VS), 60 mL liquid (glucose and trace element). Different addition amounts (0, 2, 3.33, 6.67, 10, 13g/L) and SBC loaded Ni (SBC-Ni), PBC loaded Ni (PBC-Ni) and RBC loaded Ni (RBC-Ni) were added into each serum bottle. Nitrogen was used for air evacuation to ensure anaerobic conditions. All digestion bottles were placed in a constant temperature incubator at 35 °C.

## 2.4 Sampling and analytical methods

Daily biogas production in two UASB reactors was monitored with μFlow gas meters (Bioprocess Control Sweden AB). The determination of biogas composition (CH<sub>4</sub>, CO<sub>2</sub> and N<sub>2</sub>) in batch experiment was carried out using a gas chromatography (GC-2010, Shimadzu). The effluents from the two UASB reactors were sampled and analyzed twice per week for pH, COD, suspended solids (SS). SS were detected according to the Standard Method. The pH value was determined with a pH meter (FE30k), while COD measurements were performed with COD digest vials (HACH Loveland, CO, USA).

## 3 Results and discussion

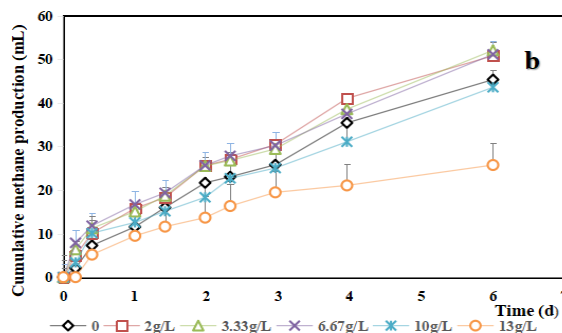
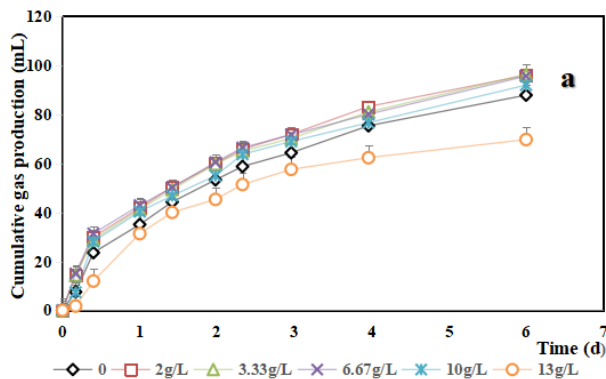


**Fig. 1. The effects of the different amount SBC-Ni on methane (a), gas production (b)**

Fig. 1(a) depicts the changes of total biogas produced by anaerobic digestion of high salinity wastewater. After 6 days of reaction, the total biogas production of 0, 2, 3.33, 6.67, 10, 13g/L SBC-Ni were 87.25, 95.88, 96.20, 95.50, 91.83 and 69.63mL, respectively. According to Fig. 1(b), the total methane volumes after the reaction were 45.32, 50.79, 52.04, 51.12, 43.57, 25.73 mL, respectively. Each bottle contained 100 mg VS of seed sludge, so the methane yields were 453.2, 507.9, 520.4, 511.2, 435.7 and 257.3 mL/(g·VS), respectively. As seen in Fig. 1(b), the addition of SBC-Ni from 2 g/L-6.67 g/L made the reactor start-up time shorter than that in unadded, and increased the average CH<sub>4</sub> content by about 10%. The reactor containing SBC-Ni was more conducive to the enrichment of methanogens in the initial stage. While, the addition of 10 g/L and 13 g/L SBC-Ni can delay the methane fermentation. High concentration can strongly inhibit the methane production rate, and the cumulative methane production is 56.8% of the unadded.

Nickel (Ni) is an important component of methanogens, cofactor and coenzyme. Although a certain concentration of Ni has a positive effort on process stability and biogas production, it takes time for microorganisms to get used to the Ni contained environment. It is reported that a high concentration of Ni<sup>2+</sup> is toxic to methanogens, which can cause oxidative stress and DNA damage [2]. Besides, the addition of high concentration biochar is proved that will strongly inhibit the accumulated methane production of anaerobic digestion.

## 4 Conclusions

So far, in this study, the effect of different amount addition of SBC-Ni on anaerobic digestion was studied. The low addition of SBC-Ni promoted the efficiency and stability of the whole methane production, and the invigorating effect of it was mainly concentrated in methanogenesis, while the inhibition effect of high addition amount of SBC-Ni was comprehensive. Appropriate amount SBC-Ni can be added into anaerobic digestion systems of high salinity wastewater for enhanced efficiencies and improved methanogenesis inhibition.

## Reference

- [1] J. Pan, J. Ma, X. Liu, L. Zhai, X. Ouyang, H. Liu, Effects of different types of biochar on the anaerobic digestion of chicken manure, *Bioresour Technol*, 275 (2019) 258-265.
- [2] X. Li, M. Wu, Y. Xue, Nickel-loaded shrimp shell biochar enhances batch anaerobic digestion of food waste, *Bioresour Technol*, 352 (2022) 127092.

# Effect of aeration intensity on a compact biofilm reactor for rural domestic sewage treatment in China: pollutant removal performance and hydrodynamic behavior

○ Weiyi WANG<sup>1\*</sup> & Yu-You Li<sup>1,2</sup>

<sup>1</sup>Department of Frontier Science for Advanced Environmental, Graduate School of Environmental Studies, Tohoku University, Miyagi 980-8579, Japan.

<sup>2</sup>Department of Civil and Environmental Engineering, Tohoku University, Graduate School of Engineering, Miyagi 980-8579, Japan.

\*E-mail: wang.weiyi.s5@dc.tohoku.ac.jp

## Abstract

The treatment of rural domestic sewage in China requires the process with low operational cost and easy maintenance. Thus, the effect of aeration intensity and aeration pattern on the treatment effect of bioreactor needs to be well investigated. In this study, the pollutant removal performance and hydrodynamic behavior of a compact biofilm reactor (purification tank) under different aeration conditions were studied. The results show that the gas rising velocity of 0.066 m/s led to a better pollutant performance and hydrodynamic behavior, compared with velocity of 0.013 and 0.120 m/s. Besides, under the multistage A/O pattern with step-feed, the average effluent concentrations of NH<sub>4</sub><sup>+</sup>-N and TN were 3 and 14 mg/L, respectively, which are lower than national discharge standards of pollutant for municipal wastewater treatment plant (GB18918-2002). The step-feed operation in the second anaerobic zone of the purification tank could well solve the problem of insufficient carbon source and strengthen the nitrogen removal function. Overall, the experimental study and hydrodynamic modelling provide the direction for the application of full-scale purification tank in rural China.

**Keywords:** wastewater treatment; domestic sewage; rural China; purification tank; CFD.

## 1 Introduction

As a compact biofilm reactor, the purification tank is a very suitable technology for in-situ treatment of rural domestic sewage, which has the advantages of good impact resistance, solid-liquid separation and simple installation. The effect of aeration intensity and aeration pattern on the treatment effect of bioreactor is particularly significant.

Effects aeration intensity and aeration pattern on removal of various pollutants were studied by experimental means. Specifically, the removal performance of pollutants under three different gas rising velocities was compared, and the nitrogen removal effect under multistage A/O process was investigated. On the other hand, 3-D transient gas-liquid two-phase flow CFD model was established to describe the hydrodynamic characteristics of the purification tank at different gas rising velocities. These studies provide reference for the practical application of the purification tank in treating rural domestic sewage in China.

## 2 Materials and methods

### 2.1 Set-up of bioreactor

The purification tank for a single household was designed to treat the sewage from 5 people's household. Schematic diagram of lab-scale purification tank for single household are shown in Fig.1. Consisted of two anaerobic zones and one aerobic zone. The volume in primary anaerobic zone, secondly anaerobic zone and aerobic zone, settling zoon were 14.5, 12.5, 11.5 and 5.0 L. To increase the surface, strength and corrosion

resistance of the biofilm in the purification tank, porous corrugated plate was used as the biofilm carrier with specific surface area of 70 m<sup>2</sup>/m<sup>3</sup> and filling volume of 60% of each zone. The volume of lab-scale experimental equipment is 1/66 that of the full-scale purification tank.

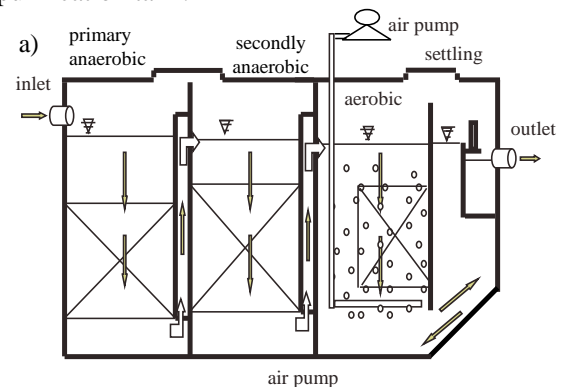


**Fig. 1. Schematic diagram of lab-scale purification tank for single household**

### 2.2 CFD mathematical model

The geometry of lab-scale purification tank was set to be length of 0.526 m, width of 0.406 m and height of 0.405 m. A total of 15 aerators were set, evenly distributed at the bottom of the purification tank. The top of the reactor was believed to be an air outlet. A schematic of the lab-scale purification reactor and its computational meshes for the 2D and 3D geometries are shown in Fig. 2. Due to the complex flow patterns in the purification tank, the standard k-ε turbulence model was chosen. The experiment adopted Euler multiphase flow mathematical model.

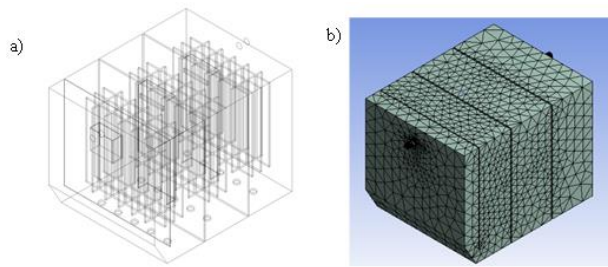


**Fig. 2. Three-dimensional computational domain: (a) reactor schematic diagram (b) computational grid**

### 3 Results and discussion

The changes of COD in each zone of the purification tank under different gas rising velocities in the aerobic tank are shown in Fig. 3a. Once the aeration was introduced, the COD degradation ability was continuously increased along with the augmentation of aeration intensity. Specifically, COD was slightly degraded to 84 mg/L at the gas rising velocity of 0.013 m/s, however it was greatly removed at the air velocity of 0.066 m/s with effluent COD concentration of 41 mg/L. Finally, it is indicated the larger air velocity of 0.120 m/s cannot greatly contribute to the higher removed COD amount. The BOD<sub>5</sub> changes of each zone in the purification tank under different gas rising velocities was shown in Fig. 3b. The changing tend of BOD<sub>5</sub> was similar to that of COD.

The effects of aeration intensity on the NO<sub>3</sub>-N and NH<sub>3</sub>-N concentrations were shown in Fig. 3c and 3d. The anaerobic condition did not change the nitrogen concentration. Along with the increase of gas rising velocity in the aerobic zone, the effluent NH<sub>3</sub>-N concentration was greatly reduced. Accompanied by the decreased of NH<sub>3</sub>, the NO<sub>3</sub>-N concentration correspondingly increased, especially up to 16 and 32 mg/L at high gas rising velocity of 0.066 and 0.120 m/s (Fig. 3d). The difference of reduced NH<sub>3</sub>-N and produced NO<sub>3</sub>-N concentration was calculated to be 30 and 23 mg/L at gas rising velocity of 0.066 and 0.120 m/s, respectively. This means that the more nitrogen was removed at the gas rising velocity of 0.066 m/s.

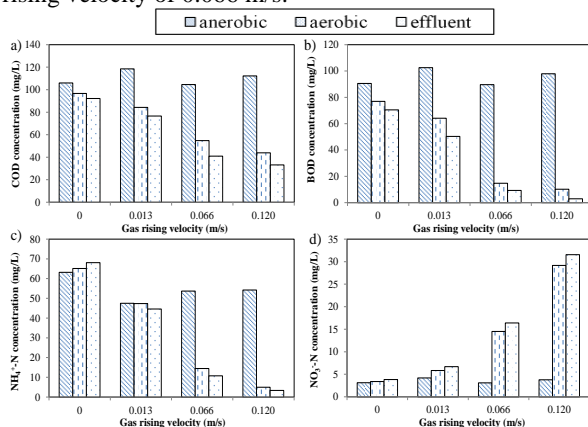


**Fig. 3. Changes of COD (a), BOD<sub>5</sub> (b), NH<sub>4</sub><sup>+</sup>-N (c) and NO<sub>3</sub><sup>-</sup>-N (d) concentrations in different zones of purification tank under three gas rising velocities**

The liquid phase flow field in the purification tank with different gas rising velocities is shown in Fig. 4. By comparing the flow charts under different gas rising velocities, when there was no aeration in the tank, a break point appeared in the flow chart inside the biofilm carrier,

indicating that the liquid phase distribution was not uniform. When the gas rising velocity arrived at 0.013m/s, the flow uniformity became better, but no eddy current was formed. Furthermore, when the gas velocity further increased to 0.066m/s, the fluid in the purification tank had the best hydrodynamic behavior being uniform. This phenomenon indicates that the gas velocity in the purification tank played an important role in the flow field distribution in the tank. The velocity of 0.120 m/s contributed to smaller vortex at the top of purification tank relative to velocity of 0.066 m/s. Since the vortex at the bottom of the biofilm carrier was more favorable for the renewal of the biofilm attached to the carrier, so the gas rising velocity of 0.066 m/s was suggested to be adopted.

Regarding with the hydrodynamic behavior, the gas rising velocity also played an important role. Firstly, the bubbles produced by aeration gather near the aerator and are cut and evenly distributed in the whole tank under the help of biofilm carrier. But the weak aeration with gas rising velocity of 0.013 m/s did not make a strong positive effect on the hydrodynamic behavior. Besides, the bubble size was relatively large, not conducive to the contact and mass transfer of gas-liquid two phases. When the gas rising velocity increased up to 0.066 m/s, the gas phase could pass through the biofilm carrier. Overall, appropriately increasing the rising velocity can not only reduce the bubble size, but also increase the turbulence between the two phases.

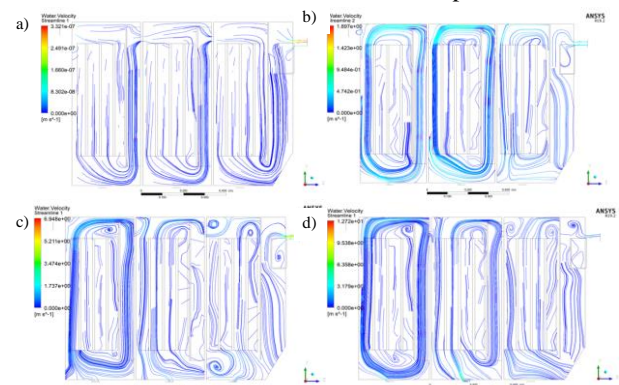


**Fig. 4. The liquid flow field diagram under anaerobic condition (a) and aerobic condition with gas rising velocities of 0.013 m/s (b), 0.066 m/s (c) and 0.120 m/s (d)**

### 4 Conclusions

The pollutant removal efficiency of purification tank could be considerably enhanced with increase of aeration intensity. But the gas rising velocity was suggested to be controlled in a medium level of 0.066 m/s. The pollutant removal and hydrodynamic behavior both performed well under this aeration intensity. Besides, appropriately increasing the gas rising velocity could not only reduce the bubble size, but also increased the turbulence between the gas-liquid phases.

### Reference

[1] P. Jin, Efficient nitrogen removal by simultaneous heterotrophic nitrifying-aerobic denitrifying bacterium in a purification tank bioreactor amended with two-stage dissolved oxygen control, *Bioresource Technology*, 281 (2019) 392-400.

# Effect of up-flow anaerobic sludge blanket reactor treating methanolic wastewater by adding complex accelerant

○Juntong Ha<sup>1\*</sup>, Liuying Song<sup>2</sup>, Qin Yu<sup>2</sup> & Yu-you Li<sup>1,2</sup>

<sup>1</sup> Department of Frontier Science for Advanced Environment, Graduate School of Environmental Studies, Tohoku University, Miyagi 980-8579, Japan.

<sup>2</sup> Department of Civil and Environmental Engineering, Tohoku University, Graduate School of Engineering, Miyagi 980-8579, Japan

## Abstract

In this study, to improve the efficiency of anaerobic digestion(AD) in an up-flow anaerobic sludge blanket reactor (UASB reactor) treating methanolic wastewater, we investigated the effect of adding a complex accelerant containing nutrients and amino acids. The experiment was divided into two parts: batch experiment and long-term continuous experiment. Firstly, the effect of the accelerant on the enhancement of anaerobic bacterial activity was verified by batch experiments. The results showed that the accelerant had a positive effect on microbial activity. Secondly, We used a lab-scale UASB reactor for the long-term continuous experiment to investigate the effect of accelerant on the performance of the reactor under different organic loading rates, and we also observed the effect on the sludge granulation. The experiments showed that the addition of the accelerant was able to operate stably at high loading conditions (OLR up to 30gCOD/L/d) with a COD removal rate of over 90%. Furthermore, the addition of the accelerant also had a positive effect on the granulation of sludge. Finally, we hypothesized that the addition of an accelerant could diversify the metabolic pathway of methanolic wastewater.

**Keywords:** Anaerobic digestion; Methanolic wastewater; UASB reactor; Accelerant; Sludge granulation.

## 1 Introduction

In recent years, with the process of industrialization and modernization, as well as the acceleration of economic globalization and the increase in chemical sales, the massive discharge of industrial wastewater has become a serious environmental problem. However, as a traditional waste treatment technology, due to incineration and landfill, greenhouse gas emissions, and soil pollution is not environmentally friendly. Therefore, there is a strong recognition of the importance of developing environmental waste treatment technologies to achieve carbon-neutral and sustainable societies, which could reduce CO<sub>2</sub> emissions, recover resources, save energy and create energy.

Anaerobic digestion(AD), with its carbon-neutral properties, is also widely used for the treatment of industrial wastewater containing large amounts of organic matter. Although AD technology is being seen as a method of generating energy from waste-based biomass resources, AD of methanolic wastewater suffers from bottleneck problems, such as lack of nutrients, sludge run-off, unstable operation, and so on. Methanol is been well known as a major component of various chemical industries and has a large annual discharge. In the meantime, methanolic wastewater has great potential for reuse because it is easily converted to methane, and does not require hydrolysis in the AD process. However, the current on-site UASB reactors are suffering from difficulties in forming granular sludge when methanol is the only substrate and a large amount of granular collapse and discharged outside the system, which severely limits its wide application in the anaerobic treatment of methanol<sup>[1]</sup>.

In this study, to improve the efficiency of AD in the UASB reactor treating methanolic wastewater, we investigated the effect by adding a complex accelerant that was obtained from the Ajinomoto plant and rich in trace metal elements and amino acids.

## 2 Materials and methods

### 2.1 Batch experiment

Sludge was obtained from the UASB reactor that treats beer wastewater on-site. The concentration of the methanol was 1.88 g-COD/L. A total of 80 ml of buffer, nutrient solution, accelerant(127mg/L), tap water, substrate, and sludge were mixed in serum vials (volume 120 ml), which were tightly closed with rubber stoppers and aluminum seals and then blown with nitrogen gas to create an anaerobic environment, and batch experiments were carried out at 35°C. The additional amount of accelerant(0.04%,0.5% of COD base) added in the different serum vials was varied. All experimental sets were run in double. An additional set of serum vials as blank was employed without accelerant added.

### 2.2 Long-term continuous experiment

A UASB reactor with a working volume of 6 L was operated at 35°C conditions. Table 1 shows the operating conditions of the UASB reactor during one-year operation, organic loading rate(OLR) was increased by a step-wise reduction in hydraulic retention time(HRT), and the effect of accelerant on reactor operation stability was investigated, furthermore, the particle size distribution of the sludge was measured periodically.

**Table 1 Operation Conditions.**

Phase	1	2	3	4	5	6	7	8	9
Duration	1	92	130	156	180	205	221	249	295
time(d)	91	129	155	179	204	220	248	294	309
HRT(h)	20	2 0	1 1	8	4.3	5	3.6	2.4	2.4
OLR	4	4	7	10	17	14	20	30	48
(gCOD/L/d)									
Methanol	3	3	3	3	3	3	3	3	5
(gCOD/L)									
Accelerant	0	0.0	0.0	0.0	0.0	0.0	0.0	0.0	0.0
(gCOD/L)		4	4	4	4	4	4	4	7
Total	3	3.0	3.0	3.0	3.0	3.0	3.0	3.0	5.0
(gCOD/L)		4	4	4	4	4	4	4	7

### 2.3 Sampling and analytical methods

All samples of influent and effluent were analyzed after being filtrated through Millipore filter units with 0.45µm pore size. The composition of the biogas(CH<sub>4</sub>, CO<sub>2</sub>)was measured once daily using a gas chromatograph with a TCD detector (Shimazu, GC-8A). The volatile fatty acids(VFAs)were quantified by gas chromatography(Agilent 6890 series)

## 3 Results and discussion

### 3.1 Batch experiment in different amounts of accelerant

As shown in Table 2, the blank group had the highest methane production rate of 133 mL/gVS/d, while it reached 108 and 76 mL/gVS/d in the amount of 0.04% and 0.5% accelerant respectively. On the other hand, the lag phase was shorter than the blank group under the condition of 0.5% accelerant added. These results indicate that the accelerant had a positive effect on microbial activity.

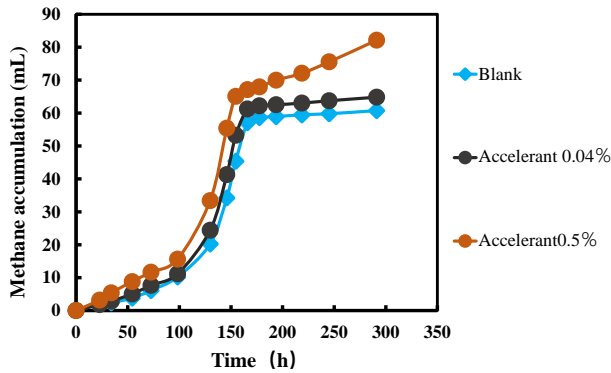


Fig. 1. Batch progress data.

Table 2 Results of fitting the batch progress data with the modified Gompertz model

	The maximum potential of CH <sub>4</sub> production (mL-CH <sub>4</sub> /gVS)	Maximum CH <sub>4</sub> production rate (mL/gVS/d)	Lag phase (d)
Blank	258	133	4.8
Accelerant 0.04%	278	108	4.2
Accelerant 0.5%	343	76	3

### 3.2 Long-term experiment with UASB reactor treating with synthetic methanolic wastewater

Fig.2 shows the results of a long-term continuous operation of the UASB reactor for approximately one year. Accelerant started to be continually added from phase2. The pH and CH<sub>4</sub> content were stable in the range of 7.2-7.5 and 83% respectively from phase 1 to phase 8. The methane production rate also increased progressively with increasing OLR. During this period, no VFA was detected in the effluent, indicating stable operation is achieved. However, in phase9, when the OLR was increased to 48 gCOD/L/d, there was a decreasing trend in pH, and alkalinity and the CH<sub>4</sub> content decreased to 75%. In addition, the rate of methane production gradually began to decrease. Although there was little change in the NH<sub>4</sub><sup>+</sup>-N concentration in the effluent. However, the COD concentration in the effluent increased to an average of 800 mg/l and the COD removal rate decreased from 90% to 80%. Besides, the accumulation of VFA was detected in this phase.

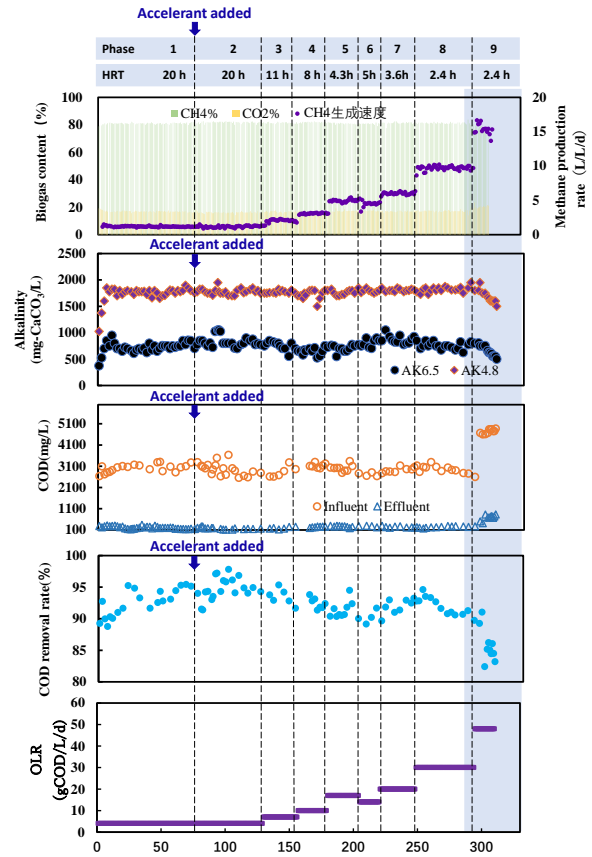


Fig. 2. Long-term performance of methanolic wastewater treatment by adding accelerant.

### 3.2 Effect on sludge granulation

To investigate the effect of the accelerant on sludge granulation, the particle size distribution of the sludge was measured periodically. Table 3 shows a summary of the median diameter (D50). It can be seen that the particle size increases significantly along the longitudinal direction of the reactor. In addition, the particles formed in the reactor did not collapse and no sludge uplift was observed.

Table 3 Comparison of median diameter (D50) results

Time	72d	109d	126d	156d	175 d	192d	248d	280d
Top(µm)	123	125	63.4	81.1	76.8	139	538	579
Medium(µm)	383	316	370	314	369	697	610	440
Bottom (µm)	579	560	533	561	578	650	620	543

## 4 Conclusions

Through batch experiments, we observed that the addition of 0.5%(COD base) accelerant could reduce the lag phase, but did not increase the rate of gas production. As for the long-term experiment, stable operation can be achieved even under high OLR conditions (up to 30g COD/L/d) with a COD removal rate of over 90%. However, when the OLR was as high as 48g COD/L/d, it resulted in the accumulation of VFA in the reactor and began to operate unstably. The addition of an accelerant can promote sludge granulation and proliferation, and also inhibits sludge collapse.

## Reference

[1] Xueqin LU, Biocatalysis conversion of methanol to methane in an up-flow anaerobic sludge blanket (UASB) reactor: long-term performance and inherent deficiencies, Bioresource technology198(2015), 691-700.

## Predictive numerical modeling of landslide susceptibility: A case study for Uma Oya catchment, Sri Lanka.

○ Abeygunasekara HASHANI<sup>1\*</sup>, Kazama SO<sup>1</sup>

<sup>1</sup>Department of Civil and Environmental Engineering, Tohoku University, Miyagi 980-8579, Japan.

\*E-mail: hashani.anuttara.abeygunasekara@dc.tohoku.ac.jp

### Abstract

Predicted landslide susceptibility offers vital input to effective disaster risk management. Landslide susceptibility is an important consideration referring to the central highlands in Sri Lanka, given the unique combination of climatic and hydro-geological conditions it is featured with. Provided the unique spatio-temporal configuration, the applicability of a global model to predict the landslide susceptibility becomes less effective, which requires much adaptation. Numerical modeling powered with globally evaluated climatic data combined with some field data provides an effective solution to model the corresponding landslide-inducing environment and predict the slope stability conditions within the local settings. The study suggests the validity and the applicability of the suggested approach to numerical modeling of slope stability within the target region, thus contributing to the fact that landslide triggering conditions are much sensitive to the input feature variables defined by both global climatic conditions and local hydro-geological settings.

**Keywords:** landslide susceptibility; slope stability; numerical modeling; disaster risk management

### 1 Introduction

Landslides are catastrophic events induced by various causes. The factors that induce landslides include both natural and anthropogenic processes. Rainfall and the geomorphology of a specific location act together to determine the slope stability of the ground leading to the generation of a slope failure. Ground water table acts a significant role in shaping the slope stability of the ground. The weight induced by the increased water table tend to induce much weight on the sliding plane which causes the land to slide along the sliding plane. Accordingly, the rainfall acts a significant role in determining the slope stability of the ground.

Comprehensive understanding of the processes related to hydrology cycle is much important which enables understanding the related mechanisms and causative factors behind the disaster events. With application to the landslides, the extreme rainfall events cause the precipitation to exceed the infiltration capacity of the ground, which in turn generate surface runoff that is added to the surface water channels shaped by the topography of the terrain. The water that is infiltrated is subjected to either interflow or deep percolation. The interflow is added to the stream network while the water that is deep percolated causes the ground water recharge. Provided the properties of the deep aquifers, and the state of equilibrium, the ground water recharge or discharge may occur in between the aquifers and the surface water resources.

The research is intended to investigate the predictability of landslide susceptibility within the region, by numerically modeling the regional hydrological processes. Accordingly, the proposed methodology is a stepwise approach i.e., to model the dynamics of the water table within the region and then use the same to evaluate the dynamics of the slope stability to predict the likelihood of a landslide event.

### 2 Materials and methods

Numerical model was developed to simulate the related hydrological processes to evaluate the dynamics of slope stability within the study region.

Step 1: Rainfall runoff model

The study period was set to 2015-2016 based on the availability of input data for the study region. Daily values for the precipitation measured at 15 rainfall gauges and minimum and maximum temperature measured at one temperature gauge were used to the net effective precipitation using the following equations.

$$\text{Effective Precipitation} = \text{Rainfall} - \text{Evapotranspiration} \quad (1)$$

$$\text{Infiltration} = \text{Min}(\text{Eff. Precipitation}, \text{Infilcapacity}) \quad (2)$$

$$\text{Surface runoff} = \text{Max}(0, \text{Eff. Precipitation} - \text{Infiltration}) \quad (3)$$

$$\text{Interflow} = \text{Infiltration} - \text{gwRecharge} \quad (4)$$

$$\text{Baseflow} = \text{gwRecharge} - \text{gwStorage} \quad (5)$$

$$\text{Streamflow} = \text{Surface runoff} + \text{Interflow} + \text{Baseflow} \quad (6)$$

$$\text{gwStorage} = \text{Surface runoff} + \text{Infiltration} - \text{Streamflow} \quad (7)$$

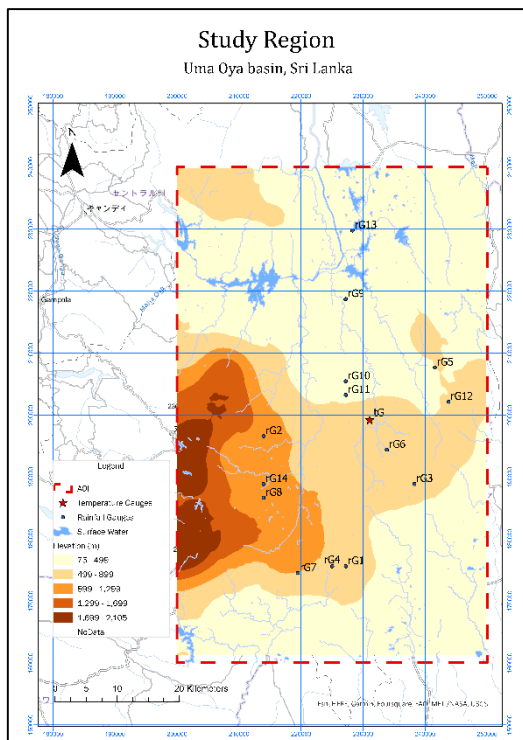


Figure 1: Study Area - Uma Oya basin, Sri Lanka

Then the landuse distribution of the region was analyzed to recategorize the existing landuse classes, which were used as the basis to determine the infiltration capacity of each unit of ground within the grid.

Provided the effective rainfall intensity exceeds the infiltration capacity of the ground, the surface runoff is generated, in terms of infiltration-excess overland flow.

Besides the mass balance of water budget was used to derive the formulae to model the daily water table within the study region.

#### Step 2: Relation to the landslide susceptibility

The evaluated temporal series of groundwater table was evaluated against various landslide occurrences recorded within the study period to identify the behavior of the water table within the designated period as simulated by the model. The attempt was focused on mapping the slope stability of the ground with the dynamics of the water table.

### 3 Results and discussion

Temporal series of factor of safety evaluations were compared with the known examples obtained from the ground surveys to evaluate the accuracy of the model results. Thus, Table 1 shows the regions that were identified as the most susceptible to landslides, which could be verified against the historical landslide records obtained from the National Building Research Organization, Sri Lanka. Moreover, the zonal statistics calculated for the same indicate that the majority of the landuse within these regions are the homesteads and tea cultivations.

**Table 1: Most landslide-susceptible regions within AOI**

Administrative Division	Code	Major Landuse
Kandededara Town	27A	Tea cultivation
Bandarawela Estate	65B	Home gardens
Hapuwalakumbura	73A	Tea cultivation
Hindagoda	78K	Home gardens
Dematawelhinna	82B	Home gardens
Medagama	84	Tea cultivation

Besides the results were analyzed for the associated trends in the characteristics of the landslide inducing environments. The same indicated a variety of combinations of the related attributes that have contributed towards defining a landslide event. Table 2 highlights few of such trends that could be observed within the landslide inducing settings.

**Table 2: Characteristics within the susceptible regions**

Characteristics	2015/1/1	2015/1/2	2015/1/3	2015/1/5	2015/1/6
	2015/1/2	2015/1/3	2015/1/5	2015/1/6	
Max Diff in WT(m)	3.97	1.58	16.28		
Attributable Regions	65B	73	27A		
	78K	84	73A		
Major Landuse	Homestead	Tea	Tea		
Gradient of Terrain	Low	High	High		

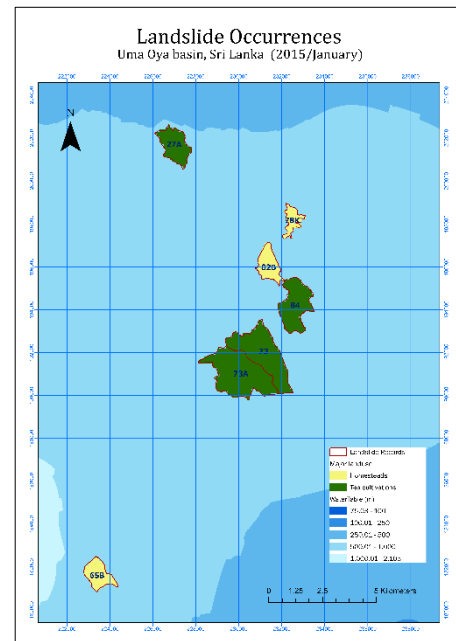


**Figure 2: Regions with landslide occurrences**

### Conclusions

The climatic conditions tend to create a significant contribution towards shaping the landslide inducing environments, whereas the extreme rainfall events, temperature variations, landuse distribution and more importantly the local geomorphology are among the stimulators.

Assessment of landslide susceptibility is of utmost importance regarding the prevention of the significant losses and the management of risks associated with the disasters to minimize the associated losses. Improved predictability of the various scenarios of risks favor to improve the community-wide awareness, alertness and the preparedness which will in turn improve the community resilience against the downturns caused by the disastrous events.

The study is expected to contribute towards the related research community in its effort to map the relationship between the dynamics of groundwater table and the vulnerability of the land to slope failures through numerical modeling. Secondly the numerical model provides the basis for further analysis by offering a structured numerical model that is conveniently be improved and adapted to a variety of scenarios in future research work.

### References

- [1] L. Chen *et al.*, "Meta-learning an intermediate representation for few-shot prediction of landslide susceptibility in large areas," *International Journal of Applied Earth Observation and Geoinformation*, vol. 110, p. 102807, Jun. 2022, doi: 10.1016/j.jag.2022.102807.
- [2] Ö. Ekmekcioğlu and K. Koc, "Explainable step-wise binary classification for the susceptibility assessment of geo-hydrological hazards," *Catena (Amst)*, vol. 216, Sep. 2022, doi: 10.1016/j.catena.2022.106379.
- [3] A. Paetzold, C. Yoshimura, and K. Tockner, "Riparian arthropod responses to flow regulation and river channelization," *Journal of Applied Ecology*, vol. 45, no. 3, pp. 894–903, Jun. 2008, doi: 10.1111/J.1365-2664.2008.01463. X.

## Validation of a watershed storage effects for the analysis of climate change

○ Sora MARUTA<sup>1</sup>, -Seiki KAWAGOE<sup>1\*</sup>

<sup>1</sup> Faculty of Symbiotic Sciences Systems, Fukushima University, 960-1296 kanayagawa1, Fukushima, Japan.

\*E-mail: kawagoe@sss.fukushima-u.ac.jp.

### Abstract

Climate change has led to an increase in precipitation and the number of rivers exceeding their flood levels in all regions of Japan. It is pointed out that the amount of precipitation and the frequency of flooding will continue to increase in the future, and there is concern that the number of disasters that cannot be prevented simply by improving river channels will increase. In recent years, basin-based flood control measures have been promoted in Japan to reduce flood damage throughout the entire basin, and estimating the effect of water storage outside the river channel can help in the planning of basin-based flood control measures. In this study, data on off-channel water storage capacity for rice paddies, parks, and school reservoirs were collected on a national scale, and their functions were evaluated. In Fukushima Prefecture, the contribution of internal and external water storage was determined in consideration of future population changes, and priority areas were selected for countermeasures.

**Keywords:** Watershed management, Off-channel storage, Storage effectiveness.

### 1 Introduction

It has been confirmed that the amount of precipitation and the number of rivers exceeding the flood risk level have increased due to climate change. According to the IPCC Sixth Assessment Report, there is no doubt that human activities are contributing to global warming, and extreme events are expected to become more severe in the future [2]. In order to prevent flooding as much as possible, it is important to understand the amount of storage in the river basin in addition to the in-channel flow rate. In a study on off-channel storage, Shimura (1982) calculated the storage effect of rice paddies for the whole of Japan, covering an area of 3.17 million m<sup>3</sup> of rice paddies in 1975 [3]. For flood inundation analysis including off-channel storage, Kawaike et al. (2018) conducted a flood inundation simulation in the Nakahama treatment area in Osaka City, including off-channel storage in residential areas, schools, and parks, and mentioned the calculation of maximum inundation depth and inundation reduction effects [4]. Thus, while there are analyses that calculate storage in rice paddies throughout Japan and that anticipate off-channel storage effects for specific areas, there have been no calculations of off-channel storage and its functional evaluation for the entire country. Therefore, in this study, we compiled data on off-channel storage on a national scale and evaluated its function. Based on the data, we attempted to understand the changes in water storage contribution due to future socioeconomic changes in Fukushima Prefecture, and to select priority areas for countermeasures.

### 2 Materials and methods

Target off-channel storage options were selected, and the storage volume for each option was estimated on a watershed basis. Three off-channel storage options were selected: rice paddies, parks, and schools, and data were obtained from numerical geographic information. For rice paddy storage, the land structure was classified into three types: plain, sloping, and fan-shaped land. The depth of waterlogging was

set to 30 cm, 10 cm, and 20 cm, respectively. For park and school storage, the storage volume was calculated by setting the required waterlogging depth to 60% of the park and school yard area and 30 cm. The maximum hourly precipitation and mean temperature (warm-season normal, analysis period: 1991-2021) data were obtained from AMeDAS stations, and the equations were derived. The obtained regression equation was applied to the mean temperature of the warm-season normal of the mesh climate value 2010 to obtain an estimate of the maximum hourly precipitation for a 1 km mesh with spatial resolution.

Population data from the socioeconomic scenario developed by Chen et al. [2] were used to evaluate the contribution of internal and external water storage to population change within the watershed. SSP1 and SSP5 were selected as the upper and lower limits of the scenarios, and were also classified into three time periods: 2015 (base year), 2050, and 2100.

### 3 Results and discussion

The amount of storage in rice paddies, parks, and schools in Japan was about 3.68 billion m<sup>3</sup>, 0.34 billion m<sup>3</sup>, and 0.05 billion m<sup>3</sup>, respectively. The storage in parks and schools is estimated to be about 340 million m<sup>3</sup> and 0.5 billion m<sup>3</sup>, respectively, and storage is expected in the Tokyo, Chukyo, and Kansai areas (Figure. 1). The storage effect in space and time was calculated, and it was found that the storage effect was high on the northern Japan side, while the effect was not so great on the Seto Inland Sea side in the Chugoku region (Figure. 2).

The area with no population as of 2015 was 33.9% of all watersheds. The proportion of watersheds with no population did not change for both SSP1 and SSP5, basically indicating that watersheds with a population distribution as of 2015 tended to increase or decrease in population. Thus, it was not possible to determine the changing water storage contribution by the unpopulated areas. The off-channel storage in these unpopulated watersheds and watersheds with significant population decline contributes to the storage of

water for the reduction of outside water. On the other hand, storage in watersheds where the population will increase in the future or where the rate of population decrease is small will contribute to water storage to mitigate internal water damage in addition to external water reduction. Therefore, areas where the population is increasing or where the population decrease is relatively small were selected as priority areas.

In SSP1 and SSP5, there were some areas where the population will increase in 2050 (Figure. 3). These areas have a high return on investment in terms of both external and internal water supply, and should be prioritized for countermeasures. In addition, since the population will decrease in all watersheds by 2100, it is necessary to take future operations into consideration.

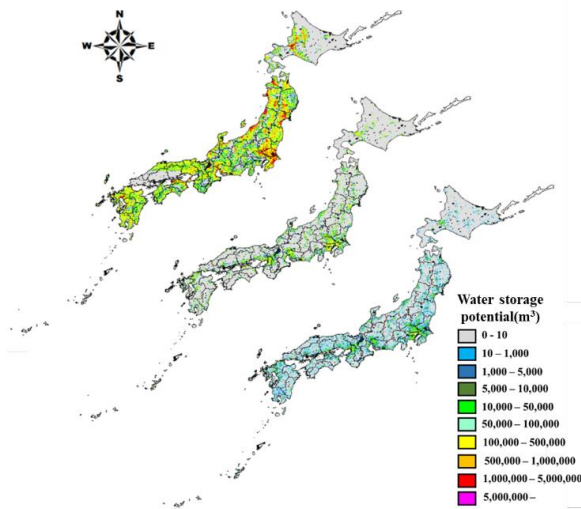


Fig. 1. Each storage potential map.

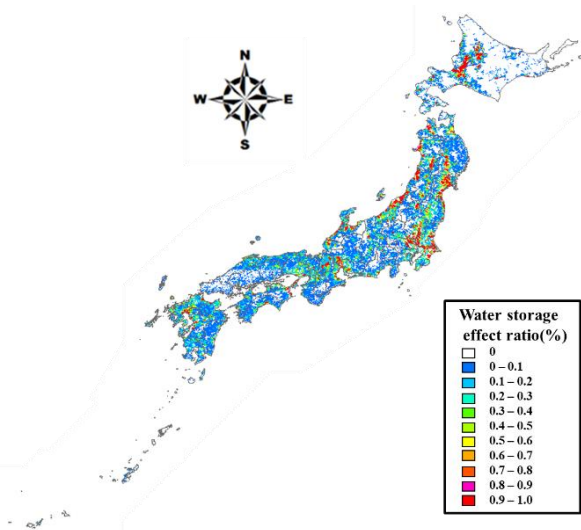


Fig. 2. Water storage effect ratio distribution.

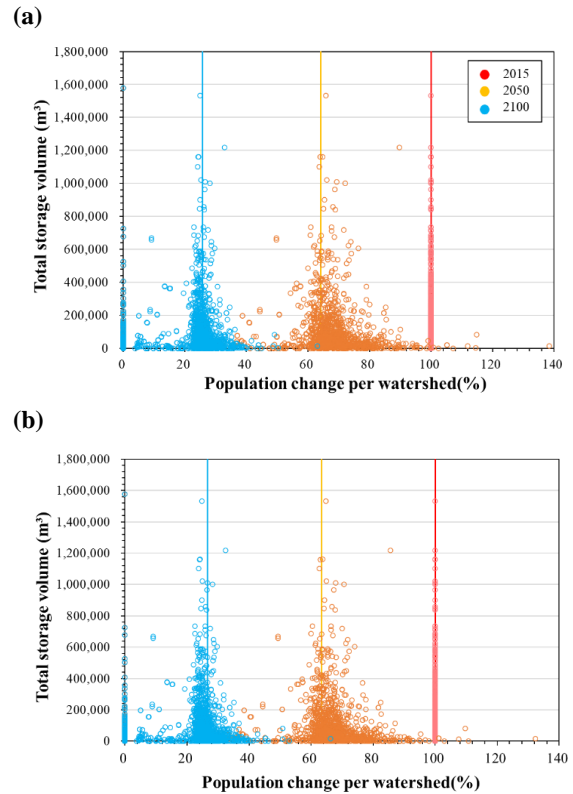


Fig. 3. Relationship between the rate of change of basin population (%) and total storage (m<sup>3</sup>) for each SSP.

#### 4 Conclusions

Among paddy field, park, and school storage, paddy field storage was found to be the most effective off-channel storage option. In the case of park and school storage, it was found that there are watersheds in the Tokyo, Chukyo, and Kansai areas that can be expected to be effective. The watersheds with the largest total storage volume were located in the northern part of Japan, which is consistent with the watersheds with high storage effectiveness.

In the analysis in Fukushima Prefecture, there were watersheds where the population will increase in 2050 for both SSP1 and SSP5. These watersheds can be considered as watersheds that function for both water storage to mitigate internal water damage and to reduce external water. Therefore, the focus should be on measures for off-channel water storage.

#### Reference

- [1] MEXT, JMA, Report of Working Group I of the IPCC Sixth Assessment Report Summary for Policymaker (2022).
- [2] Shimura, H., Evaluation of flood control function of paddy fields and rice paddies, Journal of Agricultural Civil Engineering Society, Vol.50(1), pp.25-29, (1982).
- [3] Kawaike, K, Nakagawa, H, Mitigation Effects of On-Site Storage Facilities on Pluvial Inundation in Highly Urbanized Area : Journal of Japan Society of Civil Engineers, Ser. B1 (Hydraulic Engineering), Vol.74, No4, pp. I\_1537-1542, (2018).

## Assessment of the chemical compositional characteristics as mass movements in granite zone

○ Yuki KUSAKABE<sup>1</sup>, Shiho YABUSAKI<sup>2</sup> and Seiki KAWAGOE<sup>1</sup>

<sup>1</sup>Faculty of Symbiotic Sciences Systems, Fukushima University, Fukushima 960-1296, Japan.

<sup>2</sup>Research Institute for Humanity and Nature, Kyoto 603-8047, Japan.

\*E-mail: kawagoe@sss.fukushima-u.ac.jp.

### Abstract

In this study, Actual mass movements in the Granite Zone (Abukuma highland during Hagibis) were verified environmental conditions. In particular, we focused on the chemical composition that may induce the degree of geological weathering. The mass movement cases were databased from satellite (Sentinel-2B). Spatial information based on numerical geographic information and chemical analysis of runoff were used for data on environmental conditions. The results show that the relationship between cumulative precipitation and slope gradient can indicate a large or small collapse rate. However, the chemical analysis of elemental runoff indicated that the amount of *Ca* from feldspar and *Mg* from biotite, which are leached from the granite during weathering, were also involved. The amount of these elements released from the granite varies depending on the geology and topographic position of the granite.

**Keywords:** Geological weathering, hagibis, sentinel-2, icp-ms and climate change

### 1 Introduction

In this study, the mass-movement distribution of a watershed was obtained for the Abukuma Highlands (Fig. 1), where many mass movements were caused by Typhoon East Japan in 2019. The chemical composition of the runoff in the watersheds where mass movements occurred was also determined, and the chemical characteristics of the watersheds were clarified. From these analyses, the following (1) and (2) are aimed to be achieved.

(1) To organise the environmental conditions for mass movements contributing to sediment and flood inundation.

(2) To clarify the runoff characteristics of the chemical composition that may induce the degree of weathering of the geology.

As putting these into practice and clarifying the chemical knowledge, it may be possible to derive the degree of weathering without relying on knowledge from geological maps. Such knowledge can be used for early urban relocation. This can avoid the damage from excessive combined water and sediment events that have been observed in recent years. Therefore, they provide an effect as a measure for watershed flood control.

In the East Japan Typhoon of 2019, mudflows and slope failures occurred frequently in these weathered zones, especially in the massified areas, and large amounts of sediment were washed away. Massification is a simultaneous physical and chemical reaction between the fracture of granitic rocks and the reaction of water entering the fracture surface. In granitic rocks, for example, feldspars tend to become clayey while quartz, the main element, remains unchanged. The degree of weathering can be easily determined by looking at changes in the chemical composition of the feldspar. The main elements in feldspar are *Al*, *Si*, *Ca*, *Na* and *K*, but *Al* and *Si* are not easily dissolved out, so kaolin minerals ( $Al_2O_3$ ,  $2SiO_2$ ) remain in the clayed zone. On the other hand, *Ca*, *Na* and *K* are easily dissolved in acidic water. The biotite contained in the rock is easily weathered, causing the dissolution of *K* distributed in the interlayer of the biotite. In addition, weathering also leaches *Fe* and *Mg* to form kaolin minerals. Considering the above processes of chemical compositional changes due to weathering, it may be possible to determine the degree of weathering from the dissolution and efflux of *Ca*, *Na* and *K* from feldspar and *Fe* and *Mg* from biotite<sup>[1]</sup>.

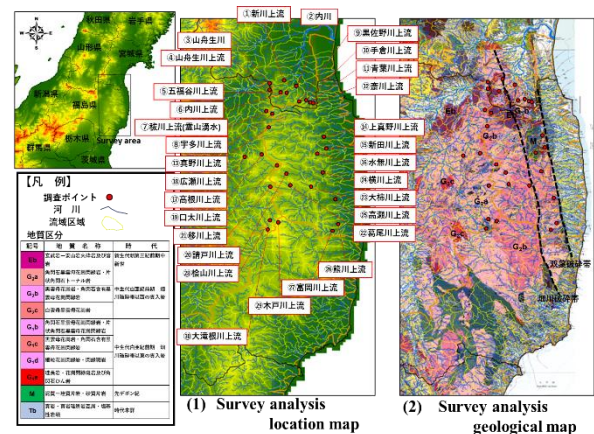


Fig. 1. Study area map

### 2 Materials and methods

The analysis in this study consists of (1) extractive analysis of mass movement distributions, (2) comparative verification of watershed environmental conditions with case studies, and (3) comparative verification with the chemical composition of runoff in the watersheds. The spatial unit of analysis was set to small watersheds, covering 30 watersheds distributed in the Abukuma Highlands.

(1) Extractive analysis of mass movement distributions

Satellite imagery was used to develop information on the spatial distribution of mass movements. Sentinel-2B was used as the dataset for satellite imagery. The images extracted to extract examples of mass movements during the East Japan Typhoon of 2019 were taken on 14 November 2018 and 9 November 2019. Two indices were used to extract mass movements: the normalized vegetation index NDVI, which indicates vegetation activity, and the grain size index GSI, which indicates bare areas. These indices were compared to determine the distribution of mass movements.

(2) Comparative verification of watershed environmental conditions with case studies

To understand the environmental characteristics of mass movements, the relationship between each environmental condition and numerical geographic information was determined. This comparative study revealed the conditions

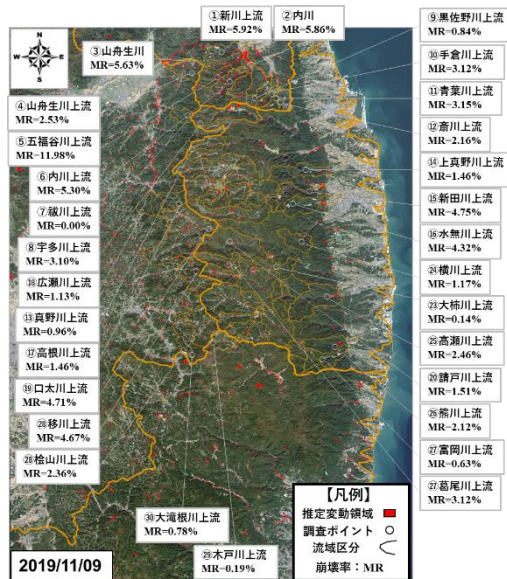


Fig. 2. Satellite image analysis results map

under which mass movements were likely to occur in the granitic zone. The conditions examined were vegetation, soil, surface geology, slope gradient and cumulative rainfall during the East Japan Typhoon of 2019(12-13 October 2019). The basin average cumulative rainfall is based on data developed by Kawagoe (2022)<sup>[2]</sup>. Comparison and verification of various information showed that a general relationship was established between vegetation with few regional differences in the Abukuma Highlands, surface geology other than soil, slope angle, and cumulative precipitation during the East Japan Typhoon of 2019 and the collapse ratio of the sub-watersheds. Therefore, this paper describes the results of the comparative verification of surface geology, slope gradient and cumulative precipitation.

(3) Comparative verification with the chemical composition of runoff in the watersheds.

The chemical composition of the runoff water from the catchment area, including the mass movement, was compared with the chemical composition of the water from the case study. The chemical composition data were obtained from surface water sampling and results analysed by inductively coupled plasma mass spectrometry (ICP-MS).

Sampling of runoff was carried out when no precipitation had been observed for five days, in order to obtain the chemical composition of runoff from base rock that had been cleared of the effects of surface runoff. In order to remove the influence of land use, such as agricultural land, sampling points were set up in mountainous areas within the catchment. Flow observations were carried out simultaneously with sampling.

### 3 Results and discussion

The points of mass movement determined from the indices obtained by satellite image results are shown in Fig.2. Mass movement is characterized by the fact that it occurs evenly on the slopes of the entire watershed in the northern Abukuma Highland area. In addition, the eastern margin of the watershed is concentrated at the valley head (zero-order valley). The collapse ratio (the ratio of mass movement area to catchment area) for each catchment was organized, and was found to be higher in the upper reaches of the Gofukuya, Shin, Uchigawa, Yamabunyu and Uchigawa Rivers in the northern Abukuma Highlands.

The relationship between slope angle and cumulative precipitation is shown in Fig.3, where a particularly clear relationship is demonstrated as a comparative study between the catchment environmental conditions and the case study.

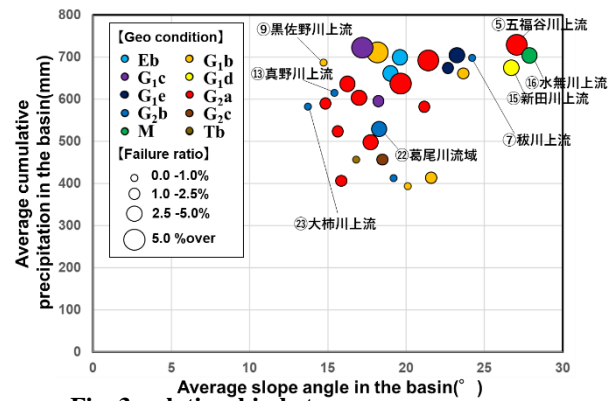


Fig. 3. relationship between slope angle and cumulative precipitation

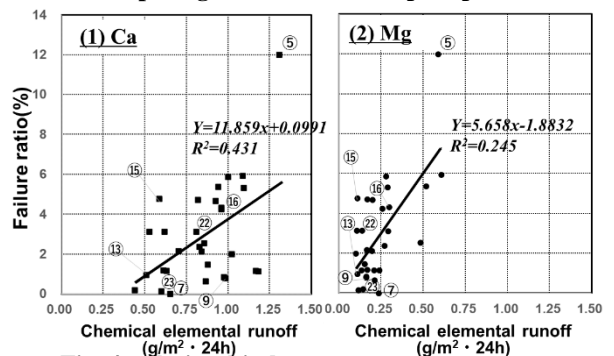


Fig. 4. relationship between failure ratio and chemical element runoff

This information is also supplemented with information on geology and failure ratios. higher failure ratios with higher cumulative precipitation and steeper slopes. However, some geological features do not fit the linear relationship. For this reason, a simple relationship was determined between the chemical composition of the runoff from the geology, In the relationship with the discharge of Ca and Mg, which is regular depending on the geology. The results are shown in Fig.4. The results show generally similar correlation coefficients between slope gradient and cumulative precipitation. This suggests that the influence of the geological interior has the same effect as that of the surface and precipitation.

### 4 Conclusions

The results show that, although the relationship between cumulative precipitation and slope gradient can generally explain the size of the collapse rate, in basins where this explanation does not apply, the tendency for the discharge of feldspar-derived Ca and biotite-derived Mg, which are leached from the granite as a result of weathering, to be involved. Therefore, the possibility of inducing the degree of weathering by the amount of Ca and Mg leached from the river was also revealed. However, these results are findings based on a case study of a specific area. Therefore, further validation by expanding the area of comparison is an issue for the future. In addition, it is also necessary to verify the specific domain in accordance with changes over time.

### Reference

[1] M. F. Thomas : Some Geomorphological Implications of Deep Weathering Patterns in Crystalline Rocks in Nigeria, Transactions of the Institute of British Geographers, No. 40, pp.173-193,1966.  
 [2] S.Kawagoe et al: Disaster characteristics of Fukushima prefecture by the 19<sup>th</sup> typhoon, Journal of JSCE, Series B1 (hydraulic Engineering), Vol.76(1), pp. 329-345, 2020.

## Population Movement caused by Flood Damage at City Level

Ayaka Okamoto<sup>1</sup>, So Kazama, Hayata Yanagihara

<sup>1</sup>Department of Civil and Environmental Engineering, Tohoku University, Miyagi 980-8579, Japan.

\*E-mail: okamoto.ayaka.s3@dc.tohoku.ac.jp

### Abstract

Flood disasters have been pointed out to have an impact on population decline in Japan. For this reason, it is important to estimate the future decline in population due to flood disasters. The results of these population estimates can be used as basic data for land use planning and economic activity planning based on flood disasters. Therefore, the objective of this study is to estimate the future population decrease caused by flood disasters. For this purpose, population loss due to flood disasters is estimated for each region and for Japan as a whole. First, we examine the population decline in cities that were severely damaged by floods in the August 2014 rainstorms. As a result, we could not confirm the impact of flood damage on population decline at the city level. Accordingly, it is necessary to analyze population loss by subregion and 500-meter resolution in the future. In Fukuchiyama City, which suffered the most damage, the population tended to decrease in the areas along the river. This suggests that floods are likely to have an impact on population decline. Based on these results, we will analyze population decline in the case of flood disasters of various sizes, such as the torrential rains in July 2020 and the East Japan Typhoon in 2019.

**Keywords:** Population movement; Flooding; City level

### 1 Introduction

Japan has entered a society with a declining population, which is a serious problem. Previous studies have indicated that flood disasters have an impact on the declining population in Japan. According to a report by the International Displacement Monitoring Centre (IDMC), floods and typhoons account for approximately 76% of the population decline due to natural disasters in Japan between 2008 and 2020 (Figure 1). Considering the above, it is important to estimate the future population decline caused by flood disasters, taking climate change into account. This is because future population estimates are used as basic data for national land policy. In order to estimate the population decline due caused by flood disasters, it is necessary to model the population decline caused by it. In previous studies, models have been developed for population estimation considering flood risk applicable only to specific regions<sup>2)</sup> and for the analysis of population movements caused by flood inundation in different countries around the world<sup>3)</sup>. On the other hand, there is no model for population decline caused by flood disasters that can be applied to a wide area. For that reason, it is not possible to estimate the future population decline caused by flood disasters taking climate change into account in the current situation. Therefore, the objective of this study is to understand the actual situation of population decline caused by flood disasters in Japan. The results obtained from this study will be used as basic data for developing a model of population decline caused by flood disasters and for estimating the future population decline caused by flood disasters, taking climate change into account. The results of this study will make it possible to predict future population decline caused by flood disasters.

### 2 Materials and methods

#### (1) Data

We obtained actual population data (2000, 2005, 2010, and 2015) from the National Population Census data. First, we

analyzed population movements by subregion (town, street, street name, etc.) using the total population by sex for the years 2000, 2005, 2010, and 2015. Currently, actual population data are available from 1995 to 2020. In this study, the number of population decline caused by flood damage is determined for the "August 2014 Torrential Rainfall". Figure 2 shows the relationship between cities and the amount of flood damage. The amount is calculated using the amount of damage to general assets by city, town, and village, by cause of flood damage, from the 2014 Flood Damage Survey. Specifically, damage from flooding is defined as damage caused by breaches of embankments, overflows at embankments, overflows at no-embankment areas, internal flooding, and internal flooding in depressions.

#### (2) Method

In this study, the number of population decline caused by flood disasters is estimated from actual population data. An overview is shown in Figure 3. The actual data include natural population movement as well as population decline caused by disasters. The number of population decline caused by flood disasters is estimated by subtracting the projected population decline in the absence of the flood from the actual population decline based on the number of population decline in the past. The flood hazards covered in this study are the various types of flood hazards listed in the National Flood Survey.

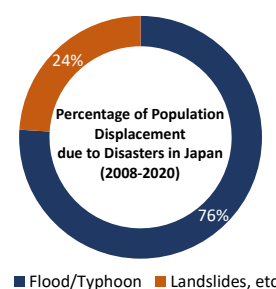


**Fig. 1. Percentage of Population Movement due to Disasters in Japan<sup>4)</sup>.**

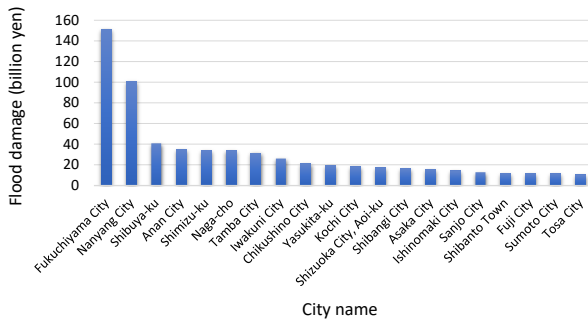


Fig. 2. Cities and Flood Damage.

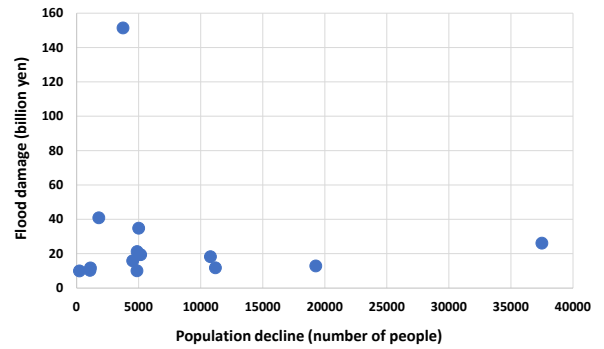


Fig. 4. Flood Damage and Population Decline.

### 3 Results and discussion

Figure 4 shows the relationship between flood damage and population decline in 13 cities. Population decline was examined for the top 20 cities with the highest flood damage, but for seven of these cities, population decline could not be calculated in the GIS. One of the reasons for this is that the key codes for each municipality have changed due to the Heisei Era's great merger and other factors. Key codes are the link codes between boundary data and statistical data, and are required when charting population data in QGIS. Therefore, some cities were unable to estimate their population in 2015 in the absence of a disaster. In consequence, only 13 cities are plotted in Figure 4. As can be seen from the figure, the effect of flood damage on population decline could not be confirmed. This suggests that it is necessary to examine population decline at the sub-region and 500-meter resolution. Sub-regions are smaller units than municipalities, such as town. Figure 5 shows the number of population decrease in Fukuchiyama City using QGIS, a cross-platform open source software with functions for viewing, editing, and analyzing geographic information systems. The blue lines indicate rivers in the direct Class 1, designated Class 1, and Class 2 river areas. The red portion indicates an increase in population, while the blue portion indicates a decline in population. The figure shows that the population tends to decline more in the areas along the rivers. Thus, it is clear that flooding has a negative impact on population decline. This suggests that floods are likely to have an impact on population decline.

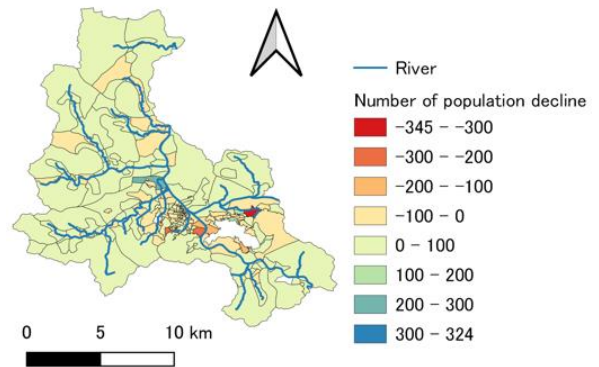


Fig. 5. Estimated number of population decline caused by flooding in Fukuchiyama City.

### 4 Conclusions

In this study, we analyzed population decline in 20 cities with large flood damage amounts for the August 2014 torrential rains. As a result, it was found that it is difficult to grasp the population decline caused by flood disasters in each municipality. In addition, due to the Heisei Era's great merger, some areas have changed from the past to the present, and key codes have also been changed. Therefore, it is difficult to accurately calculate the number of population decline in each municipality using QGIS. Thus, it is effective to study population decline in small areas or at 500-meter resolution. We would like to use the results of this study to develop a model of population decline caused by flood disasters.

### Reference

- [1] Murai et al., Characterization of population loss due to flooding based on population projections, Japan Society of Hydrology and Water Resources, 2019.
- [2] Imai et al., Development of a population distribution estimation model for future time series for land use policy evaluation considering flood risk, Journal of City Planning, Vol. 50, No. 3, pp. 656-662, 2015.
- [3] Kakinuma et al., Flood-induced population displacements in the world, Environmental Research Letters, Vol.15, 124029, 2020.
- [4] International Displacement Monitoring Centre (IDMC).

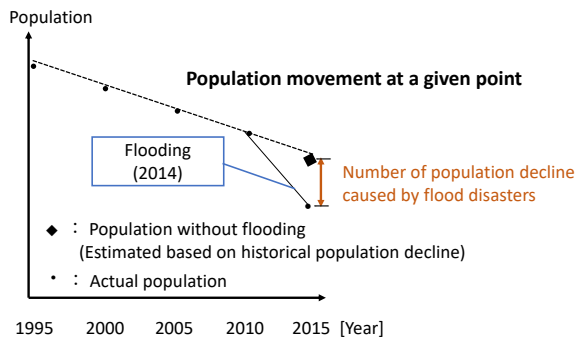


Fig. 3. Estimation of the number of population losses due to previous flood disasters.

## Innovative ensemble approach of spatial prediction of flood using bivariate index of entropy and support vector machine models

○ Kumudu Madhawa KURUGAMA<sup>1\*</sup>, So KAZAMA<sup>1</sup> & Chaminda SAMARASURIYA<sup>2</sup>

<sup>1</sup>Department of Civil and Environmental Engineering, Tohoku University, Miyagi 980-8579, Japan.

<sup>2</sup>Department of Earth Resources Engineering, University of Moratuwa, Katubedda 10400, Sri Lanka

\*E-mail: kurugama.arachchige.kumudu.madhawa.r4@dc.tohoku.ac.jp

### Abstract

In this study, we propose a novel ensemble method for improving the accuracy in flood susceptibility mapping using index of entropy (IoE) and support vector machine (SVM). The proposed method was implemented with four SVM kernels, like linear (LN), polynomial (PL), radial basis function (RBF), and sigmoid (SIG). A spatial database was created with twelve flood conditioning factors (FCFs) and a flood inventory map with 445 flood locations, produced using historical documents, satellite images and extensive field survey. First, the correlation between classes of each flood conditioning factor with flooding was evaluated using IoE. Following that, SVM was conducted using the results of the first step. Area under the curve (AUC) and seed cell area index (SCAI) methods were used to evaluate the performances of the models. The highest success and prediction rates of 94.82% and 95.81% and lowest SCAI values of 0.18, 0.878 for very high and high susceptibility classes were achieved by ensemble IoE-SVM(RBF) model. Among all the applied methods, both the individual EBF and SVM(RBF) methods achieved the lowest accuracies. It can be concluded that, using ensemble methods, a more detailed assessment of the flooding and conditioning factors can be performed, thereby increasing the accuracy of the final map.

**Keywords:** flood susceptibility; index of entropy; geographic information system (GIS); support vector machine (SVM); ensemble modelling

### 1 Introduction

Floods are among the most devastating of natural disasters and may cause immeasurable damage. Assessment of flood risk and hazard has gained significant attention in recent years from geoscientists, engineering professionals, as well as from the public and local governments in various regions of the world. Numerous studies have used a variety of techniques to map flood-prone areas [1].

In Rathnapura district, the most devastating floods have occurred during following years 2003, 2008, 2012, and 2017 resulting hundreds of fatalities and economic losses. In the current research, a GIS based, ensemble technique of IoE and SVM models is utilized to map the flood prone regions at Rathnapura city, Sri Lanka, and the main goal of this research to examine and compare the efficiency and precision of proposed ensemble method with standalone IoE and SVM methods.

### 2 Material and Method

#### 2.1 Study area

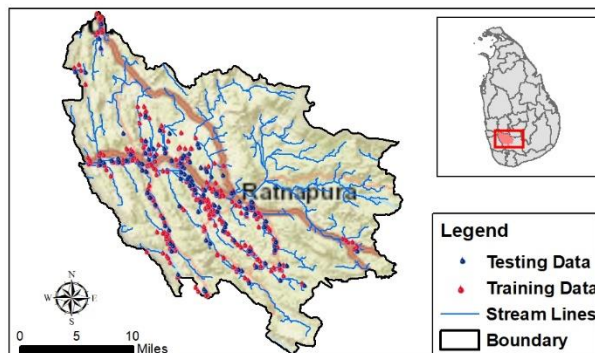


Fig. 1. Study Area

Rathnapura city is located in the western province, Sri Lanka and lies between the latitudes 6° 55' 51"N and 6° 28' 36"N, and longitudes 80° 10' 37"E and 80° 36' 57"E. The altitude ranges from 4-2174 m above mean sea level. Climatic condition of Rathnapura city is hot, humid, and cloudy with more than 3100mm average annual rainfall and average temperature ranges from 71°F to 93°F.

#### 2.2 Data and feature selection

A total of 445 flood locations were chosen as the flood inventory which was created based on satellite data, historical documentary sources and extensive field survey. Later these points were randomly divided into two sections as 70% (312 points) and 30% (133 points) for training and testing purposes, respectively. Twelve FCFs with 30m spatial grid resolution were considered. They are altitude, curvature, aspect, slope, normalized difference vegetation index (NDVI), topographic roughness index (TRI), topographic wetness index (TWI), distance from river, distance from road, land cover (LULC), soil, and rainfall.

To avoid overfitting, evaluation of correlations between the flood conditioning factors is an essential. The variance inflation (VIF) and tolerance (TOL) were used to examine the multicollinearity among the factors in this study.

#### 2.3 IoE method

The method proposed by [2]. The weight of parameters is defined by entropy level that indicates the extent of disorder in the environment, then the weight will determine which factor is more significant in occurrence of flood. The following seven equations represent the various steps in the calculation of index of entropy model. See Eq.1 and Eq.2

$$P_{ij} = \frac{A_j}{A_t} \quad (1) \quad (P_{ij}) = \frac{P_{ij}}{\sum_{j=1}^n P_{ij}} \quad (2)$$

$A_f$  : Area of the factor class after primary reclassification  
 $A_i$  : Area of flood within the given factor class  
 $(P_{ij})$  : Probability density  
 $H_j$  and  $H_{j \max}$  represent entropy values (Eq 3 and Eq4).

$$H_j = \sum_{i=1}^{S_j} (P_{ij}) \log_2(P_{ij}) \quad j = 1, \dots, n \quad (3)$$

$$H_{j \max} = \log_2 S_j \quad (4)$$

$S_j$  : Number of classes  
 $H_j, H_{j \max}$  : Entropy values  
 $I_j$  : Information coefficient

$$I_j = \frac{H_{j \max} - H_j}{H_{j \max}} \quad (5) \quad W_j = I_j \times P_{ij} \quad (6)$$

$W_j$  : represents the weight of each parameter  
 The final flood susceptibility map was prepared by summation of weighted multiplications of the secondarily reclassified parametric maps, see (7).

$$FSI = \sum_{i=1}^n (fac\_recl2) * W_j \quad (7)$$

Where factor\_recl2 is the value in a particular pixel after reclassifying the parametric map of the conditioning factors.

## 2.4 SVM method

The SVM algorithm is a cogent prediction machine learning method based on the structural risk minimization principle and statistical learning theory. The model creates a hyperplane in the original space of the coordinates between the points of the two classes. The hyperplane is classified in the central part of the peak edge. Separating hyperplane can be expressed as;

$$y_i((w \cdot x_i) + b) \geq 1 - \xi_i \quad (8)$$

where  $w$  : norm of normal hyperplane  
 $x_i$  : vector of each input space  
 $b$  : offset of the hyperplane from the origin  
 $\xi_i$  : positive slack variables

Lagrangian multipliers can be used for determine the optimal hyperplane as;

$$\text{Minimize } \sum_{i=1}^n \alpha_i - \frac{1}{2} \sum_{i=1}^n \sum_{j=1}^n \alpha_i \alpha_j y_i y_j (x_i x_j) \quad (9)$$

$$\text{Subject to } \sum_{i=1}^n \alpha_i y_i = 0, \quad 0 \leq \alpha_i \leq C \quad (10)$$

Where  $\alpha_i$  : Lagrange multipliers,  
 $C$  : is the penalty,  
 $\xi_i$  : slack variables

In the case of non-separation of a hyperplane, input data may be transformed into high dimensional feature space using non-linear kernel functions. New data is classified using decision function:

$$g(x) = \text{sign}(\sum_{i=1}^n \alpha_i y_i K(x_i, x_j) + b) \quad (11)$$

where  $K(x_i, x_j)$  is the kernel function.

**Table 1 Different SVM kernel types**

Kernel	Equation	Variables
LN	$K(x_i, x_j) = x_i^T \cdot x_j$	-
PL	$K(x_i, x_j) = (-\gamma x_i^T \cdot x_j + r)^d$	$\gamma, d$
SIG	$K(x_i, x_j) = \text{Tanh}(-\gamma x_i^T \cdot x_j + r)^d$	$\gamma$
RBF	$K(x_i, x_j) = \exp(-\gamma \ x_i - x_j\ ^2)$	$\gamma$

## 2.5 Model performance evaluation

As statistical measures, the specificity, sensitivity, and accuracy were used to evaluate the performances of the trained models. These indices reflect the ability of the model to correctly differentiate the flood pixels from the non-flood pixels. The seed cell area index (SCAI) was used to compare the ratio of the density of the flood locations and the areas of the susceptibility classes in this study.

$$SCAI = \frac{\text{Area extent of susceptibility classes}(\%)}{\text{Inventory of flood in each susceptibility classes}(\%)} \quad (12)$$

Finally, to validate the analytical outcomes, the popular AUC method was used. In this study, training and testing dataset were used to determine success and prediction rate curves which reflect the goodness of fit and prediction power of the models, respectively.

## 3 Results

### 3.1 Multicollinearity analysis

Table 2 presents the results of multi-collinearity analysis of the twelve FCFs. When  $VIF > 5$  or  $TOL < 0.1$ , the factor has multiple collinearity problems and needs be eliminated.

**Table 2 Results of multicollinearity analysis**

Conditioning Factor	Tolerance	VIF
Altitude	0.3076	3.2514
Aspect	0.7621	1.3125
Slope	0.5005	1.9979
TRI	0.4305	2.3224
Soil	0.8299	1.2049
LULC	0.9085	1.1005
Dist.River	0.6063	1.6493
Rainfall	0.6474	1.5444

Although altitude had the highest VIF(3.2514) and lowest TOL(0.3076), neither of these values exceeded the threshold values(5 and 0.1, respectively.) indicating the absence of multicollinearity among the eight FCFs. Thus, all eight FCFs were used in modeling.

### 3.2 Analyzing the weights derived from each method

The weights of entropy for each FCFs were calculated based on the aforementioned equations. For an example, the tabulated values of the rain are shown in Table 3. According to the findings, in the case of altitude, the class intervals of 4–22m, 22–47m, and 47–88 m were found as highly susceptible regions indicating flood occurs predominantly in low-altitude areas rather than on mountain tops. Slope classes within the range 0°–8.6 °, nearly flat with low elevation showed higher relationship on flooding. Mainly flat aspect exhibits the highest effect on flooding. Distances of up to 150 m from the river had the most significant impact on flooding. Further, the distance range of 150–300 m also found to be important indicating long coverage and spread of alluvial floods over the studied area. Since the type of soil has an apparent influence on drainage, water storage, permeability, this factor was used in this study. According to the results Alluvial soil type had the greatest influence on flooding. Rainfall is a major trigger in flood formation, and flooding will not occur if this factor is not present. Therefore, the most significant rainfall classes were found to be ranging from 3640–3850mm. LULC is a critical component in

**Table 3 IoE calculation result for rainfall weight**

Factor	Class	No.of pixels	flood points	$P_{ij}$	$(P_{ij})$	$H_j$	$H_{j\max}$	$I_j$	$W_j$	Fac_recal2
Rainfall	2863-3640	278102	56	0.9126	0.1884	1.69	2.32	0.27	0.26	3
	3641-3735	286992	106	1.6739	0.3455					4
	3736-3850	303519	139	2.0755	0.4284					5
	3851-3996	273380	11	0.1824	0.0376					2
	3997-4486	272019	0	0.0000	0.0000					0
Summation		1414012	312	4.8444	1.0000					

identifying vulnerable areas prone to floods. According to the results, waterbodies, homesteads, and paddy classes showed higher effect on flooding. The friction exerted on the water flow by the underlying surface is determined by TRI where lowest classes of 0.9-15, 15-26 were the most significant on flood occurrence.

**Table 4 Prediction performance of SVM models based on validation dataset**

Model	Specificity	Sensitivity	Accu.
SVM-rbf	0.9098	0.9398	0.9286
IoE+SVM-rbf	0.9774	0.9699	0.9737
IoE+SVM-poly	0.9549	0.9474	0.9511
IoE+SVM-sig	0.9699	0.9474	0.9549
IoE+SVM-ln	0.9248	0.9624	0.9436

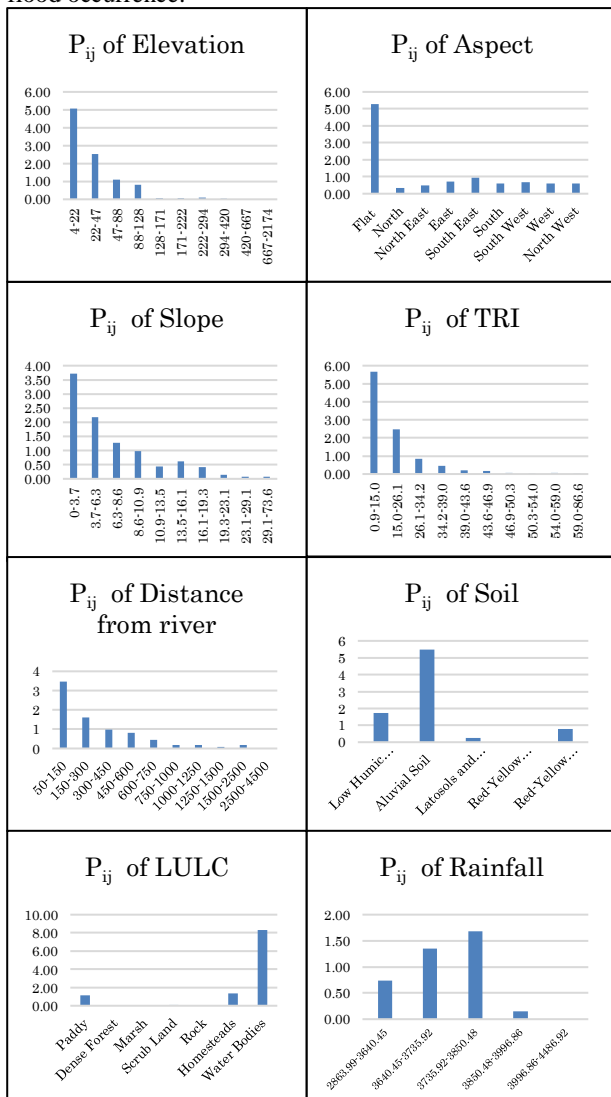


**Fig. 2. Distribution of flood in each factor classes based on probability density ( $P_{ij}$ )**

The ensemble method was applied using all four SVM kernels. Cross validation technique was used to derive kernel parameters. The final step involved the derivation of four flood probability maps. In addition, another flood probability map was generated using a stand-alone SVM -RBF kernel. The individual SVM was performed using the original FCFs, which were not classified by the IoE results.

According to SVM results, highest sensitivity, specificity, and accuracy of 96.99%, 97.74% and 97.37% was obtained for the ensemble IoE and SVM model with RBF kernel, respectively. Lowest sensitivity, specificity, and accuracy of 93.98%, 90.98% and 92.86% were obtained from standalone SVM model with RBF kernel. SVM model with Sigmoid kernel obtained higher accuracy compared to linear and polynomial kernel models.

To generate the flood susceptibility maps, the flood probability indices obtained from SVM models has to be classified into different zones of susceptibility. Natural breaks classification method which follows the Gauss normal distribution, was used to classify the probability index into 5 susceptibility classes as low, low, moderate, high, and very high (Fig. 3.).

**Table 4 SCAI values of the flood susceptibility classes**

Model	Very low	Low	Moderate	High	Very High
IoE	59.21	66.02	18.45	2.29	0.21
SVM-rbf	250.19	9.39	10.04	1.36	0.20
IoE+SVM-pol	148.30	7.47	2.78	1.07	0.19
IoE+SVM-rbf	283.75	7.47	2.02	0.878	0.18
IoE+SVM-sig	151.89	6.24	4.12	1.87	0.19
IoE+SVM-ln	54.74	4.69	2.41	0.98	0.19

Lower SCAI values indicate a higher flood susceptibility and vice versa. This approach is helpful in evaluating the consistency and effectiveness of the models. SCAI values of very high, high, and moderate susceptibility classes were found to be lower in the ensemble IoE and SVM model with rbf kernel than the other four models. Thus, the IoE and SVM model with rbf kernel model was found to be the most effective model for analyzing flood susceptibility in the study area.

To evaluate the reliability of the derived susceptibility maps, an accuracy assessment was performed using the AUC method. The AUC results showed that the highest prediction (95.81%) and success (94.82%) rates were achieved by the ensemble IoE+SVM (rbf) method. The individual SVM (rbf) and IoE methods produced lower success and prediction rates as (SVM-rbf:86.17% success rate and 84.90% prediction rate; IoE: 82.57% success rate and 81.78% prediction rate) relative to all four ensemble methods. The IoE+SVM (ln)

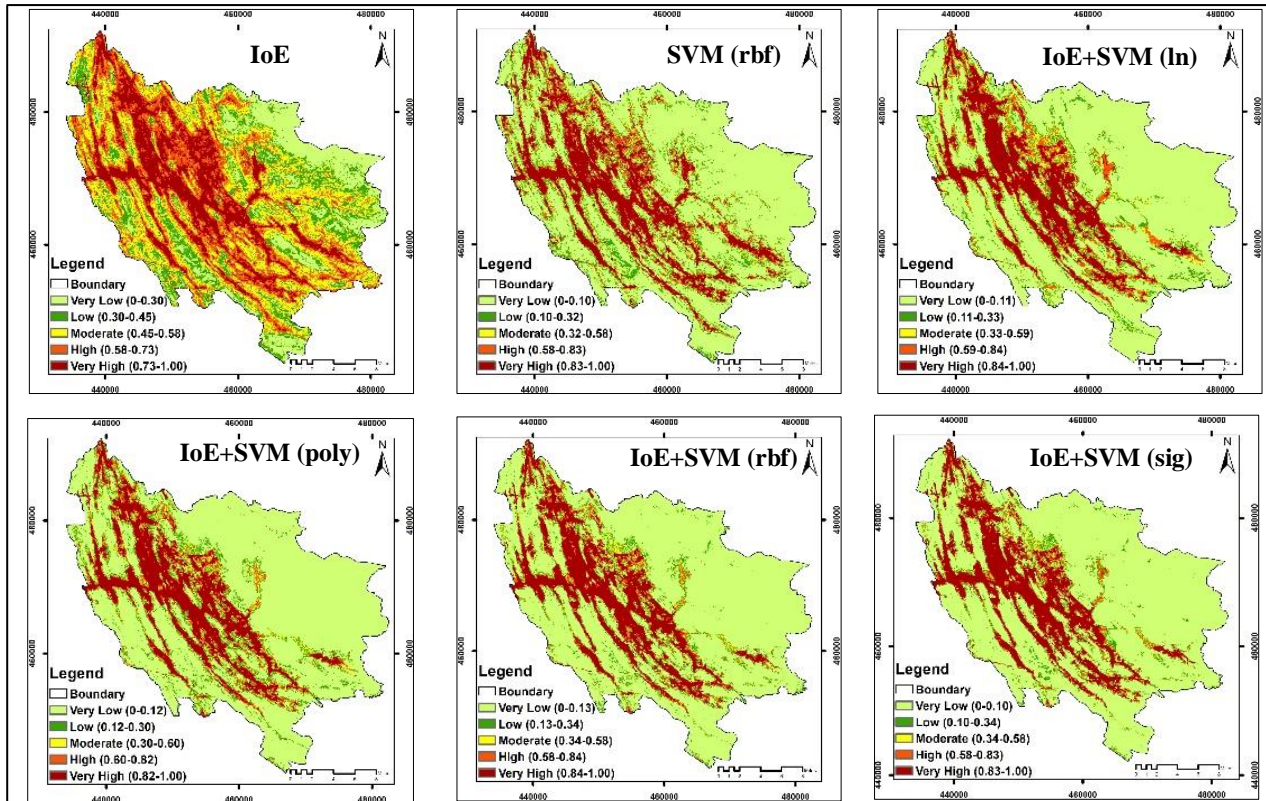


Fig. 3. Flood Susceptibility maps

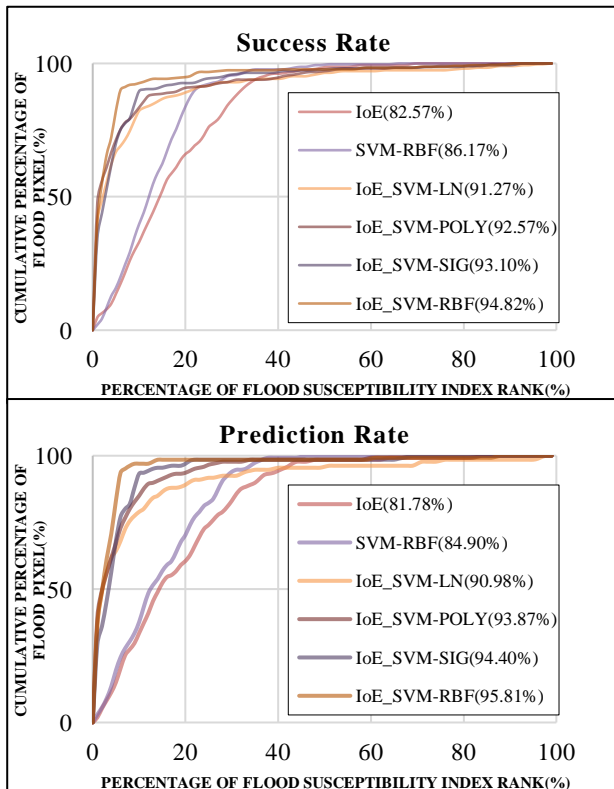


Fig.4. Success and prediction rate curves

model showed lower success and prediction rates as 91.27% and 90.98% among all ensemble models, respectively. Based on the obtained accuracies, the integrated IoE and SVM (rbf) technique can be utilized as opposed to the standalone approaches.

#### 4 Conclusions

A unique ensemble IoE-SVM approach was utilized to evaluate flood susceptibility in the Rathnapura city and its surrounding, Sri Lanka. Bivariate and multivariate statistical analysis performed using IoE and SVM respectively. Four SVM kernels were used to build the ensemble models and their impacts were also evaluated. The accuracy of the models was assessed through ROC curves and SCAI. The lowest SCAI values were obtained for very high, high and moderate flood susceptibility classes in the case of ensemble IoE+SVM(rbf) model. According to AUC results, highest accuracies were obtained for ensemble IoE+SVM(rbf) model with 95.81% and 94.82% for prediction and success rates, respectively. Lowest accuracies were obtained for the individual IoE and SVM(rbf) models. It can be concluded that the integration of the standalone methods improved their performances. We hope that this research will be useful to policymakers as a framework for taking proper measurements in prior identification of flood prone regions and minimizing the adverse effects of flooding.

#### Reference

- [1] Dano, U., Balogun, A., Matori, A., Wan Yusouf, K., Abubakar, I., Said Mohamed, M., Aina, Y. and Pradhan, B., Flood Susceptibility Mapping Using GIS-Based Analytic Network Process: A Case Study of Perlis, Malaysia, Water, 2019, 11(3), p.615.
- [2] Constantin, M., Bednarik, M., Jurchescu, M. and Vlaicu, M., Landslide susceptibility assessment using the bivariate statistical analysis and the index of entropy in the Sibiciu Basin (Romania). Environmental Earth Sciences, 2010, 63(2), pp.397-406.

# Understanding drought risk in the coastal region of Bangladesh using gridded meteorological data

○Sheikh Hefzul Bari<sup>1</sup>, Noor-E-Ashmaul Husna<sup>2</sup> and Yoshiyuki Yokoo<sup>1</sup>

<sup>1</sup>Graduate School of Symbiotic Systems Science and Technology, Fukushima University, Japan.

<sup>2</sup> Bangladesh University of Engineering and Technology, Bangladesh.

\*E-mail: shbari.bd@gmail.com.

## Abstract

The coastal region of Bangladesh is prone to different hydro climatological calamities. Drought has recently been recognized as one of them. To understand the long-term drought scenario of this area, we derived SPI (Standardized Precipitation Index) and RDI (Reconnaissance Drought Index) indices using 100 years of gridded meteorological data. Drought indices show that the region has experienced moderate to extreme drought in the past. In many cases time series of indices show a dry and wet cycle. Non-parametric Mann-Kendall test shows statistically significant trend in annual initial RDI. Which is a climate change indicator for this area. The trend result identifies that grid 5, 6, and 10 (Southwestern part) have a greater tendency of drought.

**Keywords:** Coastal Bangladesh, Drought, Reconnaissance Drought Index, Climate change, Water security.

## 1 Introduction

Due to the global climate change effects frequency of droughts are likely to increase in recent years. This will also affect Bangladesh, especially the coastal region. This region is already susceptible to numerous natural calamities. Increasing drought events might stress the already existing food and water security issues. As drought was identified as a barrier to accessing safe drinking water in the southwestern coastal region [1]. Assessing drought risks, vulnerabilities, and hazards is crucial to putting mitigation and adaptation into action to decrease the effects of the drought. Because a lack of comprehensive knowledge about drought behavior in a specific region frequently causes difficulties in decision-making [2] in the relevant field. Besides, the groundwater deficit is causing concern due to rising demand. Drought-induced surface water depletion will hasten groundwater over-exploitation, particularly during the cropping season. Also, the growing threat of salinity will impose additional stress on the existing water resources. The combined effects pose a serious threat to Integrated Coastal Zone Management (ICZM) approach as well as the Integrated Water Resource Management (IWRM) approach.

## 2 Materials and methods

The coastal zone of Bangladesh lies within the tropical zone between 21-23° N and 89-93° E. The area is characterized by a massive network of rivers, with a large number of islands among channels where horrendous tropical cyclones are common [3].

River flow reductions during the dry season have a significant negative impact on river morphology and salinity in coastal Bangladesh. Recurring drought events, as well as reduced flow volume of major rivers, drying of water channels, and depletion of groundwater tables from over-exploitation, exacerbate the area's water crisis, particularly during the dry season.

Estimation of drought indices requires rainfall and temperature data. High-resolution 0.5 degree by 0.5 degree gridded monthly land surface air temperature and precipitation data from 1910-2010 was collected from NOAA (National Oceanic and Atmospheric Administration).

For the coastal region of Bangladesh, the grid centers were assigned a number ranging from 1 to 12 for convenience (Figure 1).

The Standardized Precipitation Index (SPI) [4] and Reconnaissance Drought Index (RDI) [5] were used to assess the severity of drought occurrence in the study area. The RDI employs PET (potential evapotranspiration) in addition to rainfall, which is expected to improve drought detection efficiency. The RDI has three forms: initial value ( $\alpha_k$ ), normalized RDI ( $RDI_n$ ), and standardized RDI ( $RDI_{st}$ ). The initial value is aggregated using a monthly time step and can be calculated monthly, seasonally, or annually. Because the Standardized RDI and SPI perform similarly, the results are interpreted similarly. The initial form of RDI is equivalent to Aridity Index, enabling it to use as a climate change indicator.

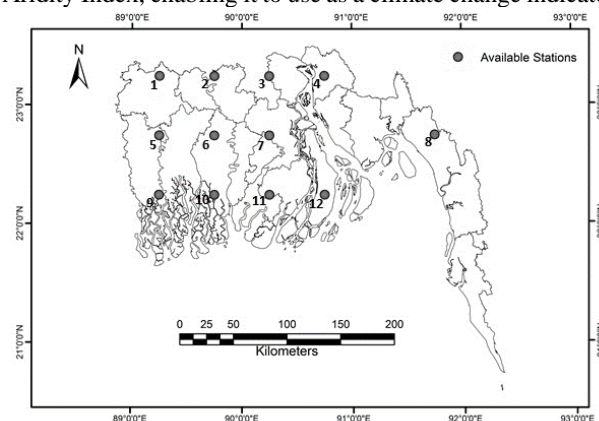


**Fig. 1. Coastal region of Bangladesh.**

PET was estimated using Thornthwaite method [5,6]. Non-parametric Mann-Kendall [7] test was used to identify the trend. While spatial distribution of Mann-Kendall Z scores and severe drought events were computed using Empirical Bayesian Kriging (EBK) in ArcGIS.

## 3 Results and discussion

The annual SPI and RDI data reveal a wet cycle. For example, grid twelve RDI time series, which includes major

flood and drought events (Figure 2). Similar cycles were observed using the 6-month SPI and RDI although there are some interruptions in the cycle where the SPI and RDI values approach zero or became negative for a short time. The indices respond more slowly to short-term precipitation variation as the time scale increases from six to twelve months, and cycles of positive or negative values become more visible. Several flood events occurred during the cycle of positive SPI and RDI values, while this area was experiencing a long-wet period. Following the wet period, a long dry period influences agricultural production.

Several noticeable drought events occurred during the cycle of negative SPI and RDI values. The sharper negative inclination of RDI<sub>12</sub> compared to SPI<sub>12</sub> reveal a possible increasing trend of temperature in this area. Based on the overall analysis of SPI and RDI, grid six (the Southwestern part) was identified as the most vulnerable.

The occurrence of the negative indices value displays that the region has suffered from comparatively more serious drought in recent times than that in the past years. Analyzing the time series plot of the drought indices, four major droughts and at least twenty moderate drought events were detected.

It was discovered that the frequency of negative SPI and RDI values is relatively low at grid eight. This could be interpreted based on where it is. For the time being, this region is less susceptible to meteorological drought risk. Overexploitation and sea level rise, on the other hand, makes it vulnerable to safe drinking water access.

RDI was found more sensitive to drought events while SPI were to flood event. This slightly better performance of RDI could be the use of evapotranspiration in RDI index calculation. Therefore, using RMSE, the relative performance of SPI and RDI were calculated. The results were satisfactory. RMSE was calculated between RDI and SPI by using the following equation:

$$RMSE = \sqrt{\frac{\sum_{i=1}^N (RDI_i - SPI_i)^2}{N}}$$

Here, N= Length of each SPI or RDI time scales.

Trend analysis of the dry six months (October - March) RDI series exhibited a negative trend except at grid twelve. Only grid twelve showed an increasing trend. In contrast, trend analysis of the annual RDI series showed a significant negative trend at all grids except grid eight. From both the six months and annual RDI trend analysis results, we can conclude that there is an overall annual moisture deficiency.

#### 4 Conclusions

The goal of this study was to present an analysis of the characteristics and recurrence of droughts in the coastal region of Bangladesh. According to the findings, the southwestern coastal zone is more vulnerable to drought. The Mann-Kendall trend test showed a significant negative trend interpreting possible increment of drought phenomenon in the future and possible climate change.

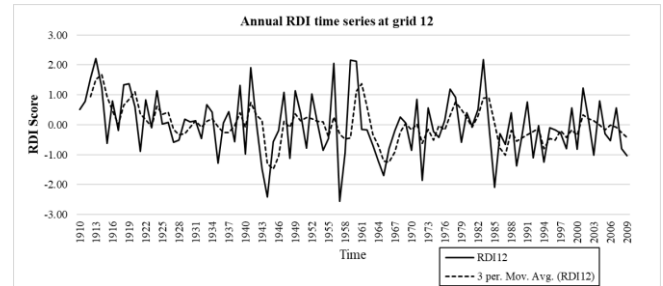


**Fig. 2. Annual RDI series at grid 12 with 3-year moving average. The X-axis denotes the hydrologic year (1910 denotes 1910-11 hydrologic year and so on).**

In general, this study has shown that most of the coastal areas were affected by drought but the severity and occurrence of this phenomenon are greater in the western coastal part, especially at grid five and six. Therefore, future research on these regions should be prioritized to improve the water resource management and development programs and to resolve the socio-economic and agricultural problems faced by the people in this part of the country.

In general, the SPI and RDI series show almost similar results. But in some cases, RDI was found more sensitive to the dry period and SPI was found more sensitive to the wet period. The SPI is a widely used drought monitoring index. Mainly, due to its fewer data requirements. However, meteorological drought depends not only on rainfall but also depends on evapotranspiration, temperature, and other climatic parameters. On this basis, the RDI could be a promising alternative to best represent the drought scenario. It is seen that drought severity is increasing in the coastal area of Bangladesh. Apart from the impacts that drought can impose on natural resources and the environment, huge economic losses are likely to happen. To overcome the drought effects comprehensive and coordinated planning should be taken.

#### Reference

- [1]. Abedin, M.A., Habiba, U., Shaw (Eds), R., Water Insecurity: A Social Dilemma. Emerald Group Publishing, 2013.
- [2]. Mishra, a. K., Desai, V.R., Drought forecasting using stochastic models, *Stoch. Environ. Res. Risk Assess.* 19 (2005), 326–339.
- [3]. Alam, E., Collins, A.E., Cyclone disaster vulnerability and response experiences in coastal Bangladesh, *Disasters*, 34(2010), 931–954.
- [4]. Mckee, T.B., Doesken, N.J., Kleist, J., The relationship of drought frequency and duration to time scales, 1993, 17–22.
- [5]. Vangelis, H., Tigkas, D., Tsakiris, G., The effect of PET method on Reconnaissance Drought Index (RDI) calculation, *J. Arid Environ.* 88(2013), 130–140.
- [6]. Thornthwaite, C.W., An Approach toward a Rational Classification of Climate, *Geogr. Rev.* 38 (1948), 55–94.
- [7]. Mann, H.B., Nonparametric tests against trend, *Econ. J.* 55(1945), 245–259.

# POTENTIAL OF IRRIGATION RESERVOIRS FOR FLOOD PREVENTION AND EVALUATION OF THE REDUCTION RATE OF FLOOD DAMAGE COST FOR EACH PREFECTURE

○ Atsuya IKEMOTO<sup>1\*</sup>, So KAZAMA<sup>1</sup>, Takeo YOSHIDA<sup>2</sup>, Hayata YANAGIHARA<sup>1</sup>  
and Yoshiya TOUGE<sup>1</sup>

<sup>1</sup>Department of Civil and Environmental Engineering, Graduate of School of Engineering, Tohoku University, Miyagi 980-8579, Japan.

\*E-mail: ikemoto.atsuya.s1@dc.tohoku.ac.jp

<sup>2</sup>National Agriculture and Food Research Organization

<sup>3</sup>Water Resources Research Center, Disaster Prevention Research Institute, Kyoto University

## Abstract

In order to grasp the potential flood prevention of the irrigation reservoir, the flood inundation model was performed for the whole of Japan assuming that the maximum reservoir capacity can work. In addition, the rate of change in inundation depth with and without reservoirs was calculated. The results suggest that effectiveness of flood control using by reservoir is expected in Kagawa, Hyogo, Osaka, Hiroshima and Saga. In addition, effectiveness of flood control using by reservoir is not expected in Kanto region.

**Key Words:** *flooding, flood inundation analysis, reservoir*

## 1 Introduction

In Japan, water control focus on each water system. The river basin management<sup>[1]</sup> is finalized river planning, rainwater storage and infiltration facilities, landuse regulation and forecasting to prior release in dams. The project uphold utilization of agricultural land, facilities for agriculture; paddy field, reservoir is upheld. Storage of rainwater and floodwater on agricultural land and facilities for agriculture is expected to reduce flooding disaster. To help water control which is expected to utilize agricultural land and facilities for agriculture, flood damage mitigation effect using agricultural land and facilities for agriculture needs to be measured. Tanakamaru *et al.*<sup>[2]</sup> and Yoshisako *et al.*<sup>[3]</sup> studied the flood control effectiveness of reservoirs in Hyogo and Hiroshima prefectures. However, studies evaluating the effect of reservoir utilization on flood damage reduction across Japan are rare. The purpose of this study is to examine the effectiveness of the use of reservoirs in Japan in reducing the damage caused by flood inundation. Flood inundation analysis is conducted considering the reservoir capacity to achieve the purpose. The study focused particularly on areas with large changes in inundation depth.

## 2 Materials and methods

The rainfall data which is used for flood inundation analysis in this study is the stochastic flood-contributing distribution of fifth-order made by Yamamoto *et al.*<sup>[4]</sup>. A two-dimensional unsteady flow model<sup>[5]</sup> in Cartesian Coordinate System is used for flood inundation analysis, which has been applied and shown to be valid for the Naruse River basin, which was severely damaged by the East Japan Typhoon 2019<sup>[6]</sup>.

The inundation analysis is conducted for gamut in Japan at a time. The two-dimensional unsteady model is uniformly applied to river and floodplain. The mesh size is fifth-order. The inundation analysis is conducted on condition that rainfall-intensity of the stochastic flood-contributing distribution is steady for 24 hours. The resistance of house is

taken in account by assuming that house area is not gotten flooded in the two dimensional model. The value of Manning coefficient is same as Yamamoto *et al.*<sup>[7]</sup>. The proportion of house in each cell is calculated in the same way as Yanagihara *et al.*<sup>[6]</sup>. The proportion of Land for building use is 0.411. Other parameter values in analysis are same as previous researches. When the analysis is conducted by using elevation data of fifth-order mesh, occurrence of unlikely inundation as real phenomenon in dip is noted. Dips are removed by in the same way as Yanagihara *et al.*<sup>[6]</sup>.

Tanaka *et al.*<sup>[8]</sup> established the level of flood control safety for each river section by mapping the planned scale of the water system to the data of the type of manager of the river section. Tanaka *et al.*<sup>[8]</sup> used data which is about the planned scale of the water system and the type of the river section to decide the level of flood control safety for each river. The assigned flood control safety level is reflected by calculating excavation depth at which a flood of that scale can be safely discharged each river section. The excavation depth is calculated by inundation analysis. The level of flood control safety is assumed to be 50% of the planned level of flood control maintenance, because the flood control structures are in the middle of improving in Japan. In this study, method which is improved is applied the inundation analysis. The way of improved is following. The manager of the river section was allocated by using order stream of Strahler in this study. Connection order stream of Strahler and the data of the type of manager of the river section was decided that is consistent with the type of manager of the river section in Digital National Land Information<sup>[9]</sup> for every first-class river and second-class river. The level of flood control safety for each river section was allocated as previous studies<sup>[7],[8]</sup>. The reservoir data in Japan is provided by National Agriculture and Food Research Organization. Some irrigation dams are not listed in the reservoir data in Japan. So the irrigation dams are added to reservoir data in Japan from the dam data(W01-05) in 2014 Digital National Land



Fig.1 Rate of inundation depth change ( Hokkaido )



Fig.3 Rate of inundation depth change  
 ( Kanto, Chubu, Kinki )

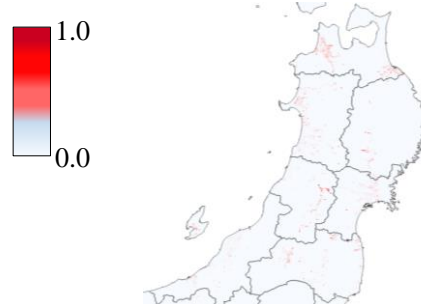


Fig.2 Rate of inundation depth change (Tohoku, Niigata )

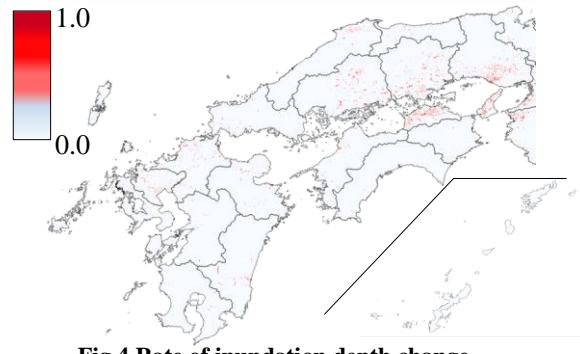


Fig.4 Rate of inundation depth change  
 ( Chugoku, Shikoku, Kyushu, Okinawa )

Information<sup>[9]</sup>. The dam data stored in the Digital National Land Information download services.

expected in Kanto region. This study intend in the future to consider water system basis and municipality basis.

### 3 Results and discussion

In this study, the inundation analysis is conducted that simulates damage due to the 200 year return period. The analysis is conducted that considers reservoir capacity or not. After analyzing, rate of inundation depth change is calculated by the following equation.

$$r = D / D_{res} \quad (1)$$

where  $r$  is rate of inundation depth change,  $D$  is inundation depth which does not consider reservoir capacity,  $D_{res}$  is inundation depth which considers reservoir capacity. The rate of inundation depth change is shown in Fig.1, Fig.2, Fig.3, and Fig.4. The size of rate of inundation depth is white to black gradient. Fig.1, Fig.2, Fig.3 and Fig.4 shows that areas which have big rate of inundation depth change distribute near estuary. This indicates that reservoir capacity and reservoir distribution mainly affect downstream. In addition, prefectures such as Kagawa, Hyogo, Osaka, Hiroshima and Saga are distributed a lot of big rates of inundation depth change. In these prefectures, effectiveness of flood control using by reservoir is expected. The other, the distributions areas that big rates of inundation depth change are small in Kanto region, such as Kanagawa, Tokyo, Tochigi, Ibaraki, Gunma, Saitama. This suggests that effectiveness of flood control using by reservoir is not expected in Kanto region.

### 4 Conclusions

The purpose of this study is to examine the effectiveness of the use of reservoirs in Japan in reducing the damage caused by flood inundation. The results suggest that effectiveness of flood control using by reservoir is expected in Kagawa, Hyogo, Osaka, Hiroshima and Saga. In addition, effectiveness of flood control using by reservoir is not

### Reference

- [1] Council for Social Infrastructure Development: Water-related Disaster Countermeasures in Light of Climate Change: Shift to Sustainable "Basin Flood Control" to be Carried Out by All Stakeholders throughout the Basin Report, 2020.
- [2] Tanakamaru, H. *et al.*: Simple estimation method of flood mitigation effect of irrigation ponds, IRRIGATION, DRAINAGE AND RURAL ENGINEERING JOURNAL, Vol. 88, No. 9, pp.23-26, 2020.
- [3] Yoshisako, H. *et al.*: Flood Peak Mitigation Effects by Irrigation Ponds Group of Valley type in the Mukunashi River Valley, Hiroshima Prefecture, Japan, IRRIGATION, DRAINAGE AND RURAL ENGINEERING JOURNAL, Vol. 81, No.3, pp.205-214, 2013.
- [4] Yamamoto, T. *et al.*: Evaluation of flood damage reduction throughout Japan from adaptation measures taken under a range of emissions mitigation scenarios, Climatic Change, Vol.165, Article number: 60, 2020.
- [5] Machida, S. *et al.*: EVALUATION OF FLOOD DAMAGES FOR CLIMATE CHANGE, Proceedings of the Symposium of Global Environment, Vol. 15, pp. 155-160, 2007.
- [6] Yanagihara, H. *et al.*: CHANGES IN FLOOD DAMAGE THROUGHOUT JAPAN DUE TO CLIMATE CHANGE AND LAND-USE CHANGE USING SHARED SOCIOECONOMIC PATHWAYS, Journal of Japan Society of Civil Engineers, Ser. G (Environmental Research), Vol. 77, No. 5, pp. I\_33-I\_42, 2021.
- [7] Yamamoto, T. *et al.*: Estimation of the mitigation and the landuse control for climate change based on the flood analysis in Japan, Journal of Japan Society of Civil Engineers, Ser. G (Environmental Research), Vol. 76, No. 5, pp. I\_141-I\_150, 2020.
- [8] Tanaka, Y. *et al.*: Assessment of the risk on flood and storm surge with flood control facilities. J Jpn Soc Civ Eng Ser B1 (Hydraul Eng) 75(2):I\_109-I\_114 (in Japanese).
- [9] Ministry of Land, Infrastructure, Transport and Tourism (MLIT) (n.d.-b) Digital National Land Information download services : <https://nlftp.mlit.go.jp/ksj/> Accessed 22 Oct 2020.

# The Survey of Extreme Flood Events in The Downstream Area of Citarum Watershed, Indonesia as Preliminary Study of Hazard Assessment and Socio-hydrology Approach

○ Muthiah SADIDAH<sup>1\*</sup> & Daisuke KOMORI<sup>1,2</sup>

<sup>1</sup>Graduate School of Environmental Studies, Tohoku University, Miyagi 980-8579, Japan.

<sup>2</sup>Department of Civil Engineering, Tohoku University, Miyagi 980-8579, Japan.

\*E-mail: muthiah.sadidah.t2@dc.tohoku.ac.jp

## Abstract

Citarum River, the longest river in West Java, is one of the most strategic rivers yet one of the most flood-prone rivers throughout history. Based on National Agency for Disaster Countermeasure of Indonesia (BNPB), Karawang regency is the most flooding-prone area in Citarum watershed with the highest number of flood events compared to the upper areas. This research aims to prepare data of socio-hydrology study by analysing three extreme events in the target area which occurred in 2013, 2014 and 2021. The human-flood interaction is assessed in the target area by discussing societal vulnerability and exposure to flood risk. The study of the interplay between social and physical processes is conducted based on 2007 until 2014 precipitation data from Yanto et al., 2017 and damages data reported by local News. The result shows that there is a sign of “adaptation effect” in the study area. This result supported the existence of the dynamics of human-flood system in the target area. This research hopefully will be able to be a starting point of the further study of flood hazard and socio-hydrological assessment in Citarum Watershed.

**Keywords:** Flood; Human-flood; Adaptation-effect; System dynamic; Socio-hydrology; Hazard

## 1 Introduction

The International Disaster Database reported that in the last 21 years, flood is the major disaster event in The World with total 3656 events. The situation appears to get worse related to the facts that rapid urbanization continues to increase the number of people living in floodplains and flood levels might rise up due to climate change [Hinkel et al., 2014; Jongman et al., 2014]. Reviewing 20 years of NASA satellite data, researchers discovered that between 58 and 86 million more people might be found residing in floodplains worldwide between the years 2000 and 2015. During that time, major floods had an impact on more than 255 million individuals at least once [Tellman et al., 2021].

The interaction between social and physical processes still lacks a fundamental understanding while there has been a lot of studies assessing flood risks quantitatively. Consequently, the dynamics emerging from this interaction cannot be well explained by the current analytical frameworks [Di Baldassare et al., 2015]. Seeking to achieve greater insights into causal relationships within human-water systems, process socio-hydrology employs nonlinear, organic thinking (i.e., systems thinking; Sivapalan et al., 2012). System dynamics (SD), a branch of systems thinking (Ford, 1999), was introduced by Forrester (1961) to support studies related to representing complex systems and analyzing their dynamic behavior (Hjorth and Bagheri, 2006).

“Adaptation effect” is a first type dynamics discussed in this research, which is associated with the relationship between the frequency of flood events and societal vulnerability. This term explains that the more frequent flooding happens the more decreasing the societal vulnerability is. Based on an empirical study, the impacts resulted by flood are decreasing while there was a similiar event happened not long before [Di Baldassare et al., 2015]. For example, despite having similar

magnitudes, the 1995 Meuse River flood caused substantially less damage than the one in 1993 [Wind et al., 1999].

A second type of dynamics is “levee effect” which is explained by a decrease in risk awareness when flooding becomes less frequent because of the introduction (or reinforcement) of structural protection measures (White, 1945). A previous study explained that increasing the levels of flood protection can generate a sense of satisfaction among protected people, which can reduce preparedness, thereby increasing vulnerability (Tobin, 1995). An example of levee effect was described in the case of New Orleans (1930’s-2005), where the construction and raising of levees caused frequent, minor flooding to become infrequent but catastrophic disasters [Kates et al., 2006].

The aforementioned two types of dynamics arises from the interaction between physical and social processes which have been considerably studied in many floodplains around the world. Nevertheless, conventional methods are not able to correctly explain these dynamics. For instance, the current methods would logically imply that flood-rich periods would result in more flood damage. However, the adaptation effect (the case of 1995 Meuse River flood) that has been explained before shows that this is not always the case. Another example, current research consistently indicates that putting flood prevention systems in place would result in less flood damage but the levee effect explains (such as the case of New Orleans happened in 1930’s-2005 explained before) that this is not necessarily the case [Di Baldassare et al., 2015]. Socio-hydrological modeling is a tool to explore and to have better understanding in the dynamics of human-flood system explained before hence our ability to interpret flood risk changes over time can be improved thereby better policies and measures that will decrease the negative impacts of floods can be developed [Di Baldassare et al., 2013].

This research is a part of socio-hydrology study which aims to prepare data of socio-hydrology study by pairing up events in the target area to examine the hazards and exposure resulted. Pairing up events is important for socio-hydrological study as it helps gain better understanding of interaction and feedback mechanism between hydrological and social processes in the target area.

## 2 Materials and methods

This research surveyed extreme flood events in 2013, 2014 and 2021 in Karawang regency, West Java, Indonesia. This area was chosen based on the database of The National Agency for Disaster Countermeasure of Indonesia (BNPB) and Citarum official website. Based on the data, the total number of flood events in Karawang from 1980 until 2021 is at least twice as much as the number in upper regencies.

Hazard assessment of this research is supported by gauge observation data of daily gridded precipitation from 1985 until 2014 over Java Island, including West Java sourced from Yanto et al., 2017. On the other hand, human-flood interactions are assessed in respect to exposure such as the number of victims and vulnerability such as the preparedness of the nearby society.

## 3 Results and discussion

### (1) The transition of flood hazard and flood exposure

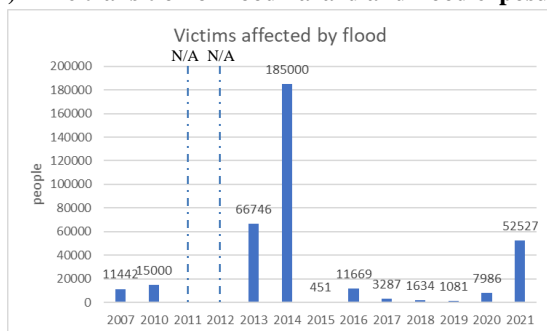


Fig. 2. Karawang Flood Victims 2007-2021

As it can be seen in Figure 2 the flood events happened in 2013, 2014 and 2021 resulted great damages of 66,746; 185,000 and 52,527 victims, respectively. The damages are much higher compared to those in other years. Hence, these three flood events are considered extreme cases within the study period in Karawang.

As shown in Figure 3, the annual maximum daily precipitation in Karawang from 2007 until 2014 depicts a fluctuative trend with the highest value occurred in 2014.

As it can be seen, the extreme cases discussed using Figure 2 are supported by hazards shown in Figure 3. The maximum daily precipitation of 2013 and 2014 is higher than that in other years which is around 45 mm and 51 mm, respectively. However, due to data limitation from Yanto et al., 2017 the data of 2021 precipitation was gathered from Kompas news, it is reported that the daily rainfall in 2021 at least reached 50 mm. These facts conclude that the hazards data of 2013, 2014 and 2021 support the extreme flood cases shown in Figure 2.

Figure 4 depicts the return periods based on maximum daily precipitation calculated using Log Normal distribution. Based on this figure, the extremes cases of 2013, 2014 and 2021 in Karawang with the value of rainfall hazards 45 mm, 51 mm, and 50 mm have the estimated magnitude of floods in terms of return periods of 4, 6, 8 return periods respectively.

Measures have been taken to reduce the risk over the intervening period.

Besides maximum precipitation. The probability of river discharge is one of the typical indicators of the scale of river flooding. However, due to data limitation, the analysis using river discharge will be employed in the further discussion.

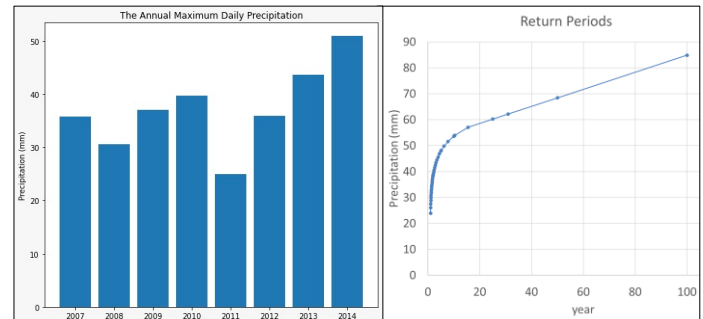


Fig. 3. Annual maximum daily precipitation in Karawang

Fig. 4. Return Periods

### (2) Extreme events comparison

The flood events that happened in 2013, 2014 and 2021 resulted in great damages of 66,746; 185,000 and 52,527 victims, respectively. The damages are much higher hence these three flood events are considered extreme cases within the study period in Karawang.

As it is shown in Figure 2 the damages of the 2021 flood in Karawang were much lower than those in 2013 and 2014 even though their magnitudes do not show great difference. This condition may consider “adaptation effect” which relates to the observation that the occurrence of more frequent flooding is often associated with decreasing societal vulnerability. The effect we can see in Figure 2 is there is a possibility that explains that the experience of floods in 2013-2014 and every year after may have reduced flood damages in 2021. This condition might have happened due to the increase of preparedness such as evolving early warning system, fixing emergency management and so on. The increasing preparedness is what really happened in Karawang as it is reported by Regional Disaster Management Agency of Karawang regency (BPBD) that in 2019 they has installed an early warning system tool that is directly connected to the disaster warning alarm at the BPBD office. So that the handling of disaster preparedness can be directly handled by the officers.

## 4 Conclusions

The estimation of the dynamics which comes from the interaction between human and flood has been applied in Karawang regency, West Java, Indonesia. The result shows that there is a sign of “adaptation effect” in the study area. “Adaptation-effect” is one type of system-dynamic arising from human-flood interaction. As it is stated by Baldassare et al., 2013, interaction and feedback mechanism between hydrological and social processes in the floodplain area is complex. Therefore, it is needed to conceptualise human-flood interactions through socio-hydrological modeling. The role of this model is to be a tool to explore possible future trajectories of flood risk so that the government and stakeholders can improve policies and measures that will decrease the negative impact of flood hazard itself.

## Reference

- [1] Di Baldassarre, G., Viglione, A., Carr, G., Kuil, L., Salinas, J.L. and Blöschl, G., 2013. Socio-hydrology: conceptualising human-flood interactions. *Hydrology and Earth System Sciences*, 17(8), pp.3295-3303.
- [2] Di Baldassarre, G., Viglione, A., Carr, G., Kuil, L., Yan, K., Brandimarte, L. and Blöschl, G., 2015. Debates— Perspectives on socio-hydrology: Capturing feedbacks between physical and social processes. *Water Resources Research*, 51(6), pp.4770-4781.
- [3] Hinkel, J., D. Lincke, A. T. Vafeidis, M. Perrette, R. J. Nicholls, R. S. J. Tol, B. Marzeion, X. Fettweis, C. Ionescu, and A. Levermann (2014), Coastal flood damage and adaptation costs under 21st century sea-level rise, Proc. Natl. Acad. Sci. U. S. A., 111(9), 3292–3297, doi:10.1073/pnas.1222469111.
- [4] Hjorth, P. and Bagheri, A., 2006. Navigating towards sustainable development: A system dynamics approach. *Futures*, 38(1), pp.74-92.
- [5] J. Forrester. 1961. *Industrial Dynamics* The MIT Press, Cambridge, MA and Wiley, New York.
- [6] Kates, R. W., C. E. Colten, S. Laska, and S. P. Leatherman (2006), Reconstruction of New Orleans after Hurricane Katrina: A research perspective, Proc. Natl. Acad. Sci. U. S. A., 103(40), 14,653–14,660, doi:10.1073/pnas.0605726103.
- [7] Livneh, B. and Rajagopalan, B., 2017. Development of a gridded meteorological dataset over Java island, Indonesia 1985–2014. *Scientific data*, 4(1), pp.1-10.
- [8] Sivapalan, M., Savenije, H.H. and Blöschl, G., 2012. Socio-hydrology: A new science of people and water. *Hydrol. Process*, 26(8), pp.1270-1276.
- [9] Sukowati, K.A.D. and Kusratmoko, E., 2019, August. Analysis of the distribution of flood area in Karawang Regency using SAR Sentinel 1A image. In *IOP Conference Series: Earth and Environmental Science* (Vol. 311, No. 1, p. 012085). IOP Publishing.
- [10] Tobin GA (1995) The levee love affair: a stormy relationship? *Water Resour Bull* 31:359–367. <https://doi.org/10.1111/j.1752-1688.1995.tb04025.x>
- [11] White, G. F.: Human Adjustments to Floods, Department of Geography Research, Paper no. 20, 29, The University of Chicago, Chicago, 1945.
- [12] Wind, H. G., T. M. Nierop, C. J. de Blois, and J. L. de Kok (1999), Analysis of flood damages from the 1993 and 1995 Meuse Floods, *Water Resour. Res.*, 35(11), 3459–3465, doi:10.1029/1999WR900192. Levermann (2014), Coastal flood damage and adaptation costs under 21st century sea-level rise, Proc. Natl. Acad. Sci. U. S. A., 111(9), 3292–3297, doi:10.1073/pnas.1222469111.

## Evaluation on high-altitude snow observation for snowmelt flood forecasting

○ Shoichi KUROSAWA<sup>1,2\*</sup> & So KAZAMA<sup>1</sup>

<sup>1</sup>Department of Civil Engineering, Graduate School of Engineering, Tohoku University, Miyagi 980-8579, Japan.

<sup>2</sup> Mitsui Consultants Co., Ltd, Tokyo 141-0032, Japan.

\*E-mail: kurosawa@mccnet.co.jp

### Abstract

In order to contribute to flood prevention activities and damage minimization against flood disasters exceeding the planned scale, provision of more accurate flood forecast information is required. This includes not only summer floods caused by rainfall, but also snowmelt floods in early spring. This paper presents the results of a study to improve the accuracy of flood forecasting by observing snow cover at high altitudes, taking the Yoneshiro River as an example.

**Keywords:** Flood forecast; Snowmelt flood; Snow depth observation; Snow depth gauge; Snowmelt model.

### 1 Introduction

In recent years, in order to contribute to flood prevention activities and damage minimization against flood disasters exceeding the planned scale, provision of more accurate flood forecast information is required. However, many flood forecasting systems currently in operation target summer floods caused by rainfall, and the problem is that they cannot be applied to snowmelt floods in early spring. For this reason, snow observations were carried out at high altitudes so that floods including snowmelt floods can be predicted throughout the year, and using those values, accuracy improvement was studied using the flood forecasting model.

In this paper, the Yoneshiro River was used as an example. Yoneshiro River is a river with a catchment area of 4,100 km<sup>2</sup>, which originates from Mt. Nakadake located on the border of Akita, Aomori, and Iwate prefectures, flows through the northern part of Akita prefecture from east to west, and empties into the Sea of Japan. (Fig. 1)

### 2 Implementation of snow depth observation

A snow depth gauge was installed at Mt. Moriyoshi Ani Ski Resort (1,167m above sea level) (November 2017). In addition, since the ski resort is famous for frost-covered trees (Japan's top three frost-covered trees), a Teflon-coated snow depth gauge sensor was manufactured, and countermeasures against low temperature such as use of an observation equipment that can withstand temperatures of up to -25°C and heating equipment were implemented. The initial status of the observation is shown in Fig. 2, Fig. 3. In early February, the sensor part became covered in frost and some missing data were confirmed, but observation has been consistent since early March. (Fig. 2, Fig. 3)

### 3 Snow depth observation results

Snow observation of the Yoneshiro River is carried out by the Japan Meteorological Agency AMeDAS at low altitudes. According to the annual AMeDAS snow depth data, snow melting begins at low altitudes around mid-March, and tends to melt at all the low altitude AMeDAS around early April. Comparing the ski resort (elevation 1,167m) and Aniai (elevation 120m) from March to May 2018, the snow at Aniai disappeared on April 6, but at this point, about 150 cm of

snow was observed at Ani ski resort, and the snow melted on May 11, one month later than the observed value at low altitude, showing a clear difference between the two. From this situation, it was judged appropriate to use the snow depth observation value at high altitudes, for snowmelt flood forecasting. (Fig. 4)



Fig. 1. Location Map of Yoneshiro River

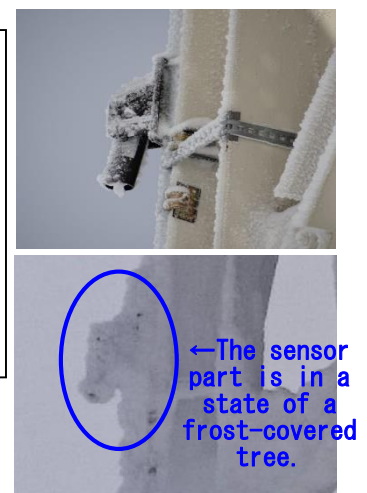


Fig. 2. Photos of the sensor. Top: At the beginning of the snowfall, Bottom: Early February.

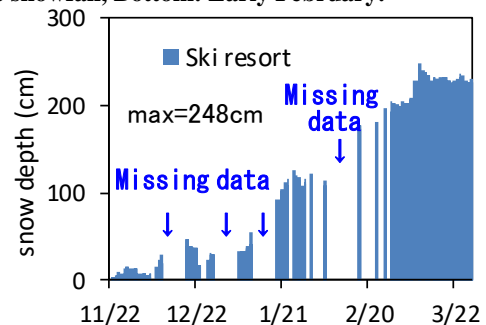


Fig. 3. Ski Resort Observation Values (November 2017 to March 2018).

### 4 Reproduction results of the flood forecasting model

The basic runoff model is the distributed runoff model in which kinematic wave method is applied to the ground

surface and Darcy's law is applied to the underground layer, so that the permeation process of rainfall and snowmelt can be expressed.

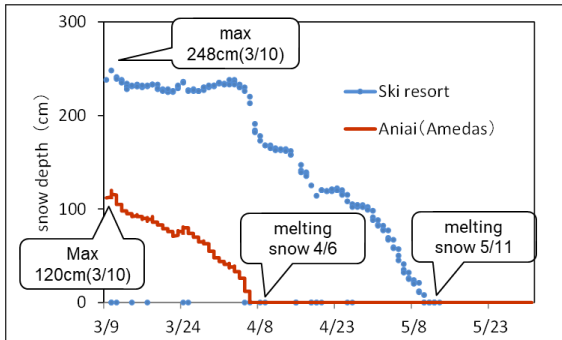


Fig. 4. High and low altitude observations (2018).

In addition, the amount of snowmelt on the base was set at 2.0mm/day, and the amount of snowmelt on the surface was determined by the degree hour method, and was assigned to each 1km mesh of the distributed runoff model. The following is the formula for calculating the amount of snowmelt. In addition, as a method of correcting the snow observation data (density difference), correction of the amount of snow water (assimilation method [1] [2]) was incorporated.

$$\text{SM} = K \times T + 2.0/24$$

T: hourly average temperature (°C)

K: snowmelt coefficient (mm/°C·hr).

The snowmelt coefficient K was set to a constant value during the snow cover period, and was set so as to coincide with the AMeDAS (Aniai) snowmelt day in the basin. In addition, the air temperature was corrected against altitude with a temperature lapse rate of 0.006°C/m.

As the model reproduction result, the river discharge was compared with each observed value. Originally, the reproducibility of flood forecasting is confirmed by river water level, but in order to include the influence of snowmelt in the evaluation, the river flow rate at Junisho where the outflow area is prominent was compared with the observed value. (Fig.5)

As a result, although the snowmelt discharge could not be reproduced due to the lack of flow volume in the calculation that did not consider the amount of snowmelt, it was possible to reproduce the peak water level etc. by considering the amount of snowmelt, and it was judged that the snowmelt model was generally appropriate.

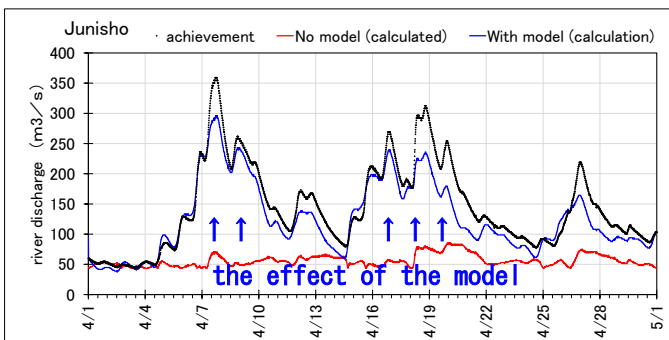


Fig. 5. Reproduction results of river discharge (Junisho).

## 5 Results and discussion

A result has been obtained that the reproducibility of river discharge will improve by building a snowmelt model based on high-altitude observation values. The reason for this is that the snow cover distribution (snowmelt amount) that remained in the mountains could be roughly reproduced.

On the other hand, new observation issues have emerged, such as data delivery delays even after maintenance and inspection, due to deterioration of the equipment installed and severe situation where the sensor part was covered with frost.

Until 2019, the observation equipment consisted of (1) sensor unit, (2) data logger, (3) communication unit, and (4) battery.

In particular, it has been determined that the data delivery delay was caused by the communication unit, so the data logger and communication unit have been updated to an integrated type. Before the update, the data logger and the communication unit operated separately, and the two devices were connected using a USB connector, so it is possible that they were affected by the outside air (temperature drop), and stable operation can be expected after the device update. (Fig. 6, Fig. 7)

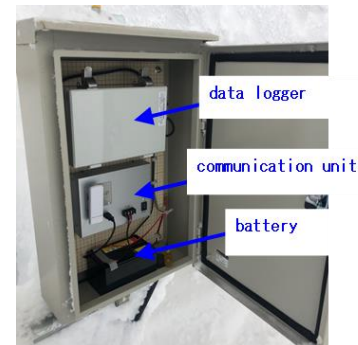


Fig. 6. Equipment configuration (until 2019).



Fig. 7. Updated equipment configuration (from 2020).

## 6 Conclusions

It has been concluded that the reproducibility of the river discharge will improve by using the observed value of the ski resort and combining it with the snowmelt model and the distributed runoff model. For this reason, stable observation is also important, and we believe that it is necessary to take countermeasures against missing measurements by covering the entire sensor with a windbreak plate that takes into account the direction of the wind.

## Reference

- [1] 柏俊輔, 朝岡良浩, 風間聡, 積雪深データ同化による融雪出水解析, 水工学論文集, 55, 2011.
- [2] 風間聡, 広域における積雪全層密度推定に関する研究, 水工学論文集, 41, 1997.

## Satellite and UAV derived vegetative roughness in Nanakita river: case of Typhoon Hagibis

○ Andre FORTES<sup>1\*</sup>, Masakazu HASHIMOTO<sup>2</sup> & Keiko UDO<sup>1</sup>

<sup>1</sup>Department of Civil and Environmental Engineering, Tohoku University, Miyagi 980-0845, Japan.

<sup>2</sup>International Research Institute of Disaster Science, Tohoku University, Miyagi 980-8572, Japan.

\*E-mail: andre.araujo.fortes.p6@dc.tohoku.ac.jp

### Abstract

Typhoon Hagibis hit Japan on October 12, 2019, causing severe floods. Hydraulic models are powerful tools for flood control strategies but depend on several input parameters. With the riparian vegetation strongly related to the Manning roughness coefficient in these areas, many studies aim to quantify the effect. Remote sensing techniques facilitated the acquisition of vegetation parameters, which enabled hydraulic models that adopt a dynamic Manning value that better represents the vegetation relationship with roughness. The objective of this study is to recreate the typhoon event with a dynamic Manning model that considers the vegetation parameters to calculate the roughness. The dynamic approach presented more accurate results when compared to the traditional static approach. The results suggest that the proposed dynamic Manning model can be a powerful tool for river management, capable of accurately representing the vegetation effect on flow dynamics.

**Keywords:** Flood modeling; Manning's coefficient; Remote sensing; Vegetative roughness; Typhoon 19.

### 1 Introduction

On October 12, 2019, typhoon Hagibis hit Japan, causing flood in many rivers in the territory [1]. To protect the population and mitigate the damage of the floods, river management uses hydraulic models for flood control strategies. But these models have a dependency on uncertain parameters like the Manning roughness coefficient.

The Manning value depends on a variety of factors [2], and among all factors, vegetation is the primary determinant of the roughness value [3]. Many studies have related the vegetation parameters with the roughness in different flow conditions, relating the friction factor with the vegetation density expressed by the leaf area index (LAI) when the vegetation is emergent [4], and relating the roughness to the degree of submergence of the plants, which is defined by the ratio of water depth over the plant height, in submerged vegetation scenario [5].

Studies that implement roughness as a dynamic variable related to vegetation are important but acquiring detailed vegetation parameters in large areas is a difficult task.

Vegetation identification and parameters acquisition became possible with remote sensing techniques from UAV and satellite imagery. Parameters like the canopy height have been obtained by combining machine learning techniques with UAV imagery [6] while other parameters, like the LAI, with satellite images [7].

The study area of this study is a 2 km stretch of the Nanakita river, a class B river with 45 km of length in total and a catchment area of 229 km<sup>2</sup>. Figure 1 shows the 2 km stretch location inside the river catchment area.

The objective of this study is to recreate the typhoon event in the 2 km stretch using a dynamic roughness model that uses both the vegetation height and the LAI to calculate the Manning value.

### 2 Materials and methods

The typhoon event was recreated using a 2D unsteady hydraulic model that uses continuity and momentum equations as governing equations [8]. The input parameters are the topography, the upstream discharge and the Manning values in channel and floodplain.

The topography digital elevation model (DEM) was created with 10 m resolution by interpolating 21 cross sections provided by the Miyagi prefecture. The discharge used in the upstream of the stretch was obtained with RRI model [9].

Three simulations were performed to recreate the event. A static model (SM) was performed with Manning values of 0.022 and 0.038 for channel and floodplains, respectively. For the other two simulations, a subroutine to calculate the Manning in the vegetated grid cells was created. The Manning calculation was done in the submerged state of vegetation using the degree of submergence relationship with the roughness found in [10]. The data was used to create a formula with regression analysis, shown in Eq. (1).

$$n = 0.084 * (SD)^{-0.98} + 0.023 \quad (1)$$

Where  $n$  is the Manning coefficient and  $SD$  is the degree of submergence of the vegetation.

In the emergent state, Darcy-Weisbach friction factor was calculated based on the LAI value in the grid cell with the formula proposed by Järvelä [4], shown in Eq. (2) and converted to Manning by Eq. (3).

$$f = 4C_{Dx}LAI \left( \frac{u}{u_x} \right)^x \quad (2)$$

$$n = \sqrt{f/8gh^{-1/3}} \quad (3)$$

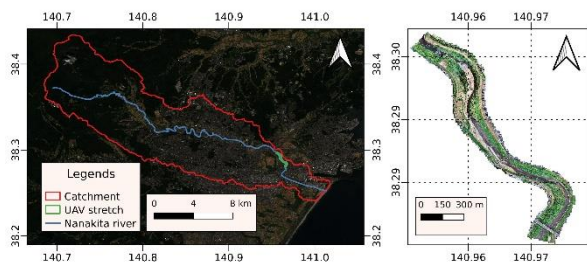


Fig. 1. Study area.

Where  $C_{Dx}$  is the vegetative drag coefficient,  $x$  is a species-specific parameter,  $u_x$  is the minimum velocity used to acquire  $x$  and  $u$  is the flow velocity.

The full dynamic model (FDM) considered both emergent and submerged Manning calculation, and the partial dynamic model (PDM) used only the submerged state, where the water was blocked in the vegetated cells while the vegetation was still emergent.

The vegetation location and height were obtained by a combination of UAV 3D point cloud data and machine learning, for more details, refer to [6].

The LAI with 10 m resolution was obtained by downscaling the LAI from MODIS (500 m) using machine learning and Sentinel-2 images, like the methodology used in [7].

### 3 Results and discussion

The simulated event with the SM produced a similar water level profile to the observed. Regarding the dynamic models, the FDM achieved results more accurate than the SM and the PDM. The FDM and SM peak water level profile were very similar, with the FDM presenting the best result. The RMSE of SM and FDM were 0.141 and 0.137, respectively. The PDM produced the largest RMSE of 0.189, with the water level profile higher than the observed. Figure 2 shows the water level profiles of the SM, FDM and PDM over the ground level and with the right and left banks.

The overestimation of the inundation produced by the PDM was due to the use of only the submerged Manning calculation routine. By blocking the water flow in the vegetated grid cells while it was emergent, a fast accumulation of water occurred in these locations, leading to the increase of the water level profile. The similar result of the FDM and SM means that the proposed emergent and submerged Manning calculation routines combined produced an equivalent overall Manning value that substituted the static Manning of 0.038 in the floodplains previously calibrated and proposed by Miyagi prefecture. This is important because the FDM can shorten the trial-and-error process of calibration of the static model, and it correctly verifies the effect of the vegetation on the floodplain roughness.

With the FDM, it is possible to perform sensitivity analysis on the vegetation LAI and height to assess the appropriate amount of vegetation in the floodplains in order to provide the safety of the nearby residents while maintaining the ecological properties of the environment.

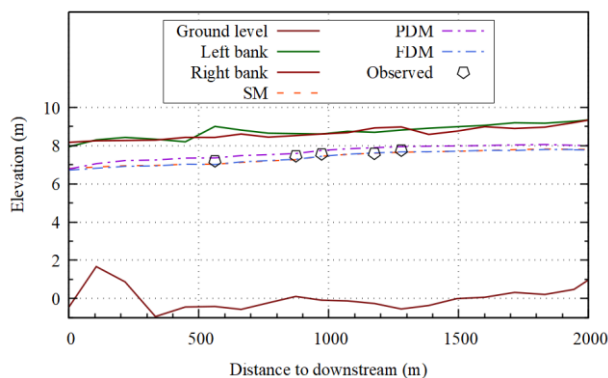


Fig. 2. Simulated and observed water level profiles.

### 4 Conclusions

Remote sensing is an important tool to provide data in river environments. Both UAV and satellite can provide vegetation parameters with moderate resolution to be used in hydraulic modeling.

The proposed dynamic Manning model considering both emergent and submerged vegetation obtained more accurate results than the traditional static Manning model. Although, the simulated water levels from the FDM and SM were very close, which suggests that the floodplain roughness value of 0.038 was appropriate. This also suggests that the FDM has the advantage of not requiring the same time-consuming process of calibration and represents well the effect of the vegetation in the roughness. The results suggest that the dynamic Manning model can be an important tool for river management.

### Reference

- [1] Kazama, M., Yamakawa, Y., Yamaguchi, A., Yamada, S., Kamura, A., Hino, T., and Moriguchi, S., Disaster report on geotechnical damage in Miyagi Prefecture, Japan caused by Typhoon Hagibis in 2019, *Soils Found.*, 61 (2021) 549-565.
- [2] Cowan, W., Estimating hydraulic roughness coefficients, *Agricultural Engineering*, 37 (1956) 473-475.
- [3] Ebrahimi, N. G., Fathi-Moghadam, M., Kashefipour, S. M., Saneie, M., and Ebrahimi, K., Effects of Flow and Vegetation States on River Roughness Coefficients, *Journal of Applied Science*, 8 (2008) 2118-2123.
- [4] Järvelä, J., Determination of flow resistance caused by non-submerged woody vegetation, *Int. J. River Basin Manage.*, 2 (2004) 61-70.
- [5] Nikora, V., Larned, S., Nikora, N., Debnath, K., Cooper, G., and Reid, M., Hydraulic Resistance due to Aquatic Vegetation in Small Streams: Field Study, *J. Hydraul. Eng.*, 134 (2008) 1326-1332.
- [6] Fortes, A., Hashimoto, M., Udo, K., Ichikawa, K., and Sato, S., Obtaining Riparian Vegetation Characteristics from UAV Optical Imagery 3D Point Cloud Data, in: *Proceedings of the 39th IAHR World Congress*, (2022) 4855-4862.
- [7] Gokool, S., Kunz, R.P., and Toucher, M., Deriving moderate spatial resolution leaf area index estimates from coarser spatial resolution satellite products, *Remote Sens. Appl.: Soc. Environ.*, 26 (2022) 100746-100758.
- [8] Hashimoto, M., Yoneyama, N., Kawaike, K., Deguchi, T., Hossain, M. A., and Nakagawa, H., Flood and Substance Transportation Analysis Using Satellite Elevation Data: A Case Study in Dhaka City, Bangladesh, *J. Disaster Res.*, 13 (2018) 967-977.
- [9] Sayama, T., Ozawa, G., Kawakami, T., Nabesaka, S., and Fukami, K., Rainfall-runoff-inundation analysis of the 2010 Pakistan flood in the Kabul River basin, *Hydrol. Sci. J.*, 57 (2012) 298-312.
- [10] Japan Institute of country-ology and engineering, *Manual of plans for river channel* (in Japanese), Sankaidou (2002).